THE SCHOOL OF HARD NOX:

Characterization of human Nox1 and cyclized Rab7

DISSERTATION

zur Erlangung des akademischen Grades
eines Doktors der Naturwissenschaften (Dr. rer. nat.)
des Fachbereichs Chemie der Technischen Universität Dortmund

Angefertigt am
Max-Planck-Institut für medizinische Forschung in Heidelberg,
Max-Planck-Institut für molekulare Physiologie in Dortmund,
und an der Technischen Universität Dortmund in Dortmund

Eingereicht von Tammy T. Woo
aus San Diego, U.S.A.

Dortmund, 2008

1. Gutachter : Prof. Dr. R.S. Goody
2. Gutachter : Prof. Dr. R. Winter

THE SCHOOL OF HARD NOX

Characterization of human Nox1 and cyclized Rab7

DISSERTATION

submitted to achieve the degree of

Doktor der Naturwissenschaften (Dr. rer. nat.)

from the Department of Chemistry,

Technical University Dortmund, Germany

Tammy T. Woo

Max Planck Institute for Medical Research, Heidelberg
Max Planck Institute of Molecular Physiology, Dortmund
and the Technical University Dortmund

2008

Die vorliegende Arbeit wurde in der Zeit von April 2004 bis Mai 2008 am Max-Planck-Institut für molekulare Physiologie in Dortmund unter der Anleitung von Prof. Dr. Roger S. Goody und Dr. Alexey Rak, an der Technischen Universität Dortmund im Fachbereich Chemie unter der Anleitung von Prof. Dr. Roland Winter, und am Max-Planck-Institut für medizinische Forschung in Heidelberg unter der Anleitung von Prof. Dr. Ilme Schlichting durchgeführt.

Hiermit versichere ich an Eides Statt, dass ich diese Arbeit selbstständig und nur mit den angegebenen Hilfsmitteln angefertigt habe.

Dortmund, 2008 Tammy T. Woo

CONTENTS

ABBREVIATIONS

$^{\cdot}OH$	hydroxyl radical
ACE	angiotensin converting enzyme
ADP	adenosine 5'-diphosphate
AIR	autoinhibitory region
ATP	adenosine 5'-triphosphate
BSA	bovine serum albumin
cGMP	cyclic guanosine 5'-monophosphate
CMC	critical micelle concentration
diaphorase	a flavoprotein capable of oxidizing NADPH
DLS	dynamic light scattering
DPI	diphenyleneiodonium
DTE	dithioerythritol
DTT	dithiothreitol
EDTA	ethylene diamine tetraacetic acid
EGF	epidermal growth factor
eNOS	endothelial nitric oxide synthase
FAD	flavin adenine dinucleotide
GAP	GTPase activating protein
GDI	GDP dissociation inhibitor
GDP	guanosine 5'-diphosphate
GEF	guanine nucleotide exchange factor
GppNHp	guanosine 5'-(β, γ)-imidotriphosphate
GTP	guanosine 5'-triphosphate
H_2O_2	hydrogen peroxide
HEPES	N-(2-Hydroxyethylpiperazine)-N'-2-ethanesulfonic acid
HOCl	hypochlorous acid
HPLC	High performance liquid chromatography
ICAM-1	endothelial intracellular adhesion molecule-1
IPTG	isopropyl β-D-thiogalactopyranoside
LB	Luria-Bertani media
LDL	low-density lipoprotein
mantGppNHp	2'-(or 3')-*O*-(*N*-methylanthraniloyl)-β:γ-imidoguanosine 5'-triphosphate
MCP-1	monocyte chemoattractant protein-1
M-CSF	macrophage colony stimulating factor
MMP	matrix metalloproteinase
NADPH	nicotinamide adenine dinucleotide phosphate, reduced form
NBT	nitroblue tetrazolium
Ni-NTA	nickel-nitrilotriacetic acid chromatography resin
$NO^{\cdot}$	nitric oxide
$O_2^{\cdot -}$	superoxide
$ONOO^-$	peroxynitrite
PC	L-α-phosphatidylcholine
PCR	polymerase chain reaction
PDGF	platelet-derived growth factor
PE	L-α-phosphatidylethanolamine
PI	L-α-phosphatidylinositol
PI(3)P	phosphatidylinositol-3-phosphate

$PI(3,4)P_2$	phosphatidylinositol-3,4-bisphosphate
PIP_3	phosphatidylinositol 3,4,5-triphosphate
PMA	phorbol 12-myristate 13-acetate
PRR	proline-rich region
PTEN	phosphatase with sequence homology to tensin
PTP	protein tyrosine phosphatases
PVDF	polyvinylidene difluoride membrane
REP-1	Rab Escort Protein-1
RILP	Rab Interacting Lysosomal Protein
ROS	reactive oxygen species
SDS-PAGE	sodium dodecylsulfate polyacrylamide gel electrophoresis
SH3	Src Homology 3
SM	sphingomyelin
SOD	superoxide dismutase
ST1	Standard 1 media
TB	Terrific Broth media
TEV	Tobacco etch virus
TNF-α	tumor necrosis factor-α
TPR	tetratricopeptide repeats
VCAM-1	vascular cell adhesion molecule-1
VSMC	vascular smooth muscle cell

ABSTRACT

Deliberate enzymatic production of superoxide ($O_2^{\cdot-}$) was originally thought to be restricted to the membrane-associated multi-subunit NADPH Oxidase in phagocytic cells, which use superoxide as a precursor to secondary reactive oxygen species (ROS) to destroy engulfed pathogens as a part of innate immunity. Recent discovery in nonphagocytic tissues of an entire family of proteins (Nox) homologous to the catalytic subunit of the phagocytic NADPH Oxidase has led to the recognition of the role of ROS in normal cellular signaling, with an increasing awareness of the pathological consequences when this signaling becomes dysregulated. These Nox proteins normally produce low-level, intracellular superoxide, although many factors can stimulate their activity. Nox1 has emerged as a key oxidase in the vasculature with the discovery that factors which promote vascular disease additionally stimulate its activity. Knowledge of the three-dimensional structure of the holoenzyme or of the cytosolic domain, which catalyzes the first electron transfer step, could aid in the design of specific inhibitors as novel therapeutics. In this work, methods were developed to produce recombinant human Nox1 suitable for structure determination by X-ray crystallography. Investigations to promote the heterologous expression of recombinant full-length human Nox1 in *E. coli* did not result in observable overexpression. In contrast, four constructs containing the cytosolic domain of human Nox1 were solubly expressed in low amounts. Expression and purification protocols were developed for these constructs. Of these, an N-terminally His-tagged truncated human Nox1 containing residues 290-564 was found to possess an intrinsic NADPH-dependent diaphorase activity of 0.95 mol reduced NBT/min/mol protein. This activity is similar in magnitude to that of a longer construct of the phagocytic homologue, and is higher than Nox1 activity measured *in vivo*. The purified truncated human Nox1 required high ionic strength conditions for stability, and incubation with phagocytic regulatory proteins slightly enhanced its intrinsic activity. This active truncated human Nox1 would be suitable for future structure determination studies.

Protein backbone cyclization is a method to increase the inherent stability of a target protein, and may also be a useful tool to aid in the crystallization of proteins through stabilization of flexible loops. To evaluate the potential of this application, Rab7 GTPase (residues 7-185) was cyclized, characterized, crystallized in both GDP- and GTP-bound forms, and the corresponding structures were determined. Cyclization did not significantly alter the secondary structure of Rab7, but increased its thermal stability by 3.7°C. Cyclized Rab7 demonstrated similar GTPase activity and effector association–dissociation kinetics as an equivalent linear Rab7 construct. Cyclized Rab7•GDP crystallized readily and diffracted to significantly higher resolution than uncyclized Rab7•GDP. Crystal contacts involving residues from the linker used for cyclization stabilized the Switch I loop, which is disordered in Rab7•GDP structures, such that its structure could be determined. Cyclized Rab7•GppNHp was also crystallized, but these crystals were found to be pseudomerohedrally twinned with a high twinning fraction. In contrast to the stabilization seen in the cyclized Rab7•GDP structure, the final model of cyclized Rab7•GppNHp contained several regions of flexibility, including the Switch II loop, which is visible in other active Rab7 structures. These structures indicate that the N- and C- termini normally point in opposite directions. The linker used for cyclization may not be long enough to allow the protein to adopt this conformation, generating a strained conformation that affects other regions of the protein, like Switch II. In general, protein backbone cyclization can be a useful method to aid in the crystallization of proteins in which the N- and C-termini lie in close proximity to each other.

ZUSAMMENFASSUNG

Bisher wurde angenommen dass die gezielte enzymatische Produktion von Superoxid ($O_2^{\cdot-}$) ausschließlich in der membran-assoziierten NADPH-Oxidase in Phagozyten stattfindet. Diese verwenden Superoxid als Vorstufe sekundärer reaktiver Sauerstoff-Spezies (ROS), um im Rahmen der angeborenen Immunantwort umhüllte Pathogene zu zerstören. Die in letzter Zeit in nicht-phagozytischem Gewebe entdeckte „Nox" Protein-Familie, welche homolog ist zur katalytischen Untereinheit der phagozytischen NADPH-Oxidase, hat zu der Erkenntnis geführt dass ROS auch außerhalb von Phagozyten als Signalmoleküle eine wichtige Rolle spielen. Damit einher ging auch ein Verständnis für die pathologischen Konsequenzen einer Fehlregulation von ROS. Nox-Proteine produzieren normalerweise kleine Mengen intrazellulares Superoxid, obwohl viele verschiedene Faktoren diese Aktivität stimulieren können. Mit der Erkenntnis dass viele Herzkreislauferkrankungen verursachende Faktoren auch die Aktivität von Nox1 stimulieren können, wurde in Nox1 eine der wichtigsten NADPH-Oxidasen des Gefäßsystems erkannt. Die Kenntnis der dreidimensionalen Struktur des ganzen Enzyms Nox1 oder seiner cytosolischen Domäne, welche den ersten Elektronübergang katalysiert, würde die Entwicklung spezifischer Inhibitoren als potentielle neuartige Medikamente unterstützen.
Im Rahmen dieser Arbeit wurden zur Strukturaufklärung mit Hilfe der Röntgenstrukturanalyse ein Expressionsprotokoll und ein Reinigungsprotokoll für die rekombinante Proteinerzeugnung des menschlichen Nox1s (hNox1) entwickelt. Untersuchungen der Expression des Volllängenproteins hNox1 in *E. coli* zeigten keine nennenswerte Protein-Produktion. Im Gegensatz wurden vier Konstrukte der zytosolischen Domäne in niedrigen Mengen löslich exprimiert. Eines dieser Konstrukte, welches einen N-terminalen Hexahistidin-Tag und die Aminosäurereste 290-564 einschließt, zeigte eine Aktivität von 0,95 mol reduziertes NBT/min/mol Protein. Diese Aktivität ist vergleichbar mit der Aktivität eines längeren verkürzten Konstrukts des phagozytischen Homologs, und größer als die für Nox1 *in vivo* gemessene Aktivität. Dieses gereinigte, verkürzte Konstrukt von hNox1 benötigte zur Stabilisierung Puffer mit einer hohen Ionenstärke. Die Inkubation mit phagozytischen zytosolischen Regulator-Proteinen führte zu einer leichten Erhöhung der intrinsischen Aktivität. Dieses aktive verkürzte Konstrukt könnte sich gut für zukünftige Röntgenstrukturanalysen eignen.

Proteinzyklisierung ist eine Methode, die inhärente Stabilität eines Proteins zu erhöhen. Dadurch kann auch die Kristallisation eines Proteins ermöglicht werden, da z.B. flexible Bereiche des Proteins stabilisiert werden können. Um das Potential dieser Methode zu validieren, wurde die kleine GTPase Rab7 (Aminosäurereste 7-185) zyklisiert, charakterisiert, und in Komplex mit GDP und GTP kristallisiert. Die Zyklisierung verändert die Sekundärstruktur von Rab7 nicht bedeutsam, jedoch erhöht sich dadurch die thermische Stabilität des Proteins um 3,7°C. Zyklisiertes Rab7 hat eine mit linearem Rab7 vergleichbare GTPase-Aktivität und Assoziations/Dissoziations-Kinetik für Effektormoleküle. Zyklisiertes Rab7 hat die Kristallisation und Diffraktion von Rab7•GDP erheblich verbessert. Neue Kristallkontakte, welche Aminosäurereste des zur Zyklisierung verwendeten Linker-Bereichs involvieren, stabilisieren den normalerweise ungeordneten Switch I Bereich so weit dass die Kristallstruktur dieses Bereichs aufgeklärt werden konnte. Zyklisiertes Rab7•GppNHp wurde auch kristallisiert, aber die erhaltenen Kristalle waren hochgradig pseudomerohedral verzwillingt. Im Gegensatz zum zyklisierten Rab7•GDP zeigt die Kristallstruktur von zyklisiertem Rab7•GppNHp viele flexible Bereiche, welche auch den normalerweise sichtbaren Switch II Bereich einschließen. In Strukturen von aktivem Rab7 zeigt der N- und C-Terminus in entgegengesetzte Richtungen. Der zur

Zyklisierung verwendete Linker scheint jedoch zu kurz zu sein um eine vergleichbare energetisch günstige Konformation zu ermöglichen. Dadurch wird eine weniger günstige Konformation erzwungen, in der einige Bereiche des Proteins wie Switch II eine hohe Flexibilität aufweisen. Allgemein kann Proteinzyklisierung als eine sehr nützliche Methode zur Unterstützung der Kristallisation von Proteinen eingesetzt werden, in denen der N- und C-Terminus in enger räumlicher Nähe zueinander liegen.

Chapter 1.

NADPH Oxidase 1

1. INTRODUCTION

Traditionally, reactive oxygen species have been regarded as harmful to the cell (Chance *et al.*, 1979; Harman, 1981; Halliwell and Gutteridge, 1989; Davies, 1995), as evidenced by the numerous antioxidant mechanisms to detoxify these molecules (Yu, 1994). The classical exception to this was the NADPH Oxidase complex of phagocytic immune cells, which produces superoxide as a defense mechanism against invading bacteria (Babior *et al.*, 2002). However, in recent years, an entire family of proteins homologous to the catalytic component of the phagocytic NADPH Oxidase has been discovered in nonphagocytic cells (Kikuchi *et al.*, 2000; Geiszt *et al.*, 2000; Yang *et al.*, 2001; Shiose *et al.*, 2001; Cheng *et al.*, 2001; Banfi *et al.*, 2001), and investigation of their biological roles has revealed the importance of reactive oxygen species as signaling molecules that affect a number of normal and pathophysiological processes. These NADPH Oxidases are found in diverse cell and tissue types, and modulate processes which include angiogenesis, cell growth, innate immunity, apoptosis, regulation of the extracellular matrix, and thyroid hormone biosynthesis (Lambeth, 2004). Recently, interest has increased in this family of proteins with the discovery of their participation in a wide variety of cardiovascular related diseases and most recently in neurodegenerative diseases and cancer, making them attractive novel therapeutic targets.

1.1 REACTIVE OXYGEN SPECIES

Although itself a radical, molecular triplet oxygen is not very reactive due to the fact that its two unpaired electrons reside in different molecular orbitals with parallel spins (Beckman and Ames, 1998). Since acceptance of two electrons would require them to both possess spins which are antiparallel to the spins of the unpaired electrons of oxygen (which is unlikely to be fulfilled by a typical pair of electrons in atomic or molecular orbitals), oxygen participates in one-electron transfers (Beckman and Ames, 1998). Reactive oxygen species (ROS) are oxygen-derived molecules, which, due to their high reactivity, readily participate in oxidation-reduction (redox) reactions. Biologically relevant reactive oxygen species can be divided into two types: those which exist as radicals, which include superoxide ($O_2^{\cdot -}$), hydroxyl radical ($^{\cdot}OH$), nitric oxide ($NO^{\cdot}$), and alkoxyl radical ($R\text{-}O^{\cdot}$); and those which do

not, such as hydrogen peroxide (H_2O_2), peroxynitrite ($ONOO^-$), singlet oxygen ($^1O_2$), hypochlorous acid (HOCl) and lipid peroxides (LOOH) (Guzik and Harrison, 2006).

Many biologically relevant ROS can be derived from superoxide, the product of a one-electron reduction of molecular oxygen. The cell possesses many enzymatic sources of superoxide. These include mitochondrial enzymes, cyclooxygenase, cytochrome P-450 enzymes, xanthine oxidase, and NADPH Oxidases (Lassegue and Clempus, 2003; Guzik and Harrison, 2006). Superoxide has a half-life of a few seconds (Ray and Shah, 2005) and can function as both a reductant or an oxidant depending on the redox potential of the target molecule (Lambeth, 2004). Although a strong reductant, superoxide oxidizes a limited number of biological targets (Lambeth, 2004) such as [Fe-S] clusters in dehydratases like aconitase and fumerase, releasing Fe^{2+} (Kuo *et al.*, 1987; Gardner and Fridovich, 1991; Gardner and Fridovich, 1992; Liochev and Fridovich, 1994; Gardner *et al.*, 1994; Gardner *et al.*, 1995). Much of superoxide's harmful effects are due to the ability to further convert it into many other types of ROS that are far more damaging, such as hypochlorous acid (HOCl), hydroxyl radical ($^{\cdot}OH$), and peroxynitrite ($ONOO^-$). When produced in low amounts in the picomolar range, detoxification by superoxide dismutase isoenzymes [copper-zinc-SOD (CuZnSOD), manganese-SOD (MnSOD), and extracellular SOD (ecSOD)] accelerates its otherwise spontaneous dismutation into hydrogen peroxide (Faraci and Didion, 2004), which, due to its ability to permeate cell membranes, can extend the range of its effects (Ray and Shah, 2005; Cai, 2005).

Hydrogen peroxide is a stronger oxidant than superoxide, reacting with methionines or highly reactive cysteines in enzyme active sites of proteins like protein tyrosine phosphatases (Lee *et al.*, 1998). Hydrogen peroxide can be neutralized to water by the action of catalase or glutathione peroxidase (Droge, 2002), or it can be further converted into a still more powerful ROS by the action of myeloperoxidase in neutrophils (a subtype of white blood cells) which generates HOCl as a potent antiseptic against engulfed bacteria (Hampton *et al.*, 1998). In addition, hydrogen peroxide can react with Fe^{2+} via the Fenton reaction to form the hydroxyl radical (McCord and Day, Jr., 1978; Chance *et al.*, 1979), the most reactive ROS which reacts with nearly diffusion-limited rates (reaction occurs immediately upon collision) (Beckman and Ames, 1998).

Hydroxyl radicals react unselectively with any biological molecule within a short range of their formation (Halliwell and Gutteridge, 1986). They readily react with polyunsaturated

fatty acid chains in the membrane to initiate peroxidation chain reactions. Such reactions produce various radicals that damage the membrane in many ways. This includes reduced membrane fluidity from cross-linked fatty acid chains, compromised membrane integrity as a result of fragmented fatty acid side chains, and inactivation of membrane-bound enzymes (Halliwell and Gutteridge, 1989). Additionally, hydroxyl radicals can react with DNA causing DNA base modifications and strand breaks (Mello Filho *et al.*, 1984; Mello Filho and Meneghini, 1984), which is the main mechanism of damage caused by ionizing radiation (von Sonntag, 1987).

Superoxide also readily reacts with nitric oxide (rate constant 6.7 x 10^9 $M^{-1}s^{-1}$) (Huie and Padmaja, 1993) to form peroxynitrite ($ONOO^-$) (Beckman *et al.*, 1990), a strong oxidant which nitrosylates proteins, oxidizes lipoproteins (Guzik and Harrison, 2006), reacts readily with thiols and initiates lipid peroxidation (Fridovich, 1995). It is worthy to note that superoxide reaction with $NO^\cdot$ is 3 times faster than dismutation by SOD (2 x 10^9 $M^{-1}s^{-1}$) (Klug *et al.*, 1972; Rotilio *et al.*, 1972), resulting in significant production of $ONOO^-$ when $NO^\cdot$ and $O_2^{\cdot-}$ are present at high nanomolar amounts (Darley-Usmar *et al.*, 1995; Beckman and Koppenol, 1996; Ray and Shah, 2005; Cave *et al.*, 2006).

1.2 ROS AND VASCULAR DISEASE

A growing body of evidence describes the role of low levels of ROS in normal cellular function. Dysregulation of their production can lead to pathological situations, which have recently been widely documented in many vascular diseases.

1.2.1 Anatomy of the vascular wall

Blood vessels are composed of three layers that enclose the lumen, the hollow area in which blood flows. The innermost layer is known as the intima, and is topped by a single layer of endothelial cells (the endothelium), which contacts circulating blood. The intima is a thin layer comprised of extracellular connective tissue, such as proteoglycans and collagen, surrounded by an elastic membrane termed the internal elastica lamina. The second layer around the intima is a muscular layer known as the media, which consists of smooth muscle cells. The outer layer of the artery is known as the adventitia, which is made of fibroblasts and smooth muscle cells interspersed in connective tissues (Gray, 1918; Lusis, 2000).

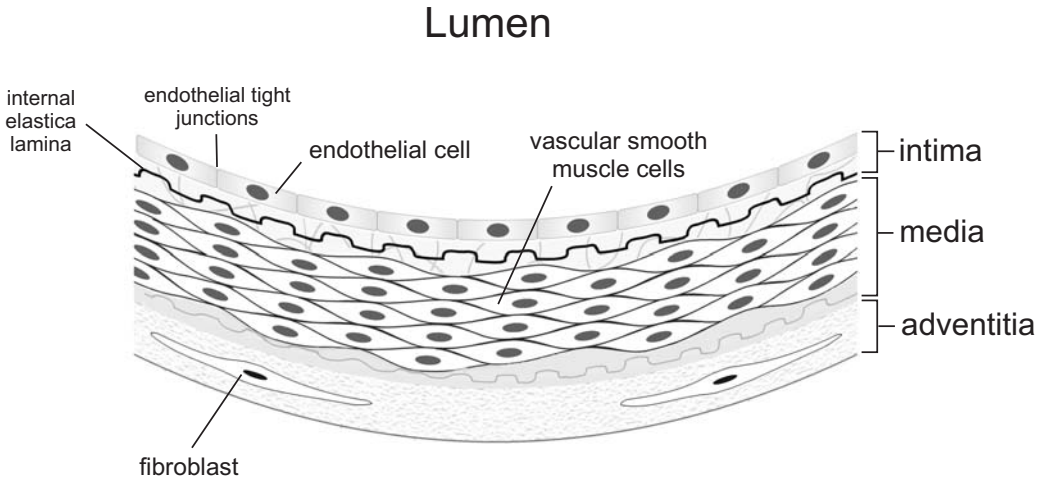

Figure 1. Anatomy of the vascular wall, showing the three main layers of blood vessels and the cells that compose them.

1.2.2 Normal endothelial function

Contrary to the earlier idea that the endothelium serves only as an inert lining of blood vessels and the heart, it is now clear that this monolayer of cells has important roles in cardiovascular homoeostasis that affect vascular tone, hemostasis (the process that stops bleeding) and vascular cell growth (Kaiser and Sparks, Jr., 1987; Ray and Shah, 2005). It does this by sensing local environmental changes and blood borne signals to modulate the equilibrium between vasoconstriction and vasodilation, anti-thrombotic and procoagulant factors, and cell proliferation and apoptosis (Ray and Shah, 2005). In general, the endothelium has vasoprotective functions to maintain a vasodilated, anti-inflammatory and anti-coagulant environment within blood vessels.

The vascular endothelium interfaces the bloodstream and the vessel wall, and mediates the effect of shear stress (tangential drag force of flowing blood over the endothelium; Fung and Liu, 1993) with the production of vasoactive substances such as $NO^{\cdot}$ and prostacyclin (both vasodilators), and endothelin-1 (a vasoconstricting peptide) (Nerem *et al.*, 1993; Guzik and Harrison, 2006). Endothelial $NO^{\cdot}$ is a key mediator of vasodilation, and is produced by the enzyme endothelial nitric oxide synthase (eNOS) (Bredt and Snyder, 1990). $NO^{\cdot}$ (previously known as endothelium-derived relaxing factor) diffuses from the endothelium to activate soluble guanylate cyclase in vascular smooth muscle cells, which increases cyclic GMP levels, leading to vasorelaxation (Rapoport *et al.*, 1983; Moncada *et al.*, 1991). Additionally, $NO^{\cdot}$ helps to maintain many areas of normal endothelial function, including inhibition of

platelet aggregation (de Graaf *et al.*, 1992), inhibition of monocyte adhesion to the endothelium (Kubes *et al.*, 1991; Gauthier *et al.*, 1995), as well as inhibition of vascular smooth muscle cell proliferation (Cornwell *et al.*, 1994). Thus, $NO^{\cdot}$ has many protective roles in the vasculature, which are critical for maintaining blood vessels in a healthy state.

1.2.3 Roles of ROS in endothelial dysfunction: impairing the cell's protective mechanisms

In light of its unique role as an interface between the blood and underlying tissues, disruption of the ability of the endothelium to modulate the equilibrium between opposing signaling mechanisms has wide-reaching effects. Endothelial dysfunction is observed in a number of vascular disease states, such as atherosclerosis, hypertension, heart failure and diabetes mellitus (Ray and Shah, 2005). Recently it has been recognized that impaired endothelial function is a strong indication of future cardiovascular complications and mortality (Halcox *et al.*, 2002; Fichtlscherer *et al.*, 2004). Endothelial dysfunction is characterized by impaired endothelium-dependent vasodilation, and an increase in factors that promote inflammation and thrombosis (Gimbrone, Jr. *et al.*, 1995; Cave *et al.*, 2006). It has become clear in recent years that elevated production of ROS are observed in many of the same pathological settings as endothelial dysfunction, such as hypercholesterolemia, hypertension and diabetes (Rajagopalan and Harrison, 1996; Harrison *et al.*, 2003). ROS, and in particular superoxide, can interfere with normal endothelial function by interfering with the bioavailability of $NO^{\cdot}$ (Guzik and Harrison, 2006).

There are a number of ways that superoxide can affect endothelial $NO^{\cdot}$ bioavailability, and thus contribute to endothelial dysfunction. As mentioned earlier, reaction of superoxide with $NO^{\cdot}$ occurs faster than dismutation by SOD. Therefore, if superoxide and $NO^{\cdot}$ are in the high nanomolar range, they will form $ONOO^{-}$. This depletes the cell of $NO^{\cdot}$ and removes the protective effects of $NO^{\cdot}$ on the vasculature (Mugge *et al.*, 1991). The resulting $ONOO^{-}$ can in turn oxidize tetrahydrobiopterin, an essential cofactor of nitric oxide synthase (NOS) (Vasquez-Vivar *et al.*, 1998; Laursen *et al.*, 2001). NOS, a multi-domain heme enzyme, produces $NO^{\cdot}$ and citrulline by transferring electrons from its heme via tetrahydrobiopterin to its substrate L-arginine (Alderton *et al.*, 2001). Loss of tetrahydrobiopterin causes the intermediate Fe^{2+}-O-O to form superoxide instead of $NO^{\cdot}$, a process known as NOS

uncoupling (Xia *et al.*, 1998). $ONOO^-$ can also oxidize the zinc-thiolate center of endothelial NOS, which also leads to uncoupling to produce superoxide instead of $NO^{\cdot}$ (Zou *et al.*, 2002). This uncoupling of NOS leads to enhanced superoxide production at the expense of $NO^{\cdot}$ production, which depletes the endothelium of $NO^{\cdot}$, the major vasorelaxing factor in the endothelium, and leads to endothelial dysfunction. There exists, therefore, a delicate balance in the cell between different ROS species like nitric oxide and superoxide, which if disrupted can lead to pathological states such as atherosclerosis.

1.2.4 Overview of atherosclerosis

Atherosclerosis is a progressive disease of large and medium-sized arteries, including the coronary, carotid and aorta (Collins, 1993). The disease is characterized by a thickening of the normally thin intimal layer with lipid-ingested macrophages (termed foam cells) intertwined with fibrous elements. Established risk factors include hyperlipidemia, hypertension, smoking, and diabetes mellitus (Collins, 1993). Observations of disease progression from animal models indicate that following a diet high in fat and cholesterol, low-density lipoproteins (LDLs) accumulate in the intima, where they can be progressively oxidized. This is followed by adhesion of monocytes (circulating, phagocytic white blood cells) and T lymphocytes to the surface of endothelial cells, which subsequently cross the endothelial layer through intercellular endothelial tight junctions and enter the intima. Once in the intima, monocytes differentiate into macrophages, immune cells which normally act as scavengers that remove toxic substances from the cell. These macrophages engulf and sequester oxidized LDLs in an effort to protect endothelial and smooth muscle cells. However, macrophage ingestion of oxidized LDLs leads to the formation of foam cells, which subsequently mix with lymphocytes to form early atherosclerotic lesions known as the “fatty streak”, and develop into intermediate lesions with the migration and proliferation of smooth muscle cells (SMCs) from the media of the blood vessel. Alternating layers of macrophages and SMCs begin to form with the continued migration of new monocytes and subsequent propagation of macrophages. Foam cells eventually die, spilling their lipid contents (predominantly free and esterified cholesterol) and depositing cell debris in the core of the lesion. Smooth muscle cells secrete fibrous elements such as collagen and other extracellular matrix proteins that form a fibrous cap over this core and intermediate lesions progress to fibrous plaques, which increase in size and protrude into the lumen of the artery.

The lesion continues to grow with the entry of new monocytes and the formation of new foam cells at the lesion edge, which make the plaque vulnerable to rupture and thrombosis particularly if the fibrous cap is thin (Ross, 1993; Ross, 1999; Lusis, 2000; Madamanchi *et al.*, 2005). This progressive occlusion of the arteries that typifies atherosclerosis can lead to an acute occlusion of the artery, which may result in clinical events such as a myocardial infarction (heart attack) or stroke.

1.2.5 Roles of ROS in atherosclerosis: The Oxidative Stress Hypothesis of Atherosclerosis

Not only can elevated levels of ROS, such as superoxide, interfere with the cell's vasoprotective mechanisms, they additionally promote events in the progression of atherosclerosis. Previously regarded as merely a disease of lipid accumulation, it is now recognized that atherosclerosis is a result of the body's chronic inflammatory response to tissue injury in the vasculature, sparked by endothelial dysfunction (Ross, 1999; Lusis, 2000).

Oxidation of low-density lipoprotein

Oxidized low-density lipoprotein (oxLDL) is key among the factors that can injure the endothelium, as well as promote adherence of monocytes and T lymphocytes to the endothelium and their subsequent migration into the intima (Ross, 1993). Oxidized LDL induces the expression of adhesion molecules of the selectin family, such as P-selectin (Vora *et al.*, 1997), which are involved in the initial attachment of monocytes to the surface of the endothelium, and participate in monocyte rolling (Madamanchi *et al.*, 2005). This rolling action brings integrins on the surface of the monocyte in contact with adhesion molecules such as endothelial intracellular adhesion molecule (ICAM-1) and vascular cell adhesion molecule (VCAM-1) on the endothelium to produce a firmer attachment (Behrendt and Ganz, 2002; Libby *et al.*, 2002) (Figure 2). Oxidized LDL additionally induces the expression of monocyte chemoattractant protein-1 (MCP-1) (Cushing *et al.*, 1990), the chemotactic factor that is responsible for monocyte migration into the intima, and also induces endothelial cells to release macrophage colony stimulating factor (M-CSF) (Rajavashisth *et al.*, 1990), which is involved in monocyte differentiation into macrophages.

Additionally, oxidized LDL is a chemoattractant for T lymphocytes (McMurray *et al.*, 1993), and can activate them to secrete numerous cytokines which interact with macrophages and enhance the inflammatory response (Mahmoudi *et al.*, 2007). Cytokines are small proteins involved in immune responses and cell-cell communication (Dyer and Fifer, 2003). Oxidized LDL is also cytotoxic to endothelial cells (Hessler *et al.*, 1983), and can inhibit endothelial dependent vasodilation, contributing to endothelial dysfunction (Ohgushi *et al.*, 1993). Thus, oxidized LDL affects multiple processes that can lead to the formation and progression of atherosclerosis.

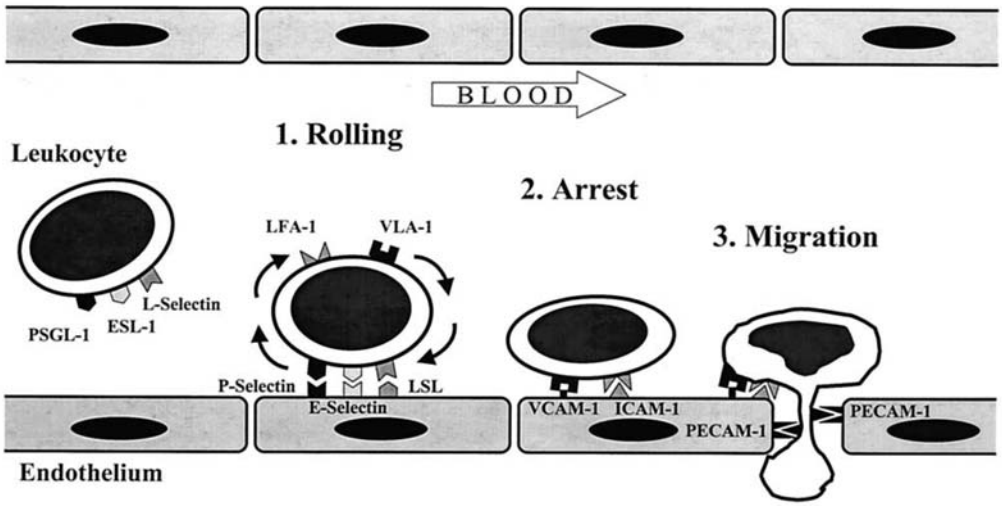

Figure 2. Role of adhesion molecules in leukocyte adhesion and transmigration across the endothelium. Members of the selectin family mediate the initial interaction of leukocytes with endothelial cells and rolling of leukocytes on the endothelial surface. Adhesion occurs if the integrins leukocyte function-associated antigen (LFA-1) and very late antigen (VLA-4) on leukocytes encounter endothelial intracellular adhesion molecule (ICAM-1) and vascular cell adhesion molecule (VCAM-1), respectively, during the rolling interval. Leukocytes transmigrate across the endothelium through the mutual interaction of platelet/endothelial cell adhesion molecule (PECAM-1) expressed at endothelial cell junctions and on leukocytes, as well as involving integrins. *ESL-1*, E-selectin ligand-1; *LSL*, L-selectin ligand; *PSGL-1*, P-selectin glycoprotein ligand-1. Figure from Behrendt *et al*, 2002.

ROS contribute to this initial injury of the endothelium through the initial oxidation of native low-density lipoprotein, a modification that causes it to be readily taken up by scavenger receptors on macrophages, and thus leads to foam cell formation (Shihabi *et al.*, 2002). Although there are numerous candidates proposed to oxidize LDL (and many agents used *in vitro* to produce oxidized LDL), *in vivo* there is evidence for the involvement of $ONOO^-$ and HOCl (both of which can be produced from superoxide) based on gas chromatography and mass spectrometry studies performed on LDL isolated from human atherosclerotic lesions (Heinecke, 1999; Mashima *et al.*, 2001). α-tocopheroxyl radical has

also been implicated based on the accumulation of α-tocopherol-derived oxidation products such as 9-*trans, cis* and 13-*cis, trans* regio-isomers of hydroperoxides of cholesteryl esters in human lesions (Mashima *et al.*, 2001). Modification of LDL by either $ONOO^-$ or HOCl, has been shown to produce forms that are recognized and readily taken up by the scavenger receptor on macrophages (Hazell and Stocker, 1993; Graham *et al.*, 1993).

ROS and endothelial activation: induction of proinflammatory molecules

Endothelial activation is an important initial step in the inflammatory response, and refers to the induction of 1) proteins involved in cell surface adhesion which mediate the attachment of monocytes from the circulating blood to the endothelium, and 2) chemotactic factors responsible for their subsequent migration into injured tissues. As mentioned above, it also plays a key role in the inflammatory response-to-injury caused by oxidized LDL in atherogenesis. ROS can contribute to endothelial activation through their ability to induce cell adhesion molecules. Prolonged exposure to ROS, such as hydrogen peroxide, have been found to induce P-selectin expression on the surface of endothelial cells (Patel *et al.*, 1991), and administration of scavenging enzymes such as SOD and catalase demonstrated significant inhibition of monocyte adhesion to endothelial cells, thus implicating the involvement of superoxide and hydrogen peroxide in monocyte attachment to endothelial cells (Godin *et al.*, 1993).

The activation of cell adhesion molecules by hydrogen peroxide was found to affect a ubiquitous eukaryotic transcription factor known as NF-κB (nuclear factor κB). This discovery helped cast ROS in a new light as important signaling molecules, and not merely destructive by-products of aerobic metabolism (Reth, 2002). Many proteins involved in cell adhesion (VCAM-1, ICAM-1, E-selectin) and migration (MCP-1) are induced by inflammatory cytokines such as TNF-α (tumor necrosis factor-α), a process regulated at the transcriptional level by NF-κB (Marui *et al.*, 1993; Chen and Medford, 1999; Baldwin, Jr., 2001). NF-κB is involved in immune and stress responses, inflammation and apoptosis (Li and Karin, 1999).

Interestingly, $NO^{\cdot}$ prevents monocyte adhesion to endothelial cells on several levels that affect NF-κB mediated transcription. $NO^{\cdot}$ donors have been shown to inhibit cytokine-induced transcription of adhesion molecules VCAM-1 and ICAM-1 (Spiecker *et al.*, 1997;

Spiecker *et al.*, 1998), as well as the monocyte chemoattractant M-CSF (Hong *et al.*, 1997). In the case of VCAM-1, it has been demonstrated in endothelial cells that $NO^{\cdot}$ donors increase the transcription and nuclear translocation of IκBα (Spiecker *et al.*, 1997), one of a family of proteins (IκBs) that inhibit NF-κB. IκBs can do this by either binding NF-κB in the cytosol and masking its nuclear localization signal (Collins and Cybulsky, 2001), which prevents its translocation to the nucleus and subsequent transcription of NF-κB target genes (Zabel and Baeuerle, 1990; Baeuerle and Baltimore, 1996), or by displacing NF-κB from its cognate DNA within the nucleus (Traenckner *et al.*, 1994). Additionally, $NO^{\cdot}$ can directly react with superoxide to prevent superoxide-mediated induction of proinflammatory molecules (Griendling *et al.*, 2000). Once again, nitric oxide and superoxide mediate opposing signaling pathways in the vasculature.

ROS and plaque stability: induction of matrix metalloproteinases

A main cause for the clinical complications of atherosclerosis arises from plaque instability and subsequent rupture, which can occlude the artery and result in a myocardial infarction or stroke (Lusis, 2000). The activity of extracellular matrix-degrading enzymes such as matrix metalloproteinases (MMPs) can promote plaque rupture, and active forms of these enzymes have been shown to co-localize in vulnerable shoulder regions of plaques from human atherosclerotic lesions (Galis *et al.*, 1994). These shoulder regions are rich in foam cells (Lusis, 2000), and it has been shown that foam cells isolated from hypercholesterolemic animal models are abundant sources of MMP activity that can be inhibited *in situ* with the ROS scavenger, *N*-acetyl-L-cysteine (Galis *et al.*, 1998). Like many proteases of the coagulation cascade, MMPs exist as proenzymes (Murphy *et al.*, 1994) in an autoinhibited form, which, upon proteolytic cleavage, releases the active enzyme. MMPs contain a catalytic zinc which is coordinated by a conserved cysteine that maintains the propeptide in its autoinhibited state (Visse and Nagase, 2003). ROS can easily disrupt this interaction by reaction with the thiol group of cysteine leading to autoactivation (Suzuki *et al.*, 1990). Interestingly, both H_2O_2 and $ONOO^-$ have been found to activate MMPs secreted by human vascular smooth muscle cells (Rajagopalan *et al.*, 1996b).

1.2.6 Ineffectiveness of global antioxidant therapy to counter ROS effects in atherosclerosis

In light of the growing body of evidence that implicate ROS in the pathophysiology of vascular disease, it was quite surprising and disappointing that administration of global antioxidants such as vitamin C, β-carotene, and vitamin E supplements failed to give conclusive beneficial results for patients with atherosclerosis (Landmesser and Harrison, 2001; Shihabi *et al.*, 2002). In some cases, antioxidant supplements exacerbated disease and increased mortality in vitamin E supplementation trials (Lonn *et al.*, 2005; Miller, III *et al.*, 2005), increased the occurrence of lung cancer in β-carotene treatment (Lee *et al.*, 1999), as well as negated the beneficial effects of statin-niacin therapy in lipid lowering studies (Cheung *et al.*, 2001). Such results, while appearing to cast doubt on the oxidative stress hypothesis of atherosclerosis, may in fact highlight an incomplete understanding of the complicated nature of the role of oxidation as well as antioxidants in the disease.

There are several important reasons why use of vitamin E would fail to prevent progression of atherosclerosis. A major factor to consider is that vitamin E does not effectively scavenge the ROS responsible for many of the events in the disease. Much of the motivation for global antioxidant therapy came from the observation that α-tocopherol, biologically and chemically the most active form of vitamin E (Burton and Ingold, 1986), is the most abundant lipid-soluble antioxidant in LDL (Thomas and Stocker, 2000). Additionally, *in vitro* oxidation experiments on LDL using non-physiologically high concentrations of transition metals as oxidants (predominantly Cu^{+1}) (Esterbauer *et al.*, 1989) or aqueous peroxyl radicals (Bowry and Stocker, 1993; Neuzil *et al.*, 1997) demonstrated an initial lag phase in the rate of lipid peroxidation when α-tocopherol was present (Esterbauer *et al.*, 1989). Free transition metals, however, rarely occur *in vivo*, and as noted previously, analysis of LDL isolated from human atherosclerotic lesions identified HOCl and $ONOO^-$ as potential ROS sources of oxidation. It is interesting to note that α-tocopherol does not protect against apolipoprotein B-100 oxidation by myeloperoxidase *in vitro*, and HOCl-induced lipid peroxidation occurs at a slower rate when α–tocopherol is depleted (Hazell and Stocker, 1997; Hazell *et al.*, 1999). Apolipoprotein B-100 is the protein found in human LDL. As noted above, increased production of superoxide is associated with many vascular disease states. Vitamin E reacts with superoxide with a rate of 5×10^3 $M^{-1}s^{-1}$ (Gotoh and

Niki, 1992), 6 orders of magnitude slower than superoxide reaction with nitric oxide. Together, these findings indicate that vitamin E is unable to effectively protect against the physiologically relevant oxidants in atherosclerosis.

Contrary to its proposed antioxidant nature, α–tocopherol can also help initiate and promote free radical chain reactions in lipid peroxidation, especially under mild oxidizing conditions (Bowry and Stocker, 1993; Neuzil *et al.*, 1997). Interestingly, this process can be accelerated by enriching LDL with α–tocopherol, and is significantly suppressed in LDL lacking α–tocopherol (Thomas *et al.*, 1996; Neuzil *et al.*, 1997). LDL isolated from a patient with familial isolated vitamin E deficiency showed a high degree of resistance to oxidation, which could be reversed by dietary supplementation of vitamin E (Thomas *et al.*, 1996). In this study, supplementation with only vitamin E led to LDL that was more prone to oxidation, whereas co-administration of coenzyme Q (another antioxidant found to a much lesser extent in human LDL) and vitamin E yielded LDL that was more resistant to oxidation. These results lend more support for co-supplementation of vitamin E with other antioxidants such as vitamin C or coenzyme Q, as perhaps a more beneficial therapy than vitamin E alone. The pro-oxidant nature of α–tocopherol can be understood if one considers that by reacting with a radical, α–tocopherol itself becomes a radical, which is thermodynamically stable (Bisby and Parker, 1991), and can perpetuate the chain reaction instead of terminating it. Vitamin C on the other hand can be enzymatically converted back to ascorbic acid after reacting with a radical, which might explain the protective nature of this combination (Salonen *et al.*, 2000).

1.2.7 Success of angiotensin converting enzyme inhibitors and statins: effects on NADPH Oxidase

In contrast to non-specific antioxidant treatment, two existing therapies that have shown significant clinical improvement in individuals with increased risk for cardiovascular disease have recently been shown to additionally inhibit NADPH Oxidase activity. These treatments reduce hypertension and hypercholesterolemia, respectively- two conditions that play a role in atherosclerosis and are strong risk factors for further cardiovascular complications. The first class of compounds, angiotensin converting enzyme inhibitors, inhibit the production of angiotensin II and block its effects on blood pressure. The second

family of compounds, statins, act to lower circulating levels of LDL by inhibiting cholesterol synthesis.

The renin-angiotensin system

The renin-angiotensin system is involved in regulation of fluid and electrolyte balance, as well as blood pressure, through the actions of angiotensin II on vascular smooth muscle, adrenal cortex, kidney, and brain (Reid, 1998). Angiotensin II is a peptide agonist, a substance that acts like a hormone, binding to its receptor, and mediating various signaling mechanisms to produce a desired action. It is produced after cleavage of angiotensin I by angiotensin converting enzyme (ACE), a dipeptidyl carboxypeptidase.

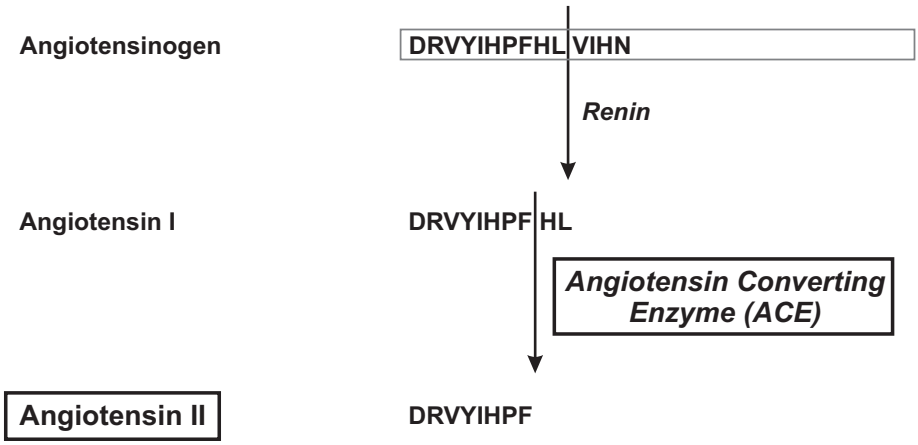

Figure 3. Proteolytic processing of angiotensinogen to form angiotensin II. Amino acids are represented by one-letter codes. Figure made after Reid, 1998.

Angiotensin II plays a role in blood pressure regulation and is a potent vasoconstrictor (Reid, 1998), whose levels are often elevated in individuals with hypertension (Ross, 1999). It affects not only the vasculature, but additionally acts on the hypothalamus in the brain to stimulate thirst, and the adrenal cortex to increase secretion of aldosterone, a hormone that increases sodium reabsorption and water retention (Dyer and Fifer, 2003; Xiao *et al.*, 2003). Angiotensin II can additionally exert effects by inducing proinflammatory cytokines (Libby *et al.*, 2002). ACE inhibitors prevent the formation of angiotensin II, thus reducing high blood pressure. They additionally improve endothelial dysfunction in patients with coronary artery disease, which may involve increased local $NO^{\cdot}$ production and bioactivity through a bradykinin-mediated increase in expression and activity of endothelial NOS (Mahmoudi *et*

al., 2007). Bradykinin is another peptide agonist that is also a major substrate of ACE (Yang *et al.*, 1970), but acts as a vasodilator in contrast to angiotensin II. In addition, unlike angiotensin II, bradykinin is inactivated by ACE through the cleavage of the last two C-terminal residues (Xiao *et al.*, 2003) and is subsequently degraded by the same enzyme (Dendorfer *et al.*, 2001).

Statins

Statins are a class of compounds that competitively inhibit the rate-limiting step in cholesterol biosynthesis (Figure 4). Cholesterol is synthesized by nearly all cells in the human body, but a majority of it is produced by the liver (Ucar *et al.*, 2000). Statins bind with nanomolar affinity to the liver enzyme 3-hydroxy-3-methylglutaryl coenzyme A (HMG-CoA) reductase, which catalyzes the generation of L-mevalonate from HMG-CoA (Greenwood *et al.*, 2006). In addition to direct reduction of endogenous cholesterol production, this decrease in intracellular levels of cholesterol increases transcription and expression of the LDL receptor at the surface of liver cells, which increases LDL uptake from the bloodstream (Brown and Goldstein, 1986). Independent from its lipid lowering abilities, statins have a broad range of effects that counter many steps in the progression of atherosclerosis, which has lead to much enthusiasm for its widespread use. They have been found to upregulate endothelial NOS expression, increase fibrinolytic activity, inhibit smooth muscle cell proliferation and instead stimulate apoptosis, and inhibit expression of the monocyte chemoattractant MCP-1 (Palinski, 2001), in addition to having many anti-inflammatory effects (Sparrow *et al.*, 2001; Greenwood *et al.*, 2006). Many of these effects can be attributed to the inhibition of isoprenoid intermediates in the cholesterol synthesis pathway, which are involved in prenylation, a post-translational lipid modification of proteins. Protein prenylation involves the transfer of lipid moieties such as farnesyl or geranylgeranyl groups to the C-terminus of a protein, and is required for the membrane localization of small GTPases which have critical regulatory roles affecting a wide variety of cell signaling cascades (Takemoto and Liao, 2001; Greenwood *et al.*, 2006).

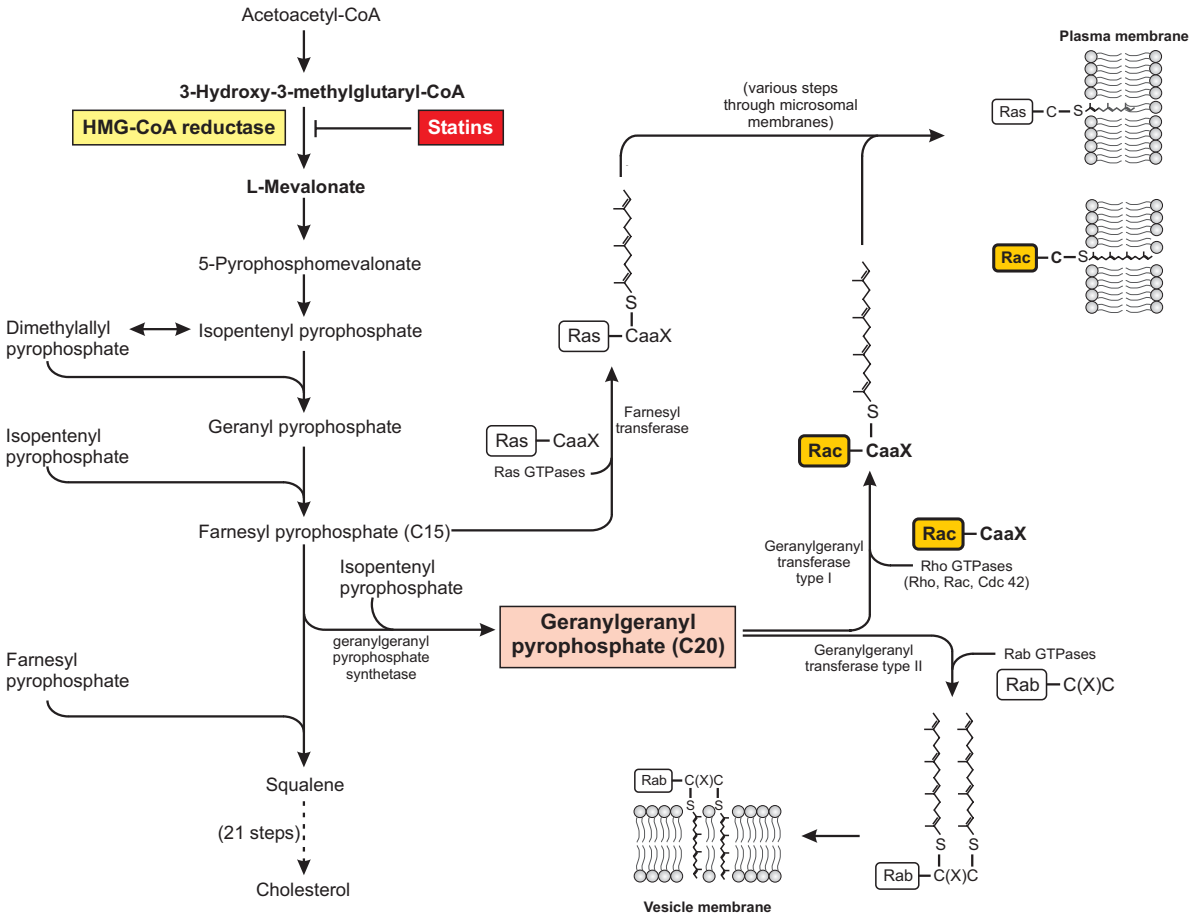

Figure 4. Synthesis of cholesterol and protein prenylation. Statin inhibition of HMG-CoA reductase not only inhibits cholesterol synthesis but also the biosynthesis of isoprenoids such as farnesyl pyrophosphate and geranylgeranyl pyrophosphate, which are crucial to the post-translational modification of the small GTPases, Ras, Rac, Rho and Rab. Each has a specific C-terminal consensus sequence for the site of prenylation (C, cysteine; a, an aliphatic amino acid; X, any amino acid), and are targeted to specific membranes after prenylation. Cdc 42, cell-division cycle 42. Figure after Greenwood *et al*, 2006.

Disadvantages of each therapy

Due to their ability to affect multiple cellular processes, therapeutic use of ACE inhibitors or statins are associated with a few risks. As a consequence of ACE inhibition, inactivation and degradation of the pharmacological peptide bradykinin is prevented, resulting in maintained bradykinin levels. This is responsible for the side effect of dry cough, which makes ACE inhibitors less well tolerated by some patients (Sleight, 2002). As for statins, many of its pleiotropic effects are not fully understood, and recent reports have spotlighted some unfavorable actions of statins (Ucar *et al.*, 2000; SoRelle, 2001; Staffa *et al.*, 2002; Omar and Wilson, 2002), including skeletal muscle damage that can lead to the severe muscle

disorder rhabdomyolysis, where apoptosis of muscle cells can result in kidney failure and death. This is particularly true if statins are taken together with either another lipid-lowering drug derived from fibric acid or with inhibitors of cytochrome P450 3A4 (the enzyme which normally metabolizes them), taken in high doses (Graham *et al.*, 2004), or taken over a long period of time (Ucar *et al.*, 2000). Concerns are also growing that the concept of administering statins to individuals with no overt occlusive vascular disease as a preventive measure may also result in detrimental side effects rather than preventing disease (Abramson and Wright, 2007). Considering the broad scope of statin actions, it is clear that thorough and extensive investigations of its mechanisms of action outside of lipid lowering and interaction with other drugs are imperative to determine the optimal way to administer this widely prescribed drug.

Mutual link with NADPH Oxidase point to a new therapeutic target

It was, therefore, of great interest when it was discovered that both ACE inhibitors and statins could act to inhibit the actions of NADPH Oxidase. Initial studies in cultured vascular smooth muscle cells exhibited potent angiotensin II stimulation of NADPH Oxidase activity (Griendling *et al.*, 1994), and this effect was confirmed in animal studies (Rajagopalan *et al.*, 1996a; Pagano *et al.*, 1997) and demonstrated in human blood vessels (Berry *et al.*, 2000). As mentioned above, statins show many cholesterol-independent effects, which are mainly mediated through its concomitant inhibition of protein prenylation, affecting the small GTPases Ras, Rho, Rac, Rab, Ral and Rap. Rac is required for activation of NADPH Oxidase, and must be prenylated with a geranylgeranyl lipid moiety for proper membrane targeting. This modification is disrupted by the actions of statins, which have been found to reduce angiotensin II-induced superoxide production in vascular smooth muscle cells (Wassmann *et al.*, 2002), as well as in cardiac myocytes (Takemoto *et al.*, 2001) via mechanisms that specifically involve Rac. In the study using cardiac myocytes, the role of prenylation in angiotensin II-induced superoxide production was thoroughly demonstrated. Total intracellular oxidation was increased 2.7-fold upon addition of angiotensin II, which was completely inhibited when statin was co-administered. This inhibition could be reversed with the addition of L-mevalonate and geranylgeranylpyrophosphate, but not farnesylpyrophosphate, indicating the involvement of Rho GTPases (of which Rac is a member) and not Ras GTPases. Additionally, use of

dominant-negative and constitutively active forms of three different Rho GTPases: RhoA, Rac1, and Cdc42 clearly showed Rac1 as the GTPase responsible for angiotensin II-induced increase in and statin inhibition of superoxide production.

1.3 NADPH OXIDASE: A MAJOR SOURCE OF ROS IN VASCULAR DISEASE

Over the last several years, a great deal of interest has grown in NADPH Oxidases, beginning with the discovery that these enzymes are expressed in virtually all tissues, and intensifying with the discovery that their activity can be regulated by a number of factors that are commonly associated with pathological settings (Harrison *et al.*, 2003; Ray and Shah, 2005), particularly in cardiovascular diseases. Such factors include agonists like angiotensin II, thrombin, platelet-derived growth factor (PDGF), and TNF-α (Madamanchi *et al.*, 2005). Many studies using animal models of different vascular diseases have found elevated superoxide production, including hypercholesterolemia (Ohara *et al.*, 1993; Warnholtz *et al.*, 1999), hypertension (Rajagopalan *et al.*, 1996a; Fukui *et al.*, 1997; Bauersachs *et al.*, 1998), heart failure (Bauersachs *et al.*, 1999), and diabetes (Kojda and Harrison, 1999). Superoxide production was shown to derive from NADPH Oxidase through the use of substrates (West *et al.*, 2001) and/or inhibitors for various potential enzymatic sources of superoxide, including mitochondrial enzymes, xanthine oxidase, and uncoupled NOS (Warnholtz *et al.*, 1999; Shi *et al.*, 2001; West *et al.*, 2001; Paravicini *et al.*, 2002; Hathaway *et al.*, 2002). Each study indicated NADPH Oxidase as the source, with the exception of hyperlipidemic rabbits, where oxypurinol (an inhibitor of xanthine oxidase) additionally caused a partial reduction of superoxide production (Warnholtz *et al.*, 1999). Studies of human blood vessels revealed that NADPH Oxidases are major sources of superoxide, with increased superoxide production correlating with impaired $NO^{\cdot}$-dependent vasodilation and increased atherosclerotic risk factors (Guzik *et al.*, 2000). Investigations of human lesions have confirmed the role of NADPH Oxidase in vascular disease, with the finding that $p22^{phox}$ protein (a component of the NADPH Oxidase complex) and oxidase activity are present in atherosclerotic coronary arteries (Azumi *et al.*, 1999). Subsequent studies demonstrated co-localization of oxidized LDL, oxidase protein and ROS generation in human atherosclerotic arteries (Azumi *et al.*, 2002). Elevated NADPH Oxidase activity

was also found in human heart failure, compared to non-failing hearts (Heymes *et al.*, 2003).

1.3.1 Nox proteins and tissue distribution

The term Nox (***N***ADPH ***Ox***idase) refers to a family of enzymes that are homologous to the catalytic subunit, gp91^{phox}, of the NADPH Oxidase complex, which deliberately produces superoxide from molecular oxygen and NADPH. This enzyme complex was originally thought to be restricted to phagocytic cells of the immune system until several homologues of gp91^{phox} (also known as Nox2) were found in nonphagocytic cells by several groups independently (Kikuchi *et al.*, 2000; Geiszt *et al.*, 2000; Yang *et al.*, 2001; Shiose *et al.*, 2001; Cheng *et al.*, 2001; Banfi *et al.*, 2001). To date, five human Nox proteins and two Duox proteins have been discovered, each with specific tissue distribution. All are membrane spanning proteins with a C-terminal cytosolic domain which shares distant homology to the ferredoxin-NADP^{+}-reductase (FNR) family (Segal *et al.*, 1992; Rotrosen *et al.*, 1992; Sumimoto *et al.*, 1992). Duox proteins contain an additional N-terminal calcium binding domain and an extracellular peroxidase domain, and thus are called Duox for ***du***al ***ox***idase (Cheng *et al.*, 2001). In contrast to Nox enzymes, Duox enzymes produce hydrogen peroxide instead of superoxide (De Deken *et al.*, 2002). They are found in the thyroid and are involved in thyroid hormone synthesis (Dupuy *et al.*, 1999; De Deken *et al.*, 2000).

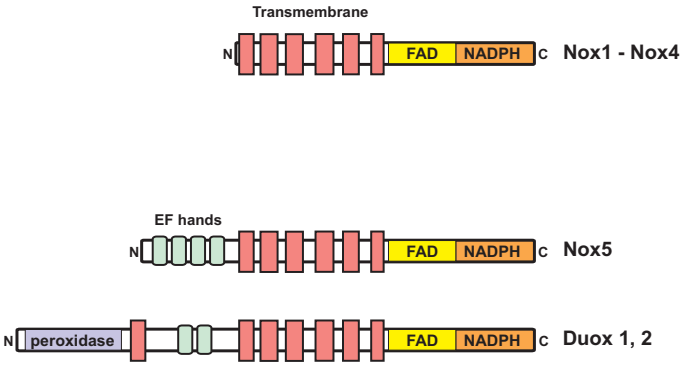

Protein	Expression
Nox1	colon, prostate, uterus, VSMC
gp91phox (Nox2)	phagocytes, endothelium, cardiomyocytes, lung
Nox3	fetal tissues, adult inner ear
Nox4	kidney, pancreas, placenta, heart, endothelium, VSMC, ovary, testis, skeletal muscle, bone
Nox5	lymphoid tissue, testis, spleen, ovary, placenta, pancreas, fetal tissues
Duox1	thyroid, lung
Duox2	thyroid, colon

Figure 5. Domain structure and tissue expression of Nox family members. Figure after Takeya *et al*, 2003.

The first known Nox protein, gp91^{phox} (Nox2), is found in phagocytic cells and is involved in host defense. It has subsequently been found to also be expressed in the endothelium (Jones *et al.*, 1996; Bayraktutan *et al.*, 1998; Gorlach *et al.*, 2000; Bayraktutan *et al.*, 2000), cardiac myocytes (Xiao *et al.*, 2002), and lung (Cheng *et al.*, 2001). Nox1 (58% sequence identity with gp91^{phox}) was the first homologue of gp91^{phox} discovered, with predominant expression in colon epithelial cells (Suh *et al.*, 1999; Kikuchi *et al.*, 2000), and additional expression in prostate, uterus, and cultured vascular smooth muscle cells (VSMC) (Suh *et al.*, 1999). Nox3 (56% sequence identity with gp91^{phox}) is found in fetal tissues and the adult inner ear (Banfi *et al.*, 2004), and is required for the formation of specialized structures called otoconia, which are involved in the perception of balance and gravity (Paffenholz *et al.*, 2004). Nox4 (39% sequence identity with gp91^{phox}), also known as the kidney oxidase due to its high expression in epithelial cells of the renal tube (Geiszt *et al.*, 2000; Shiose *et al.*, 2001), is also found in vascular endothelial cells (Wingler *et al.*, 2001; Ago *et al.*, 2004; Kuroda *et al.*, 2005), and has the broadest tissue distribution among homologues (Cheng *et al.*, 2001) (Figure 5). Its precise function is still not known, but has been implicated in cell differentiation (Cucoranu *et al.*, 2005), apoptosis (Mochizuki *et al.*, 2006), growth (Menshikov *et al.*, 2006; Sturrock *et al.*, 2006) and endothelial cell proliferation (Petry *et al.*, 2006). Nox5 is the most divergent of the five Nox proteins (26% sequence identity with gp91^{phox}), bearing more similarity to the Duox proteins. It contains an additional calmodulin-like EF domain with four Ca^{2+} binding sites N-terminal to the regions homologous to gp91^{phox} (Cave *et al.*, 2006). Nox5 is present in lymphoid tissue, testis and spleen (Banfi *et al.*, 2001), and its function is also unknown.

In contrast to the high catalytic output and stimulus-dependent phagocytic NADPH oxidase, nonphagocytic Nox proteins constitutively produce low levels of superoxide without the need for stimulation, although various factors can increase oxidase activity (Cave *et al.*, 2006). Additionally, nonphagocytic Nox proteins produce intracellular superoxide, as is the case with Nox1 and Nox4, which localize in the caveolae and cytoskeleton of VSMCs, respectively (Hilenski *et al.*, 2004). Nonphagocytic pools of gp91^{phox} can produce superoxide intracellularly or extracellularly, depending on its location. It has been found preassembled in oxidase complexes in the perinuclear region of endothelial cells for intracellular ROS production (Li and Shah, 2002), as well as at or near the plasma membrane in endothelial and adventitial cells, which are capable of extracellular superoxide

production (Meier *et al.*, 1993; Meyer *et al.*, 1999; Wang H.D. *et al.*, 1999; Barbacanne *et al.*, 2000).

1.3.2 The phagocytic NADPH Oxidase: the classical NADPH Oxidase

The first discovered and most well studied NADPH Oxidase is that of a class of immune system cells (phagocytes), which initiate the cell's defense against foreign pathogens. In response to invading bacteria and microbes, certain phagocytic cells called neutrophils mobilize to sites of inflammation and engulf pathogens and/or parts of damaged tissues (DeLeo and Quinn, 1996). They dramatically increase their oxygen uptake, known as "the respiratory burst," and elicit a tremendous burst in superoxide production to destroy the phagocytosed material as a primary action of innate immunity. The enzyme responsible for this is a carefully regulated, multi-component enzyme complex known as the phagocytic NADPH Oxidase. When active, it comprises six different proteins, two that are membrane-bound, three cytosolic proteins, which translocate to the membrane upon stimulation, and the small GTPase Rac. The membrane heterodimer is composed of a Nox protein, gp91^{phox} (or Nox2), and p22^{phox}, another phagocytic oxidase protein component. For historical reasons they are collectively known as cytochrome b_{558}, for b-type cytochrome with a maximal absorbance near 558 nm (Cross and Segal, 2004). All of the catalytic machinery resides in gp91^{phox}, which contains putative sites for NADPH and FAD binding in its cytosolic C-terminal half, as well as four conserved histidines, which coordinate two hemes in the N-terminal transmembrane domain. p22^{phox} serves to stabilize gp91^{phox} and is essential for oxidase activity (Parkos *et al.*, 1989; Maly *et al.*, 1993; Cross and Segal, 2004). To generate superoxide, gp91^{phox} and p22^{phox} require interaction with four cytosolic proteins: three oxidase proteins called p47^{phox}, p40^{phox} and p67^{phox}, and the small GTPase Rac (Figure 6). The essential nature of this enzyme complex is highlighted by the occurrence of chronic granulomatous disease (CGD) caused by mutations in the genes for gp91^{phox}, p22^{phox}, p47^{phox}, or p67^{phox}. CGD is an inherited disorder characterized by severe and recurrent, often fatal, infections (Cross and Segal, 2004; Segal, 2005). Individuals develop granulomas where the pathogens have been phagocytosed, but are not destroyed due to an inactive NADPH Oxidase (Quinn and Gauss, 2004).

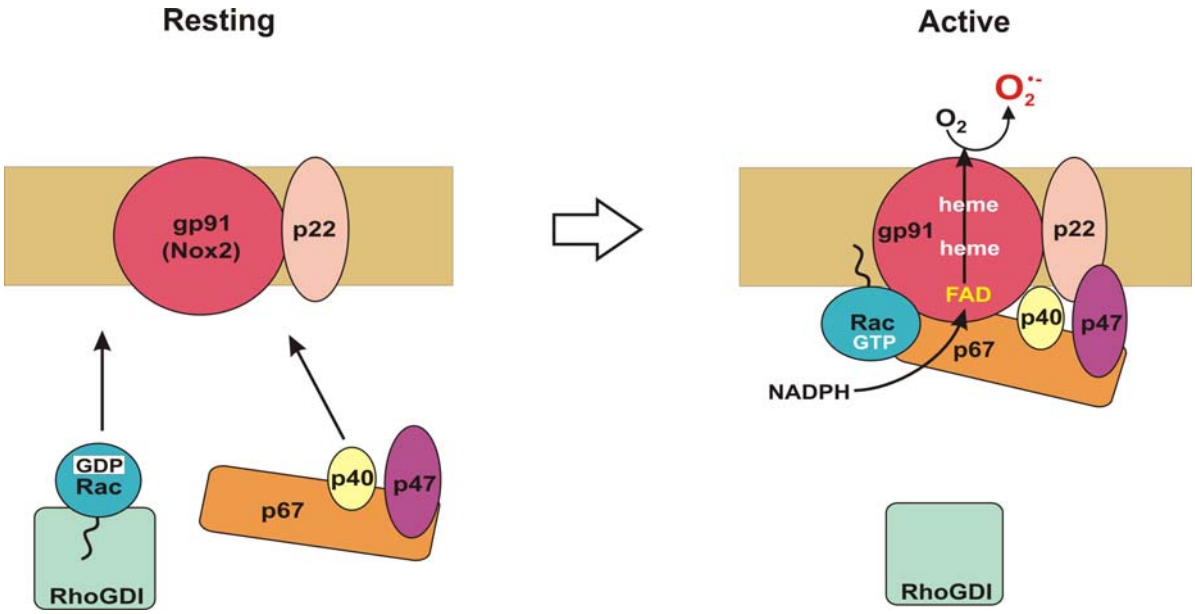

Figure 6. Overview of the activation of phagocytic NADPH Oxidase. In resting neutrophils, oxidase components are segregated between membrane-bound subunits and cytosolic regulatory proteins. Upon stimulation, these regulatory proteins translocate to the membrane to produce the active NADPH Oxidase, which transfers an electron from cytosolic NADPH to FAD, onto two hemes in the gp91phox subunit and finally to molecular oxygen, producing superoxide.

Molecular details of phagocytic NADPH Oxidase components

As mentioned above, many details regarding the phagocytic NADPH Oxidase have been established. These serve as a basis to discuss the recently discovered homologues, with emphasis on Nox1 for the present work. The proteins that comprise the phagocytic NADPH Oxidase complex have historically been named according to their apparent molecular weight on SDS-PAGE, with the extension "*phox*" designating their participation in the phagocytic oxidase.

gp91^{phox}

So termed for the heavy glycosylation that causes the protein to run at an apparent molecular weight of ***91*** kDa on SDS-PAGE, this 65 kDa membrane-associated ***g***lyco***p***rotein is the catalytic center of the ***ph***agocytic ***ox***idase. Since its initial discovery in 1961 (Hattori, 1961) and rediscovery in 1978 (Segal *et al.*, 1978; Segal and Jones, 1978), there has not been any three-dimensional structure of gp91^{phox} available. Its cytosolic C-terminal domain shows weak sequence homology to the family of ferredoxin-NADP$^+$ reductase (FNR) proteins, that allow the recognition of proposed binding sites for FAD and NADPH (Segal *et al.*, 1992; Rotrosen *et al.*, 1992). A model of the topology for the N-terminal domain

proposes six transmembrane helices, placing the N-terminus on the cytosolic side of the membrane. Four conserved histidines, residues 101, 115, 209 and 222 (Biberstine-Kinkade *et al.*, 2001), coordinate two hemes with differential reduction potentials [E_{m7} = -265 mV and E_{m7} = -225 mV; (Cross *et al.*, 1995)], which allow electron transfer from the cytosol, across the membrane, to the phagosome interior to destroy engulfed pathogens (Figure 7). Studies on the biosynthesis of cytochrome b_{558} have revealed the necessity of heme incorporation into gp91^{phox} for heterodimer formation to occur (DeLeo *et al.*, 2000). This is followed by asparagine (N)-linked glycosylation of gp91^{phox} (Harper *et al.*, 1985; Yu *et al.*, 1997) which is not required for catalytic activity (Kleinberg *et al.*, 1989; Paclet *et al.*, 2000), but instead may protect the protein from the degradative environment present in the phagocytic vacuole (Wallach and Segal, 1997).

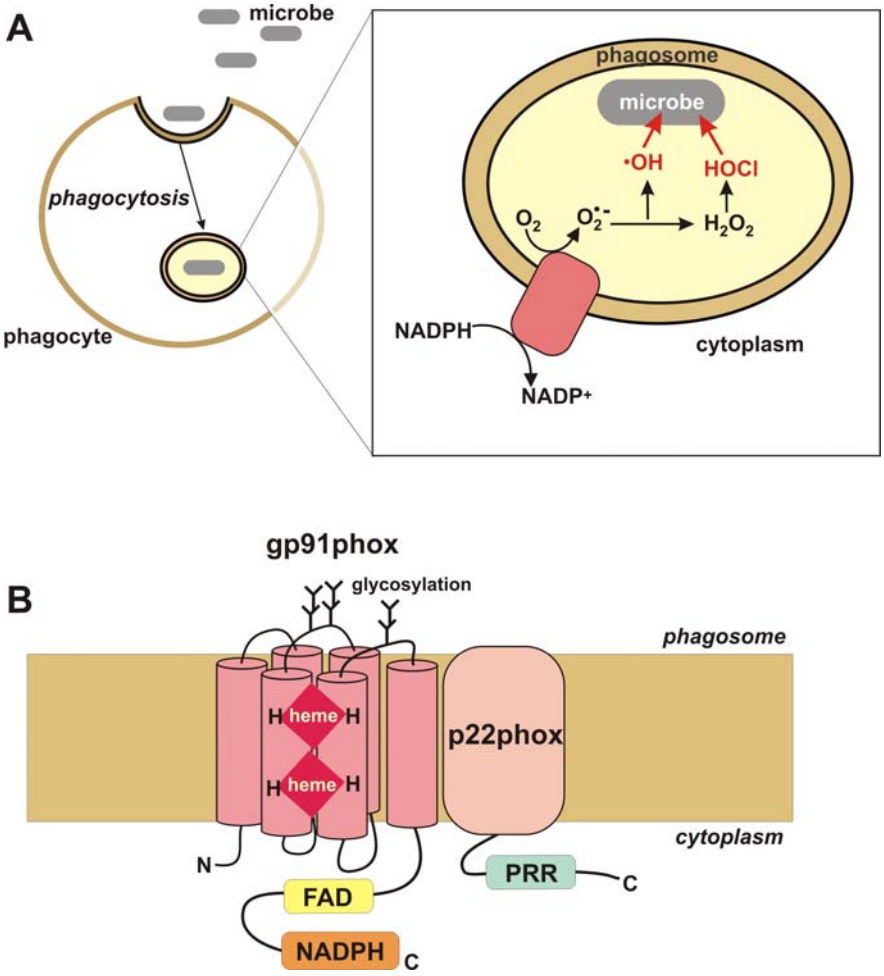

Figure 7. *A*, Destruction of foreign pathogens by phagocytic cells of the immune system. Phagocytes engulf microbes, forming phagosomes, which contain a membrane-bound NADPH oxidase that when activated produces superoxide from NADPH and molecular oxygen. This superoxide serves as a precursor to secondary ROS such as HOCl and ·OH, which kill the microbes. *B*, Model of the structure of the complex between gp91^{phox} and p22^{phox}. Figures made after Sumimoto, 2005.

p22 phox

The second member of the membrane-bound heterodimer is $p22^{phox}$, a protein of approximately 21 kDa. Similar to $gp91^{phox}$, little is known about its three-dimensional structure. It also has a hydrophobic N-terminal region (residues 1-132) and a hydrophilic C-terminus (residues 132-195). Hydropathy analysis predicts three or four hydrophobic regions (Parkos *et al.*, 1988). The cytoplasmic C-terminus contains a proline-rich region (PRR) which interacts with the cytosolic protein $p47^{phox}$ (Sumimoto *et al.*, 1994; Leto *et al.*, 1994). Although not required for the glycolysation of $gp91^{phox}$, $p22^{phox}$ is required for the processing of the high mannose-content carbohydrate chains to N-acetylglucosamine and galactose to form the mature $gp91^{phox}$ (Maly *et al.*, 1993; Porter *et al.*, 1994). Each member of the heterodimer is mutually stabilized by the presence of the other as evidenced by the absence of both subunits in CGD patients with mutations in either gene (Parkos *et al.*, 1988; Parkos *et al.*, 1989; Verhoeven *et al.*, 1989). $p22^{phox}$ mRNA shows broad and abundant tissue distribution (Parkos *et al.*, 1988; Cheng *et al.*, 2001), but protein expression is dependent on the presence of Nox proteins (Ambasta *et al.*, 2004).

p47 phox

$p47^{phox}$ is a cytosolic, multi-domain adapter protein that serves as an "organizer" in the assembly of the NADPH Oxidase complex (Takeya and Sumimoto, 2006). A highly basic protein of 390 amino acids, (pI = 9.6), $p47^{phox}$ contains many motifs involved in protein-protein interactions: an N-terminal PX (for ***P***ho***x*** homology) domain that binds phosphoinositides and is involved in membrane association; two consecutive SH3 (Src Homology 3) domains, which bind proline-rich sequences (Ren *et al.*, 1993), like that which is found in the C-terminal tail of $p22^{phox}$; an autoinhibitory region (AIR) that maintains $p47^{phox}$ in an autoinhibited state when the oxidase is not active; and a C-terminal proline-rich region (PRR) which is involved in interaction with $p67^{phox}$ (Cross and Segal, 2004).

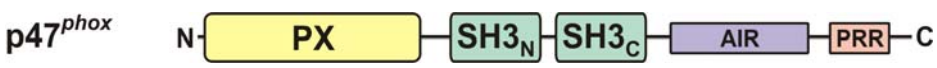

Figure 8. Domain structure of $p47^{phox}$.

The PX domain was originally discovered in two phagocytic oxidase proteins, $p47^{phox}$ and $p40^{phox}$, and was subsequently found in other proteins involved in signal transduction and membrane association (Ponting, 1996). Membrane association is mediated through its ability to bind phosphoinositides. The PX domain of $p47^{phox}$ preferentially binds phosphatidylinositol-3,4-bisphosphate ($PI(3,4)P_2$) (Kanai *et al.*, 2001), and a recent x-ray crystal structure revealed two potential binding sites for phosphoinositides occupied by two bound sulfates (Karathanassis *et al.*, 2002). The PX domain of $p47^{phox}$ also contains a proline-rich motif, which was found to interact with the C-terminal SH3 domain with an affinity of 50 μM based on NMR chemical shift perturbations (Hiroaki *et al.*, 2001). This interaction may represent an intramolecular regulatory mechanism for membrane targeting, by preventing $p47^{phox}$ binding to phosphoinositides prior to oxidase activation (Figure 9).

Following the PX domain are two SH3 domains which bind a polybasic region within the autoinhibitory domain (Ago *et al.*, 1999; Huang and Kleinberg, 1999), maintaining autoinhibition. The tandem SH3 domains have also been crystallized along with the autoinhibitory region (Groemping *et al.*, 2003). The structure revealed a "super SH3" domain comprised of both SH3 domains creating a groove with the autoinhibitory region bound in between. This autoinhibitory region contains a number of basic residues as well as several serines which undergo phosphorylation (El Benna *et al.*, 1994) in response to stimuli that activate the resting NADPH Oxidase. This multiple phosphorylation disrupts the interactions with the SH3 domains, releasing $p47^{phox}$ from its autoinhibited form (Figure 9). It additionally allows two regions of the protein to bind to membrane targets: binding of the PX domain to phosphoinositides (Karathanassis *et al.*, 2002; Ago *et al.*, 2003) and binding of the tandem SH3 domains to the proline-rich region of $p22^{phox}$ (Ago *et al.*, 1999; Shiose and Sumimoto, 2000; Nobuhisa *et al.*, 2006). The very C-terminus of $p47^{phox}$ contains a proline-rich region that binds the C-terminal SH3 domain of $p67^{phox}$ independently of phosphorylation (Leto *et al.*, 1994; Finan *et al.*, 1994; Leusen *et al.*, 1995) (Figure 10), and this interaction recruits $p67^{phox}$ to the membrane (Heyworth *et al.*, 1991; Dusi *et al.*, 1996).

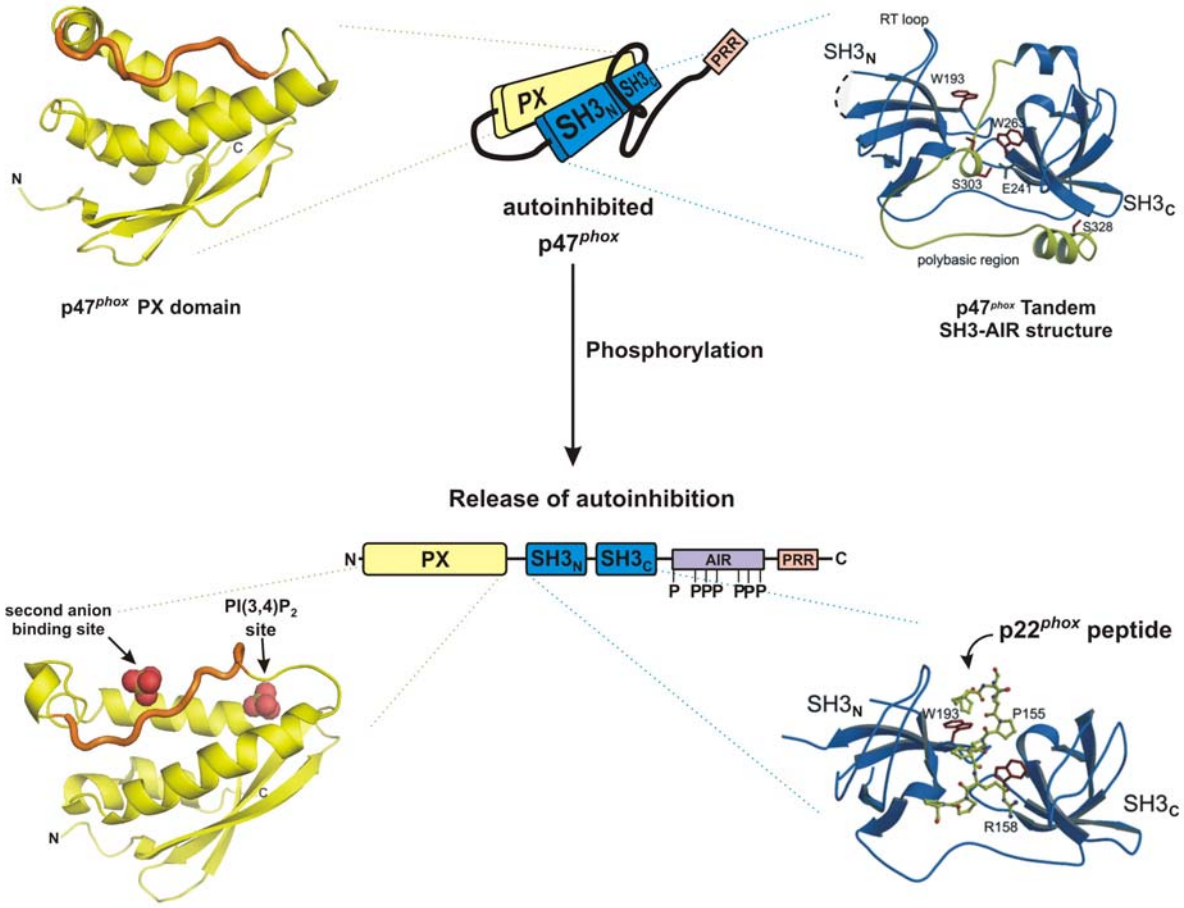

Figure 9. Intramolecular autoinhibition of p47^{phox}. Prior to oxidase activation, p47^{phox} exists in an autoinhibited form, with the proline-rich region of its PX domain interacting with the C-terminal SH3 domain, and the AIR binding between the SH3 domains (*center schematic*). The corresponding NMR solution structure (PDB Code 1GD5, Hiroaki, *et al* 2001) of the p47^{phox} PX domain is shown as a ribbon representation with the proline-rich region highlighted in orange, as well as the crystal structure of the tandem SH3 domains (blue ribbon) of p47^{phox} bound by the AIR (yellow). In response to stimuli, p47^{phox} is heavily phosphorylated at 11 sites within the AIR which disrupts the intramolecular interactions and allows p47^{phox} to bind membrane targets. Shown are the corresponding crystal structures of the p47^{phox} PX domain (yellow ribbon) with the phosphoinositide binding sites indicated by two bound sulfate ions (red) (PDB Code 1O7K, Karathanassis *et al*, 2002), and the crystal structure of the tandem SH3 domains with a bound peptide of the p22^{phox} C-terminus indicated by yellow stick representation, (which coincides with the site that binds the AIR). Both figures of the crystal structures of the tandem SH3 domains from Groemping and Rittinger, 2005 ((Groemping and Rittinger, 2005).

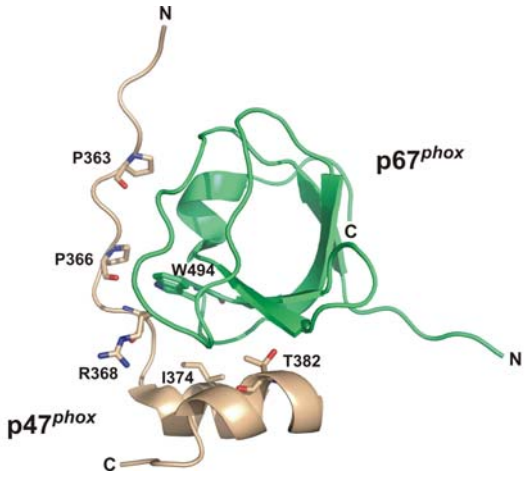

Figure 10. Interaction of the C-terminal proline-rich region of p47^{phox} (beige ribbon) with the C-terminal SH3 domain of p67^{phox} (green ribbon) as solved by NMR (Kami *et al.*, 2002), with residues essential for the interaction shown as stick representations.

p67 phox

The second obligatory cytosolic oxidase component is p67^{phox} (526 amino acids, pI= 6.21) (Cross and Segal, 2004). In contrast to p47^{phox}, it plays a critical role in activation of NADPH oxidase activity, and is believed to participate in the electron transfer steps from NADPH to FAD (Cross and Curnutte, 1995). Like p47^{phox}, it is also a protein composed of several motifs involved in protein-protein interactions. Its N-terminus contains 4 tetratricopeptide repeats (TPR) which mediate Rac binding, followed by an activation domain (residues 199-210) that is needed for activation of oxidase activity. p67^{phox} additionally contains two SH3 domains with a PB1 domain sandwiched in between.

Figure 11. Domain structure of p67^{phox}.

The TPR motif is a repeating 34 amino acid motif (Sikorski *et al.*, 1990) that characteristically forms an extended domain composed of pairs of antiparallel α-helices that adopt a right-handed superhelical twist creating an amphipathic groove (Melville *et al.*, 2000). The N-terminal region of p67^{phox} comprising the TPR motifs have been shown to bind Rac (Diekmann *et al.*, 1994; Ahmed *et al.*, 1998; Koga *et al.*, 1999), and as revealed in the crystal structure of the complex between the N-terminal region of p67^{phox} (1-203) and Rac1, the binding interface is actually mediated by a β-hairpin insertion between TPR3 and

TPR4, and not the TPR groove (Lapouge *et al.*, 2000). Instead, residues 168 to 186 fold back into the hydrophobic groove.

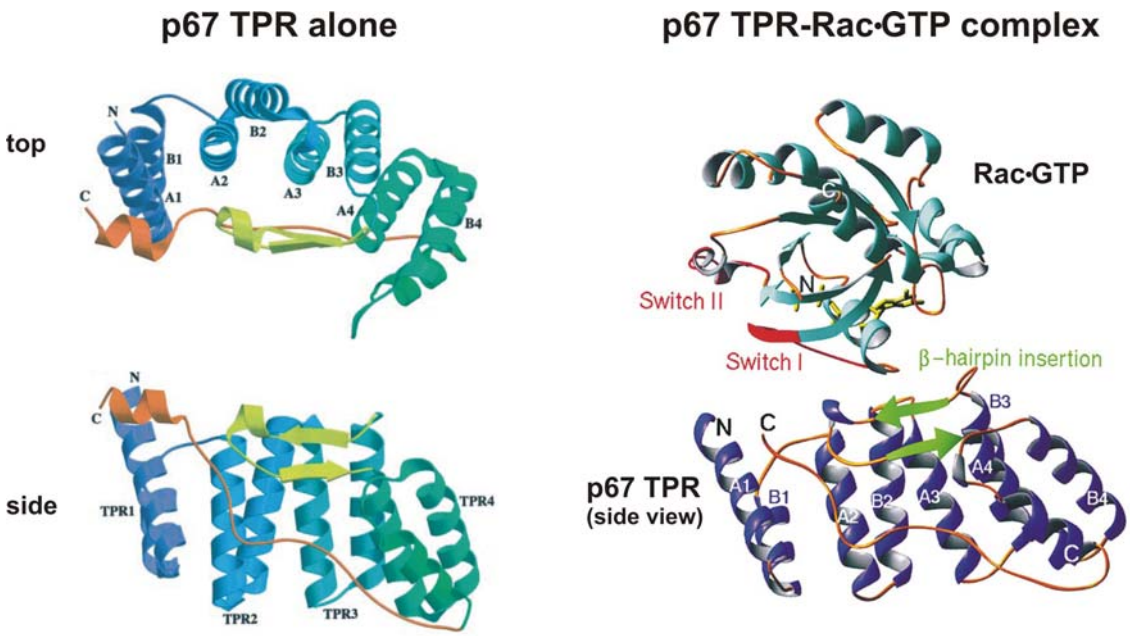

Figure 12. Crystal structures of the p67^{phox} TPR domain alone and in complex with Rac•GTP. *Left*, Ribbon representation of the p67^{phox} TPR domain alone with the β-hairpin insertion colored in yellow-green, and the additional C-terminal helix in orange. *Right*, Ribbon representation of the p67^{phox} TPR-Rac•GTP complex highlighting the Switch I and II regions in red, and the β-hairpin insertion colored green. Figures from Grizot *et al*, 2001 (*left*, PDB Code 1HH8) and Lapouge *et al*, 2000 (*right*, PDB Code 1E96).

The TPR domain has also been crystallized alone (Grizot *et al.*, 2001), utilizing a longer construct that includes the activation domain (although this region is not seen in the electron density), in contrast to the construct used in the Rac complex. Binding of Rac does not cause large structural rearrangements in p67^{phox}, with the only difference between the two structures being a small additional helix that is present at the end of the loop that packs into the TPR groove. There is some inconsistency with affinity measurements for the Rac-p67^{phox} interaction, with fluorescence titration determinations yielding affinities of 120 nM (Nisimoto *et al.*, 1997), and 31 nM (Han *et al.*, 1998) and ITC measurements giving 1.7 µM (Lapouge *et al.*, 2000).

Studies using various truncations of p67^{phox} led to the identification of an activation domain (residues 199-210) that is essential for NADPH Oxidase activity (Han *et al.*, 1998). As for the proline-rich region and N-terminal SH3 domain of p67^{phox}, the identity of the respective

binding partners for these regions are still unknown. As mentioned earlier, the C-terminal SH3 domain of p67^{phox} binds the C-terminal proline-rich region of p47^{phox} (Leto *et al.*, 1994; Finan *et al.*, 1994; Leusen *et al.*, 1995).

The PB1 domain of p67^{phox} has been shown to bind the PB1 domain in another oxidase protein, p40^{phox}. PB1 domains are so named because they were originally found in ***P***hox proteins and the budding yeast protein ***B***em1p (Ito *et al.*, 2001). The crystal structure of this complex is also known (Wilson *et al.*, 2003), and shows the mode of binding involves a front-to-back interaction of each PB1 domain mediated by electrostatic interactions, with the highly basic, concave back of PB1$_{p67phox}$ binding to the acidic, convex front of PB1$_{p40phox}$.

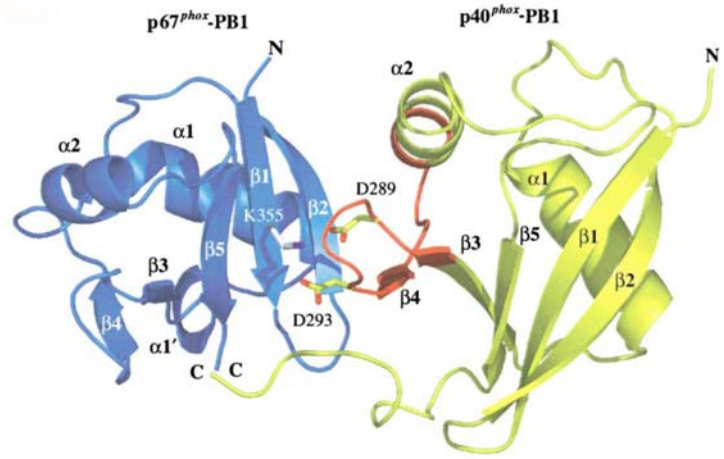

Figure 13. Ribbon diagram of the p40^{phox} PB1 (yellow)/p67^{phox} PB1 (blue) heterodimer. A short sequence found in some PB1 domains is highlighted in orange, and the D289$_{p40phox}$, D293$_{p40phox}$/K355$_{p67phox}$ electrostatic interaction is shown with stick representation. Figure from Wilson *et al*, 2003 (PDB Code 1OEY).

p40 phox

p40^{phox} (339 amino acids) is an oxidase protein whose exact role is not entirely understood. It is constitutively associated with p67^{phox} in resting neutrophils (Wientjes *et al.*, 1996), mediated by the PB1 domains of each protein. This interaction is quite strong: 4 nM for the isolated PB1 domains of each protein (Wilson *et al.*, 2003), and 10 nM for the full-length proteins (Lapouge *et al.*, 2002). Similar to p47^{phox} and p67^{phox}, it is composed of protein-protein interaction motifs: an N-terminal PX domain, followed by a SH3 domain, and a C-

terminal PB1 domain. Although much is known regarding the PX and PB1 domains, the binding partner and role of the SH3 domain has not been established yet.

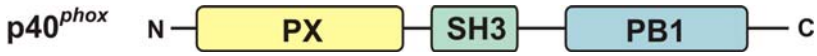

Figure 14. Domain structure of p40^{phox}.

In contrast to the PX domain of p47^{phox}, the PX domain of p40^{phox} binds phosphatidylinositol-3-phosphate (PI(3)P) (Kanai *et al.*, 2001; Ellson *et al.*, 2001b) which has been shown recently to stimulate NADPH Oxidase activity (Ellson *et al.*, 2001b). Its structure has also been determined to 1.7 Å in complex with di-butanoyl-PI(3)P (Bravo *et al.*, 2001).

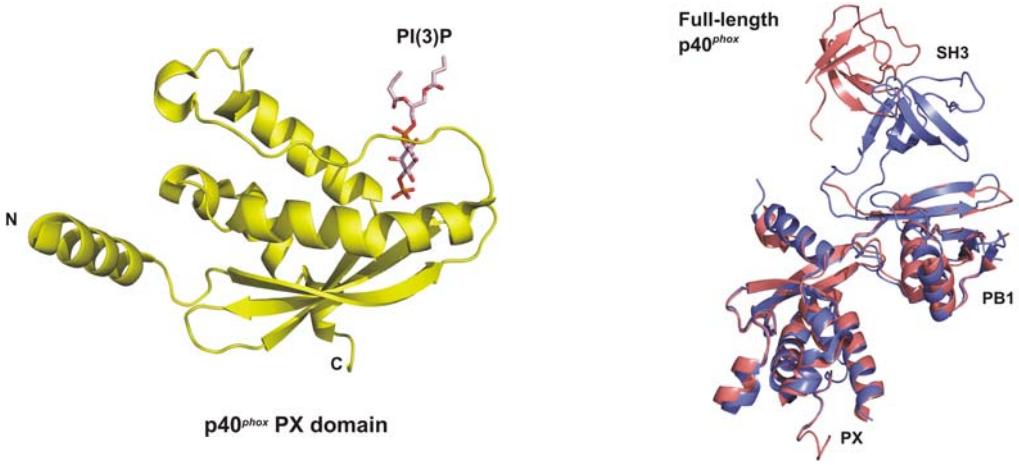

Figure 15. *Left*, Ribbon representation of the crystal structure of the p40^{phox} PX domain in complex with di-butanoyl-PI(3)P (pink stick; Bravo *et al*, 2001, PDB Code 1H6H). *Right*, Ribbon representation of the crystal structure of full-length p40^{phox} (Honbou *et al* , 2007, PDB Code 2DYB). The superposition of the two molecules in the asymmetric unit is shown, demonstrating the flexibility in the position of the SH3 domain.

Recent cellular studies indicate that p40^{phox} can enhance NADPH Oxidase activation, the degree of which seems to depend on the stimulus used (Kuribayashi *et al.*, 2002). The full-length p40^{phox} has recently been crystallized (Honbou *et al.*, 2007), and gives insight into another form of autoinhibition when the oxidase is not active. *In vivo* studies confirmed that the PB1 domain inhibits interaction of the PX domain with its membrane lipid target PI(3)P (Honbou *et al.*, 2007), a lipid that is enriched in phagosomal membranes (Kanai *et al.*, 2001; Ago *et al.*, 2001; Ellson *et al.*, 2001a). The structure of the full-length protein indicates the interaction occurs at another region of the PB1 domain, which leaves the PB1$_{p67phox}$ - PB1$_{p40phox}$ interaction undisturbed. In this way, p40^{phox} may help in the recruitment of p67^{phox} to the membrane upon stimulation.

Rac

Rac is a small (21 kDa) GTP-binding protein that belongs to the Rho (Ras homology) family of small GTPases. These proteins cycle between inactive GDP-bound and active GTP-bound forms, regulating signal transduction cascades that affect actin cytoskeletal organization, cell growth, endocytosis and secretion (Hall, 1994; Ridley, 1996). Rac undergoes prenylation at its C-terminal tail with the 20-carbon geranylgeranyl isoprenoid, which enables it to target to membranes (Zhang and Casey, 1996). In its inactive form, prenylated Rac•GDP is bound by its cytosolic chaperone, Rho GDP dissociation inhibitor (RhoGDI) (Abo *et al.*, 1991; Chuang *et al.*, 1993; Abo *et al.*, 1994), which prevents unsignaled exchange to GTP and sequesters the geranylgeranyl group, maintaining prenylated Rac in a soluble form (Gregg *et al.*, 2003). Stimuli-induced Rac activation targets the complex near the membrane, with subsequent dissociation of prenylated Rac•GDP from RhoGDI for Rac membrane localization. Guanine nucleotide exchange factors (GEFs) accelerate the dissociation rate of GDP (Vetter and Wittinghofer, 2001), allowing Rac to bind GTP, which is normally present at a ~10-fold higher concentration than GDP inside the cell. This active form of Rac is available to interact with many different effector molecules to transduce the desired signal. The duration of this signal is regulated by GTP hydrolysis. Rac, like all small GTPases, has a slow intrinsic GTPase activity, which is accelerated by GTPase activating proteins (GAPs) (Moon and Zheng, 2003), and returns Rac to the GDP-bound state. The cycle is completed with the extraction of prenylated Rac•GDP from the membrane by RhoGDI.

In addition to its roles in cytoskeleton rearrangement and cell growth, Rac is also required for NADPH Oxidase activation, with both Rac1 (Abo *et al.*, 1991) and Rac2 isoforms (Knaus *et al.*, 1991) capable of supporting oxidase activity in cell-free studies. In human neutrophils, Rac2 is the predominant Rac isoform (Knaus *et al.*, 1991), whereas Rac1 is expressed ubiquitously (Bokoch and Zhao, 2006) and has been used in many of the studies investigating the role of Rac in NADPH Oxidase. The two isoforms share 92% sequence identity, with the main differences found in the composition of their C-terminal tails (residues 183-188) that are involved with membrane association (Bokoch and Zhao, 2006).

All small GTPases have two characteristic regions termed Switch I and Switch II, which are involved in nucleotide binding and undergo conformational changes with respect to GDP and GTP binding (Vetter and Wittinghofer, 2001). Many downstream effector molecules

regulated by GTPases recognize these changes and form complexes with the active GTP-bound form that involve one or both of the Switch regions (Vetter and Wittinghofer, 2001). In the case of the phagocytic NADPH oxidase complex, the TPR region of $p67^{phox}$ binds Rac via the Switch I region (residues 26-45) (Diekmann *et al.*, 1994; Freeman *et al.*, 1994; Xu *et al.*, 1994; Lapouge *et al.*, 2000) (Figure 12). Two residues of Switch I, Ala 27 and Gly 30, mediate the specificity of $p67^{phox}$ interaction with Rac (Lapouge *et al.*, 2000).

Like all members of the Rho family, Rac contains an additional 12 residue "insert region" (residues 124-135) relative to other GTPases. The exact function of this region is not clear, with some reports implicating its involvement in NADPH oxidase activation (Freeman *et al.*, 1996; Joneson and Bar-Sagi, 1998; Diebold and Bokoch, 2001) and Rac-induced DNA synthesis leading to cell proliferation (Joneson and Bar-Sagi, 1998), while others finding no effect on oxidase activity (Toporik *et al.*, 1998; Alloul *et al.*, 2001). Translocation experiments have suggested a direct interaction of Rac with cytochrome b_{558} via the insert region (Diebold and Bokoch, 2001), with only 25% of Rac translocated to the membrane in X chromosome-linked CGD neutrophils deficient in cytochrome b_{558} (Heyworth *et al.*, 1994).

Phagocytic NADPH Oxidase activation

Due to its role in the destruction of pathogens and its high catalytic output, the phagocytic NADPH oxidase is tightly regulated such that superoxide production occurs only when pathogens have been phagocytosed to avoid injury to normal cellular tissues. Therefore, neutrophils must be stimulated to signal the assembly of the cytosolic regulatory proteins to the phagosome membrane. By-products from bacterial protein secretion, like the *N*-formylated peptide *N*-formyl-Met-Leu-Phe, or opsonized particulate stimuli bind to cell surface receptors and stimulate neutrophils (Bokoch and Zhao, 2006). Many researchers use the phorbol ester, PMA (phorbol 12-myristate 13-acetate), a soluble protein kinase C agonist (Nauseef, 2004) to stimulate cells since PKC is responsible for the phosphorylation of several serines in the AIR of $p47^{phox}$, a key event in phagocytic NADPH oxidase activation. Additionally, phospholipase A2 generation of intracellular arachidonic acid seems to be required for phagocytic oxidase activation (Dana *et al.*, 1994; Dana *et al.*, 1998), although the precise mechanism of this action is still unknown.

Cell stimulation leads to translocation of all three cytosolic oxidase components $p47^{phox}$, $p67^{phox}$, and $p40^{phox}$ to the membrane (Wientjes *et al.*, 1993). Phosphorylation of the autoinhibitory region in $p47^{phox}$ releases autoinhibition, allowing its tandem SH3 domains to bind to the proline-rich region in $p22^{phox}$, and its PX domain to bind phosphoinositides in the membrane. $p47^{phox}$ carries $p67^{phox}$ to the membrane via a tail-to-tail interaction between the C-terminal SH3 domain of $p67^{phox}$ and the C-terminal proline-rich region of $p47^{phox}$. Translocation of $p67^{phox}$ to the membrane is further enhanced by interactions of $p40^{phox}$ with membrane phosphoinositides via its N-terminal PX domain. Once positioned at the membrane, $p67^{phox}$ requires interaction with the small GTPase Rac to initiate electron transfer in $gp91^{phox}$ for superoxide production. Rac translocates to the membrane independently from the cytosolic oxidase proteins (Heyworth *et al.*, 1994) after dissociation from RhoGDI. Membrane associated GEFs exchange GDP for GTP, and prenylated Rac•GTP binds the TPR domain of $p67^{phox}$, enabling the activation domain of $p67^{phox}$ to activate superoxide production through $gp91^{phox}$.

1.3.3 Nox1

Nox1 was the first discovered homologue of $gp91^{phox}$ and was initially considered to be mitogenic, based on subsequent tumor formation when NIH-3T3 cells overexpressing Nox1 were injected into nude mice (Suh *et al.*, 1999). This was later found to be caused by a mutant form of Ras present in these cells (Lambeth, 2004). Although Nox1 is present in colon cancer cell lines, its suppression does not affect cell proliferation (Geiszt *et al.*, 2003a). Instead, Nox1 expression is increased in more differentiated colon tumors, suggesting another role which at present remains to be characterized.

Nox1 is most abundant in the colon, and is believed to participate in host defense in the digestive tract based on findings that specific microbial components recognized in innate immune responses induce Nox1 expression and subsequent ROS generation. For example, lipopolysaccharides from the pathogenic *Helicobacter pylori* (a Gram-negative bacterium which infects the stomach) can elicit increased ROS release by activation of Nox1 in guinea pig gastric pit cells (Kawahara *et al.*, 2001). Lipopolysaccharides are components in the cell wall of Gram-negative bacteria that allow pathogenicity. Nox1 is similarly induced in human colon cancer cells in response to recombinant flagellin from *Salmonella enteriditis*,

which increases ROS release as well as ROS-dependent release of the inflammatory cytokine interleukin-8 (IL-8) (Kawahara *et al.*, 2004).

Nox1 is 58% identical to gp91^{phox} and of all the Nox homologues it is the most functionally similar to gp91^{phox}, as indicated by its ability to rescue gp91^{phox} deficiency in CGD neutrophils (Geiszt *et al.*, 2003a). It can be activated by p47^{phox} and p67^{phox}, although superoxide production is only marginally increased (Takeya *et al.*, 2003). Nox1 possesses its own regulatory proteins, termed Noxo1, for ***Nox*** ***o***rganizer ***1*** (the equivalent of p47^{phox}) and Noxa1, for ***Nox*** ***a***ctivator ***1*** (the equivalent of p67^{phox}), both of which are expressed in the colon (Banfi *et al.*, 2003; Geiszt *et al.*, 2003b). Nox1 produces little or no superoxide on its own (Takeya *et al.*, 2003), and this can be significantly increased through interaction with Noxo1 and Noxa1 (Takeya *et al.*, 2003; Banfi *et al.*, 2003; Geiszt *et al.*, 2003b).

Comparison of regulatory proteins for Nox1 and the phagocytic oxidase

Noxo1 and Noxa1 share a majority of the motifs found in p47^{phox} and p67^{phox}, respectively, with some exceptions. Noxo1 lacks the autoinhibitory region present in p47^{phox}, while Noxa1 lacks the N-terminal SH3 domain of p67^{phox}.

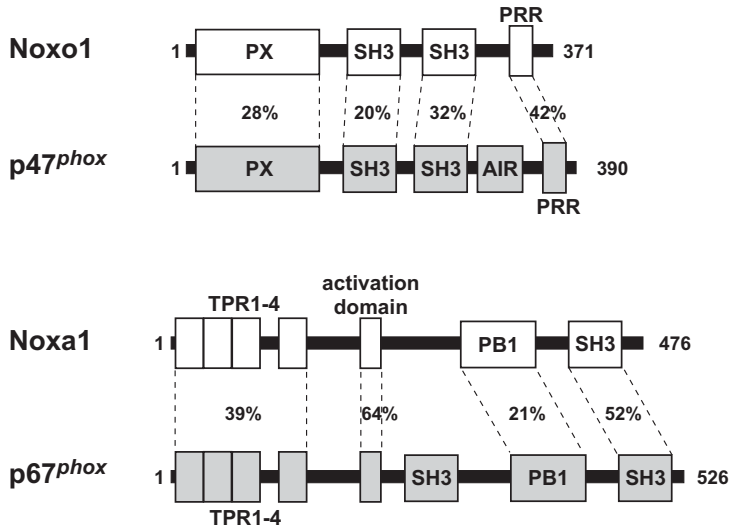

Figure 16. Domain structure of Noxo1 and Noxa1, with comparison to p47^{phox} and p67^{phox}, respectively. Figure after Takeya and Sumimoto, 2003.

Both proteins show relatively low overall sequence identity to their phagocytic counterparts (23% identity of Noxo1 to p47^{phox} and 28% identity of Noxa1 to p67^{phox}), yet they both are

capable of most of the interactions seen for phagocytic oxidase proteins. Site-specific mutations that define the molecular interactions of the phagocytic oxidase components have confirmed this. The tandem SH3 domains of Noxo1 recognize the proline-rich C-terminus of $p22^{phox}$, confirmed with a loss of interaction with a P156Q mutation, a naturally occurring mutation in $p22^{phox}$ from a CGD patient. Similarly, the SH3 domain of Noxa1 binds the C-terminal proline-rich region of Noxo1, with disruption of the interaction when Trp 436 of the Noxa1 SH3 domain is mutated to Arg. Additionally, the TPR domain of Noxa1 binds Rac•GTP, with loss of interaction when Arg 103_{Noxa1} is substituted by Glu (Takeya *et al.*, 2003).

Noxo1 and Noxa1 do not exclusively regulate Nox1. They have been found to regulate Nox3 in a Rac-independent manner, as well as in mixed complexes with $p47^{phox}$ and $p67^{phox}$. They can additionally activate $gp91^{phox}$, although they activate Nox1 more efficiently (Takeya and Sumimoto, 2006). In contrast to $gp91^{phox}$, Nox1 and Nox3, Nox4 is capable of generating superoxide without the need for additional regulating proteins like $p47^{phox}$, $p67^{phox}$, Noxo1 or Noxa1 (Geiszt *et al.*, 2000; Shiose *et al.*, 2001; Ambasta *et al.*, 2004; Martyn *et al.*, 2006).

Alternative splice forms of Noxo1 have also been found, designated Noxo1α, β, γ, and δ (Cheng and Lambeth, 2005; Takeya and Sumimoto, 2006). Noxo1β is the predominant form expressed in most tissues, like the colon. Noxo1α and Noxo1δ each have a single amino acid deletion of Lys 50 in the PX domain with respect to Noxo1β, and exhibit weaker ability to activate Nox1. Both splice forms are found in much lower abundance in tissues such as testis, fetal liver and the human colon cancer cell line T84, and therefore may have little biological relevance. Noxo1γ, on the other hand, possesses a five amino acid insertion in the PX domain with respect to Noxo1β, and is expressed in the testis at similar levels as Noxo1β. This insertion apparently allows Noxo1γ to localize primarily in the cytoplasm, in contrast to the exclusive membrane association of Noxo1β in resting cells. The activity of Noxo1γ is still controversial, with some reports of equal activation as Noxo1β (Cheng and Lambeth, 2005), and others observing lower activation (Takeya *et al.*, 2006). The subsequent use of the term Noxo1 in this writing refers to Noxo1β, the first published form without insertions or deletion.

Regulation of Nox1

The Nox1 oxidase shares several aspects analogous to the regulatory mechanisms of the phagocytic NADPH oxidase (Ueyama *et al.*, 2006). Nox1 functionally associates with $p22^{phox}$ in the plasma membrane and exhibits enhanced superoxide production when $p22^{phox}$ is coexpressed (Takeya *et al.*, 2003; Ambasta *et al.*, 2004; Hanna *et al.*, 2004). Both proteins have mutually stabilizing effects on each other, as evidenced by increased protein expression when the other is coexpressed (Hanna *et al.*, 2004). Like $p47^{phox}$, Noxo1 interacts with the proline-rich region of $p22^{phox}$ and interacts in a tail-to-tail fashion with Noxa1 to recruit it to the membrane. Noxa1 also binds Rac•GTP via the TPR region, and both proteins (like $p67^{phox}$and Rac) can support Nox1 superoxide generation in the absence of Noxo1 (Ueyama *et al.*, 2006).

Although Nox1 shares many features of the phagocytic oxidase, there are several important differences in the regulation of Nox1, most notably with respect to Noxo1. In contrast to $p47^{phox}$, Noxo1 is localized in the membrane, independent of cell activation. Since it lacks the region homologous to the autoinhibitory region in $p47^{phox}$, it is constitutively associated with the membrane via its PX domain (Cheng and Lambeth, 2004). A consequence of this feature is seen in the ability of Nox1 to spontaneously produce superoxide once Noxo1 and Noxa1 are coexpressed, without the requirement for PMA stimulation (Takeya *et al.*, 2003; Geiszt *et al.*, 2003b). PMA is still capable of slightly increasing Nox1 superoxide production (Takeya *et al.*, 2003). A second area of difference lies with Noxa1. Despite possessing a PB1 domain like $p67^{phox}$, it does not interact with $p40^{phox}$, due to the substitution of a conserved Lys at position 355 by Glu within this domain, which is essential for this interaction (Takeya *et al.*, 2003).

Recent studies on Nox1 with regards to host defense have demonstrated that Nox1 is additionally regulated at the transcriptional level. In gastric mucosal cells of guinea pigs, lipopolysaccharides from *Helicobacter pylori* activate Rac1 and transcription of Nox1 and Noxo1 mRNA (Kawahara *et al.*, 2005). Interestingly, Noxa1 mRNA is constitutively expressed in these cells, indicating that activation of Rac1 and induction of Nox1 and Noxo1 serve as triggers to activate oxidase activity in these cells. Once activated, these cells continuously and spontaneously produced superoxide at a rate of ~100 nmol·mg $protein^{-1}\cdot h^{-1}$ for more than 24 hours. Although this oxidative output is not sufficient to kill *H. pylori*, compared to 348 nmol·mg $protein^{-1}\cdot \boldsymbol{min^{-1}}$ for the phagocytic oxidase (Cross *et al.*, 1985),

Nox1 may serve as an initial signal for the cell to mount immune and inflammatory responses against such pathogens.

Role of Nox1 in disease

This inducible nature of Nox1 has captured the attention of many researchers with regards to factors that can induce Nox1 expression and which have been found to promote vascular disease. Angiotensin II (Lassegue *et al.*, 2001), growth factors like PDGF (Lassegue *et al.*, 2001), LDL (Holland *et al.*, 1996; Holland *et al.*, 1997), and mechanical stimuli (Grote *et al.*, 2003; Castier *et al.*, 2005; Jo *et al.*, 2006) have all been found to upregulate Nox1 mRNA. In the case of mechanical stimuli, hemodynamic forces have been shown to profoundly affect the vasculature. Normal blood flow in straight portions of the artery is uni-directional and is termed laminar shear stress. Disturbed blood flow, which includes oscillatory shear stress, is found in areas such as branched and curved regions in the artery, which are more likely to develop atherosclerotic lesions (Zarins *et al.*, 1983; Ku *et al.*, 1985). Interestingly, laminar shear stress stimulates eNOS production of $NO^{\cdot}$, whereas oscillatory shear stress activates Nox oxidases in endothelial and vascular smooth muscle cells. Disturbed blood flow increases Nox-derived superoxide, leading to reaction with $NO^{\cdot}$ and the production of $ONOO^{-}$, thereby decreasing the bioavailability of $NO^{\cdot}$, which in turn leads to increased endothelial dysfunction. In some cases, like high pressure in some models of hypertension, mechanical stimuli do not alter Nox mRNA expression but rather increase Nox oxidase activity (Ungvari *et al.*, 2006). This mechanosensitivity may derive from increases in intracellular Ca^{2+} concentration, as well as phosphorylation and activation of the kinase PKC-α (Ungvari and Koller, 2000; Ungvari and Koller, 2001; Ungvari *et al.*, 2004).

Oscillatory shear stress additionally stimulates inflammation through the induction of adhesion molecules and subsequent monocyte adhesion to endothelial cells, which has been found to depend on a Nox1 and $p47^{phox}$ containing oxidase in endothelial cells (Hwang *et al.*, 2003; Sorescu *et al.*, 2004). This involves the cell adhesion molecule, ICAM-1 (Chiu *et al.*, 1997), a molecule involved in monocyte adhesion and transendothelial migration, through the actions of the potent inflammatory cytokine, bone morphogenic protein 4 (BMP4), a member of the transforming growth factor-β (TGF-β) super family (Jo *et al.*,

2006). As mentioned earlier, induction of adhesion molecules plays a critical role in the pathogenesis of atherosclerosis and lesion development.

Mechanical forces have also been recently shown to affect Nox1 with regards to matrix remodeling. Vascular smooth muscle cells from mice respond to mechanical stretch with rapid ROS formation which correlates with $p47^{phox}$ translocation to the membrane, an increase in Nox1 mRNA, and an increase in both mRNA and activity of the matrix metalloproteinase, MMP-2. Each of these effects were dependent on $p47^{phox}$ (Grote *et al.*, 2003). Recent studies using mice deficient in $gp91^{phox}$ or $p47^{phox}$ have also implicated Nox1 as the oxidase that responds to chronic increase in blood flow with increased superoxide generation (Castier *et al.*, 2005). This study confirmed the subsequent production of $ONOO^-$, and demonstrated MMP activation in carotid arteries. Superoxide production, expression of MMP-9 and upregulation of MMP-2 were all found to depend on $p47^{phox}$, but not $gp91^{phox}$, implicating a role for Nox1. Thus, Nox1 containing oxidases may mediate flow-induced vascular remodeling, which has important implications with regards to atherosclerosis in lesion formation, development, and plaque rupture.

It is important to note that multiple Nox isoforms exist in the vasculature, which adds additional layers of complexity. Three Nox proteins, $gp91^{phox}$, Nox1 and Nox4 have emerged as key sources of superoxide in the vasculature. All are expressed at the mRNA level in all three layers of human arteries to distinctly varying degrees (Sorescu *et al.*, 2002). $gp91^{phox}$ mRNA is found most in endothelial cells, with much lower levels in smooth muscle cells and adventitial fibroblasts. Nox4 mRNA is abundant in all cells of the vasculature, with the highest expression in endothelial cells, followed by adventitial fibroblasts and smooth muscle cells. Conversely, Nox1 mRNA is expressed in low levels in each of these cells. Levels of mRNA, however, do not necessarily equate with protein levels, as seen by the localization of these Nox proteins in human coronary arteries. $gp91^{phox}$ was found mostly in the adventitia, to a lesser degree in the intima, and was nearly absent from the media. In contrast, Nox4 protein was found abundantly in the media, with a weaker presence in adventitial fibroblasts and the intima. Although Nox4 is abundant in the medial layer of the vessel wall, many of the agonist-induced superoxide production in VSMCs has been found to depend on $p47^{phox}$, which is not required for Nox4 activity. In fact, $p47^{phox}$ has been found to play a pivotal role with regards to early stages of atherosclerosis. In an animal model of atherosclerosis, mice deficient in $p47^{phox}$ demonstrated a 75% reduction in the total

lesion area of descending aortas (where early lesions appear), regardless if fed a normal or high fat diet. gp91^{phox}-deficiency did not affect the level of agonist-induced superoxide production, implicating the involvement of Nox1 (Barry-Lane *et al.*, 2001). Despite its low mRNA expression, Nox1 has been found to be the major oxidase in vascular smooth muscle cells, based on studies using Nox1 antisense mRNA and anti-Nox1 ribozymes which decreased the agonist-induced superoxide production in VSMC (Lassegue *et al.*, 2001; Katsuyama *et al.*, 2002; Lassegue and Clempus, 2003). Often only information regarding Nox1 mRNA expression is available, due to a lack of an appropriately specific Nox1 antibody (Lassegue *et al.*, 2001; Bedard and Krause, 2007). Other oxidase proteins such as p22^{phox}, p47^{phox}, and p67^{phox} are also expressed at both the mRNA and protein level in all cells of the vessel wall (Lassegue and Clempus, 2003). At present, there is little information regarding the presence of Noxo1 and Noxa1 in vascular cells. Recent work describes the localization of Noxa1 protein in the medial layer of mouse arteries and the translocation of Noxa1 and p47^{phox} in response to the proliferative agonist epidermal growth factor, suggesting that Nox1 is activated by the combination of one classical and one novel regulatory protein in vascular cells (Ambasta *et al.*, 2006).

Not only can a single Nox isoform affect many processes in vascular pathologies, multiple Nox isoforms can also collectively contribute to a single pathology. The recent use of animals deficient in a particular Nox isoform are beginning to delineate the individual contributions of different Nox proteins, suggesting specific roles of Nox isoforms in vascular disease development. One example is the role of Nox proteins in angiotensin II-induced hypertension. Hypertension can lead to smooth muscle hypertrophy (an increase in the size of smooth muscle cells) and increased vascular cross-sectional area, as a consequence of pressure-induced and pressure-independent mechanisms. In addition to its direct effects on blood pressure, angiotensin II can additionally induce medial smooth muscle hypertrophy in culture, and this was found to depend on NADPH Oxidase-derived ROS (Griendling *et al.*, 1994; Liu *et al.*, 2004). Nox1 deficiency *in vivo* was found to affect blood pressure, with Nox1-deficient mice retaining the ability of endothelium-dependent vasodilation. In contrast, mice containing a functional Nox1 showed significantly decreased cGMP levels, indicating that elevated blood pressure in response to angiotensin II occurs through $NO^{\cdot}$ depletion by Nox1-derived superoxide. Nox1 deficiency, however, did not affect hypertrophy of VSMCs in the media of mice aortas (Matsuno *et al.*, 2005).

Conversely, *in vivo* deficiency in gp91^{phox} did not affect blood pressure, but did reduce hypertrophy of VSMCs in the media (Wang *et al.*, 2001). gp91^{phox}-deficient mice exhibited significant reduction of ROS production in the endothelium and adventitia, which supports other data that suggests paracrine signaling of endothelial and adventitial ROS on the media (Liu *et al.*, 2004). With regards to hypertension, the causes of which are complex and often varied from individual to individual, these findings are significant because they allow for the possibility of specific therapies for different underlying causes.

The participation of NADPH Oxidases in multiple aspects of atherosclerosis makes them attractive targets for therapeutic intervention. Inhibitors directed at the responsible sources of ROS may be more effective than unspecific treatment with antioxidants, which have the potential to perturb normal cellular ROS signaling without effectively hindering dysregulated ROS production in pathological settings. Nox isoform-specific inhibitors may allow for targeted intervention at a particular cell, tissue, or pathway, which may enable custom therapies for individuals with different pathological backgrounds.

In addition to their roles in vascular diseases, there is an increasing appreciation for the role of NADPH Oxidases in cell proliferation and the pathogenesis of neurodegenerative diseases. Many human tumors constitutively produce large amounts of hydrogen peroxide, which can be inhibited by the flavoprotein inhibitor, diphenyleneiodonium (DPI), a known inhibitor of NADPH Oxidase (Szatrowski and Nathan, 1991). Normal cells also produce hydrogen peroxide in response to peptide growth factors such as epidermal growth factor (EGF) and PDGF. Growth factors bind their respective receptor tyrosine kinases, leading to phosphorylation of the receptors and other signaling molecules. This process is normally regulated by protein tyrosine phosphatases (PTPs), which remove phosphates, thus ensuring a limited duration of the growth signal. Hydrogen peroxide promotes growth signaling by inactivating PTPs through the oxidation of a key cysteine residue that must remain reduced to form a thiol-phosphate intermediate in the catalytic mechanism (Maehama *et al.*, 2001).

A second action of growth factor signaling is the transient activation of phosphatidylinositol (PI) 3-kinase to produce phosphatidylinositol 3,4,5-triphosphate (PIP_3). This lipid second messenger activates many downstream targets, such as the protein kinase Akt, which is involved in cell proliferation and cell survival. Levels of PIP_3 are regulated by lipid

phosphatases, such as the phosphatase with sequence homology to tensin (PTEN), which is a PIP_3 3-phosphatase. PTEN is a tumor suppressor and belongs to the PTP family of phosphatases. It has been found to undergo reversible inactivation by hydrogen peroxide through active site cysteine oxidation in growth factor stimulated cells stably expressing Nox1 or a dominant negative peroxidase, either of which results in elevated intracellular hydrogen peroxide levels. Increased PIP_3 levels observed in cells overexpressing Nox1 can further activate Nox1 by activating βPix, a guanine nucleotide exchange factor for Rac. Like all GEFs, βPix contains a pleckstrin homology domain which is activated by PIP_3 or $PI(3,4)P_2$ (Kwon *et al.*, 2004). Hydrogen peroxide production in growth factor stimulated cells has been found to require PI 3-kinase activation, with formation of a ternary complex between Rac, βPix, and Nox1 (Bae *et al.*, 2000; Park *et al.*, 2004). Other studies that suggest a role for Nox1 in cell proliferation include studies using RNA interference of Nox1 which demonstrated a requirement for Nox1 in Ras activated ROS production, oncogenic transformation, and tumor growth (Mitsushita *et al.*, 2004). Nox1 expression in lung epithelial cells was also found to promote cyclin D expression in a dose dependent manner. Cyclin D is a critical regulatory protein that controls progression of cells into the cell cycle for division. Thus, Nox1 may be a novel target for antitumor therapies.

Increasing evidence indicates a role for NADPH Oxidases in neurodegenerative diseases like Alzheimer's and Parkinson's disease, where chronic oxidative stress contributes to neuronal death, protein aggregation and pathogenesis (Giasson *et al.*, 2002; Klein and Ackerman, 2003; Norris and Giasson, 2005; Infanger *et al.*, 2006). The oxidase proteins $p47^{phox}$ and $p67^{phox}$ have been found to accumulate in post-mortem brain tissue of Alzheimer's disease patients (Shimohama *et al.*, 2000), and fragments of β-amyloid from Alzheimer's disease patients can stimulate superoxide production in rat microglial cells in a NADPH Oxidase-dependent manner (Bianca *et al.*, 1999). Microglial cells act as immune cells of the central nervous system. While many of these studies have focused on the role of $gp91^{phox}$/Nox2, Nox1 and Nox4 are also detected with $gp91^{phox}$/Nox2 in fore-, mid-, and hind-brain (Infanger *et al.*, 2006). Nox1 mRNA levels are the lowest of the three isoforms, but as seen in the vasculature where it can be subject to stimulus-induced activation, this does not necessarily negate its potential role in normal neuronal functions like long term potentiation, or possible roles in neurodegenerative diseases.

1.4 AIMS OF WORK

While significant progress has been made unraveling the intricate and complex roles of NADPH Oxidases at the cell biological level, limited information is available with regards to the enzyme at the molecular level, in particular for the membrane-associated Nox proteins. Molecular details on the mechanism of electron transfer would enable us to understand how these enzymes produce superoxide, which may shed light on ways to prevent this by therapeutic intervention. Specifically, information about the three-dimensional structure of the catalytic Nox proteins would assist in the design of novel, isoform-specific inhibitors, which may have significant therapeutic importance. Nox1 plays important roles in many facets in atherosclerosis, such as endothelial dysfunction, hypertension, induction of cell adhesion molecules and vascular remodeling, with additional potential roles in cell proliferation and neurodegenerative disease. Inhibitors of Nox1 in these pathological settings may provide a way of early intervention to prevent disease progression. This work aimed to structurally characterize human Nox1, either as a holoenzyme or only the cytosolic domain, by X-ray crystallography to gain insight into the mechanistic details of electron transfer. A prerequisite for structural studies is the ability to produce the protein of interest relatively pure and in appreciable amounts. A method was therefore developed to heterologously overexpress and purify four different constructs of human Nox1. Additionally, it is important to verify the biological integrity of the recombinant proteins. This can be accomplished by measuring a specific enzymatic activity if the protein performs an enzymatic function. In the case of human Nox1, a NADPH-dependent activity assay was used to determine if the recombinant proteins were indeed active. Characterization of interactions with biological binding partners is another way to address biological integrity. Biochemical and biophysical methods were employed to determine if the recombinant proteins were capable of biologically relevant interactions with regulatory oxidase proteins. These, together with the structural characterization of human Nox1, could provide insights into the mechanism of electron transfer of human Nox1 and molecular details on how regulatory proteins enhance this activity, which can be used to develop novel inhibitors as potential therapeutic agents.

Chapter 2.

Characterization of human Nox1

If you faint in the day of adversity,
your strength is small.
Prov. 24:10

2. RESULTS AND DISCUSSION

2.1 GENETIC ENGINEERING AND DEVELOPMENT OF EXPRESSION AND PURIFICATION METHODS FOR CONSTRUCTS OF HUMAN NOX1

Previous work (Woo, 2003, unpublished results) to establish a procedure to heterologously express and purify constructs of human Nox1 from *E. coli* involved initially two types of constructs: one that encompassed the entire sequence of human Nox1 and another consisting of only the cytosolic C-terminal domain based on sequence alignment analysis from the original work that first described the Nox homologues (Cheng *et al.*, 2001) (Figure 17). These preliminary expression studies indicated that a construct containing an N-terminal thioredoxin tag (to improve protein solubility) and the cytosolic C-terminal domain of human Nox1 could be expressed in low levels in the soluble fraction when a low temperature (20°C) was used for induction. Different *E. coli* cell strains such as BL21(DE3) Codon Plus RP, Origami and C41(DE3) were used for protein expression. BL21(DE3) Codon Plus RP contains rare tRNAs for the amino acids arginine and proline. Origami cells are recommended by the manufacturer for use with the expression vector (pET32a) in which the cytosolic C-terminal Nox1 domain was subcloned. C41(DE3) is a derivative of the commonly used BL21(DE3) strain, and was found to improve expression of problematic globular and membrane proteins (Miroux and Walker, 1996). Of these, utilization of the strain C41(DE3) improved soluble expression of the cytosolic domain of human Nox1. Co-expression of the molecular chaperones GroEL/GroES did not improve soluble expression of the cytosolic domain of human Nox1. Other N-terminal tags were tested and an N-terminal NusA tag was found to greatly improve soluble expression of the cytosolic domain of human Nox1. However, the NusA tag could not be easily removed with chromatographic measures after proteolytic cleavage, which decreased the utility of this construct for crystallization studies. This is a known disadvantage of the NusA tag (Ermolova *et al.*, 2003). In contrast to the cytosolic domain of human Nox1, initial trials of expression of full-length human Nox1 with an N-terminal GST tag in Rosetta competent cells (which contain plasmids for rare tRNAs), and in C41(DE3) cells with and without the molecular chaperone system GroEL/GroES did not result in any noticeable target protein expression.

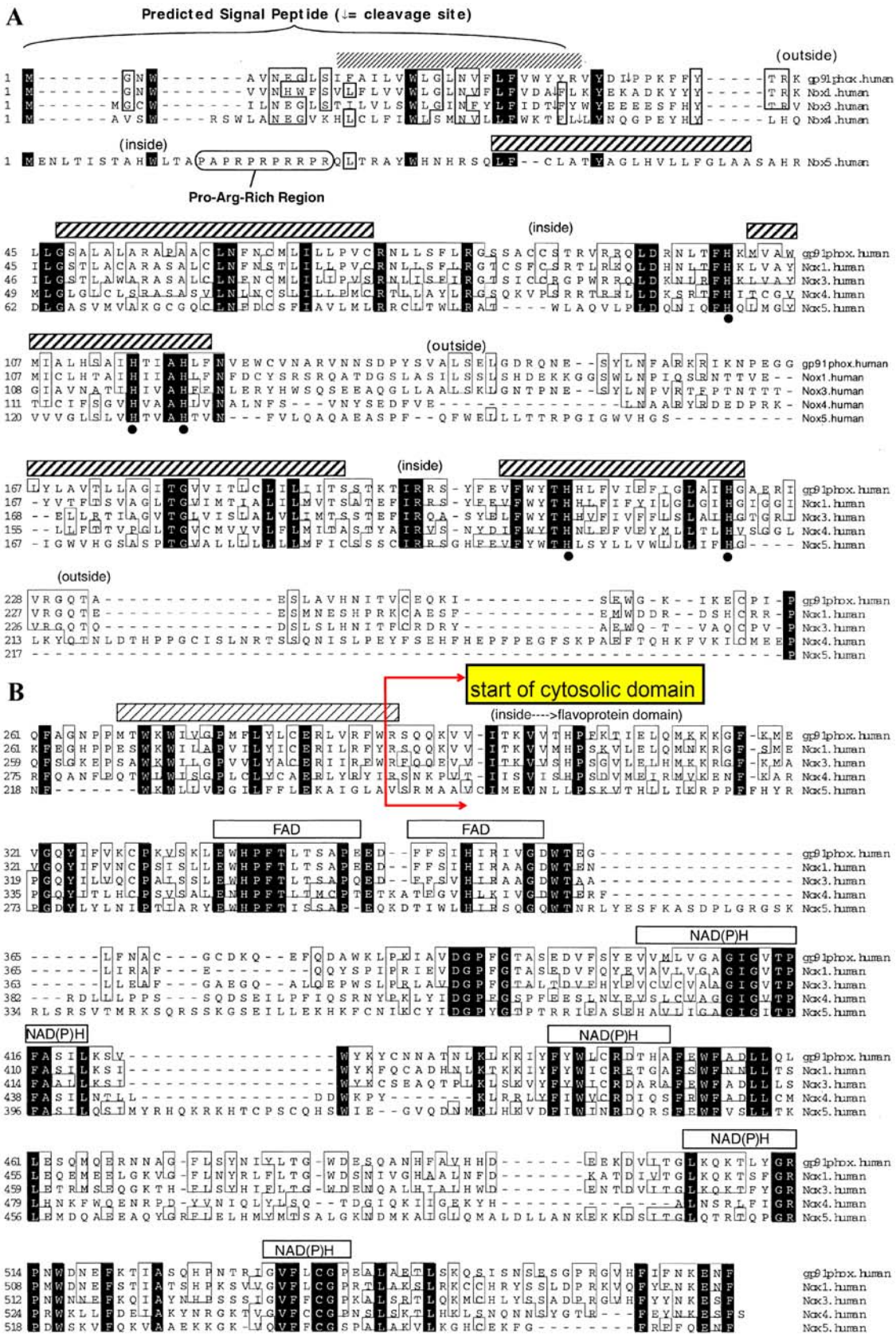

Figure 17. Sequence alignment of human Nox proteins (gp91^{phox}, Nox1, Nox3, Nox4 and Nox5). Filled circles indicate candidates for heme ligation. Predicted transmembrane α-helices are represented by heavily hashed boxes. The lightly shaded hashed box is a transmembrane helix that lies within a predicted signal peptide motif for gp91^{phox}, Nox1, Nox3, Nox4, but not Nox5, with arrows indicating the site of cleavage. FAD and NADPH binding sites are also indicated. Figure from Cheng *et al*, 2001. Red arrows indicate the start of the cytosolic domain of Nox1 used in the present work.

2.1.1 Full-length human Nox1

Two factors were tested to see whether they could promote expression of human Nox1 in *E. coli*. One addressed cofactor incorporation of the heme prosthetic group as a potentially limiting factor. Other heme containing eukaryotic proteins expressed in *E. coli* have been found to require inclusion of the heme precursor, δ-aminolevulinic acid for expression (Mulrooney and Waskell, 2000). The second examined whether providing an internal membrane environment in *E. coli* for overexpressed membrane proteins to accumulate could promote expression. Studies on overexpression of the subunit b of *E. coli* F_1F_o ATP synthase in the *E. coli* strains C41(DE3) and C43(DE3) were found to concomitantly produce intracellular membranes, and coexpression of subunit b with a target membrane protein was suggested as a potential strategy to promote overexpression of a desired membrane protein (Arechaga *et al.*, 2000).

Coexpression of human Nox1 and subunit b of E. coli F_1F_o ATP synthase

To determine if coexpression of the subunit b of *E. coli* F_1F_o ATP synthase could promote expression of full-length human Nox1, cells of the strain C41(DE3) were transformed with both a plasmid containing the gene for subunit b (a kind gift from Prof. John E. Walker, MRC, Cambridge, UK) and a plasmid containing the gene for human Nox1 inserted into the vector pET 41a via the restriction sites *Nco*I and *Xho*I (a kind gift from Prof. Dr. H.H.W. Schmidt, Monash University, Melbourne, Australia). Control cells transformed with each single plasmid were additionally prepared. Protein expression was induced with the addition of a final concentration of 0.7 mM IPTG, and two induction conditions were tested: 3 hours at 37°C and 18 hours at 25°C. Moderate expression of subunit b could be obtained in all cells transformed with this plasmid. However, no overt overexpression of human Nox1 (expected molecular weight of ~97 kDa for the construct) was seen at either induction condition, which was independent of the cell density at the time of induction.

Influence of δ-aminolevulinic acid in the coexpression of human Nox1 and subunit b of E. coli F_1F_o ATP synthase

The effect of including the heme precursor, δ-aminolevulinic acid was tested in conjunction with coexpression with subunit b on human Nox1 protein expression. To allow the cells time to incorporate heme into the protein, the induction conditions were adjusted to 20°C over 2 days. Due to the reduced induction temperature, a cold-adaption protocol (Dr. Konstanze von König, personal communication) was used where cultures were allowed to grow to cell density at 25°C instead of 37°C prior to induction. In this study, inclusion of δ-aminolevulinic acid did not improve expression of human Nox1. One factor that could have affected this result was the use of the media 2YT (from the protocol for subunit b expression) and not the richer TB (Terrific Broth) media, which can allow for sustained growth over several days.

In any case, protein expression of full-length human Nox1 in *E. coli* may be limited by other factors like mRNA secondary structure or the fact that the lipid composition of *E. coli* membranes differs from those of eukaryotic cells. Thus, continuing efforts to heterologously express a eukaryotic membrane protein in a prokaryotic system may prove less successful. Other eukaryotic expression systems such as yeast, dictyostelium, or baculovirus might prove to be more useful, especially if expressed with $p22^{phox}$. With regards to baculovirus, there has been a report of recombinant expression of the phagocytic cytochrome b_{558} using recombinant baculovirus (Rotrosen *et al.*, 1992). This seems, however, to be limited in utility since no subsequent work following this isolated report has been published, suggesting the overall level of difficulty of overexpressing the membrane-bound Nox proteins in general. Additionally, the authors admit that the system produced relatively low amounts of recombinant cytochrome b_{558} protein, which precludes its usefulness for providing the amount of protein required for structural studies.

2.1.2 The cytosolic domain of human Nox1

As mentioned earlier, previous work involved an extensive search for conditions that would promote soluble expression of the cytosolic portion of human Nox1 (residues 290-564). Of the two initial constructs tested, one that contained an N-terminal thioredoxin tag to promote solubility, was found to overexpress the fusion protein, although a majority of this protein

was insoluble. At the time of these studies, the protease required to cleave off the thioredoxin tag (should it prove to be necessary for crystallization) was a limiting factor. One way to remedy this would be to exchange the protease cleavage site with that of tobacco etch virus (TEV) protease, which can be easily produced recombinantly. In addition to this, the cytosolic domain can be cloned into a vector that possesses a simple N-terminal His-tag, followed by a TEV cleavage site. In this work, two such constructs were cloned, expressed, and purified to determine their usefulness for structure-function studies. An additional His-tagged construct, which includes the cytosolic domain and at least one transmembrane helix, was also produced and characterized. These three constructs along with the original thioredoxin tagged construct are discussed below.

Trx_E-$Nox1_{cyt}$

Of the constructs containing the cytosolic domain of human Nox1, the original thioredoxin-tagged construct was found to overexpress to the largest extent and the most reproducibly. Hence initial biochemical work was carried out with this construct to determine a template purification scheme that could then be used for the other constructs. In addition, preliminary characterizations could be made to see, for example, if the thioredoxin tag interfered at all. In the best case, the tag could provide additional crystal contacts and more importantly, could provide a method for obtaining phases via molecular replacement, should crystallization prove to be successful. This construct will be referred to as Trx_E-$Nox1_{cyt}$: Trx indicates an N-terminal thioredoxin tag, the italicized subscript refers to the protease which cleaves off the tags (in this case, enterokinase), and $Nox1_{cyt}$ indicates the cytosolic domain of human Nox1 (residues 290-564).

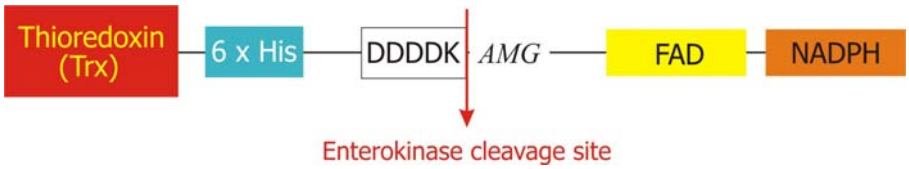

Figure 18. Schematic of the Trx_E-$Nox1_{cyt}$ construct. To encourage protein solubility, this construct contains an N-terminal thioredoxin (Trx) tag followed by a 6-His Tag for affinity purification. These tags can be removed by the protease enterokinase to produce the cytosolic domain of human Nox1 (residues 290-564) which contains the putative binding sites for FAD and NADPH. The additional amino acids alanine, methionine and glycine are inserted before the start of the Nox1 cytosolic domain as a consequence of using the *Nco*I restriction site.

Conditions for the expression of Trx_E-$Nox1_{cyt}$ were determined in a previous work (Woo, 2003, unpublished results). Briefly, C41(DE3) competent cells were transformed with the plasmid pET32a containing residues 290-564 of human Nox1 inserted via *Nco*I and *Xho*I restriction sites (a kind gift from Prof. Dr. H.H.W. Schmidt, Monash University, Melbourne, Australia). An overnight culture was made from a single colony in Standard 1 (ST1) or TB media supplemented with ampicillin, and used to inoculate larger cultures, typically 5-10L. Cells were grown to an optical density of 0.35-0.5 at 37°C and protein expression was induced with the addition of IPTG to a final concentration of 0.1 mM, and further incubated at 20°C overnight.

Chromatographic measures used previously to purify Trx_E-$Nox1_{cyt}$ indicated that Ni-NTA affinity chromatography and size exclusion chromatography were insufficient to purify the fusion protein to homogeneity (Woo, 2003, unpublished results). Subsequent purifications employed additional chromatographic steps that proved to be effective. The entire purification was made at 4°C. Initial capture proceeded via Ni-NTA affinity chromatography, and crude separation was achieved with a linear gradient of 5-800 mM Imidazole in 150 ml over two 5 ml HiTrap Ni-Chelating columns (Amersham Biosciences/GE Healthcare) connected in series (Figure 19).

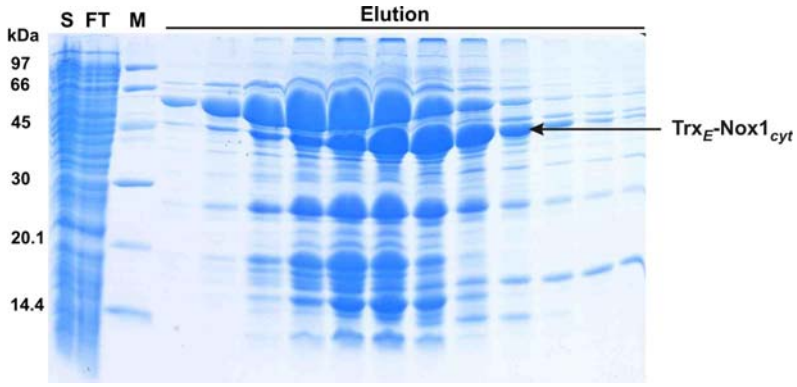

Figure 19. Initial purification of Trx_E-$Nox1_{cyt}$ with Ni-NTA chromatography. The supernatant, *S*, of clarified lysate from *E. coli* C41(DE3) cells expressing Trx_E-$Nox1_{cyt}$ was loaded via a peristaltic pump onto two 5ml HiTrap Ni-Chelating Sepharose columns connected in series. The columns were pre-equilibrated with Buffer Ni-A (20 mM Tris-HCl, pH 8, 300 mM NaCl, 5 mM Imidazole, 10% glycerol, 2 mM β-mercaptoethanol). Flow thru, *FT*, was collected and the column was washed with Buffer Ni-A until the absorbance reading at 280 nm returned to baseline and remained constant. The columns were then transferred to an ÄKTA Prime (Amersham Biosciences/GE Healthcare) and elution was made with a 0-80% Buffer Ni-B (20 mM Tris-HCl, pH 8, 300 mM NaCl, 1M Imidazole, 10% glycerol, 2 mM β-mercaptoethanol) linear gradient over 150 ml. A single elution peak was obtained and fractions (3 ml) were analyzed on SDS-PAGE. *M* represents molecular weight markers.

An initial trial using anion exchange chromatography (Resource Q, Amersham Biosciences/GE Healthcare) was moderately successful to provide intermediate separation after Ni-NTA chromatography. A gradient from 25 mM-1M NaCl over 300 ml was set up and the gradient was held at 190.75 mM NaCl, allowing weakly binding proteins to elute until the absorbance reached baseline and remained constant. The gradient was then allowed to run to completion. Trx_E-$Nox1_{cyt}$ eluted predominantly in the first peak from the hold at 190.75 mM NaCl, with many of the contaminating proteins preferentially binding the resin. Although the Resource Q resin provided some separation from contaminants, its improvement was limited, as can be seen in Figure 20.

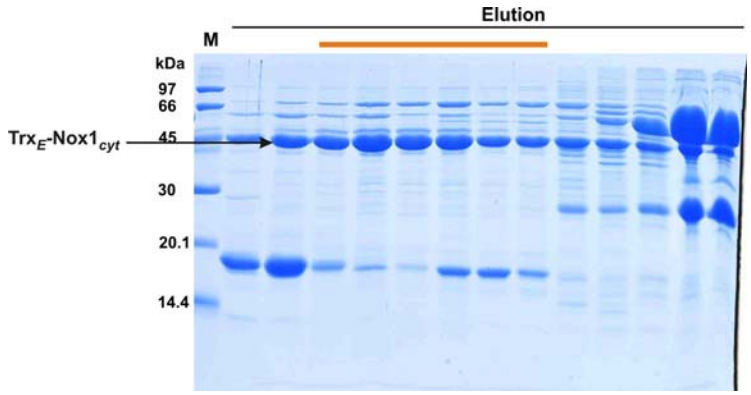

Figure 20. Purification of Trx_E-$Nox1_{cyt}$ with Resource Q chromatography. Fractions containing Trx_E-$Nox1_{cyt}$ pooled from Ni-NTA chromatography were desalted over 5x 5ml HiTrap Desalting columns (Amersham Biosciences/GE Healthcare) connected in series, and then applied to a 6ml Resource Q column pre-equilibrated with Buffer Res Q-A (20 mM Tris-HCl, pH 8, 25 mM NaCl, 10 % glycerol, and 2 mM β-mercaptoethanol). A linear gradient from 0-100% Buffer Res Q-B (20 mM Tris-HCl, pH 8, 1M NaCl, 10 % glycerol, and 2 mM β-mercaptoethanol) was run over 300 ml, and the gradient was initially held at 17% Buffer B (190.8 mM NaCl) to elute weakly binding proteins. *M* represents molecular weight markers, and an orange bar indicates fractions containing Trx_E-$Nox1_{cyt}$ pooled for further purification.

The cytosolic domain of human Nox1 is predicted to contain putative binding sites for the cofactors FAD and NADPH, and this second binding site was exploited with a second affinity chromatography step using 2'5'ADP Sepharose 4B (Amersham Biosciences/GE Healthcare). This resin selectively binds $NADP^+$-dependent dehydrogenases, and elution can proceed with a simple salt gradient for weakly binding proteins, or competitively with NAD^+ or $NADP^+$. In the case of Trx_E-$Nox1_{cyt}$, binding was weak and the fusion protein could be eluted with step gradients of NaCl. The separation achieved from this chromatographic step was so effective, it was found that anion exchange chromatography

could be completely omitted and a similar level of purification was seen. (Figure 21A and B). Western blot analysis using both antibodies against the His tag and against the C-terminus of human Nox1 (a kind gift from Prof. Dr. H.H.W. Schmidt, Monash University, Melbourne, Australia) confirmed the purified protein as the desired fusion protein, Trx_E-$Nox1_{cyt}$ (Figure 21C).

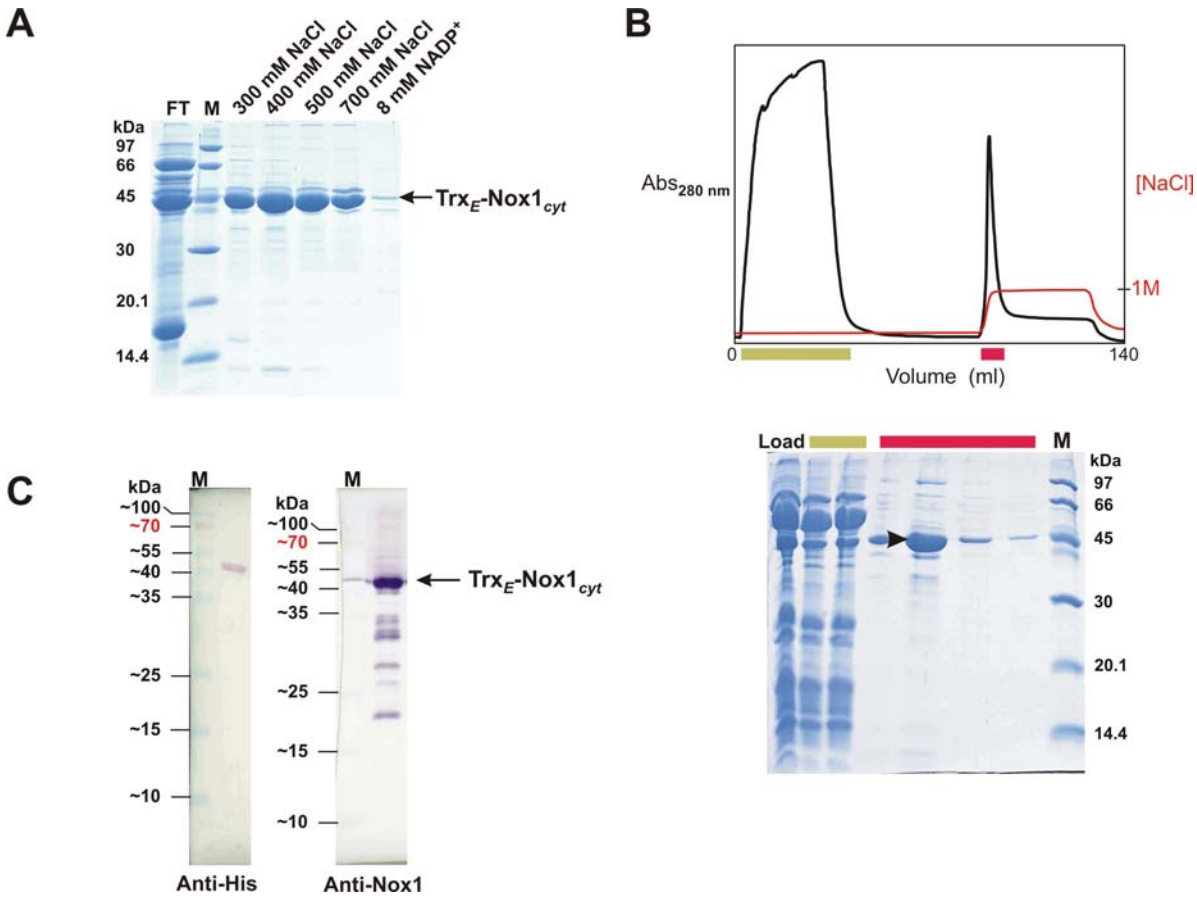

Figure 21. *A*, Purification of Trx_E-$Nox1_{cyt}$ from 2'5'ADP Sepharose 4B. Pooled fractions containing Trx_E-$Nox1_{cyt}$ from Resource Q chromatography were applied to a column containing 4 ml of 2'5'ADP Sepharose 4B resin pre-equilibrated with Buffer ADP-A (10 mM NaH_2PO_4, pH 7.3, 150 mM NaCl, 10 % glycerol, and 2 mM DTT). The column was washed by gravity with two column volumes of Buffer ADP-A, and a series of step gradients were made with 4 ml of Buffer ADP-A containing 200 mM, 300 mM, 400 mM, 500 mM, 700 mM and 1M NaCl, respectively. Competitive elution was made with 4 ml of 8 mM $NADP^+$. Flow through, *FT*, and elution fractions were analyzed on SDS-PAGE. *B*, Comparison with 2'5'ADP Sepharose 4B purification of Trx_E-$Nox1_{cyt}$ fractions pooled after Ni-NTA chromatography. Colored bars indicate peaks and respective fractions analyzed on SDS-PAGE. Arrowhead indicates Trx_E-$Nox1_{cyt}$. *C*, Western Blot analysis of purified Trx_E-$Nox1_{cyt}$. *M* represents molecular weight markers.

MALDI-TOF (matrix-assisted laser desorption ionization- time of flight) analysis (Dr. Robert Shoeman) additionally confirmed the correct molecular mass, with a calculated value of 48,616.46 Da versus the expected 48,684.55 Da for the fusion protein construct, which is within error of the instrument (Figure 22).

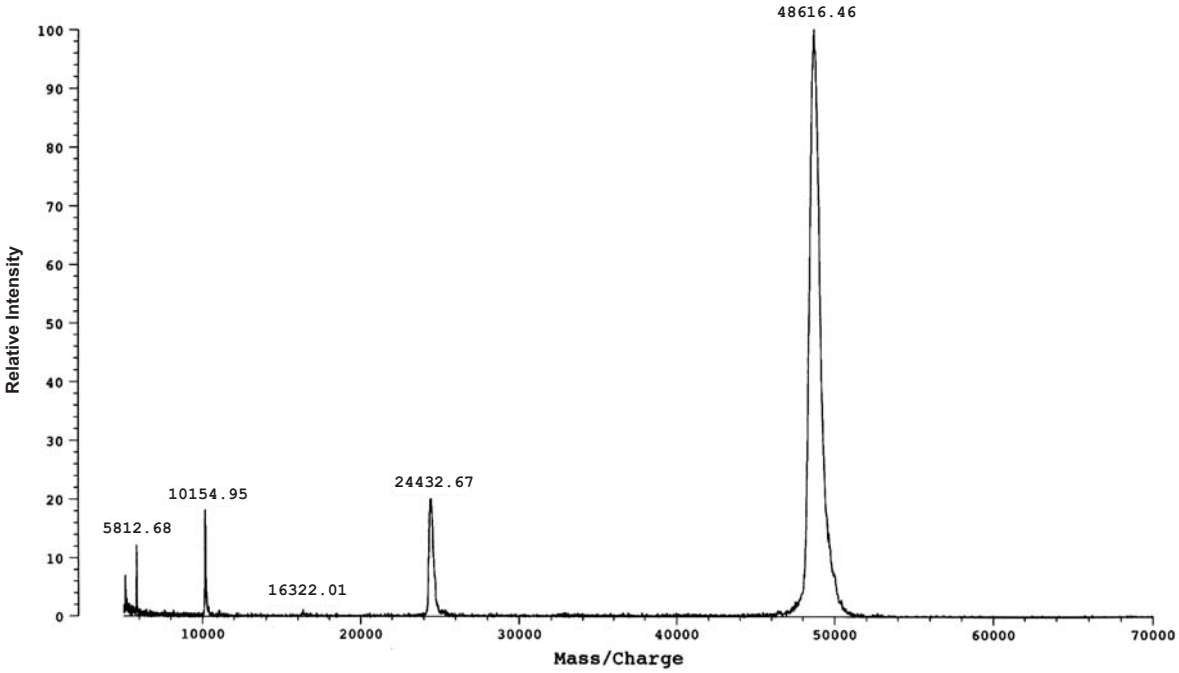

Figure 22. MALDI spectrum of purified Trx_E-$Nox1_{cyt}$, with a measured mass of 48,616.46 Da.

Although it was possible to purify Trx_E-$Nox1_{cyt}$ under native conditions from the soluble portion of *E. coli* lysate, the typical yields were significantly lower than typical yields normally obtained from proteins that overexpress well. Yields ranging from less than 0.5 mg/107 g of cells (10 L TB) to 1.2 mg/84g (7L TB) cells were not uncommon, and thus became a limiting factor for structural studies on the protein.

At the time of this work, an article was published describing the expression and purification (under denaturing conditions) of various truncations of the cytosolic domain of $gp91^{phox}$ from *E. coli* (Nisimoto *et al.*, 2004). The authors also found predominant expression of the proteins in the insoluble fraction, and used a denaturing/renaturing protocol that employed replacement of the denaturing agent with either of two detergents, Triton X-100 or Genapol X-80. This purification method was tested with Trx_E-$Nox1_{cyt}$ to determine if larger quantities of more stable protein could be obtained in like fashion.

Pellets of insoluble material (corresponding to the amount of cells from approximately 1L of induced culture) from cells lysed previously were homogenized with buffer containing 6M guanidinium hydrochloride. This is in contrast to the 8M urea used by Nisimoto, *et al*, due to a lack of solubility of Trx_E-$Nox1_{cyt}$ in urea after initial fractionation (Woo, 2003, unpublished results). The clarified supernatant was then applied to a 10 ml Ni-NTA (Qiagen) column and washed with a denaturing buffer containing 40 mM Imidazole until a stable baseline absorbance was reached. The column was then washed with a linear gradient of 0-100% Refolding buffer over 100 ml, where the denaturing agent was replaced with 0.3% Triton X-100 and supplemented with 30 µM FAD. Elution was made in this Refolding buffer with 250 mM Imidazole. As noticed in pilot denaturing trials made previously (Woo, 2003, unpublished results), the denatured Trx_E-$Nox1_{cyt}$ is not captured 100% by the Ni-NTA resin, and significant amounts were seen in the Flow through and Wash fractions (Figure 23). In addition, exclusive binding of the refolded Trx_E-$Nox1_{cyt}$ was not observed, with a considerable amount of contaminants present in the elution fractions. This indicates that further chromatographic measures would be required to purify the protein to homogeneity, which differs from what was described for the recombinant C-terminal truncations of $gp91^{phox}$. In spite of this, a denaturing/renaturing purification method for Trx_E-$Nox1_{cyt}$ could provide a more substantial protein yield, if the renatured protein was shown to retain native properties.

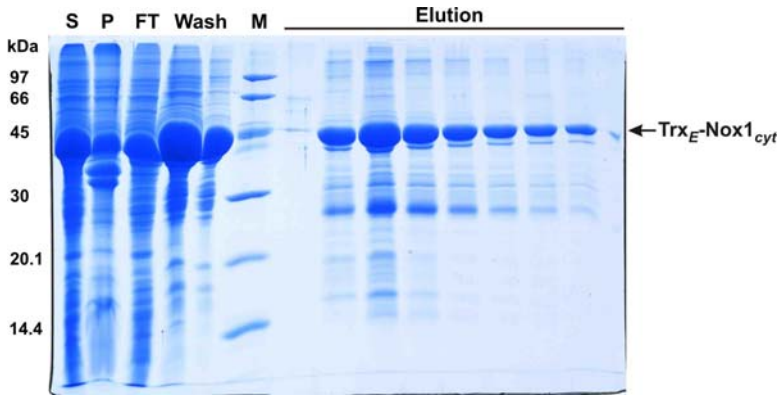

Figure 23. Denaturing/renaturing purification of Trx_E-$Nox1_{cyt}$ after Nisimoto *et al*, 2004. Insoluble material after lysis was homogenized in denaturing buffer (50 mM HEPES, pH 7.4, 150 mM NaCl, 20 mM Imidazole, 6 M guanidinium hydrochloride). The supernatant, *S*, was applied to 10 ml of Ni-NTA resin. The column was washed with 10 column volumes of denaturing buffer containing 40 mM Imidazole. Refolding buffer (50 mM NaH_2PO_4, pH 7.4, 150 mM NaCl, 30 µM FAD, 0.3% Triton X-100) was introduced by a linear gradient over 100 ml. Renatured protein was step eluted with refolding buffer containing 250 mM Imidazole. *P*, insoluble fraction from homogenization under denaturing conditions; *FT,* flow through; *M*, molecular weight markers.

H_6-Nox1$_{220-564}$

In light of the work done on the cytosolic domain of gp91^{phox} (Nisimoto *et al.*, 2004), a truncation construct of human Nox1 was cloned that encompassed the homologous regions of their longest and most active construct (residues 221-571). This corresponds to residues 220-564 of human Nox1. Although affirmed by the authors as a construct defining the cytosolic domain of gp91^{phox}, the construct includes the sixth predicted transmembrane helix in its entirety and the last three residues of the fifth predicted transmembrane helix (Figure 17).

To have a direct comparison, this was cloned into the same vector (pET 30a, Novagen) using the same restriction sites (*Eco*RI and *Xho*I) as was used for gp91^{phox}. The cloning of the construct was made by Monika Berthel and will be referred to as H_6-Nox1$_{220-564}$, for N-terminally His-tagged human Nox1 containing residues 220-564.

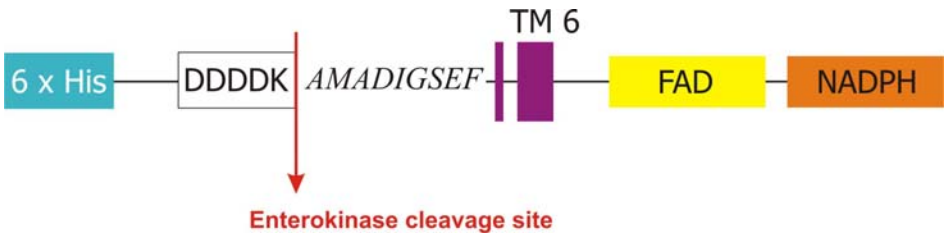

Figure 24. Details of the H_6-Nox1$_{220-564}$ construct. This construct includes the last three residues from transmembrane helix 5, the entire transmembrane helix 6 (TM6) and the cytosolic portion of human Nox1. It contains an N-terminal His-tag removable by the protease enterokinase, and a nine-residue insertion (in italics) as a consequence of the vector and *Eco*RI restriction site.

Expression studies in both BL21(DE3) and BL21(DE3) Codon Plus RIL cells showed significant overexpression of H_6-Nox1$_{220-564}$ in the insoluble fraction (Monika Berthel) (Figure 25). Attempts to purify under denaturing conditions according to Nisimoto *et al*, resulted in very low amounts of H_6-Nox1$_{220-564}$ retained on the Ni-NTA column (Monika Berthel, personal communication). A simple, fast native purification method based on a protocol presented at a course on membrane proteins (NCCR course, 2004) was employed to determine the potential usefulness of this construct. Lysis was performed in a buffer containing 2% Triton to simultaneously solubilize membranes. Clarified lysate from 1L of induced cells was applied to 100 µl of Ni-NTA resin (Qiagen) pre-equilibrated with lysis buffer and washed with step gradients of lysis buffer containing 20 mM, 40 mM and 60 mM Imidazole, respectively, and with a reduced concentration of Triton (0.3%). Elution

proceeded with lysis buffer containing 300 mM Imidazole, and 0.3% Triton. SDS-PAGE and Western Blot analysis were used to determine the progress of the purification.

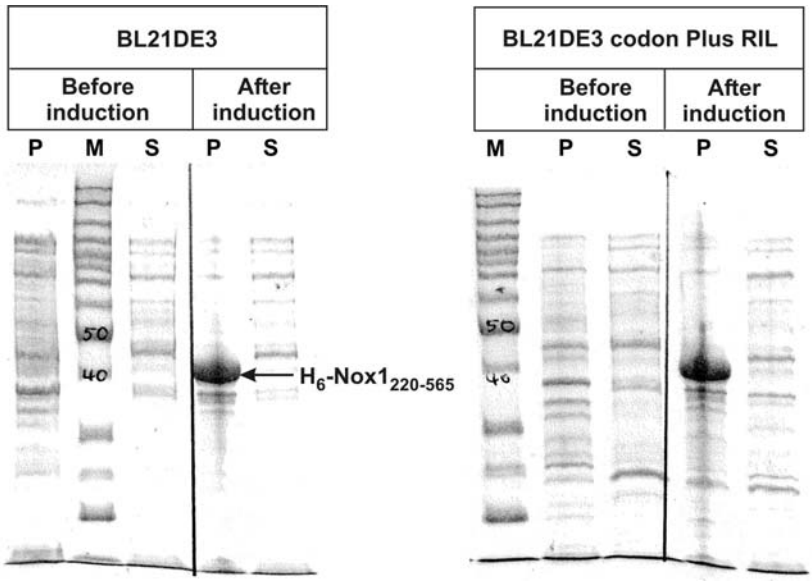

Figure 25. Overexpression of H_6-Nox1$_{220-564}$ in BL21(DE3) or BL21(DE3) Codon Plus RIL cells (Monika Berthel). Cells were grown at 37°C to a cell density of 1.2 or 1.4, respectively and induced with a final concentration of IPTG of 1mM for 3 hours at 37°C. *P*, stands for pellet, *S*, for supernatant, and *M*, for molecular weight markers.

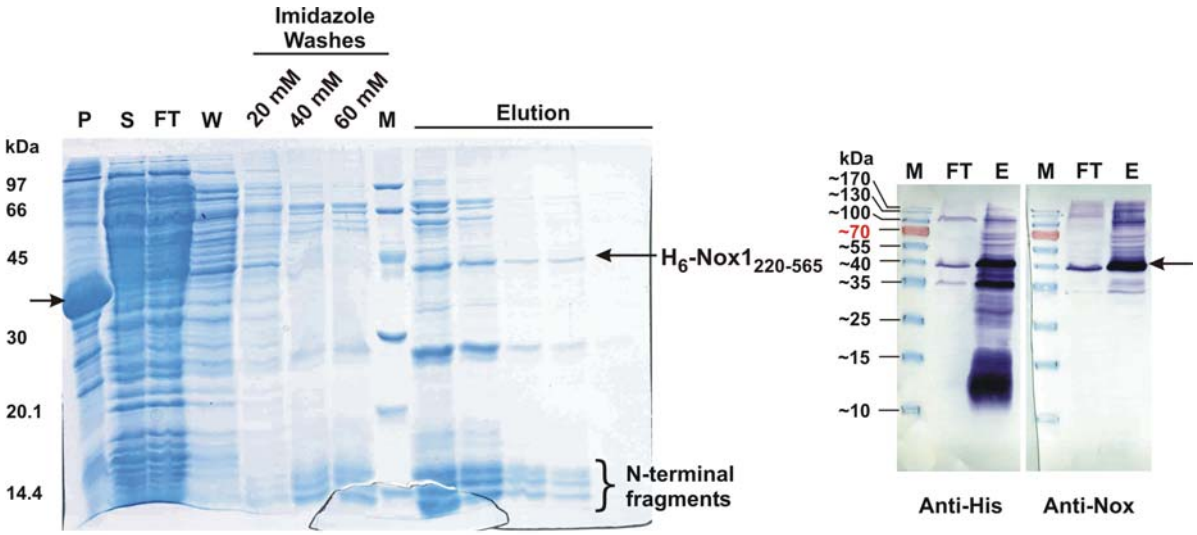

Figure 26. Native purification of H_6-Nox1$_{220-564}$ with Ni-NTA chromatography and corresponding Western blot of flow through (*FT*) and elution (*E*) fractions. *P*, stands for pellet, *S*, for supernatant, *FT*, for flow through, *W* for lysis buffer wash, and *M*, for molecular weight markers. Arrows indicate H_6-Nox1$_{220-564}$.

As can be seen in Figure 26, there are significant N-terminal proteolytic fragments from H_6-$Nox1_{220-564}$ which are present to a higher degree than the desired protein. The anti-Nox1 antibody is directed against the C-terminus of Nox1, and notably reacts only with the larger molecular weight species. In contrast, the anti-His tag antibody additionally recognizes many of the lower molecular weight protein species seen in the SDS-PAGE of the elution fractions. These results spotlight initial concerns over the usefulness of this longer construct. In the original work using $gp91^{phox}$, the authors mention this extreme susceptibility of gp91C (the equivalent construct) to proteolysis even in the presence of protease inhibitors (which was likewise observed with H_6-$Nox1_{220-564}$ in this work). This process was time dependent during dialysis at 3°C for 16 h, and after one week the 46 kDa protein was completely proteolyzed into two fragments. If one desires to perform structural characterization of a protein, clearly this kind of behavior is not desirable, and will make crystallization of the entire construct near to impossible.

It should be noted here that a recent article, published after this work, described the expression of several C-terminal truncations of Nox1, including a construct similar to H_6-$Nox1_{220-564}$ that includes three additional residues of TM5 and lacks the last 14 residues from the C-terminus (residues 217-550) (Park *et al.*, 2006). The authors describe the use of the vector pGEX4T1 with expression in *E. coli* DH5α cells, and demonstrate reasonable expression for the purpose of pull-down experiments, although smaller molecular weight species of ~28-30 kDa (possible proteolytic fragments) are also capable of binding the glutathione resin. Perhaps this vector and cell combination affords better heterologous overexpression of Nox1 proteins than those used in this work. None of the designed constructs by Park *et al* contain the last 14 residues of Nox1, perhaps suggesting that these residues destabilize the resulting proteins. While this deletion might be justified for the purposes of their study, it may not be advantageous for use in studies on the electron transfer mechanism of Nox1. As mentioned earlier, Nox proteins belong to the family of ferredoxin-$NADP^+$-reductase (FNR) proteins, which have a characteristic NADPH binding fold where the last aromatic residue of the C-terminus packs against one side of the isoalloxazine rings of FAD (Taylor *et al.*, 1993). In Nox proteins, this residue is a phenylalanine, which is strictly conserved in all five Nox proteins. Removal of this residue (and neighboring residues) may affect the ability of the enzyme to bind and transfer electrons to the FAD cofactor. Other studies on C-terminal truncations of $gp91^{phox}$ support

this, with a reduced NADPH-dependent activity observed with constructs bearing deletions of the last 13 or 20 residues from the C-terminus (Nisimoto *et al.*, 2004) (although the authors view these reductions as negligible). Interestingly, the article that describes binding interactions of Nox1 (residues 217-550) does not report any data on the activity of this construct (Park *et al.*, 2006).

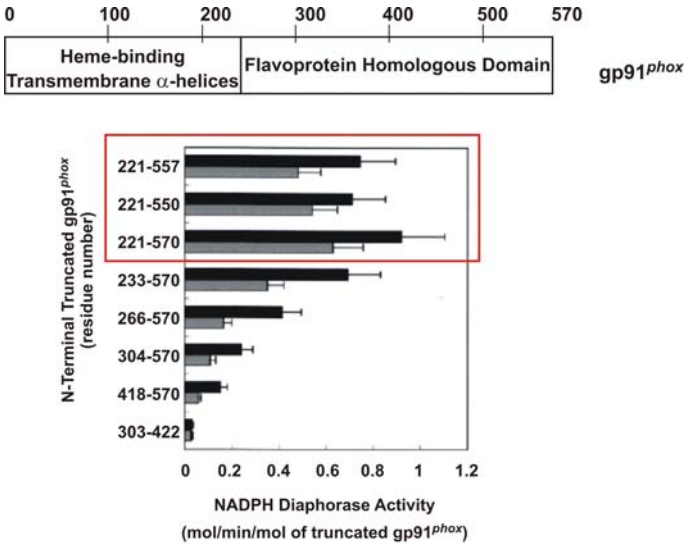

Figure 27. Domain structure of gp91^{phox} and activity of various C-terminal truncations, with the longest construct and equivalent constructs containing truncations of the last 13 and 20 residues boxed in red. Figure from Nisimoto *et al*, 2004.

H_6-Nox1$_{cyt}$

As mentioned earlier, alternative constructs were designed in case the thioredoxin tag was found to interfere. A vector containing an N-terminal His-tag followed by a TEV protease site (kindly provided by Dr. Kirill Alexandrov, MPI of Molecular Physiology, Dortmund) was used to produce a simple His-tagged construct of the cytosolic domain of human Nox1, here referred to as H_6-Nox1$_{cyt}$. In order to subclone the Δ1-289 human Nox1 insert into the vector, a Nde I site was introduced through PCR using Δ1-289 human Nox1 in pET 32a (the plasmid for Trx_E-Nox1$_{cyt}$) as a template. Vector and insert were each digested with Nde I and Xho I, and ligated after treating the digested vector with calf intestinal alkaline phosphatase to prevent vector re-ligation. Ligated plasmids were then transformed into competent XL1-Blue cells and positive clones were identified through agarose gel

electrophoresis of restriction enzyme digests and PCR reactions of isolated plasmids. Sequences were verified with DNA sequencing.

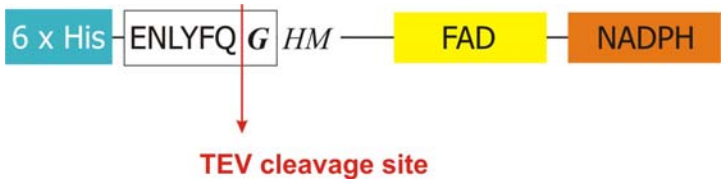

Figure 28. Schematic of the H_6-Nox1$_{cyt}$ construct. This construct contains an N-terminal His-tag removable by TEV protease, followed by a three amino acid insertion (which results from the TEV protease site and the *Nde*I restriction site) that directly precedes the cytosolic portion (residues 290-564) of human Nox1.

H_6-Nox1$_{cyt}$ was expressed in C41(DE3) competent cells, according to guidelines worked out previously for Trx$_E$-Nox1$_{cyt}$. Cells were induced at low cell density (0.3-0.5) with low amounts of IPTG (0.05 mM or 0.1 mM final concentration) and overnight incubation at 20°C. Reasonable and reproducible expression was only obtained from freshly transformed cells grown in rich media such as TB or ST1, with ST1 as the preferred media. TB media tended to produce twice as much cells for similarly sized cultures, which made the purification more cumbersome and time-consuming, without necessarily providing more protein in the end. Similar to Trx$_E$-Nox1$_{cyt}$, H_6-Nox1$_{cyt}$ showed predominant expression in the insoluble fraction, although some amount of protein could be purified from the soluble portion.

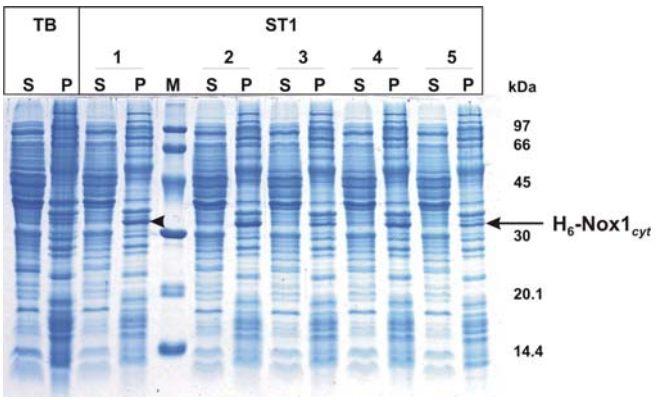

Figure 29. Comparison of H_6-Nox1$_{cyt}$ expression in TB vs. ST1 media. 1L cultures were grown to OD_{600} of ~0.52 for each media and protein expression was induced with a final concentration of 0.1 mM IPTG overnight at 20°C. The amount of harvested cells from TB media (15.12g) was more than twice that from ST1 (*1*, 6.48 g; *2*, 7.42g; *3*, 6.51g; *4*, 6.69g; *5*, 6.36g). Arrowheads indicate H_6-Nox1$_{cyt}$ expression, which is more obvious from ST1 cultures and predominantly in the pellet. They also indicate the variability of expression often observed, even with equivalent cell amounts (compare *1* with *3*).

H_6-Nox1$_{cyt}$ was purified via Ni-NTA chromatography and the enhanced binding capability of this construct allowed for improved separation from impurities in a single chromatographic step by lengthening the linear gradient from the original 70 ml to 250 ml. This proved to be necessary in light of the greater instability of H_6-Nox1$_{cyt}$ and the preclusion of many chromatographic techniques that require low salt binding conditions.

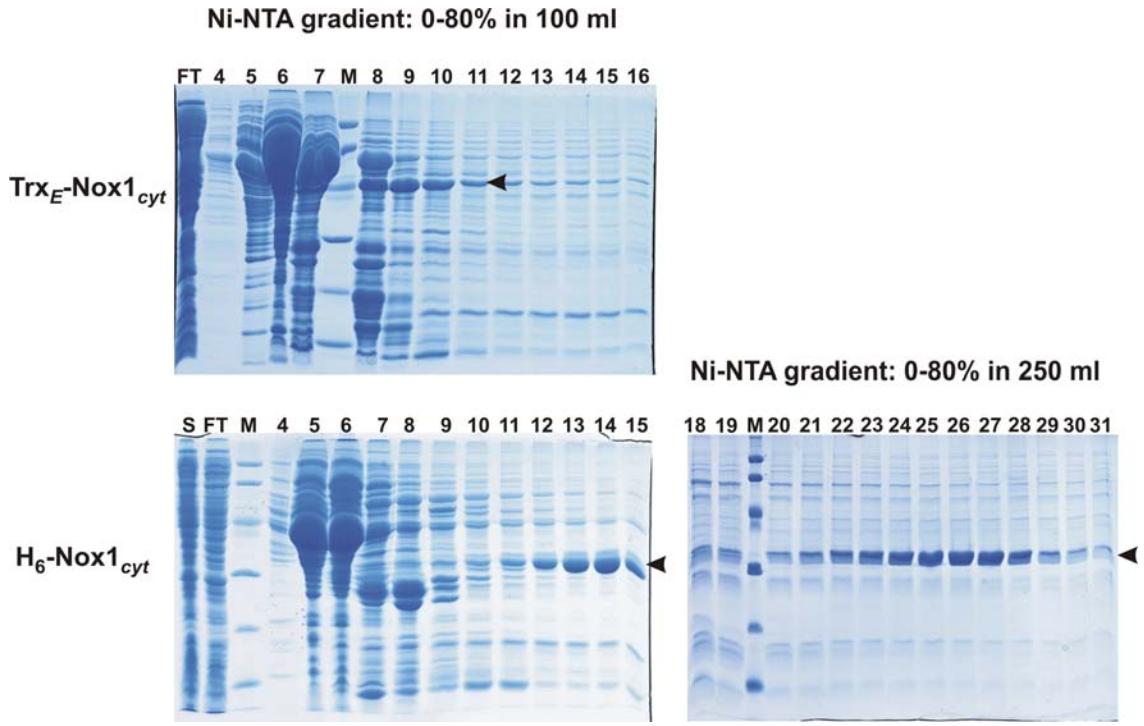

Figure 30. Enhanced binding of H_6-Nox1$_{cyt}$ and improved separation with Ni-NTA chromatography. SDS-PAGE analysis of fractions from H_6-Nox1$_{cyt}$ and Trx$_E$-Nox1$_{cyt}$ Ni-NTA chromatography with equivalent linear gradients revealed the greater binding capacity of H_6-Nox1$_{cyt}$. This property was exploited to maximize the extent of purification over a single chromatographic step through an extension of the gradient to 250 ml. *FT* stands for Flow through, *S* stands for supernatant, *M* stands for Markers, and numbers indicate fraction numbers. Arrowheads indicate Trx$_E$-Nox1$_{cyt}$ and H_6-Nox1$_{cyt}$, respectively.

Attempts to further purify H_6-Nox1$_{cyt}$ over 2'5' ADP Sepharose 4B revealed the particular sensitivity of the cytosolic domain of human Nox1, and its requirement of high concentrations of salt in the buffer. Any attempt to reduce the NaCl concentration (either by dialysis or simple dilution with a buffer not containing NaCl) for application on 2'5' ADP Sepharose 4B resin resulted in the prompt precipitation of the protein. One trial also tested the possibility of directly loading the Ni-NTA fractions onto 2'5' ADP Sepharose 4B resin, but only 7% of the loaded protein bound the column, reducing the usefulness of this effort

(data not shown). This sensitivity to salt was not noticed initially with Trx_E-$Nox1_{cyt}$ possibly because the thioredoxin tag (pI = 4.67) might have interacted favorably with the basic (pI = 8.45) cytosolic domain of human Nox1. Additionally, these samples contained many contaminating proteins that may have interacted with the cytosolic domain of human Nox1, shielding the areas that would normally precipitate if isolated. It should be noted that the higher the purity of the construct, the greater the instability of the protein and the tendency for it to precipitate (including later purifications of Trx_E-$Nox1_{cyt}$ which showed improved separation from impurities after Ni-NTA affinity chromatography). Early purifications of either Trx_E-$Nox1_{cyt}$ or H_6-$Nox1_{cyt}$ from Ni-NTA chromatography with substantial amounts of contaminating proteins did not show the same sensitivity to reduction in the NaCl concentration (Figure 31). An alternative approach to a single Ni-NTA chromatographic step might be to use a short gradient during the Ni-NTA chromatography, in order to increase the presence of stabilizing contaminating proteins, followed by 2'5' ADP Sepharose 4B chromatography, since H_6-$Nox1_{cyt}$ should be stabilized in the high salt 1M NaCl elution.

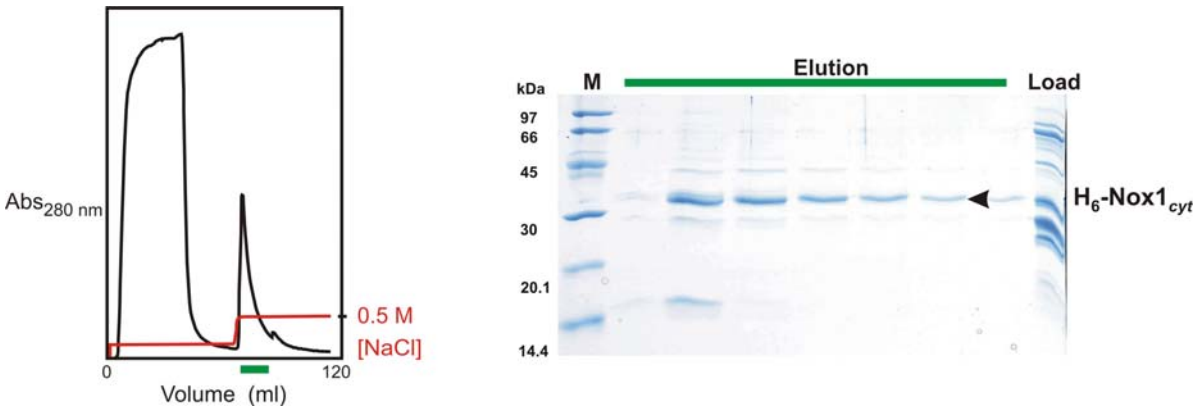

Figure 31. Purification of H_6-$Nox1_{cyt}$ with 2'5' ADP Sepharose 4B chromatography using a sample from a single step elution from Ni-NTA resin, that had also been purified with size exclusion chromatography. *Load*, indicates the sample loaded onto the column; green bars identify the elution peak and respective fractions on the SDS-PAGE. Arrowhead indicates H_6-$Nox1_{cyt}$. *M*, molecular weight markers.

The greater sensitivity of H_6-$Nox1_{cyt}$ necessitated a few adjustments as to how it was handled, in contrast to Trx_E-$Nox1_{cyt}$. The H_6-$Nox1_{cyt}$ protein not only required high salt for stability, but also had a greater tendency to be retained on the membranes of most

conventional centrifugal concentration devices. To remedy this, static concentrators (Vivapore, Sartorius, Göttingen), which use solvent absorption to concentrate the sample of interest, proved to be more effective at concentrating H_6-$Nox1_{cyt}$ without large losses in protein yield. It was important to not over-concentrate the protein, since this increased the likelihood for soluble aggregates to form. Additionally, standard methods for determining the protein concentration could not be used due to the presence of a high concentration of imidazole still present in the pooled fractions after Ni-NTA chromatography (which interferes with most standard methods such as Bradford assay and absorbance determination at 280 nm). Attempts to reduce the imidazole concentration by dialysis also resulted in prompt precipitation of the protein. Therefore, the Ni-NTA protein fractions were diluted until the imidazole concentration was between 200-300 mM and then concentrated. The high glycerol content (10%) in the buffer also interfered with the Ehresmann protein concentration determination method. For these reasons, SDS-PAGE analysis was used in lieu of standard methods to estimate protein concentration. This was done by running a series of known amounts of a low molecular weight marker (Amersham Biosciences/GE Healthcare) alongside various amounts of H_6-$Nox1_{cyt}$ and comparing these with the chymotrypsin marker at 30 kDa in the known series. The general solubility limit of H_6-$Nox1_{cyt}$ was 1-1.4 mg/ml, with typical yields of 3.15 mg/3L to 7.7 mg/5L. Western blot analysis confirmed the purified protein to be H_6-$Nox1_{cyt}$.

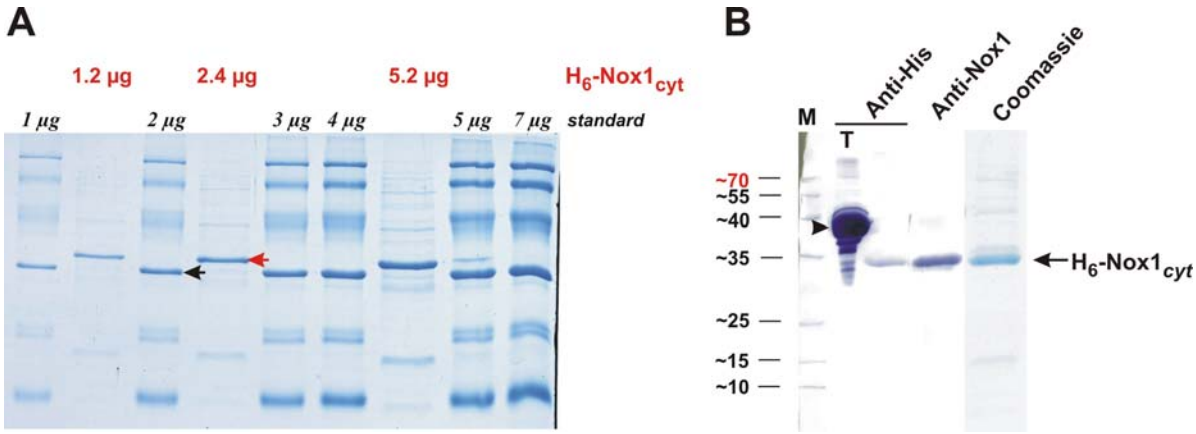

Figure 32. *A*, Determination of H_6-$Nox1_{cyt}$ protein concentration by SDS-PAGE analysis. Defined amounts of a low molecular weight marker were loaded in series alongside various amounts of H_6-$Nox1_{cyt}$ (red arrowhead). The amount of H_6-$Nox1_{cyt}$ protein loaded was estimated by visual comparison with the 30 kDa molecular weight marker (black arrowhead). Protein concentration was calculated as µg/µl loaded. *B*, Western Blot confirmation of the Ni-NTA purified protein as H_6-$Nox1_{cyt}$ with Anti-His tag and Anti-Nox1 antibodies. *M* stands for Markers, *T* (black arrowhead) indicates Trx_E-$Nox1_{cyt}$ used as a positive control for the Anti-His tag antibody since H_6-$Nox1_{cyt}$ stained more weakly.

Trx_T-$Nox1_{cyt}$

As a second alternative, a construct similar to Trx_E-$Nox1_{cyt}$ was made containing a different protease site for removal of the N-terminal tags. This construct contains a TEV protease site instead of the enterokinase protease site. Although the thioredoxin tag was later found to interfere with the NADPH-dependent activity assay (see Section 2.2.1), this construct may provide a way to stabilize the cytosolic domain during purification, while retaining the ability for removal of the tags with TEV protease for subsequent characterization experiments.

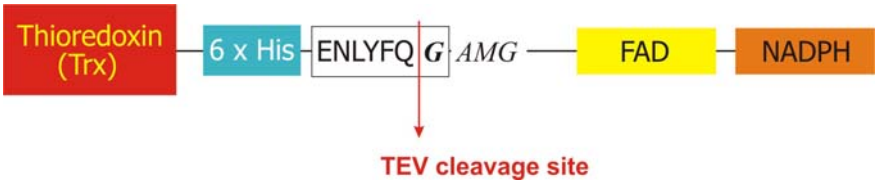

Figure 33. Details of the Trx_T-$Nox1_{cyt}$ construct. This fusion protein has the identical structure as the Trx_E-$Nox1_{cyt}$ construct, with the exception that the enterokinase protease cleavage site has been replaced with that of TEV protease, which adds an additional glycine to the short insertion before the beginning of the cytosolic domain of human Nox1.

Site directed mutagenesis was used to exchange the enterokinase protease cleavage site to that of TEV protease. This was done using the QuikChange® Site-Directed Mutagenesis Kit (Stratagene) in two sequential reactions: the first deleting the enterokinase site, and the second introducing the TEV site. The plasmid encoding the Trx_E-$Nox1_{cyt}$ construct was used as the initial template for the first deletion reaction. DNA sequencing identified positive clones, and this resulting plasmid was in turn used as the template for the second insertion reaction. DNA sequencing confirmed clones containing the TEV protease site.

Protein expression conditions worked out previously for the construct Trx_E-$Nox1_{cyt}$ were again employed for Trx_T-$Nox1_{cyt}$. These included transformation in C41(DE3) competent cells, early induction with 0.1 mM IPTG when the cell density reached approximately 0.3-0.45, and overnight incubation at 20°C. Initial expression of Trx_T-$Nox1_{cyt}$ proved to be reasonable and purification proceeded over Ni-NTA resin using step gradients containing 50, 100, and 250 mM Imidazole for elution. Trx_T-$Nox1_{cyt}$ began to elute primarily at 100 mM Imidazole and these fractions were pooled and further purified over size exclusion

chromatography containing 300 mM NaCl in the elution buffer. This chromatographic step proved to be quite effective, and although purified just short of homogeneity, this step may be an alternative to 2'5' ADP Sepharose 4B chromatography for protein preparations that are more sensitive to low salt conditions. Western blot analysis confirmed the ~ 45 kDa band to be Nox1 (Figure 34).

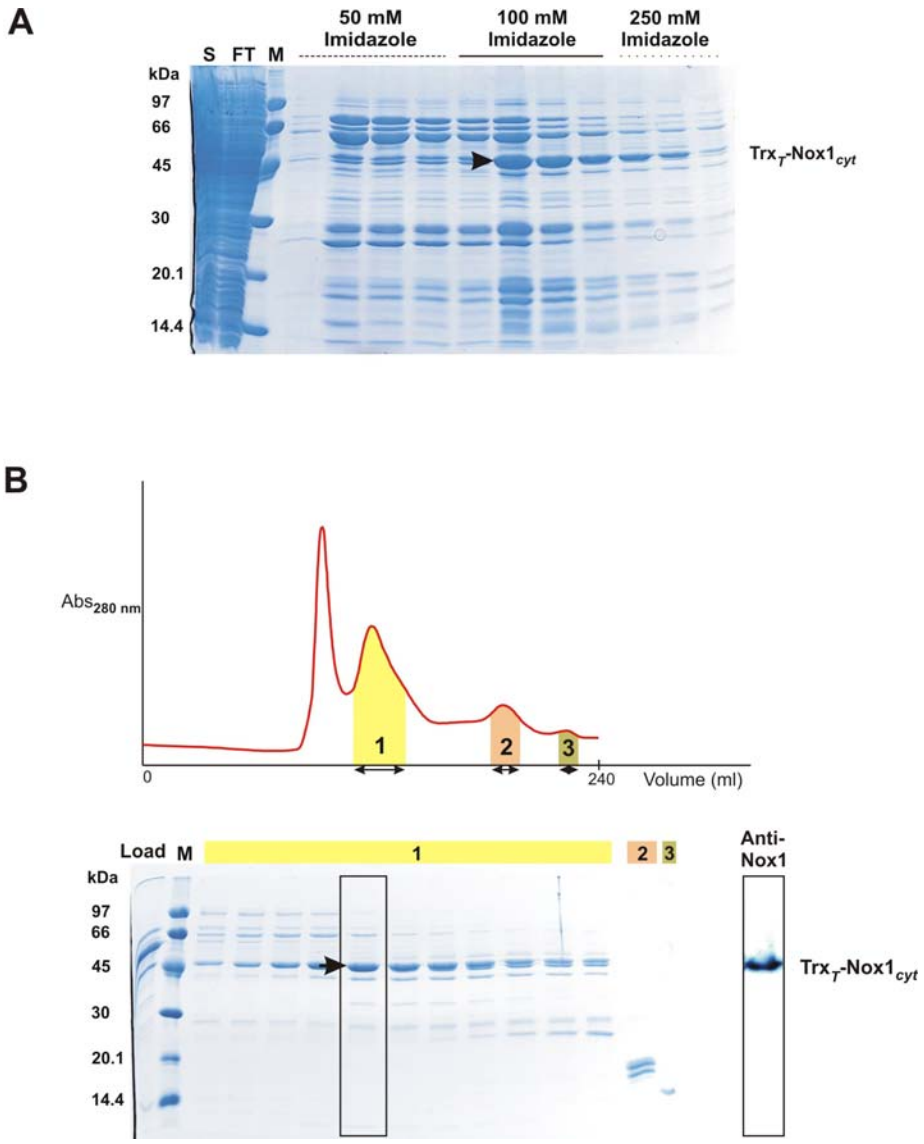

Figure 34. *A*, Ni-NTA purification of Trx$_T$-Nox1$_{cyt}$. Fractions from different step elutions with the indicated amounts of Imidazole in the elution buffer are shown. An arrow highlights Trx$_T$-Nox1$_{cyt}$, which runs slightly above the 45 kDa molecular weight marker. *S*, supernatant loaded on the column; *FT*, flow through; *M*, molecular weight markers. *B*, Chromatographic trace of further purification of Trx$_T$-Nox1$_{cyt}$ with size exclusion chromatography and SDS-PAGE of corresponding fractions. *Load*, indicates the sample loaded onto the column; *M*, molecular weight markers. Numbers indicate elution peaks and identify respective fractions on the SDS-PAGE. Western blot of boxed fraction using Anti-Nox1 antibody.

2.2 ASSESSMENT OF THE BIOLOGICAL INTEGRITY OF RECOMBINANT HUMAN NOX1 CONSTRUCTS

While determining the three dimensional structure of a new protein is significant in and of its own, it is additionally important to confirm that the purified protein is capable of native biological functions, and to relate the new structural insights to the functional role of the protein of interest. Of the four constructs, the two most promising constructs, namely Trx_E-$Nox1_{cyt}$ and H_6-$Nox1_{cyt}$, were further characterized with biochemical and biophysical methods. Biological activity was assessed with a NADPH-dependent diaphorase activity assay, which measures the electron transfer step from NADPH to FAD, using an artificial terminal electron acceptor. Of interest was whether the C-terminal truncation of human Nox1 was active and whether it contained the necessary regions to bind FAD and interact productively with cytosolic regulatory proteins.

Since the purification of Trx_E-$Nox1_{cyt}$ under denaturing conditions had the potential to generate more protein, the refolded Trx_E-$Nox1_{cyt}$ protein was characterized to determine if the refolding procedure resulted in a protein with native properties. The refolded Trx_E-$Nox1_{cyt}$ was found to have a slightly higher experimental pI, ~6.9 as determined by isoelectric focusing (Figure 35), compared to the calculated value of 6.35 using the ExPASy Proteomics Server (Gasteiger *et al.*, 2003).

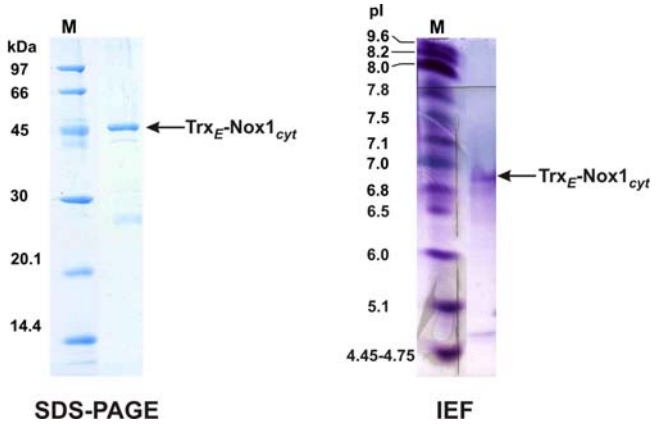

Figure 35. Isoelectric focusing gel of refolded Trx_E-$Nox1_{cyt}$. The left gel shows a SDS-PAGE of the sample loaded onto an IEF gel (right). *M* represents molecular weight markers.

Unfortunately, the Triton X-100 detergent was found to interfere with many of the methods used for characterization of the refolded Trx_E-$Nox1_{cyt}$. DLS measurements were performed

to determine if the sample was monodisperse, but the inclusion of Triton X-100 at a concentration 20 times the CMC (CMC = 0.015%, Anatrace Product Catalogue) meant that the machine detected the micelles (74 kDa) of the detergent, and could not distinguish between these and micelles containing a 48 kDa protein. This is a well known disadvantage of using DLS to determine the monodispersity of membrane proteins which require the presence of detergents, and is no longer routinely used to assess this property (NCCR course, 2004). While DLS is very useful to measure the size of detergent micelles, it cannot distinguish between two species if the difference in their molecular weights is less than 8-fold. To underscore this point, the manufacturer of DynaPro (Wyatt Technologies) admits that a mixture of standard proteins such as BSA (64 kDa) and lysozyme (14.7 kDa), which have a mass ratio of 4.4, cannot be resolved by DLS even at the highest resolution. Instead, the device measures the average radius for both particles (http://www.wyatt.com/solutions/hardware/DynaProTitan.cfm). Triton X-100 also interfered with standard protein concentration determination assays, such as Bradford. Additionally, it was found that an average lab stock of Triton X-100 was capable of reducing the terminal electron acceptor in the activity assay without the presence of the fusion protein. One disadvantage of using polyoxyethylene detergents such as Triton X-100 and Genapol X-80 is their ability to form peroxides from their reaction with oxygen, which is accelerated upon exposure to light (Lever, 1977; Miki and Orii, 1985; Jaeger *et al.*, 1994). Although purer grades can be commercially obtained that contain less than 200 µM peroxides (Calbiochem), any peroxide can interfere with the NADPH-dependent diaphorase activity assay, potentially giving false positives.

In contrast to the apparent stabilizing effects of 0.3% Triton X-100 or Genapol X-80 on C-terminal truncations of gp91^{phox}, significant precipitation was observed in the refolded Trx$_{E}$-Nox1$_{cyt}$ protein sample after only 2 days at 4°C. This prompted a small screen of a range of detergents from different classes to see whether there might be another more stabilizing detergent. This protocol was based on one which involved incubation of equal volumes of the target protein with a buffer containing approximately 10 times the CMC of a desired detergent and allowed to remain at 4°C for one week (NCCR course, 2004). This was done individually with a variety of detergents and the samples were then centrifuged after the incubation. Protein stability was determined by analyzing the amount remaining soluble after this procedure via SDS-PAGE. In this study, eight different detergents were tested: n-

Dodecyl-β-D-maltopyranoside (DDM), n-Decyl-β-D-maltopyranoside (DM), n-Octyl-β-D-glucopyranoside (OG), CHAPS, CYMAL-5, Fos-Choline-12, Triton X-100, and Genapol X-80. Of these, only Fos-choline-12 and the buffer control containing no detergent did not have any visible precipitation after centrifugation of the incubated samples. SDS-PAGE analysis of these samples indicated that the Trx_E-$Nox1_{cyt}$ fusion protein remained in the soluble fraction at levels similar to a freshly thawed control (Figure 36). Interestingly, both samples with either Triton X-100 or Genapol X-80 contained small but visible precipitation after centrifugation of the incubated samples, and at least with regards to the Trx_E-$Nox1_{cyt}$ fusion protein, these detergents may not stabilize the protein as effectively as was observed for the C-terminal truncations of $gp91^{phox}$.

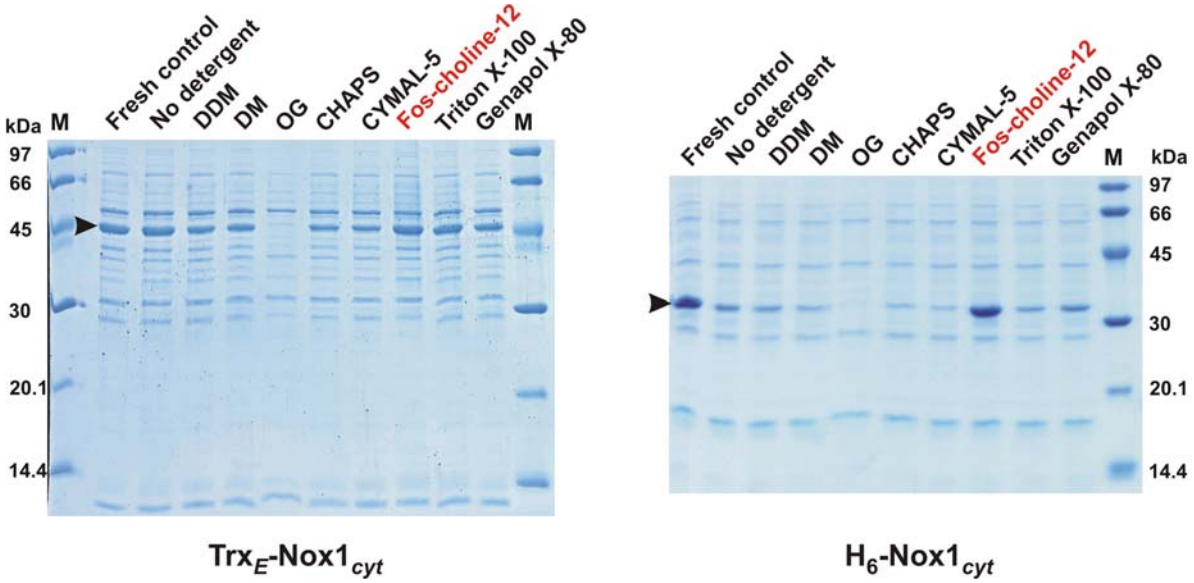

Figure 36. Stability of Trx_E-$Nox1_{cyt}$ and H_6-$Nox1_{cyt}$ in different classes of detergents. Detergent solutions containing 10 mM Tris-HCl, pH 7.5, 100 mM NaCl, and the following detergent concentrations were incubated 1:1 v/v with Trx_E-$Nox1_{cyt}$ for 9 days or H_6-$Nox1_{cyt}$ for 7 days at 4°C: 0.2% DDM, 2% DM, 5% CHAPS, 1.2% CYMAL-5, 0.5% Fos-choline-12, 0.15% Triton X-100, and 0.083% Genapol X-80. Due to solubility issues, OG was used as a 10% aqueous solution without buffer or NaCl. A non-detergent control was also made: using the storage buffer for Trx_E-$Nox1_{cyt}$, 10 mM NaH_2PO_4, 500 mM NaCl, 10% glycerol, 2 mM DTE, pH 8.0; for H_6-$Nox1_{cyt}$, using 10 mM Tris-HCl, pH 7.5 and 100 mM NaCl. Total protein amount is indicated by a gel sample made just before running the SDS-PAGE from freshly thawed protein (Fresh control). All gel samples (excluding markers) were made without boiling at 100°C. Arrowheads point to Trx_E-$Nox1_{cyt}$ and H_6-$Nox1_{cyt}$ respectively. *M* represents molecular weight markers.

A similar detergent screen was performed on H_6-$Nox1_{cyt}$, which also identified Fos-choline-12 as the only detergent of those tested that was able to maintain H_6-$Nox1_{cyt}$ in the soluble

fraction (Figure 36). H_6-Nox1$_{cyt}$ appears to be more sensitive than Trx_E-Nox1$_{cyt}$ to many common detergents, with very little of the protein remaining soluble after incubation. This includes Triton X-100 and Genapol X-80. These results explain the lack of improved stability observed when 0.3% Triton X-100 was included in a purification of H_6-Nox1$_{cyt}$. Park *et al* have included 1% Triton X-100 in buffers used for pull down assays, where various Nox1 truncations were bound to GST resin to serve as bait for investigations of various protein-protein interactions (Park *et al.*, 2006). Although in the present work, 2% Triton X-100 was found to effectively extract all of H_6-Nox1$_{cyt}$ from the pellet fraction after lysis, the protein precipitated once it was eluted from the Ni-NTA column (data not shown). The stability of truncated Nox1 in a detergent may therefore be less obvious when the protein is still retained on the resin, as opposed to being free in solution.

2.2.1 NADPH-dependent diaphorase activity of recombinant human Nox1 constructs

Intrinsic activity

Nox proteins catalyze the one-electron reduction of molecular oxygen using the two-electron donor NADPH as an electron source:

$$2\ O_2 \ + \ NADPH \ \rightarrow \ 2\ O_2^{\cdot -} \ + \ NADP^+ \ + \ H^+$$

It was additionally discovered that cytochrome b_{558} is capable of a NADPH-dependent diaphorase activity, which was independent from superoxide production (Cross *et al.*, 1994). Diaphorase refers to a flavoprotein capable of oxidizing NADPH. This diaphorase activity has been utilized to measure the intrinsic activity of various recombinant C-terminal truncations of gp91^{phox}, as well as the effect of cytosolic regulatory proteins on this activity *in vitro* (Han *et al.*, 2001; Nisimoto *et al.*, 2004). The first step of electron transfer involving NADPH and FAD can be studied using an artificial terminal electron acceptor such as the dye nitroblue tetrazolium (NBT) or cytochrome *c*, which, upon reduction, undergoes a spectrophotometric change that can be monitored over time. This work utilized NBT as the final electron acceptor since studies made on C-terminal truncations of gp91^{phox} demonstrated higher turnover rates using NBT (Han *et al.*, 2001; Nisimoto *et al.*, 2004). NBT is a dye that changes color from yellow to purple upon reduction, and can be monitored spectrophotometrically at 595 nm.

Determination of the NADPH-dependent diaphorase activity of the natively purified Trx_E-$Nox1_{cyt}$ revealed some inherent limitations of this construct. The activity of the recombinant Trx_E-$Nox1_{cyt}$ protein was assayed using a cell-free assay developed for cytosolic truncations of $gp91^{phox}$ (Han *et al.*, 2001; Nisimoto *et al.*, 2004). Unfortunately, low amounts of DTE/DTT used in the buffer for Trx_E-$Nox1_{cyt}$ (18 μM) were enough to reduce NBT at a rate similar to the intrinsic rate of H_6-$Nox1_{cyt}$ (see below). Since the thioredoxin tag itself is also capable of sulfhydryl redox chemistry, it would interfere with the assay as well. It should be noted that the authors who studied the C-terminal truncations of $gp91^{phox}$ also began with N-terminally tagged thioredoxin fusion proteins of their constructs and also found that DTT interfered with the assay (Han *et al.*, 2001). Their subsequent work (Nisimoto *et al.*, 2004) utilized N-terminal His-tagged fusion proteins instead.

To determine if H_6-$Nox1_{cyt}$ possessed the necessary regions of the protein to be biologically active, its activity was also tested using this NADPH-dependent diaphorase activity assay. Performing the assay in 1 ml cuvettes, H_6-$Nox1_{cyt}$ was found to possess a low intrinsic NADPH-dependent diaphorase activity of 0.19 mol reduced NBT/min/mol H_6-$Nox1_{cyt}$. Due to the large consumption of protein for these spectrophotometric activity measurements, the assay was modified for microtiter format. This had the additional advantage that several samples could be assayed simultaneously, including all necessary buffer controls. All samples could be rapidly (within 5 minutes) and uniformly heated, which simplified the cumbersome handling experienced with the 1ml assay version. In the microtiter format, the protein concentration used for the 1 ml spectrophotometric format was too low to generate absorbance signals at 595 nm with a satisfying signal-to-noise ratio. Therefore, the protein concentration was increased in the microtiter format. Both 5-fold (2.3 μM) and 10-fold (4.6 μM) increases in protein concentration produced acceptable signals. Due to limitations in protein yields, a concentration of 2.3 μM was used in subsequent assays.

The measured intrinsic NADPH-dependent diaphorase activity of H_6-$Nox1_{cyt}$ was found to depend on the amount of soluble aggregation in the purified sample. A protein batch that was later found to contain a large percentage of soluble aggregates (Figure 37, see next section) showed a low activity (0.22 mol reduced NBT/min/mol H_6-$Nox1_{cyt}$). A second batch of mostly non-aggregated H_6-$Nox1_{cyt}$ (Figure 38, see next section) displayed a markedly higher activity (0.95 mol reduced NBT/min/mol H_6-$Nox1_{cyt}$). This activity is

roughly 4-fold higher than that of a truncated gp91^{phox} protein of roughly similar length (residues 304-570), and is similar in magnitude to the activity of a longer truncated gp91^{phox} (residues 221-570) (Table 1) which showed the highest activity in a series of truncated gp91^{phox} constructs (Nisimoto *et al.*, 2004).

Table 1. Comparison of *in vitro* NADPH-dependent diaphorase activity of purified H_6-Nox1$_{cyt}$ (this work) to truncated gp91^{phox} proteins and intact cytochrome b_{558}, as well as to *in vivo* values. Calculations of electron flow assume that NBT is a 4 electron acceptor.

Protein	Truncation	Assay format	Activity (mol reduced NBT/min/mol Nox)	electron flow (electrons/min/molecule Nox)
in vitro (present work)				
Nox1	290-564	spectrophotometric	0.19	0.76
Nox1 *mostly aggregated*	290-564	microtiter	0.22	0.88
Nox1	290-564	microtiter	0.95	3.8
in vitro (literature values)				
gp91^{phox}	304-570	spectrophotometric	0.24 [a]	0.96[*]
gp91^{phox}	266-570	spectrophotometric	0.41 [a]	1.64[*]
gp91^{phox}	221-570	spectrophotometric	0.92 [a]	3.68[*] (0.92 [a ‡])
cytochrome b_{558}	none	NR	NR	6.5 [a]
cytochrome b_{558}, solubilized from phorbol-stimulated pig neutrophils	none	spectrophotometric	782 mol $O_2^{\cdot -}$/min/mol cyt b_{558} [b *]	30.4[*]
in vivo				
Protein			Activity (mol $O_2^{\cdot -}$/min/mol Nox)	
Nox1, unstimulated VSMCs			0.21 [c *]	0.21[*]
Nox1, Angiotensin II stimulated VSMCs			0.77 [c *]	0.77[*]
Nox1, unstimulated gastric guinea pig cells			0.011 [d *]	0.011[*]
Nox1, LPS stimulated gastric guinea pig cells			0.11 [d *]	0.11[*]

[a]Nisimoto *et al*, 2004; [b]Cross *et al*, 1985; [c]Griendling, *et al*, 1994; [d]Kawahara *et al*, 2005. *LPS*, lipopolysaccharides from *Helicobacter pylori.* [*]Calculated from values reported in the literature. [‡]For this value, the authors appear to have assumed that NBT is a single electron acceptor. *NR,* not reported.

Although the intrinsic activity of H_6-Nox1$_{cyt}$ is low if compared to the catalytic output of the phagocytic oxidase, it is consistent with the biological function of Nox1 as a source of low-level constitutive superoxide production, observed from *in vivo* studies (Table 1). Even with roughly 50% homology, many of the nonphagocytic Nox proteins produce superoxide at levels 10% or less than that of the phagocytic oxidase. The electron transfer rate of 3.8 electrons/min/molecule H_6-Nox1$_{cyt}$ is higher than that calculated from *in vivo* superoxide production by Nox1 in various tissues, which suggests that electron transfer by the truncated protein may occur via a different mechanism *in vitro*.

Effect of Fos-choline-12 on the intrinsic NADPH-dependent diaphorase activity of H_6-Nox1$_{cyt}$

The microtiter-format activity assay was exploited to address whether the detergent Fos-choline-12 was able to increase the intrinsic activity of H_6-Nox1$_{cyt}$ through increased stabilization of the protein. NADPH-dependent diaphorase activity was measured with and without Fos-choline-12 at various multiples of the CMC. Fos-choline-12 was capable of slightly increasing the activity of H_6-Nox1$_{cyt}$ at a concentration 2x the CMC (3 mM), but this effect was found to depend strongly on the protein batch, and the extent of soluble protein aggregation in the sample. In one batch, where a majority of the protein was present as soluble aggregates, this slight enhancement in activity was observed (Figure 37). In contrast, when another predominantly monomeric H_6-Nox1$_{cyt}$ batch was assayed, Fos-choline-12 actually decreased the intrinsic activity of H_6-Nox1$_{cyt}$ (Figure 38). These results indicate that while 3 mM Fos-choline-12 may improve re-solubilization of soluble aggregates of H_6-Nox1$_{cyt}$, it may not necessarily be required for optimal activity in monodisperse preparations.

It is important to note that freshly prepared solutions of Fos-choline-12, in contrast to Triton X-100, was not capable of reducing NBT, and thus does not interfere with the assay under the conditions tested (60 minutes at 37°C). Solutions made from an aqueous 10% stock solution of Fos-choline-12 (although stored at 4°C under Argon) were, however, capable of partially reducing NBT to its half-reduced form which is magenta pink in color (Altman, 1974), emphasizing the importance of making the detergent solutions fresh from solid if they are to be included.

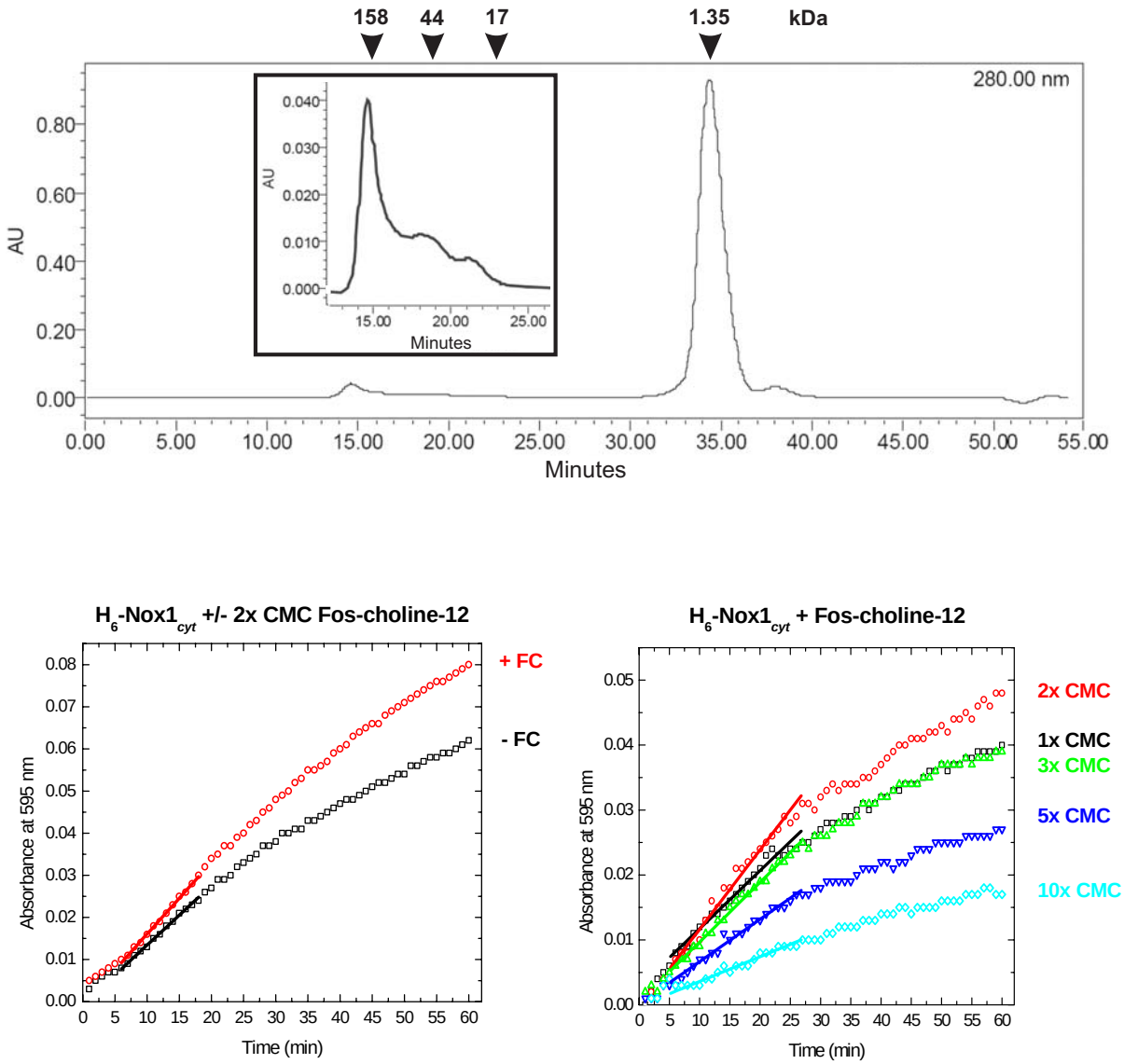

Figure 37. Analytical gel filtration of a batch of H_6-Nox1$_{cyt}$ with a large amount of aggregation in the sample (inset). H_6-Nox1$_{cyt}$ (33.5 kDa) was incubated with a 50-fold molar excess of FAD at 4°C for at least 1 hour. 95 µg was injected over an analytical Superdex 75 column pre-equilibrated with 20 mM NaH_2PO_4, pH 7.3, 300 mM NaCl, 250 mM Imidazole, and 10% glycerol. Arrowheads indicate elution profile of gel filtration standards. Corresponding effects of various concentrations of Fos-choline-12 (FC) on the intrinsic NADPH-dependent activity of this sample.

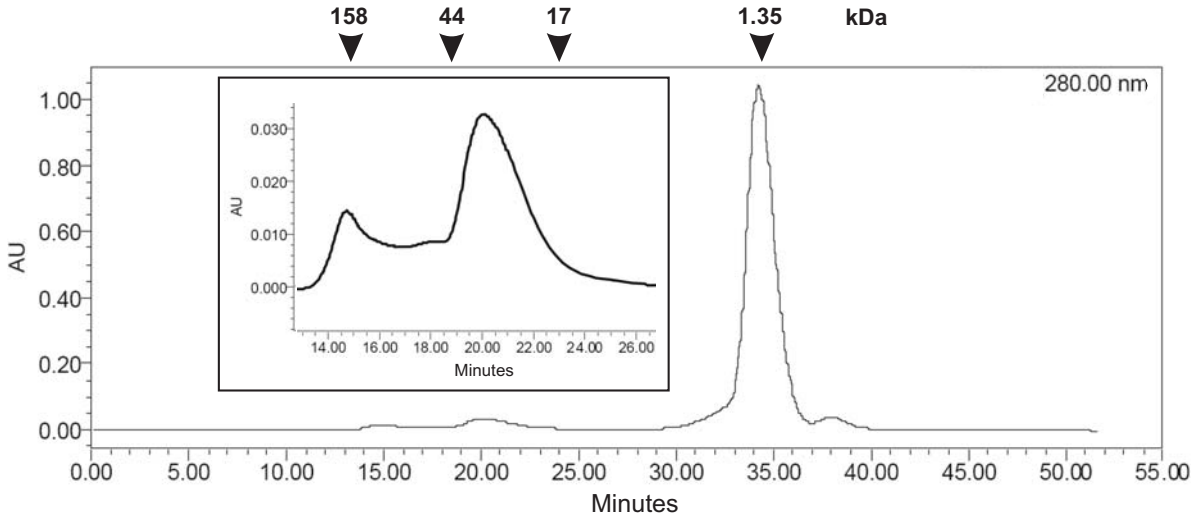

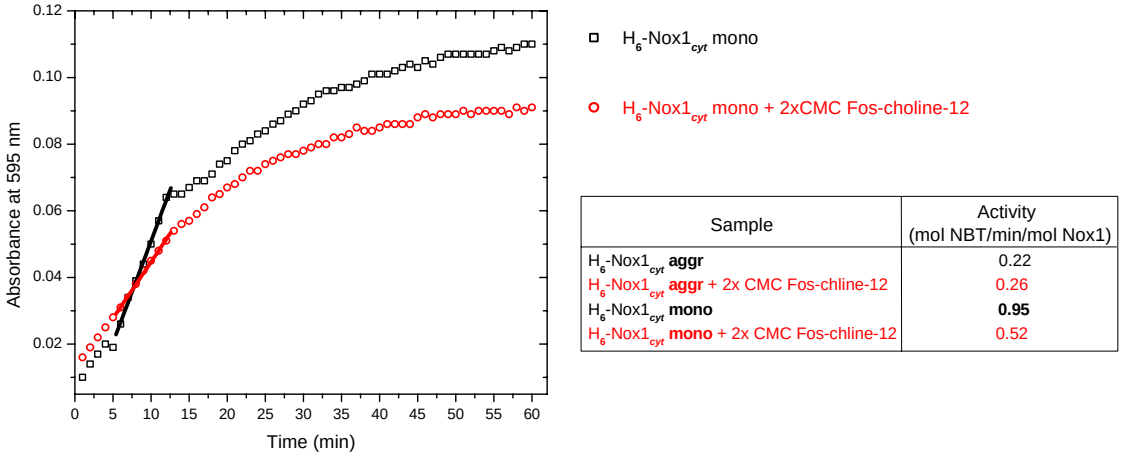

Sample	Activity (mol NBT/min/mol Nox1)
H_6-Nox1$_{cyt}$ **aggr**	0.22
H_6-Nox1$_{cyt}$ **aggr** + 2x CMC Fos-chline-12	0.26
H_6-Nox1$_{cyt}$ **mono**	**0.95**
H_6-Nox1$_{cyt}$ **mono** + 2x CMC Fos-chline-12	0.52

Figure 38. Analytical gel filtration of a more monomeric batch of H_6-Nox1$_{cyt}$ (inset). H_6-Nox1$_{cyt}$ (33.5 kDa) was incubated with a 25-fold molar excess of FAD at 4°C for at least 1 hour. 264 µg was injected over an analytical Superdex 75 column pre-equilibrated with 20 mM NaH_2PO_4, pH 7.3, 300 mM NaCl, 250 mM Imidazole, and 10% glycerol. Arrowheads indicate elution profile of gel filtration standards. Effect of 2x CMC Fos-choline-12 on the intrinsic NADPH-dependent activity of this sample.

2.2.2 Interaction of recombinant human Nox1 constructs with regulatory oxidase proteins

An important question to address was whether the C-terminal truncation of human Nox1 contained all the necessary regions of the protein to interact with regulatory proteins. Although Nox1 possesses its own cytosolic regulators, Noxo1 and Noxa1, the human proteins were found to be much more difficult to work with than their phagocytic oxidase counterparts (Dr. Yvonne Groemping, personal communication). In light of the high degree of difficulty in handling the Nox1 constructs alone and the ability of Nox1 to interact with phagocytic oxidase regulatory proteins, a recent description of a recombinant fusion of $p67^{phox}$ and Rac that acts as a minimal activator of cytosolic truncations of $gp91^{phox}$ in a cell-free assay (Miyano *et al.*, 2001; Nisimoto *et al.*, 2004) was selected as a more realistic tool to probe this question. This fusion protein, p67N-Rac, contains the N-terminal Rac-binding TPR domain and activation domain (residues 1-210), followed by a three amino acid linker (Ser-Glu-Phe), and Rac1 containing a point mutation (C189S) in a cysteine that undergoes prenylation, maintaining Rac in a soluble form (Kreck *et al.*, 1994). p67N-Rac containing a constitutively active Rac1 mutation (Q61L) was also described and both proteins were used in these studies.

Expression and purification of p67N-Rac fusion proteins

Plasmids containing the two fusion proteins, p67N-Rac and p67N-Rac(Q61L) were a kind gift from Dr. Minoru Tamura (Ehime University, Japan). Since the description of the expression and purification of the fusion proteins was very general, the detailed procedures were also experimentally developed. p67N-Rac and p67N-Rac(Q61L) were expressed in the *E. coli* strain BL21(DE3), and although described as being expressed at 37°C for 2.5 hours after the addition of IPTG, little soluble expression was actually observed under these conditions. For this reason, lower temperature (20°C) and a reduced IPTG concentration (0.05mM final) were employed and found to remedy this problem (Figure 39). Protein expression was normally determined using Bug Buster® Protein Extraction Reagent (Novagen) for lysis of analytical cell amounts, and although this often revealed little soluble expression, substantial amounts of both p67N-Rac and p67N-Rac(Q61L) were observed in the soluble fraction after lysis with a microfluidizer.

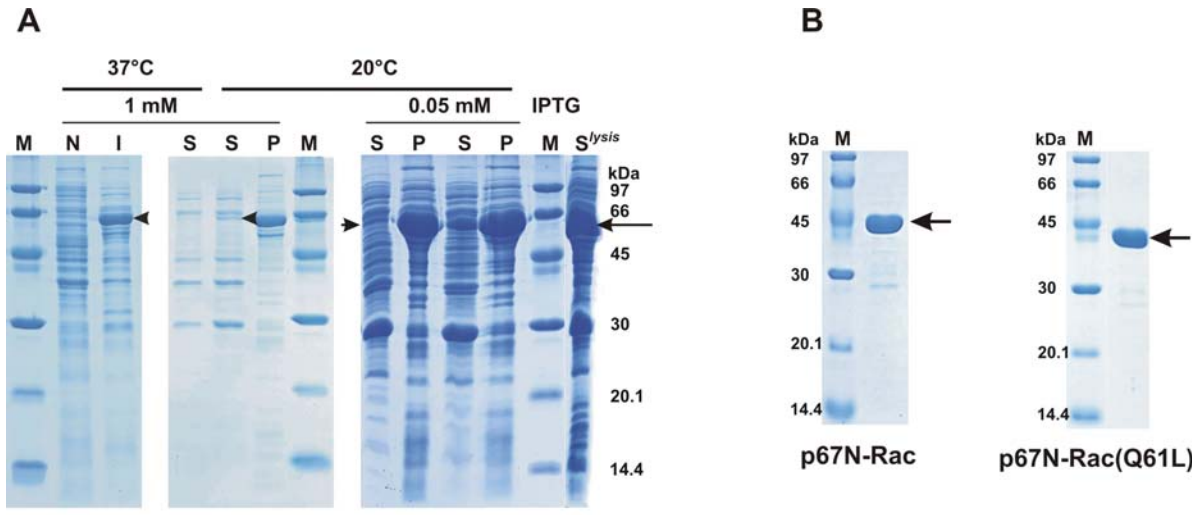

Figure 39. *A*, Expression of p67N-Rac following published protocols (37°C), and with adjustments in the expression conditions (20°C). Arrows indicate p67N-Rac. *M*, molecular weight markers, *N*, non-induced, *I*, induced, *S*, supernatant, *P*, pellet, S^{lysis}, supernatant after lysis. *B*, SDS-PAGE of the final purified p67N-Rac and p67N-Rac(Q61L) fusion proteins.

Since p67N-Rac and p67N-Rac(Q61L) are expressed as GST fusion proteins, they were purified with glutathione sepharose affinity chromatography. The high level of expression of both fusion proteins allowed for nearly exclusive binding to the affinity resin. Elution of p67N-Rac or p67N-Rac(Q61L) was initially performed with thrombin digestion as described, which cleaves after the GST tag. However, the digestion was not every efficient on the column, with a majority of the GST-fusion protein still bound to the resin. Thrombin digestion after elution of the GST-fusion proteins from the glutathione sepharose proved to be more effective, but required a week for complete digestion at 4°C. Thrombin was removed with Benzamidine chromatography and p67N-Rac or p67N-Rac(Q61L) was collected after a second glutathione chromatographic step to capture any uncut protein and GST tag. Purification was completed with size exclusion chromatography. MALDI-TOF analysis confirmed the expected molecular mass of the purified p67N-Rac (45,976.67 expected, 46,359.2 measured). The yields of both p67N-Rac (85 mg/1L medium) and p67N-Rac(Q61L) (70 mg/1L medium) after these adjustments were found to be substantially better than published yields (1-2 mg/L medium).

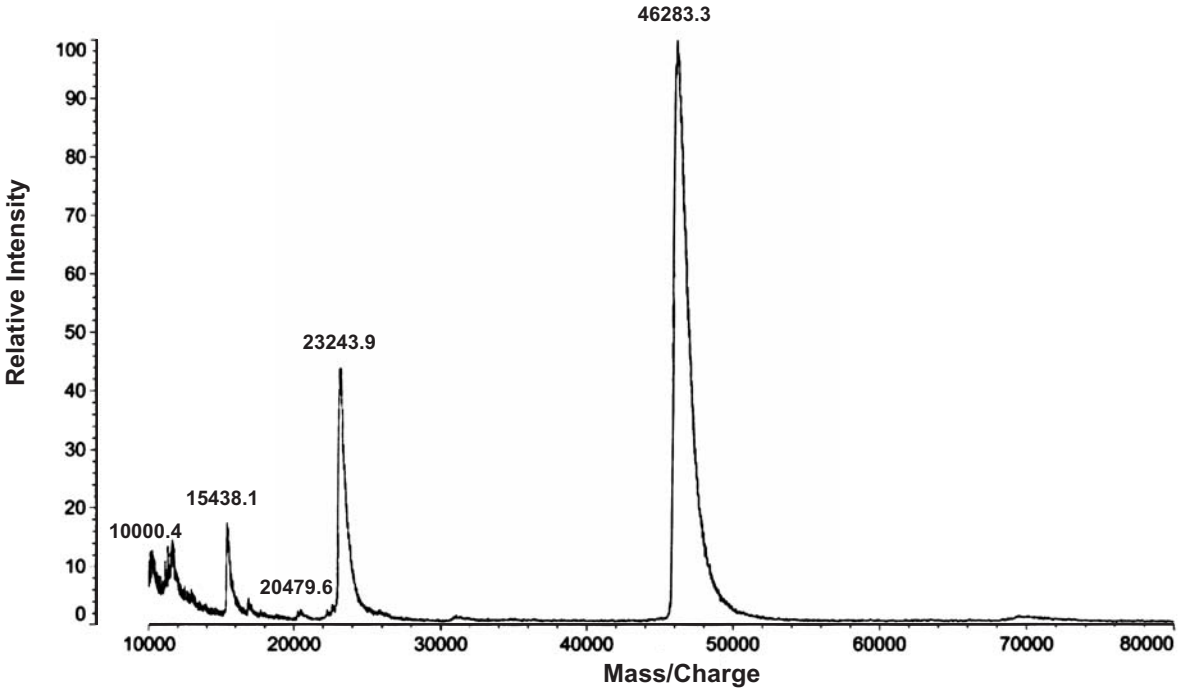

Figure 40. MALDI spectrum of purified p67N-Rac, with a measured mass of 46,283.3 Da.

To ensure that the constitutively active Rac1 mutant did not hydrolyze GTP under the conditions to be used in the NADPH-dependent diaphorase assay, the intrinsic GTPase activity of p67N-Rac(Q61L) was measured at 37°C over several days. As can be seen in Figure 41, the amount of GTP bound did not change significantly even after 5 hours incubation at 37°C.

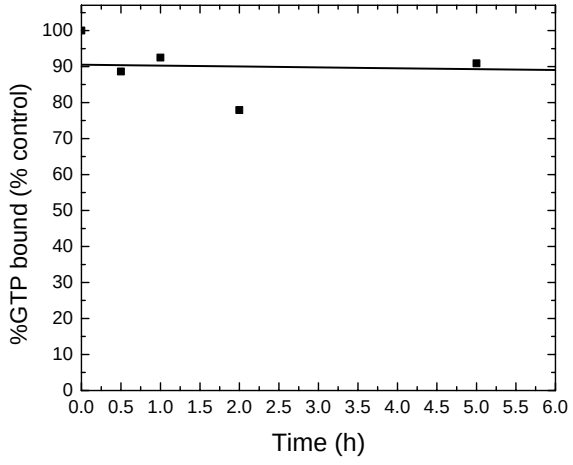

Figure 41. Intrinsic GTPase activity of p67N-Rac(Q61L) at 37°C. Aliquots were removed at the indicated times and analyzed in triplicate by HPLC.

Probing protein-protein interactions

Several methods were used to determine whether the truncated Nox1 protein was capable of interactions with cytosolic regulatory proteins. A pull-down assay using GST-p67N-RacQ61L•GTP as bait was made to determine if H_6-Nox1$_{cyt}$ could be captured from *E.coli* lysate. High salt in the H_6-Nox1$_{cyt}$ lysis buffer, however, could have prevented any interaction, revealing the shortcomings of using this method due to the major instability of H_6-Nox1$_{cyt}$ in low salt buffers. Other methods were tested to see if they would report directly on a possible interaction. Previous studies by others on the interaction of p67^{phox} with Rac utilized fluorescence changes as reported by mantGppNHp, a fluorescent, nonhydrolyzable analogue of GTP. Fluorescence was found to increase upon binding of p67^{phox} to Rac•mantGppNHp (Nisimoto *et al.*, 1997). These experiments were extended in this work to determine if any interaction between the p67N-Rac fusion protein and Nox1$_{cyt}$ also produced a change in fluorescence. Due to a lack of stability in the buffer used for fluorescence measurements (which was identical to that used in Nisimoto *et al.*, 1997), Trx$_E$-Nox1$_{cyt}$ was used instead of H_6-Nox1$_{cyt}$. Initial fluorescence measurements indicated a slow, substantial increase (46.7%) in the fluorescence emission at 445 nm upon the addition of p67N-Rac•GDP to mantGppNHp, representing the exchange of the Rac-bound GDP for the fluorescently labeled GTP analogue. In contrast, a small (1.4%), immediate increase was observed upon the addition of Trx$_E$-Nox1$_{cyt}$ to p67N-Rac•mantGppNHp (Figure 42).

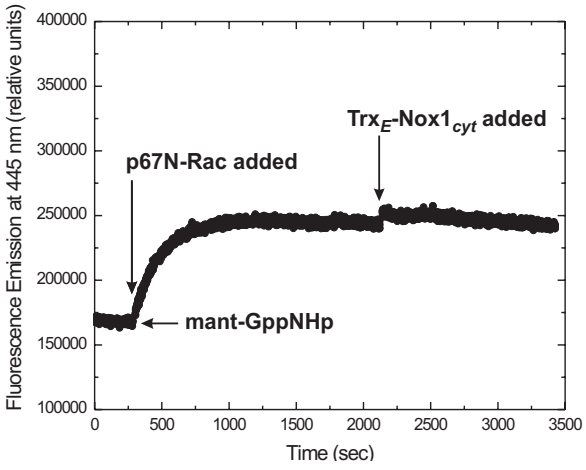

Figure 42. Interaction of Trx$_E$-Nox1$_{cyt}$ with p67N-Rac as measured by fluorescence. mantGppNHp (0.12μM) in 20 mM Tris-HCl, pH 7.45, 3 mM NaCl, 50 mM KCl, and 0.1 μM $MgCl_2$, was excited with a wavelength of 355 nm and the emission at 445 nm was monitored over 5 minutes. p67N-Rac•GDP was added to this solution at a final concentration of 0.25 μM and the emission was monitored for 30 minutes. Trx$_E$-Nox1$_{cyt}$ was then added at a final concentration of 0.35 μM and the emission monitored for 20 minutes.

These observations were further investigated using stopped flow kinetic methods in order to resolve the time scale of the interaction and increase the sensitivity of the measurement. However, these measurements gave inconsistent results, suggesting that other factors might be involved which complicate interpretation of the data. Additionally, the low magnitude of increase upon the addition of Trx_E-$Nox1_{cyt}$ to p67N-Rac•mantGppNHp may reflect the possibility that the mant moiety might be physically distant from the site of interaction and thus may not be able to report effectively on an interaction between $Nox1_{cyt}$ and the p67N-Rac complex. The NADPH-dependent diaphorase assay was therefore favored as a more likely indicator of any functional interaction of p67N-Rac with $Nox1_{cyt}$ due to effects on activity.

Effect of p67-Rac fusion proteins on the intrinsic NADPH-dependent diaphorase activity of H_6-$Nox1_{cyt}$

High concentrations of $p67^{phox}$ or only the N-terminal region of $p67^{phox}$ (residues 1-210) in combination with Rac have been shown to fully activate the phagocytic oxidase in a cell-free reconstitution assay without the requirement for $p47^{phox}$ (Koshkin *et al.*, 1996; Han *et al.*, 1998). The p67N-Rac and p67N-Rac(Q61L) fusion proteins were also found to be capable of activating NADPH oxidase activity and recombinant C-terminal truncations of $gp91^{phox}$ in a cell-free assay, with a 2-fold higher activation compared to activation by the individual $p67^{phox}$ and Rac proteins (Miyano *et al.*, 2001; Miyano *et al.*, 2003; Nisimoto *et al.*, 2004).

Preliminary studies in this work indicate that both fusion proteins, either as native p67N-Rac bound with the nonhydrolyzable GTP analogue, GppNHp, or p67N-Rac(Q61L)•GTP, slightly enhance the intrinsic activity of H_6-$Nox1_{cyt}$ (Figure 43). The activation is minimal, with p67N-Rac•GppNHp producing a 1.3-fold higher activity, and p67N-Rac(Q61L)•GTP, a 1.4-fold higher activity. This slight enhancement of activity is not due to DTT present in the buffer used to store p67N-Rac(Q61L) since volumes of each protein storage buffer equivalent to the volume of that protein used in the assay were also assayed in the same assay buffer used to assay the proteins, and the change in absorbance at 595 nm over time recorded for the respective buffer samples were subtracted from the activity measured from the corresponding protein-containing samples. The sample of p67N-Rac•GppNHp used did

not contain DTT in the storage buffer. Although the assay buffer for this measurement did not contain extra 4 mM $MgCl_2$ (which was present in the assay buffer for the p67N-Rac(Q61L)•GTP measurement), $MgCl_2$ was present in the storage buffer of p67N-Rac, which gives a final concentration of 90 µM $MgCl_2$ in the 1ml assay sample. According to fluorescence measurements made by Nisimoto, *et al*., a concentration of 0.1 µM $MgCl_2$ is still sufficient to observe nucleotide exchange of GDP for mantGppNHp by Rac (Nisimoto *et al.*, 1997). p67N-Rac•GDP was also capable of exchanging GDP for mantGppNHp in a buffer with 0.1 µM $MgCl_2$ in fluorescence measurements made in this work (Figure 42). Therefore, this lower concentration of $MgCl_2$ in the p67N-Rac•GppNHp assay sample is not expected to disrupt efficient binding of GppNHp to Rac.

It should be noted that the p67N-Rac•GppNHp measurement was made using the spectrophotometric assay format, while the p67N-Rac(Q61L)•GTP measurement was made in the microtiter format, yet both yield similar levels of activation. When compared to the roughly 1.8-fold increase in activity using a truncated $gp91^{phox}$ of roughly comparable length (306-569) (Han *et al.*, 2001), this low level of activation is consistent with this length of truncation. To determine whether the measured level of activation is statistically significant, the performed measurements could be repeated. In any case, the effect of the p67N-Rac fusion proteins on these shorter truncated proteins is less significant when compared to the more than 16-fold enhancement seen for the longest recombinant C-terminal truncated (221-570) $gp91^{phox}$. This could indicate that the truncated human Nox1 does not contain all of the necessary regions for optimal interaction to occur. A recent article describes GST fusion proteins of two constructs of Nox1, one containing residues 217-550 and one containing residues 336-550, with both constructs capable of Rac1 association when each GST fusion was incubated with lysates of the human colon cancer cell line Caco-2 (Park *et al.*, 2006). They noted that the longer Nox1 construct associated with Rac1 to a larger extent than that containing residues 336-550, suggesting that the membrane-proximal region of Nox1 is required for Rac1 binding. H_6-$Nox1_{cyt}$ contains this region, but lacks the sixth transmembrane helix, and perhaps these residues strengthen this interaction.

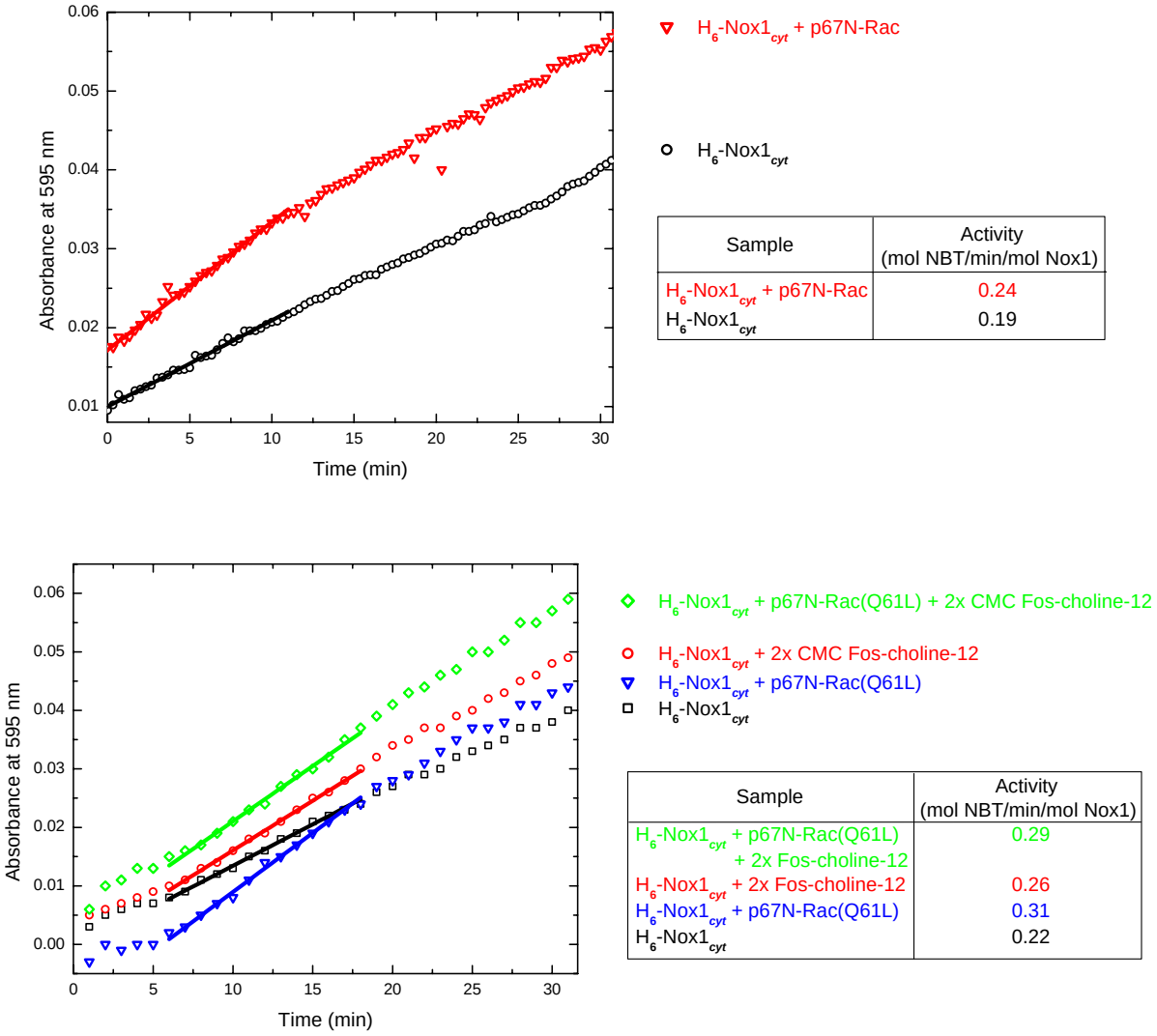

Sample	Activity (mol NBT/min/mol Nox1)
H_6-Nox1$_{cyt}$ + p67N-Rac	0.24
H_6-Nox1$_{cyt}$	0.19

Sample	Activity (mol NBT/min/mol Nox1)
H_6-Nox1$_{cyt}$ + p67N-Rac(Q61L) + 2x Fos-choline-12	0.29
H_6-Nox1$_{cyt}$ + 2x Fos-choline-12	0.26
H_6-Nox1$_{cyt}$ + p67N-Rac(Q61L)	0.31
H_6-Nox1$_{cyt}$	0.22

Figure 43. Effect of p67N-Rac and p67N-Rac(Q61L) on the intrinsic NADPH-dependent diaphorase activity of H_6-Nox1$_{cyt}$. *Top*, H_6-Nox1$_{cyt}$ (4.5 µM) was pre-incubated with 12.3 µM of p67N-Rac pre-loaded with GppNHp at 4°C for 15 minutes. 100 µl of this solution was assayed in a final volume of 1ml in a Beckman DU®640 spectrophotometer alongside H_6-Nox1$_{cyt}$ alone at 37°C. Activity was calculated from the slopes obtained from the linear region. *Bottom*, H_6-Nox1$_{cyt}$ (11 µM) was pre-incubated with 39 µM of p67N-Rac(Q61L)•GTP at 4°C for 15 minutes. 21 µl of this solution was assayed in a final volume of 100 µl in a Labsystem iEMS Reader MF microtiter plate reader alongside H_6-Nox1$_{cyt}$ alone and in the presence and absence of 2x CMC Fos-choline-12 at 37°C. Activity was calculated from the slopes obtained from the linear region.

Additionally, these results could reflect the minimal activation of Nox1 observed when mixed with phagocytic oxidase regulators, in contrast to the large activation seen with Noxo1 and Noxa1 (Takeya *et al.*, 2003; Geiszt *et al.*, 2003b). This is in spite of a 39% and 64% identity for the TPR and activation domains of p67^{phox} and Noxa1, respectively. A

recent study has demonstrated that Nox1 is regulated by $p47^{phox}$ and Noxa1 in vascular cells (Ambasta *et al.*, 2006). The lack of significant activation by p67N-Rac may therefore reflect the lower ability of $p67^{phox}$ to activate Nox1. Studies in human colon cancer cell lines T84 and Caco2 confirm the lower ability of $p67^{phox}$ to elicit a marked increase in Nox1-dependent superoxide production. Transduction of $p67^{phox}$ mRNA or overexpression of Noxa1 alone did not augment spontaneous or PMA-stimulated superoxide release by T84 cells, whereas cells overexpressing Noxo1 significantly increased their superoxide generation when stimulated with PMA. This output was not altered by transfection of $p67^{phox}$, but was further increased with overproduction of Noxa1 (Kawahara *et al.*, 2004).

With regards to the effect of detergent on the level of activation by the p67N-Rac fusion proteins, inclusion of the detergent Fos-choline-12 at a concentration 2x the CMC did not significantly enhance the activation by p67N- Rac(Q61L)•GTP, with a tendency to reduce the effect of p67N-Rac(Q61L)•GTP on H_6-$Nox1_{cyt}$ (Figure 43). Again, this suggests that detergents may have a destabilizing effect on the proteins, which is in contrast to what was observed for truncations of $gp91^{phox}$ (Nisimoto *et al.*, 2004).

2.2.3 Assessment of cofactor binding

Although all Nox proteins require the cofactor FAD to generate superoxide, early studies on cytochrome b_{558} indicated that the binding of FAD to the enzyme is quite labile. Human neutrophils lost the ability to produce superoxide in the presence of 0.045% Triton X-100, but full activity could be restored if 0.2 mM FAD was added in the presence of the detergent (Babior and Kipnes, 1977). The ability to differentially fractionate the FAD containing portion from cytochrome b_{558} led some to believe that the oxidase contained an additional flavoenzyme component (Gabig, 1983) before it was evident that the flavin-binding protein was indeed $gp91^{phox}$ itself (Rotrosen *et al.*, 1992). FAD is lost during the purification of cytochrome b_{558} (Knoller *et al.*, 1991; Rotrosen *et al.*, 1992), with the dependence on exogenous FAD for cell-free superoxide production correspondingly increasing with the level of cytochrome b_{558} purity (Sumimoto *et al.*, 1992).

Consistent with these observations, retention of FAD by H_6-$Nox1_{cyt}$ after purification was not visually obvious, with no overt absorbance maxima detected in the visible region expected for FAD binding proteins. In contrast, characterization of the longest truncated

gp91^{phox} protein (residues 221-570) by Nisimoto *et al*, found this truncation to be the only one capable of binding FAD in a nearly 1:1 molar ratio. An absorption spectrum of the re-flavinated gp91^{phox} protein (residues 221-570) contains two absorbance maxima typical for flavoproteins at 383 nm and 452 nm, although the relative intensities of these peaks is roughly 1/5 the intensity of the corresponding protein absorbance at 275 nm. This suggests that the last transmembrane helix may be involved in the stable association of FAD with Nox proteins, which is lacking in H_6-Nox1$_{cyt}$. Reflavination of cytochrome b_{558} has been shown to be sensitive to phospholipid composition (Koshkin and Pick, 1993; Koshkin and Pick, 1994), with reflavination of cytochrome b_{558} in an optimal mixture of PC, PE, PI, SM, and cholesterol (4:2:1:3:3 w/w) demonstrating 70% the activity measured in native plasma membranes (Nisimoto *et al.*, 1995). H_6-Nox1$_{cyt}$ is capable of transient, functional binding of FAD, as inferred from the ability of the enzyme to reduce NBT in the presence of excess FAD in the assay buffer used for the NADPH-dependent diaphorase assay. This diaphorase activity was still observed after subtracting the change in absorbance at 595 nm that was measured for the H_6-Nox1$_{cyt}$ protein storage buffer assayed in the same assay buffer and in the same manner as the H_6-Nox1$_{cyt}$ protein sample. Further characterization should be done to determine if H_6-Nox1$_{cyt}$ is able to retain FAD after reflavination by using HPLC methods to quantify the amount of FAD in H_6-Nox1$_{cyt}$ elution fractions after removal of excess FAD by size exclusion chromatography using a buffer that does not include FAD. Additionally, the NADPH-dependent diaphorase activity assay could be used to determine the affinity of FAD for H_6-Nox1$_{cyt}$ by varying the FAD concentration in the assay and determining any effects on activity.

2.3 SUMMARY AND PERSPECTIVES

Studies were made to heterologously overexpress human Nox1 in *E. coli*, either as the full-length protein or as C-terminal truncations containing the cytosolic domain, for the purpose of structural characterization by X-ray crystallography. Coexpression of full-length human Nox1 with subunit b of *E. coli* F_1F_o ATP synthase in the absence or presence of the heme precursor, δ-aminolevulinic acid, did not promote Nox1 expression in C41(DE3) *E. coli* cells. Eukaryotic expression systems such as yeast, dictyostelium, or baculovirus may prove to be more effective, especially if Nox1 is coexpressed with p22^{phox} to enhance the stability

of each protein. Of these, dictyostelium may be the preferred expression system, since it naturally expresses three Nox homologues, NoxA, NoxB, and NoxC, with NoxA showing homology to the Nox1-4 proteins (Kawahara *et al.*, 2007).

Heterologous overexpression of C-terminal truncations containing the cytosolic domain of human Nox1 in *E. coli* proved to be more successful. Three constructs, Trx_E-$Nox1_{cyt}$, Trx_T-$Nox1_{cyt}$, and H_6-$Nox1_{cyt}$, containing human Nox1 (residues 290-564) were solubly expressed at low levels in C41(DE3) *E. coli* cells under induction conditions using low cell density, low temperature, and low concentrations of IPTG. Purification procedures were established for each construct, which include initial capture by Ni-affinity chromatography, followed by a second affinity step using 2'5' ADP Sepharose. H_6-$Nox1_{cyt}$, was found to be less tolerant of low salt conditions, and therefore was purified over a single Ni-affinity chromatography step. Although the N-terminal thioredoxin tag present in Trx_E-$Nox1_{cyt}$ and Trx_T-$Nox1_{cyt}$ was found to interfere with the NADPH-dependent diaphorase assay used to assess the activity of the truncated Nox1, these constructs may still be useful in structural studies if the tag does not hinder crystallization. A fourth construct, H_6-$Nox1_{220\text{-}564}$, containing the cytosolic domain of human Nox1 as well as the sixth transmembrane helix and the last three residues of the fifth transmembrane helix, was also cloned and expressed in BL21(DE3) and BL21(DE3) Codon Plus RIL *E. coli* cells. Unfortunately, H_6-$Nox1_{220\text{-}564}$ was found to be prone to severe proteolysis, even in the presence of protease inhibitors, which limits its utility for structural studies.

In spite of its difficulty in handling, H_6-$Nox1_{cyt}$ does possess an intrinsic NADPH-dependent diaphorase activity of 0.95 mol/min/mol H_6-$Nox1_{cyt}$, which is consistent with its biological function of low-level, constitutive superoxide production. This activity suggests that H_6-$Nox1_{cyt}$ is capable of transient, functional interaction with the cofactor FAD (present in excess in the assay buffer), and the assay can be used to determine the affinity of this interaction. Additionally, preliminary studies suggest that H_6-$Nox1_{cyt}$ can functionally interact with fusion proteins of the phagocytic oxidase regulators $p67^{phox}$ and Rac1, resulting in a modest activation of 1.3 to 1.4-fold. This low level of activation may indicate the importance of the sixth transmembrane helix in strengthening the interaction between Nox1 and phagocytic regulatory proteins, which is lacking in H_6-$Nox1_{cyt}$. Additionally, it may reflect the ability of Nox1 to discriminate between different cytosolic regulators, as was

seen in *in vivo* experiments (Kawahara *et al.*, 2004). Of interest would be the creation of an equivalent Noxa1N-Rac1 fusion protein to examine its ability, if any, to significantly enhance the intrinsic activity of H_6-$Nox1_{cyt}$. Interestingly, detergents such as Fos-choline-12, may not be required to stabilize H_6-$Nox1_{cyt}$ as long as the protein is maintained in high salt conditions and is not subjected to conditions that would promote soluble aggregation, such as overconcentration. Thus, H_6-$Nox1_{cyt}$ may serve as a minimal active fragment that can be used in future structural studies either alone or in complex with a variety of other proteins to aid in the understanding of how auxiliary proteins can modulate its intrinsic activity. Such proteins include the proposed Noxa1N-Rac1 fusion protein and βPix, a GEF for Rac. If Noxa1N-Rac1 is found to significantly activate H_6-$Nox1_{cyt}$, structural characterization of the complex could provide molecular details on factors that promote electron transfer, as well as insights into mechanisms to disrupt this for therapeutic reasons. The role of βPix in EGF-induced ROS generation by Nox1 has been recently described (Park *et al.*, 2004; Park *et al.*, 2006), and indicates that Nox1 (residues 217-550) forms a ternary complex with Rac•GTPγS and βPix. Domain mapping of βPix revealed that its PH domain interacts with the FAD binding region (residues 335-360) of Nox1. Structural characterization of a complex between H_6-$Nox1_{cyt}$, active Rac1 and the PH domain of βPix may offer some insights as to how a GEF can modulate the activity of Nox1.

Complexes of H_6-$Nox1_{cyt}$ with small molecule inhibitors may directly shed light on mechanisms to inhibit Nox1. Several experimentally used inhibitors such as diphenyleneiodonium (DPI) or aminoethyl benzenesulfono fluoride (AEBSF) lack the appropriate specificity for therapeutic consideration. DPI is a general flavoenzyme inhibitor, inhibiting NOS (Stuehr *et al.*, 1991), xanthine oxidase (Doussiere and Vignais, 1992), and cytochrome P450 reductase (McGuire *et al.*, 1998). Inhibition of NADPH oxidase occurs via a radical mechanism, where DPI abstracts an electron from a reduced redox center in the oxidase and subsequently reacts with FAD, forming covalent adducts (O'Donnell *et al.*, 1993). AEBSF inhibits the binding of $p47^{phox}$ to cytochrome b_{558} during oxidase assembly (Diatchuk *et al.*, 1997) but is also a well known serine protease inhibitor. Currently, NADPH oxidase inhibitor design has relied on high-throughput screening due to a lack of structural information (Tegtmeier *et al.*, 2005). A novel inhibitor identified by such high-throughput screening, VAS2870 (3-benzyl-7-(2-benzoxazolyl)thio-1,2,3-triazolo[4,5-d]pyrimidine) from vasopharm BIOTECH GmbH (Würzburg), has been found to have an

IC_{50} value of 10.6 μM when assayed with membranes of human neutrophils. Additionally, preincubation of 10 and 20 μM VAS2870 abolishes PDGF-induced NADPH Oxidase activation and ROS generation in VSMC homogenates, preventing PDGF-dependent VSMC migration via Src (ten Freyhaus H. *et al.*, 2006). Structural characterization of a complex of VAS2870 with H_6-$Nox1_{cyt}$ may provide avenues for rational drug design to increase specificity for human Nox1, the major oxidase in VSMCs.

With regards to a detailed understanding of the overall catalytic mechanism of Nox proteins at the molecular level, analysis of multiple homologues in other organisms may be another alternative to identify more stable Nox proteins that retain the basic features of the human Nox proteins. A recent, comprehensive taxonomic analysis of the Nox and Duox proteins has yielded many possible candidates that could be screened to find one that might be more amenable to heterologous expression and isolation than the human Nox proteins (Kawahara and Lambeth, 2007). These include Nox1 homologues present in frog and zebrafish, as well as NoxA homologues found in dictyostelium and fungi, which contain the basic domain structure of Nox1-4 proteins.

In conclusion, methods have been developed to heterologously express and purify an active form of the cytosolic domain of human Nox1, which may be capable of biologically relevant interactions. Structural characterization of this active fragment alone and in complex with activating proteins may provide deeper insights into the first electron transfer step towards the production of superoxide by these unique enzymes, whose roles in human pathologies are increasingly recognized.

Chapter 3.

Characterization of cyclized Rab7

3. INTRODUCTION

As highlighted by the difficulties experienced with the characterization of the cytosolic domain of human Nox1, many proteins of interest lack the inherent stability outside of their natural cellular environment to be able to address questions at the biochemical and molecular level. Factors that can increase protein stability are thus of considerable interest. Since the discovery of naturally occurring circular proteins and peptides, peptide backbone cyclization of linear proteins and peptides has become a biotechnical method for protein stabilization. These circular proteins and peptides are characterized by high thermal and chemical stability, as well as resistance to proteolysis (Eisenbrandt *et al.*, 1999; Jennings *et al.*, 2001; Felizmenio-Quimio *et al.*, 2001). Such properties are attractive for industrial applications, with regard to enzyme catalysis, or in pharmaceutical drug design. Additionally, cyclization may facilitate structural determination of proteins by X-ray crystallography through stabilization of inherently flexible regions of proteins which are often not observed in the calculated electron density, or which may hinder or prevent efficient packing of the protein in a crystal lattice.

3.1 PROTEIN CYCLIZATION VIA EXPRESSED PROTEIN LIGATION

Several examples of engineered cyclic proteins and peptides have taken advantage of a technique called expressed protein ligation (Iwai and Pluckthun, 1999; Scott *et al.*, 1999; Iwai *et al.*, 2001; Williams *et al.*, 2002). This method utilizes protein splicing via inteins (***in***ternal pro***teins***) to catalytically generate the circular products. Inteins are protein domains that excise themselves out of a precursor polypeptide chain. This self-splicing reaction results in the formation of a new peptide bond between the flanking ends of the precursor polypeptide chain (the exteins). Such splicing can occur post-translationally on nascent polypeptide chains, and is termed *cis*-splicing. Alternatively, inteins can be divided into two inactive N- and C-terminal fragments, which are either fused to two different exteins, or a single extein. Plasmids containing the divided intein-extein construct(s) are transformed into *E. coli* cells. When the two intein fragments are expressed, they are able to form a functional intein independent of covalent linkage between the fragments, and perform a *trans*-splicing reaction inside the *E. coli* cells. The reaction results in ligation between the two different

exteins, or ligation of a single polypeptide chain, as is the case in cyclization (Figure 44) (Paulus, 2000).

Inteins are generally single protein sequences about 400-500 amino acids long, and consist of a protein splicing domain and an endonuclease domain. Mini-inteins are roughly 150 residues long and contain only a protein splicing domain. The cyanobacterium *Synechocystis* sp. strain PCC6803 (*Ssp*) possesses a naturally split intein, *Ssp* DnaE intein (Wu *et al.*, 1998a), which has been used to produce cyclic peptides and proteins. Generation of a circular product involves a precursor with the structure I_C-extein-I_N, where I_C and I_N are the C- and N- terminal intein domains, respectively, and the extein is the linear sequence of the target peptide or protein (Scott *et al.*, 1999; Evans, Jr. *et al.*, 2000; Iwai *et al.*, 2001). Inteins that exist as a single, continuous sequence have also been engineered to be split, and retain the ability to perform *trans*-splicing after reconstitution. Examples of this include the Psp Pol-1 intein (Southworth *et al.*, 1998), PI-*Pfu*I intein from *Pyrococcus furiosus* (Iwai *et al.*, 2001), and the *Ssp* DnaB mini-intein (Wu *et al.*, 1998b). The *Ssp* DnaB mini-intein has the advantage that the *trans*-splicing reaction occurs efficiently *in vivo* in *E. coli* cells, without the need for a denaturation/renaturation step required by the separately purified fragments of the Psp Pol-1 intein. It requires neither a spacer sequence nor the presence of native exteins for efficient splicing. The superior performance of the *Ssp* DnaB mini-intein compared to other inteins in heterologous systems has led to its use in protein engineering applications, and is used in this work to produce a cyclized Rab7 protein.

The mechanism of intein-mediated protein splicing occurs in four steps. (1) Nucleophilic attack by the side chain of cysteine or serine/threonine at the I_N–target junction on the carbonyl of the adjacent peptide bond results in a N-S or N-O acyl shift, creating a (thio)ester. (2) Transesterification, with nucleophilic attack on the (thio)ester by the side chain of the first residue at the I_C-target junction, producing a branched (lariat) intermediate. (3) Cyclization of a conserved asparagine at the intein C-terminus involving attack by the β-amide nitrogen on the carbonyl of the peptide bond, which cleaves at the carboxyl terminal splice junction, releasing the cyclized target. (4) A final N-S or N-O shift in the circularized target, producing a peptide bond and completing the splicing reaction (Figure 44) (Paulus, 2000; Perler and Adam, 2000).

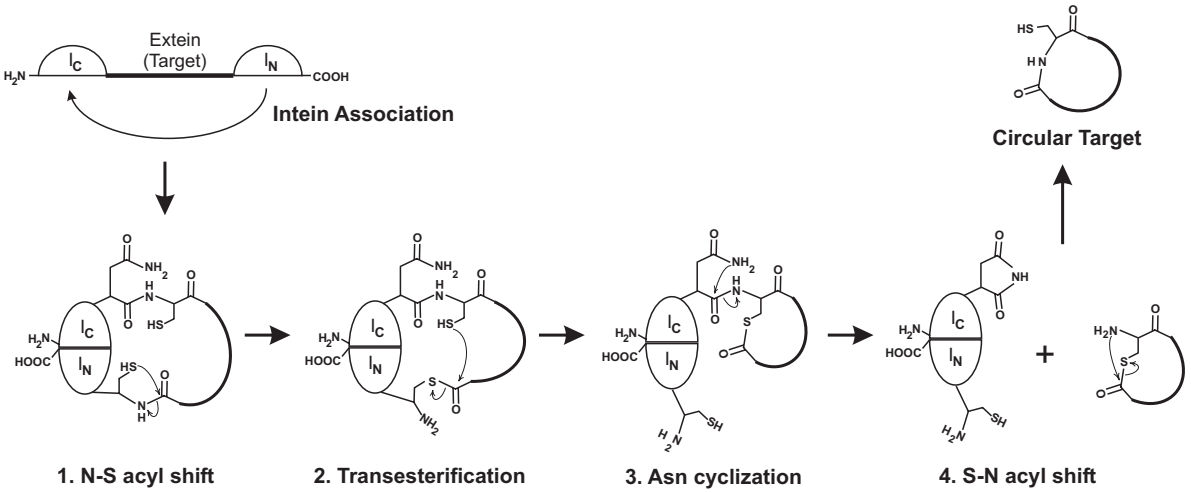

Figure 44. Schematic of a split intein and mechanism of protein splicing to produce a circularized target. Generation of a circular product involves a split intein precursor with the structure I_C-extein-I_N, where I_C and I_N are the C- and N- terminal intein domains, respectively, and the extein is the linear sequence of the target peptide or protein. Association of I_C and I_N produces a fully functional intein that catalyzes the circularization of the target in four steps. Figure after Perler and Adam, 2000.

3.2 THE MODEL SYSTEM: RAB7 GTPASE

3.2.1 Rab GTPases

Rab GTPases (Ras genes from rat brain) represent the largest branch of Ras related small GTPases, with 11 yeast proteins (Ypt proteins, yeast protein involved in transport) and over 60 mammalian members identified thus far. They regulate major steps in intracellular vesicular membrane transport during cellular processes such as exocytosis and endocytosis. Nascent proteins destined for secretion and integral membrane proteins are sorted to their appropriate locations by exocytosis, passing from the endoplasmic reticulum, through the Golgi, to the plasma membrane. Extracellular nutrient uptake and recycling of membrane proteins and receptors via internalization is accomplished through endocytosis. Cargo is transported to the early endosome and moves onto either recycling endosomes to be recycled, or to late endosomes and then lysosomes for degradation. Rab GTPases mediate steps in this transport such as vesicle budding, vesicle delivery via molecular motors along microtubules or actin filaments, vesicle tethering close to the target membrane, and vesicle fusion with the membrane of the target compartment (Zerial and McBride, 2001; Pfeffer, 2001; Grosshans *et al.*, 2006).

Rab GTPases are posttranslationally modified at two cysteines in their C-terminus with a 20-carbon geranylgeranyl lipid moiety that allows them to anchor to membranes. Some Rab proteins (such as Rab8 and Rab13) are geranylgeranylated at a single cysteine. In contrast to other GTPases, Rab prenylation requires Rab escort protein (REP) to present it to the cytosolic heterodimeric Rab geranylgeranyltransferase (Rab GGTase or GGTase type II). Mammalian cells contain two REP isoforms (REP-1 and REP-2) that bind Rab in its GDP form. Once prenylated, REP sequesters the lipid modification, keeping inactive prenylated Rab•GDP soluble, and delivers it to the membrane.

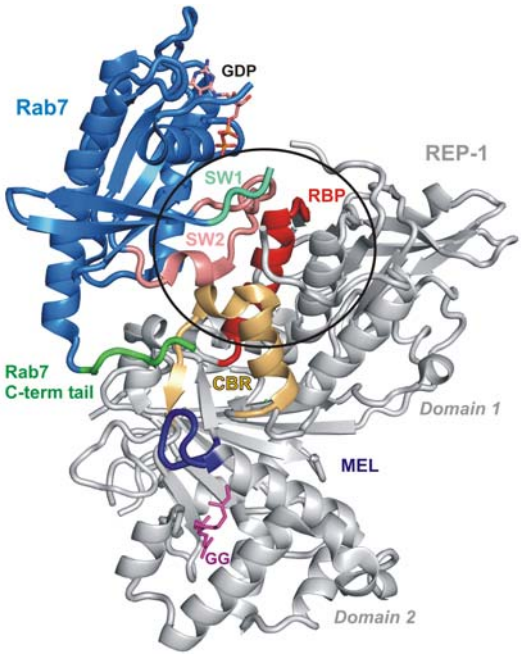

Figure 45. The Rab7•GDP(monoprenylated):REP-1 complex (PDB Code 1VG0, Rak *et al*, 2004). Rab7 (blue)•GDP(salmon stick) prenylated with a single geranylgeranyl group (*GG*, magenta stick) interacts with three main regions in REP-1 (white). The globular core of Rab7 mainly interacts with the Rab binding platform (*RBP*, red) of REP-1 through its Switch II region (*SW2*, salmon). The extended C-terminal tail (green) of Rab7•GDP interacts with the C-terminal binding region (*CBR*, yellow orange) of REP-1. A mobile effector loop (*MEL*, dark blue) lies between Domain 1 and Domain 2 of REP-1, with Domain 2 sequestering the geranylgeranyl moiety. Switch I (*SW1*, blue-green) is not well-defined in this structure.

Like all small GTPases, Rab GTPases cycle between an inactive GDP-bound and an active GTP-bound state. Guanine nucleotide exchange factors (GEFs) increase the dissociation rate of GDP, allowing GTP to bind, which is present at concentrations 10 times that of GDP in the cell. This leads to the active Rab•GTP state, which is recognized by a myriad of effector proteins that participate in the various steps of vesicular transport. GTPase activating proteins (GAPs) regulate the duration of this signal by accelerating the normally slow intrinsic GTPase activity, which returns Rab•GTP to the inactive Rab•GDP state. Rab proteins are then extracted out of the membrane by Rab GDP dissociation inhibitor (RabGDI), and are recycled back to the cytosol where they can repeat the cycle (Goody *et al.*, 2005) (Figure 46).

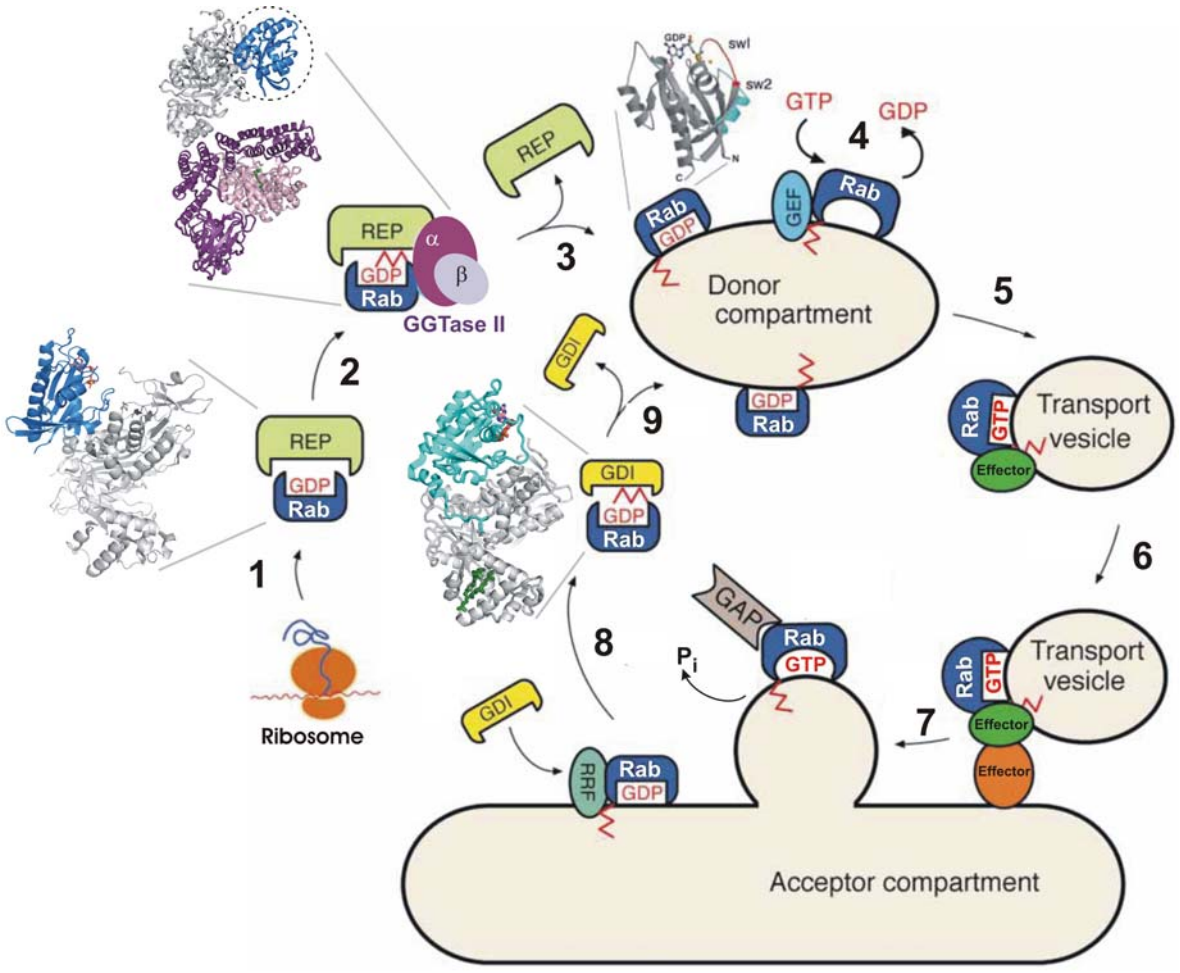

Figure 46. Rab GTPase cycle. *1* and *2*, In the cytosol, newly synthesized Rab•GDP GTPases are escorted by REP to GGTase II for geranylgeranylation. *3*, REP delivers prenylated Rab•GDP to the membrane for use in vesicular transport. *4*, GEFs accelerate GDP dissociation from Rab, allowing GTP to bind. *5* and *6*, Active prenylated Rab•GTP is recognized by effector molecules that participate in various steps of vesicular transport. *7*, GAPs accelerate Rab's intrinsic GTPase activity, returning it to the inactive GDP form. *8*, GDI retrieves prenylated Rab•GDP from the membrane through Rab recycling factor (RRF), recycling it back into the cytosol, *9*, where it can repeat the cycle. Corresponding crystal structures of Rab7ΔC22•GDP:REP-1 (PDB Code 1VG9) and REP-1:GGTaseII:isoprenoid (PDB Code 1LTX) are shown, with a dashed circle indicating the hypothetical position of Rab7 based on superposition of the two structures. Additionally, the crystal structure of doubly geranylgeranylated (green stick) Ypt1•GDP (a yeast homologue, cyan; PDB Code 2BCG) in complex with GDI (white) is shown. Figure modified from Alory and Balch, 2001.

Sequence alignment of Rab proteins led to the identification of regions that are specific to the Rab family (Figure 47). These regions (RabF1-5) lie in or around the Switch regions, which change conformation depending on whether GDP or GTP is bound, and together with conserved regions for phosphate/Mg^{2+} and guanine nucleotide binding (PM/G) motifs define the Rab family of proteins. Additional regions of high conservation were observed

within Rab subfamilies, and these areas (RabSF1-4) are proposed to confer effector specificity (Pereira-Leal and Seabra, 2000).

3.2.2 Rab7 GTPase

Rab7 regulates late endocytic transport from early to late endosomes, from late endosomes onto lysosomes, as well as lysosome biogenesis (Feng *et al.*, 1995; Meresse *et al.*, 1995; Bucci *et al.*, 2000). It is additionally involved in cellular response to the withdrawal of growth factors, contributing to the initiation of apoptosis (Edinger *et al.*, 2003). Two Rab7 effectors have been identified, Rab7-interacting lysosomal protein (RILP) (Cantalupo *et al.*, 2001) and Rabring7 (Mizuno *et al.*, 2003), both of which are recruited to late endosomes/lysosomes by Rab7•GTP. The three-dimensional structure of a constitutively active Rab7 mutant in complex with RILP indicates that both the Switch regions and two Rab specific regions (RabSF1 and RabSF4) are involved in the interaction interface (Wu *et al.*, 2005).

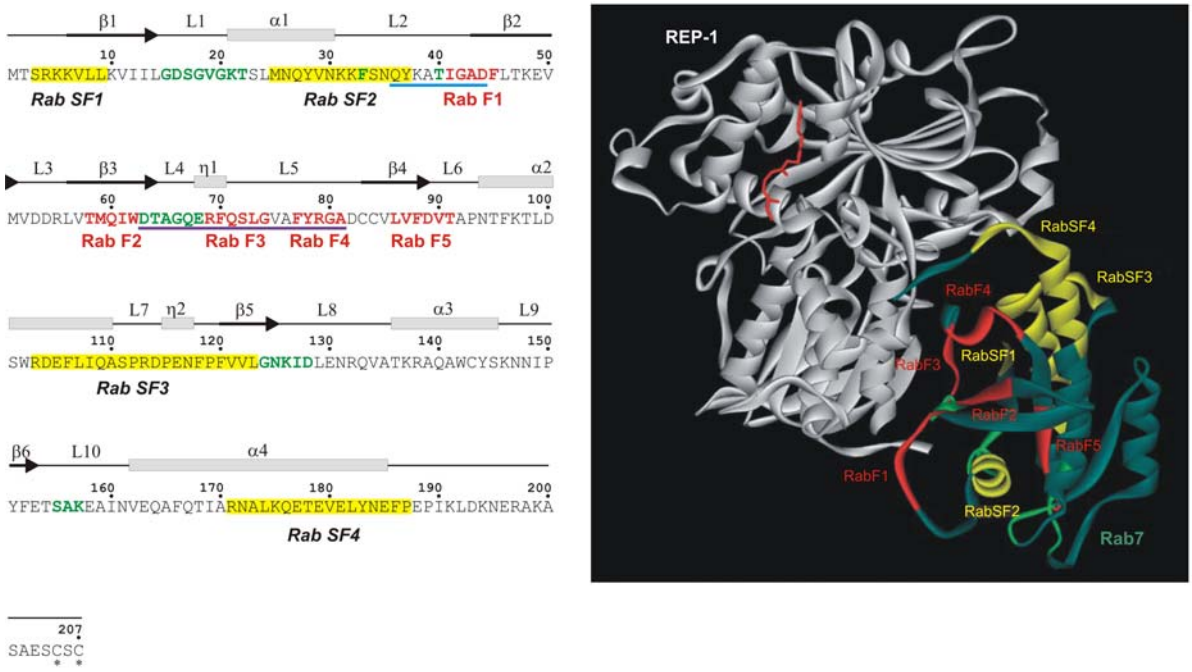

Figure 47. Rab7 protein sequence with secondary structure shown above, and RabF (red, bold) and RabSF (yellow highlight) regions indicated below. A blue line underlines Switch I, and a purple line underlines Switch II. Conserved nucleotide binding (PM/G) motifs are shown in green. The two C-terminal cysteines that undergo prenylation are indicated by *. Ribbon representation of the Rab7 (dark green):REP-1 (white) complex (PDB code 1VG0) with RabF and RabSF regions indicated in red and yellow, respectively, and PM/G motifs in light green. Geranylgeranyl is shown in red stick representation. Ribbon representation figure taken from Leung *et al*, 2006.

3.3 AIMS OF WORK

Rab7 was selected as a model system to study the effects of cyclization on protein stability and in stabilization for crystallization. Fluorescence and circular dichroism spectroscopy were used to assess the extent of thermal stabilization imparted by cyclization. Native biological function was evaluated by measurement of the intrinsic GTPase activity and interaction with a yeast homologue of REP-1 (Mrs6) to determine if cyclization of Rab7 disturbed its biological activity. Finally, structural characterization by X-ray crystallography was made on cyclized Rab7•GDP and cyclized Rab7•GppNHp to determine (1) if cyclization improved the ability to crystallize both inactive and active forms of Rab7, and (2) if cyclization could stabilize flexible protein loops and allow for their structure determination.

3.4 RESULTS AND DISCUSSION

3.4.1 Protein expression and purification

The generation of cyclized Rab7 took advantage of split-intein mediated protein ligation. Rab7 truncated to residues 7-185 flanked by linker residues (Figure 48A) was inserted via *Eco*RI and *Mlu*I restriction sites into a plasmid containing the split *Ssp* DnaB mini-intein under a thermally controlled promoter (Williams *et al.*, 2002) (a kind gift from Prof. Nick Dixon, University of Wollongong, New South Wales, Australia). This plasmid was transformed into BL21(DE3) *E. coli* cells. Protein expression was induced via heat shock, and found to be sensitive to the cell density at the time of induction. Reasonable expression was found when the cell density reached an optical density at 600 nm of at least 0.7 but not above 0.8 absorbance units. Although overexpression was not obvious from SDS-PAGE analysis (Figure 48B), further purification resulted in typical yields of 12 mg of cyclized Rab7 per 5L of cell culture. Prior to harvesting the cells, cyclization was promoted by incubating the cultures for at least 2 hours at 4°C.

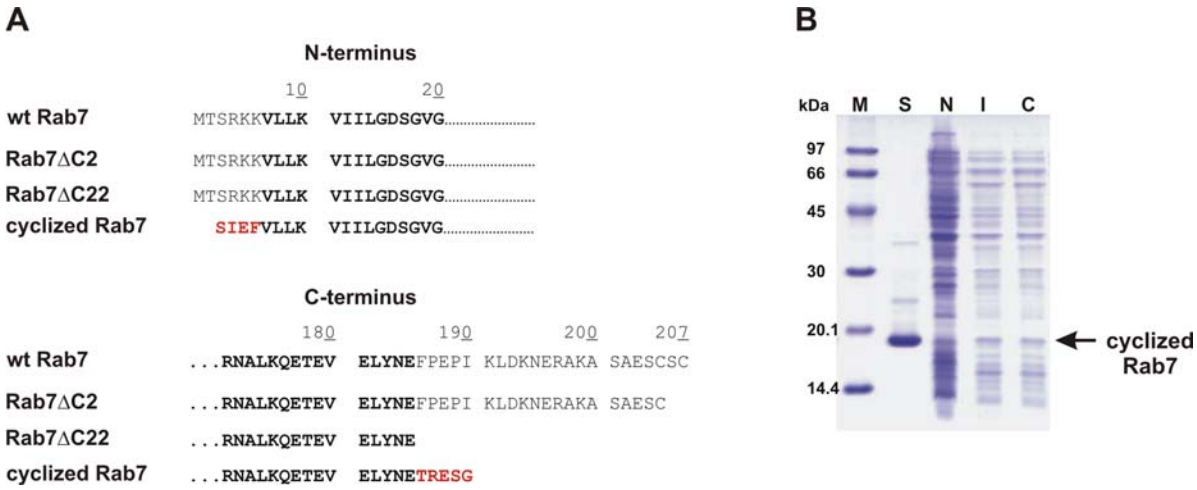

Figure 48. *A*, Design of cyclized Rab7: a truncated version of Rab7 containing residues 7-185 (bold) was used with a 9 residues linker (red) that becomes covalently linked upon cyclization. Two other constructs used in this work, Rab7ΔC2 and Rab7ΔC22, are also shown aligned with excerpts of the protein sequence of wild type Rab7. *B*, Expression pattern of cyclized Rab7 in BL21(DE3) *E. coli*. *M*, Markers; *S*, cyclized Rab7 standard; *N*, non-induced cells; *I*, cells after thermal induction; and *C*, induced cells after promotion of cyclization at 4°C for 2 hours.

Since the construct lacks affinity tags, a traditional purification scheme was employed with crude fractionation via ammonium sulfate, followed by initial separation over DEAE-Sepharose, a weak anion exchange resin. Higher molecular weight contaminants were removed by size exclusion chromatography, and a final run over Porous HQ resin, a strong

anion exchanger, allowed for the final polishing step (Figure 50A). A previous protocol using a linear gradient from 0-1M NaCl over 100 ml for the final elution showed significant amounts of contaminating proteins, in spite of a single peak in the elution profile (Nathalie Bleimling, unpublished results, Figure 49A). It was noted that cyclized Rab7 was the first species to elute, with other proteins following later on in the elution peak. This protocol was modified in two ways: 1) the gradient volume was extended to 300 ml, and 2) the gradient was held once the absorbance at 280 nm began to increase from baseline to allow selected elution of weaker binding proteins. When the first elution peak began, the gradient was held at 80 mM NaCl, allowing improved separation of different protein species (Figure 49B). As the absorbance reading at 280 nm reached a plateau, the gradient was then allowed to continue until the next elution peak began (at 110 mM NaCl), and again held until no further elution was seen. This was continued until the gradient reached 500 mM NaCl, at which point the elution was stepped to 1 M NaCl, since all of the protein had eluted before 500 mM NaCl in the original 100 ml linear gradient. SDS-PAGE analysis on fractions from this modified elution scheme indicated that most of the contaminating proteins were retained longer on the anion exchanger with respect to cyclized Rab7, allowing cyclized Rab7 to elute nearly exclusively.

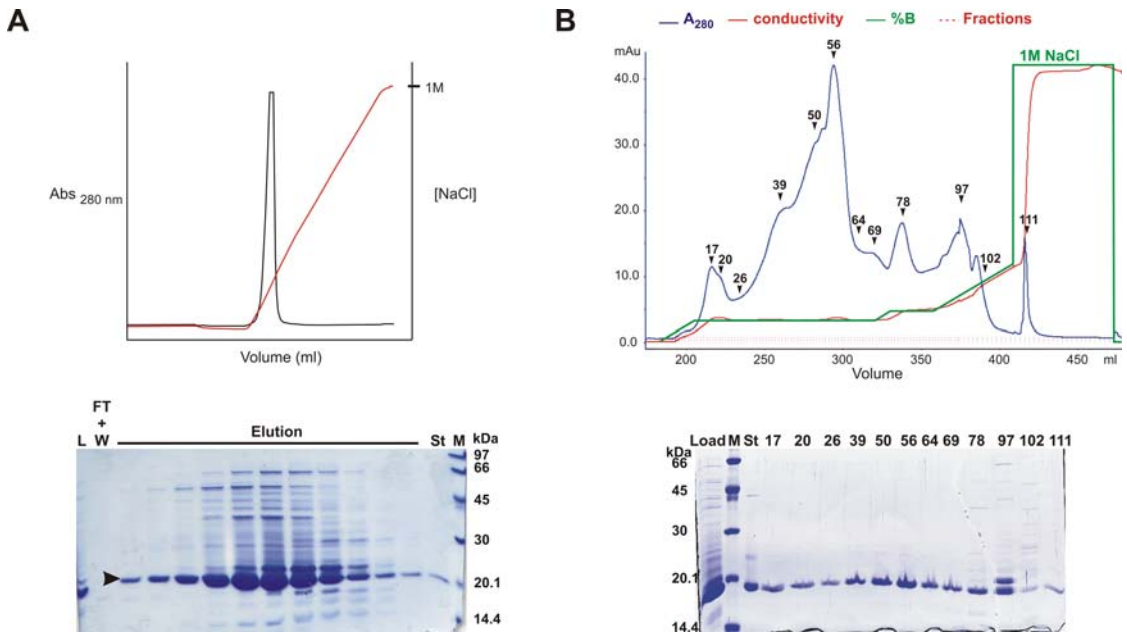

Figure 49. Optimization of cyclized Rab7 purification over Porous HQ chromatography. *A*, Chromatographic profile of a single linear gradient over 100 ml and respective SDS-PAGE on elution fractions. Arrowhead indicates cyclized Rab7. *L*, sample loaded; *FT+W*, flow through and wash samples; *M*, Markers; *St*, cyclized Rab7 standard. *B*, Chromatographic profile of the modified elution method and corresponding SDS-PAGE analysis of respective fractions. *Load*, loaded sample; numbers indicate fractions.

This modified protocol was successful to produce pure cyclized Rab7 as judged by SDS-PAGE (Figure 50A). Cyclization was confirmed with ESI-MS, with a measured mass of 21,353 Da, indicating a loss of 18 Da due to a water molecule upon cyclization (expected mass for the linear form: 21,373.20 Da) (Figure 50B).

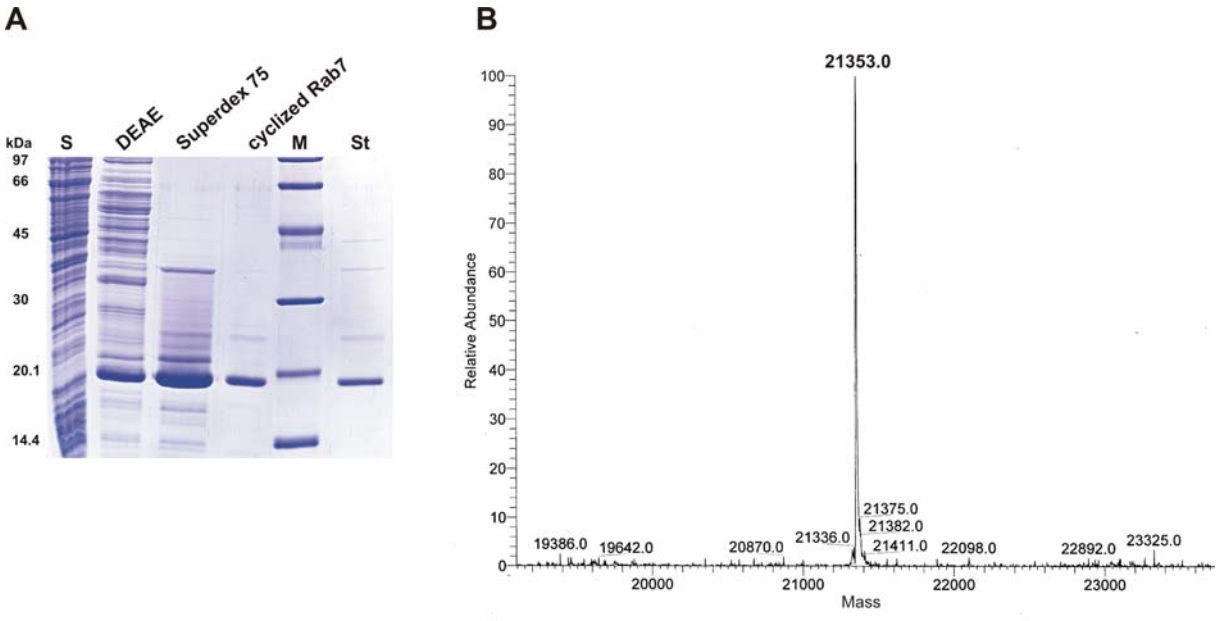

Figure 50. *A*, Purification of cyclized Rab7. *S*, supernatant after protein induction; *M*, markers; *St*, cyclized Rab7 standard. *B*, ESI-MS spectra of the final purified protein, confirming successful cyclization.

3.4.2 The effect of cyclization on the secondary structure of Rab7

Circular dichroism measurements were made on cyclized Rab7•GDP and compared to a linear version missing the equivalent 22 residues from the C-terminus (Rab7ΔC22•GDP), as well as wild-type Rab7 missing the last two amino acids from the C-terminus (Rab7ΔC2•GDP). As can be seen from Figure 51 and Table 2, cyclization does not significantly alter the percentage of secondary structural elements, and is actually more similar to the nearly full-length Rab7ΔC2 protein than the linear truncated Rab7. These are in good agreement with the values of 37% α-helix and 19% β-sheet calculated from the crystal structure of human Rab7(Q67L)•GTP (PDB code 1T91) (Wu *et al.*, 2005), and 41% α-helix and 19% β-sheet for rat Rab7•GppNHp (PDB code 1VG8) (Rak *et al.*, 2004). The percentage of α-helix varies from the two crystal structures based on the fact that more of

the C-terminal helix is visible in the Rab7•GppNHp structure as compared with the Rab7(Q67L)•GTP structure.

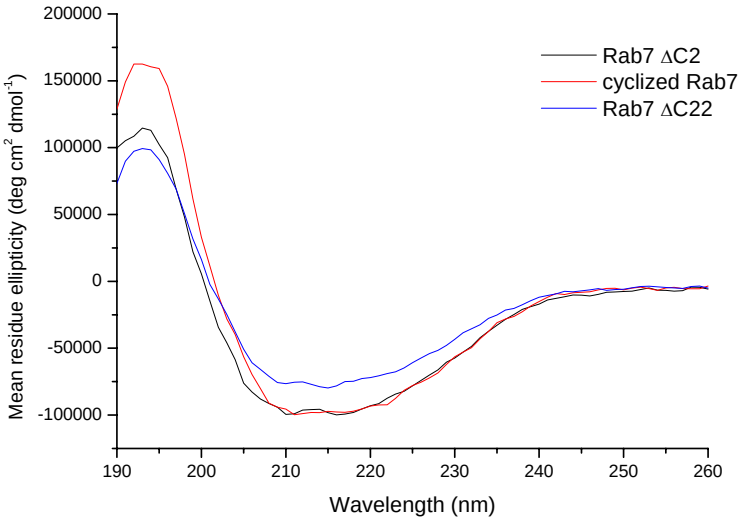

Figure 51. Overlay of circular dichroism spectra of Rab7ΔC2, Rab7ΔC22, and cyclized Rab7.

Table 2. Percent secondary structure of different Rab7 constructs determined by circular dichroism.

Protein	% α-helix	% β-sheet	% β-turns	% Unordered
Rab7ΔC2•GDP	29.1	16.4	19.3	35.1
Rab7ΔC22•GDP	22.5	21.5	20.8	35.0
Cyclized Rab7•GDP	30.6	18.2	16.0	35.1

3.4.3 The effect of cyclization on protein stability: Temperature-dependent fluorescence and circular dichroism measurements

To determine whether cyclization conferred additional thermal stability, both cyclized Rab7•GDP and a linear version, Rab7ΔC22•GDP, were monitored by fluorescence and circular dichroism with increasing temperature. Fluorescence measurements were made monitoring the intrinsic tryptophan fluorescence using an excitation wavelength of 290 nm. Thermal recovery of the respective proteins was checked after the last temperature by cooling the sample to 20°C and re-measuring its fluorescence emission. In the case of the cyclized Rab7•GDP, the fluorescence emission measured at 20°C was lower than that at 30°C, even though the same sample and cuvette were used and the measurements performed on the same day. Therefore, the measurement at 20°C has been excluded from Figure 52. Cyclized Rab7•GDP appears to retain more fluorescence than its linear counterpart (Figure

52A), and even demonstrated an apparent ability to regain intrinsic tryptophan fluorescence after re-cooling to 20°C (data not shown).

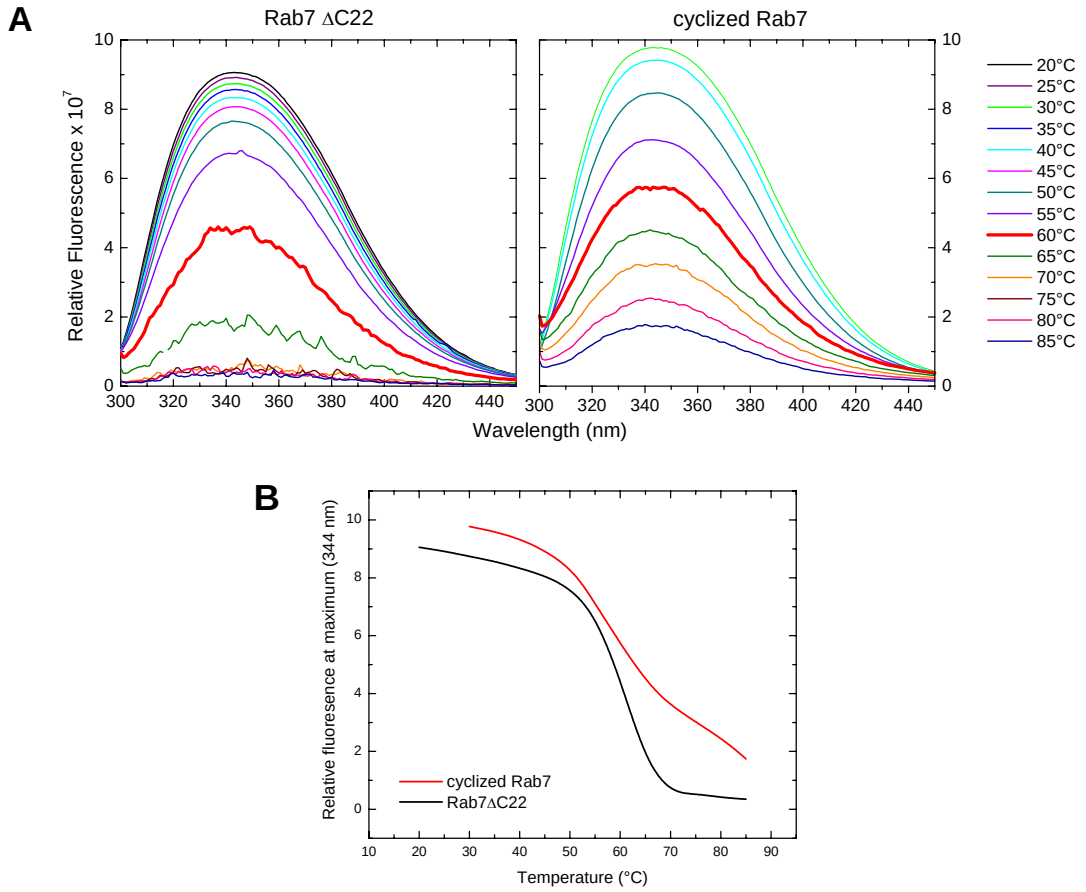

Figure 52. *A*, Comparison of the intrinsic tryptophan fluorescence emission of Rab7ΔC22 and cyclized Rab7 upon thermal denaturation. *B*, Fluorescence at 344 nm with respect to temperature.

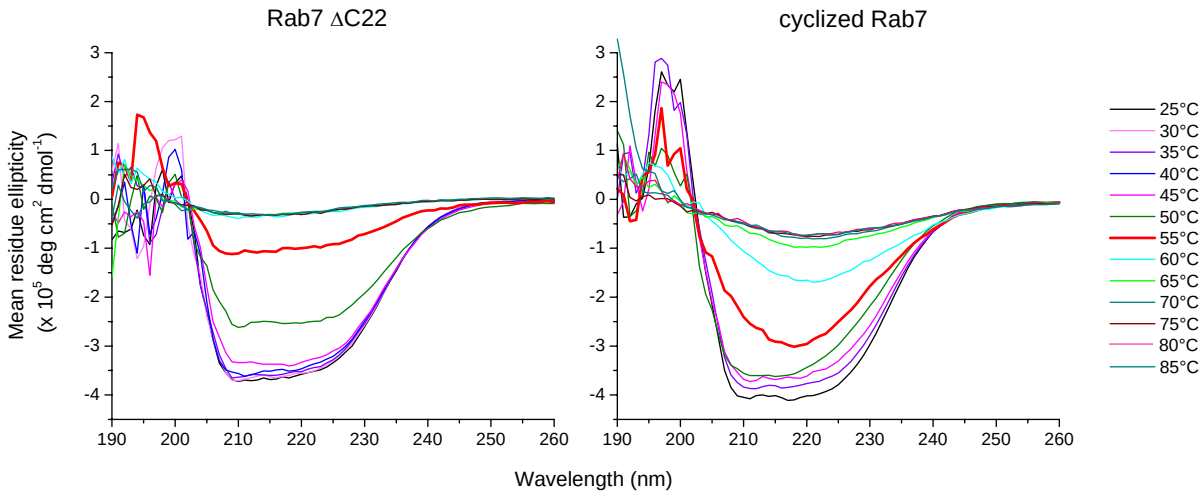

Figure 53. Comparison of circular dichroism spectra of Rab7ΔC22 and cyclized Rab7 upon thermal denaturation.

The nature of this effect was clarified with subsequent circular dichroism measurements (Figure 53). With increasing temperature, both proteins increase their β-strand content, with cyclized Rab7 demonstrating a more pronounced alpha to beta transition. In contrast to the recovery of fluorescence of cyclized Rab7 observed upon re-cooling, the protein did not regain any secondary structure when the 85°C sample was re-cooled to 20°C. Rab GTPases have a conserved 6-stranded β-sheet core that is surrounded by 4 α-helices. For the cyclized protein, thermal denaturation causes the surrounding α-helices to unfold but the protein is prevented from melting further possibly by the constraints of the covalent attachment of the N- and C-termini. Thus the final denatured protein is "trapped" with some elements of β-sheet remaining. Since Rab7 contains a tryptophan in the β-sheet core (W62), the apparent retention and recovery of tryptophan fluorescence may be due to an enhanced hydrophobic environment upon denaturation that prevents quenching of the fluorescence by water.

The extent of thermostability imparted by cyclization was quantified by determining the melting temperature for cyclized Rab7 and Rab7ΔC22. This was measured using the temperature dependence of the CD signal at 210 nm (α-helix) and 220 nm (β-sheet) (Figure 54). Cyclization modestly increased the melting temperature by 3.7°C (210 nm), which falls short of the typical 5°C increase in thermostability observed for cyclization of other proteins such as β-lactamase and subunit IIA of the *E. coli* glucose transporter (Iwai and Pluckthun, 1999; Siebold and Erni, 2002), and is less significant when compared with the ~14°C increase in melting temperature obtained with cyclized DnaB-N (Williams *et al.*, 2002).

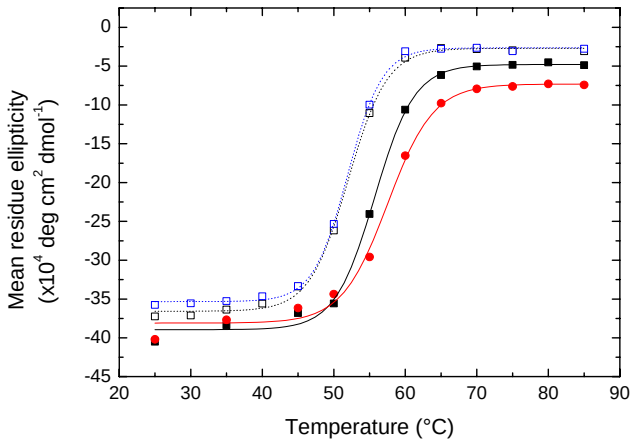

Rab7 ΔC22 (210 nm)
Rab7 ΔC22 (220 nm)
cyclized Rab7 (210 nm)
cyclized Rab7 (220 nm)

Protein	*T*m
Rab7 ΔC22 (210 nm, 220 nm)	52°C
cyclized Rab7 (210 nm)	55.7°C
cyclized Rab7 (220 nm)	57.5°C

Figure 54. Melting temperature of Rab7ΔC22 and cyclized Rab7 determined by the CD signal at 210 nm and 220 nm with increasing temperature.

3.4.4 The effect of cyclization on biological function

As is the case with all modifications, it is important to determine whether they influence the native state of the protein of interest. In this regard, several measurements were made with cyclized Rab7 and its linear counterpart, Rab7ΔC22 to see if they differed significantly from each other.

GTPase Activity

The intrinsic GTPase activity was measured by incubating either Rab7ΔC22•GTP or cyclized Rab7•GTP in 40 mM HEPES, pH 7.5 at 37°C in the presence of 10 mM $MgCl_2$. Aliquots were collected every 20 seconds, flash frozen in liquid nitrogen to stop the GTPase reaction, and analyzed by HPLC to quantify the amounts of GTP and GDP. Cyclization caused a slight decrease in the hydrolysis rate, with a rate constant of 0.0032 s^{-1} compared to 0.0054 s^{-1} for the linear form (Figure 55).

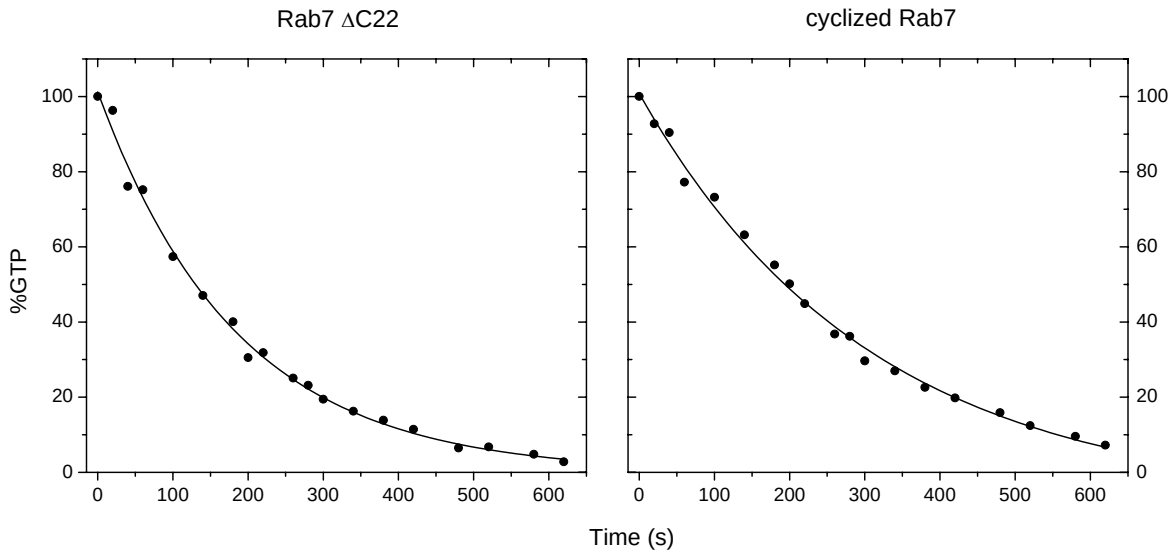

Figure 55. Intrinsic GTPase activity of cyclized Rab7 compared to Rab7ΔC22. Cyclized Rab7•GTP or Rab7ΔC22•GTP at a concentration of 150 µM in 40 mM HEPES, pH 7.5 was incubated at 37°C in the presence of 10 mM $MgCl_2$. Aliquots were collected at the given time points, flash frozen in liquid nitrogen and analyzed on HPLC to quantify the amounts of GTP and GDP. The amount of GTP for each time point was normalized with the initial amount of GTP.

Effector binding and dissociation

Association and dissociation kinetics were measured for both cyclized Rab7 and its linear counterpart, Rab7ΔC22 to determine if cyclization affected the biological activity of Rab7. For association measurements, each Rab7 construct was complexed with a fluorescent analogue of GDP (mantGDP) at a final protein concentration of 0.5 µM and titrated against varying excess concentrations of Mrs6, the yeast homologue of REP-1. Fluorescence resonance energy transfer (FRET) was exploited by excitation of the intrinsic tryptophan fluorescence of the Rab7 protein and measurement of the emission of the mantGDP moiety. Binding was associated with an increase in the FRET signal over time, whereas displacement showed a decrease in the FRET signal over time. Cyclization of Rab7 did not drastically alter the association kinetics of Rab7 to Mrs6. Both cyclized Rab7 and Rab7ΔC22 showed double exponential binding kinetics, with apparent K_D's of similar order of magnitude, 3.58 ± 0.75 µM and 1.36 ± 0.40 µM, respectively, using amplitude analysis (Figure 56). Each construct lacks the C-terminal tail, and therefore represents the globular core of Rab7. The affinity of these constructs to Mrs6 is decreased 40- to ~100-fold when compared to wild type Rab7 [c.f. K_D = 35 ± 2 nM, (Constantinescu, 2001)]. Thus, the measured values can be regarded as the affinity of the globular core of Rab7 to REP-1.

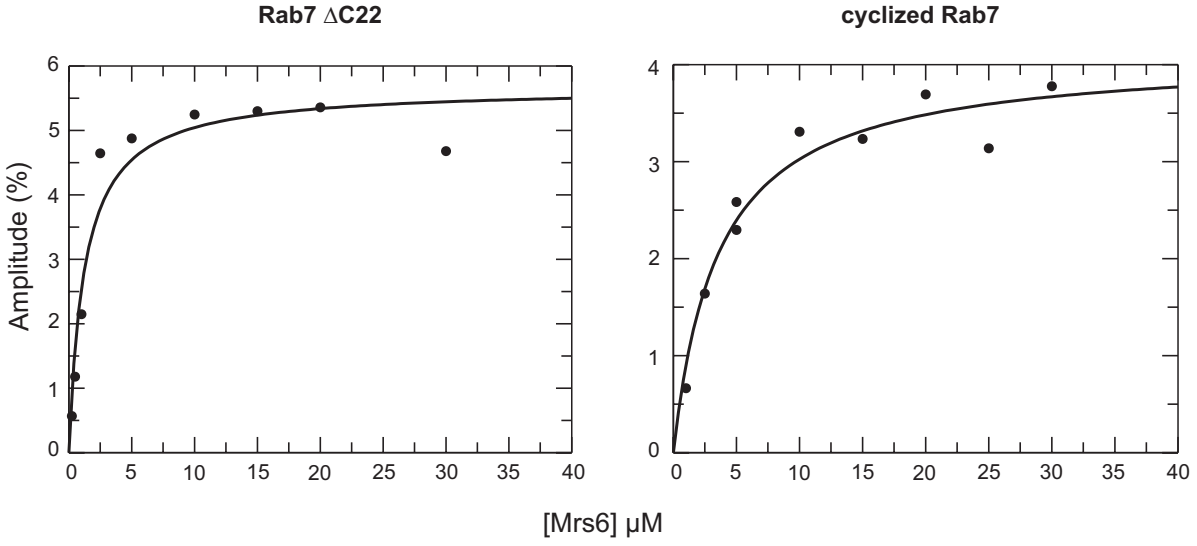

Figure 56. Independent determination of the affinity of Rab7ΔC22•mantGDP and cyclized Rab7•mantGDP, respectively, for Mrs6 using amplitude analysis.

The association of two proteins is a bimolecular process, and is therefore a second order reaction. Under certain conditions, a second order reaction can be made to approximate a first order reaction if one of the species is present in a large excess of the other. Although such conditions were employed in the studies presented here, simple exponential behavior expected from pseudo-first order conditions was not observed. Earlier measurements of REP-1 association with Rab7 also indicated double exponential behavior, and this was explained by a 2-step binding model with fluorescence changes in both steps (Alexandrov *et al.*, 1998). Displacement measurements in the present work also showed biphasic behavior. Here, there was a clear difference in the behavior, with Rab7ΔC22 being more obviously biphasic.

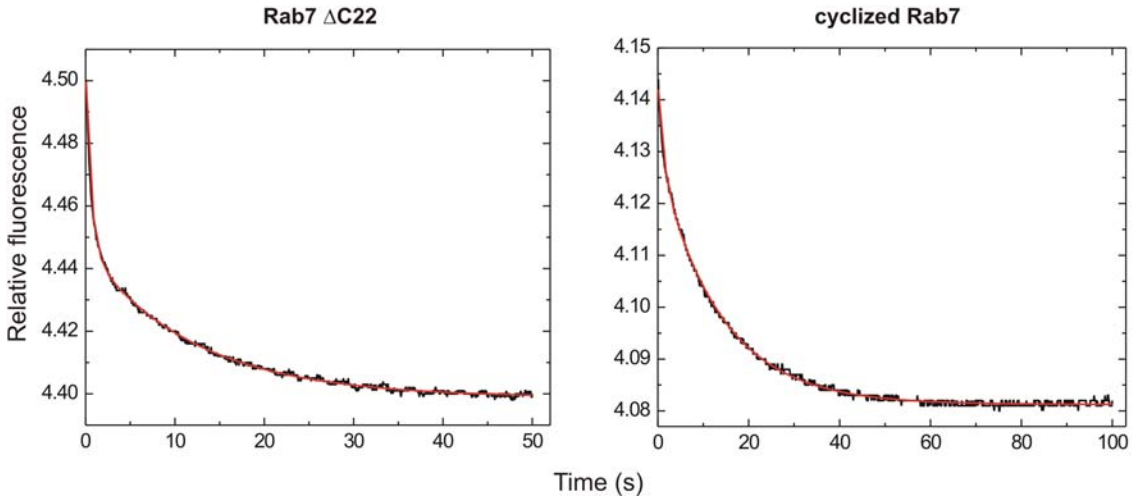

Figure 57. Displacement of Rab7ΔC22•mantGDP and cyclized Rab7•mantGDP, respectively, from Mrs6. Kinetic transients were fit to a double exponential equation. The fitted rate constants for Rab7ΔC22 are k_1=1.6 ± 0.022 s^{-1}, k_2= 0.083 ± 0.00052 s^{-1}, and for cyclized Rab7, k_1 = 0.87± 0.04 s^{-1}, k_2= 0.074 ± 0.00036 s^{-1}.

Biphasic kinetics suggests, but is not limited to, two binding steps, and in this case may represent the overall behavior of several different factors. It is interesting to note that Rab7 contains three tryptophans, each of which are within 25 Å of the 3'-oxygen of the nucleotide ribose, which is the usual site of attachment for the mant moiety (PDB Code 1VG9: Trp 62, 22.42 Å; Trp 102 ,17.96 Å; and Trp 142, 24.69 Å). Two of these lie in the vicinity of Switch I and II, with Trp 62 just below the interface between Switch I and the Rab binding platform of REP-1, and Trp 102 situated just behind the short helix in Switch II (Figure 58A and B). Switch II makes extensive contacts with the Rab binding platform in REP-1 (Figure 45).

Trp 62 additionally participates directly at the Rab7:REP-1 interface, and undergoes a rotation of 19.8° upon REP-1 binding (Figure 58C). It is thus conceivable that the observed fluorescence changes represent a combination of several conformational changes of Rab7 upon REP-1 binding as sensed by the tryptophans, which may not all occur simultaneously with association. This would be consistent with the previously observed fast, concentration-dependent phase, followed by a slower, concentration-independent phase of Rab7 association with REP-1 (Alexandrov *et al.*, 1998). In this case, the initial association of Rab7 to REP-1 would be concentration dependent, while the subsequent conformational changes would not depend on REP-1 concentration since the two proteins are already associated with each other.

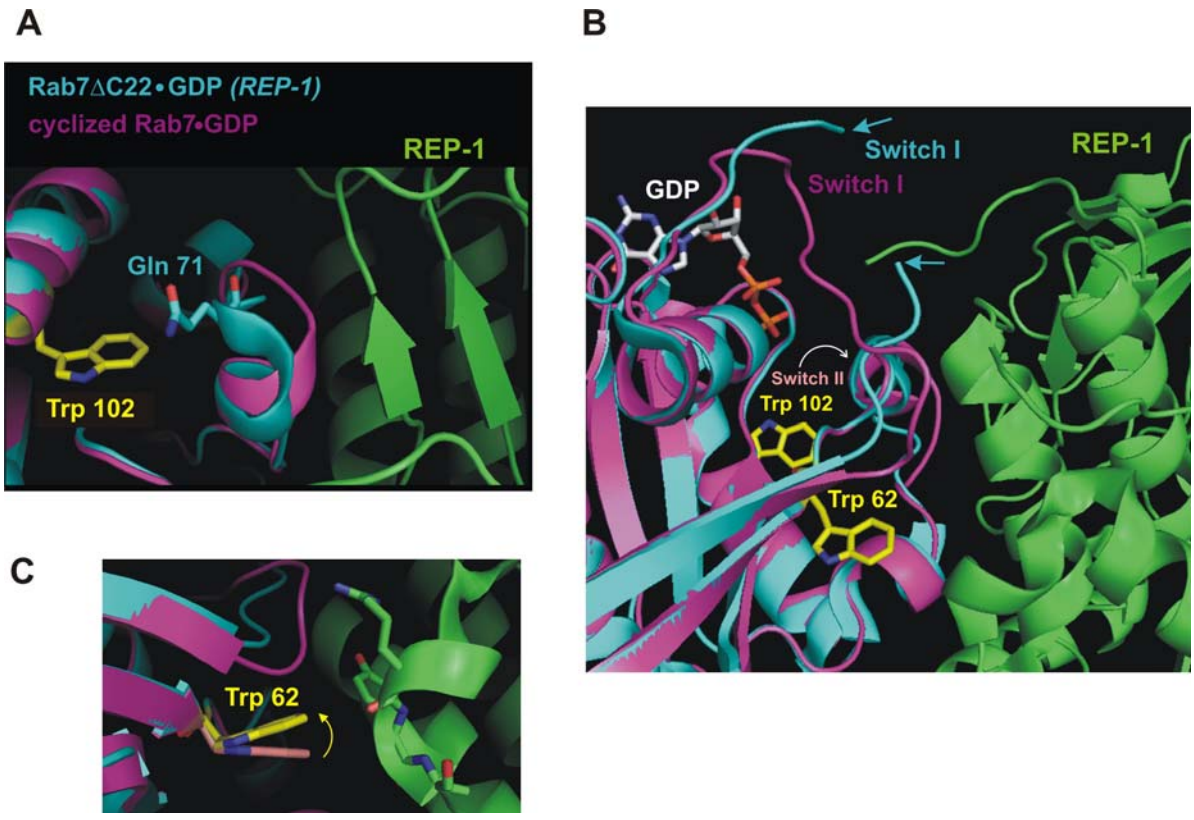

Figure 58. Location of tryptophans in the vicinity of Switch I and II in Rab7. *A*, Ribbon representations of cyclized Rab7•GDP (magenta) superposed on Rab7ΔC22•GDP (cyan) in complex with REP-1 (green). Trp 102 lies behind the short helix in Switch II that moves in toward Rab7 upon binding of the N-terminal region of Domain I in REP-1. *B*, View of Trp 62 at the Rab7:REP-1 interface, below Switch I, and next to Switch II, which undergoes conformational changes upon REP-1 complex formation. Arrows indicate the ends of the visible region of Switch I in the linear Rab7ΔC22•GDP structure. Bound GDP is shown as white stick representation. *C*, Rotation of Trp 62 that must occur in cyclized Rab7•GDP (peach stick) upon Rab7:REP-1 complex formation (yellow stick).

As mentioned previously, although cyclization of Rab7 does not prevent Rab7 association to Mrs6, it does slightly lower its affinity. The similar dissociation rate constants for cyclized and linear Rab7 indicate that the difference in affinity is due to different association rate constants. A direct consequence of covalent linkage of the termini is a reduction of the degrees of freedom available for Rab7, which may affect its association with Mrs6. It is well known that Ras GTPase effectors bind Ras with an induced-fit binding mechanism (Sydor *et al.*, 1998; Linnemann *et al.*, 1999), and this has also been observed when Rab3A forms a complex with its effector, Rabphilin-3A (Ostermeier and Brunger, 1999). Superposition of the crystal structure of uncomplexed cyclized Rab7•GDP on the Rab7ΔC22•GDP in complex with REP-1 reveals that the short helix consisting of Arg 69, Phe 70, and Glu 71 in Switch II is compressed towards Rab7 upon REP-1 binding (Figure 59). In cyclized Rab7•GDP, Glu 71 would have to rotate approximately 180°C to avoid collision with Tyr 395 of REP-1, and form a hydrogen bond between its backbone carbonyl and the side chain of Arg 398 from REP-1. Covalent linkage of the termini may constrain the protein in such a way that this rotation is less favorable, which could contribute to the slight reduction in affinity measured for cyclized Rab7. Interestingly, in contrast to uncomplexed wild type Rab7•GDP, which possesses a different conformation of Switch II prior to REP-1 binding, cyclized Rab7•GDP alone and Rab7ΔC22•GDP in complex with REP-1 share a similar overall conformation in some areas of Switch II. In spite of this, REP-1/Mrs6 may require a different initial conformation of Rab7•GDP to induce the final bound conformation. It is worthy to note here that in most of the determined inactive GDP-bound Rab GTPase structures, the switch regions are largely disordered (Eathiraj *et al.*, 2005). REP-1/Mrs6, thus, may require a more flexible Rab7•GDP in order to produce a productive binding event. The reduced degrees of freedom in turn may hinder the larger conformational changes required by cyclized Rab7•GDP for REP-1/Mrs6 association.

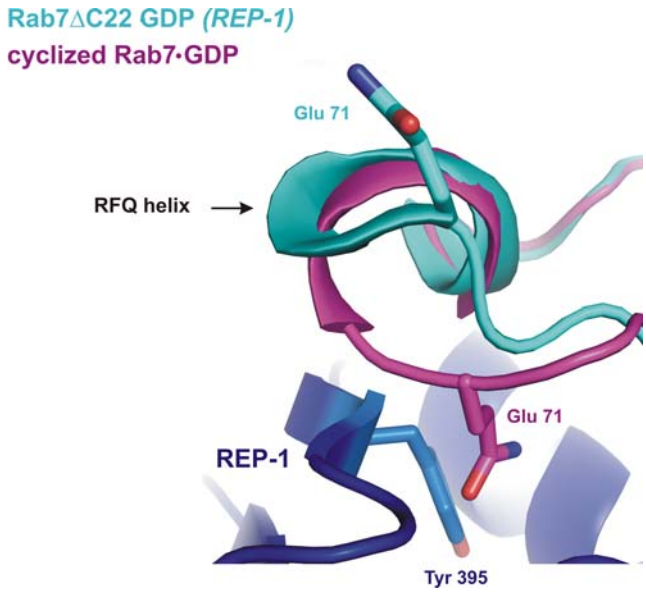

Figure 59. Rearrangement of the short helix (Arg69-Phe70-Glu71) of Rab7 with 180° rotation of Glu 71 upon REP-1 binding to Rab7. Superposed ribbon representations of cyclized Rab7•GDP (magenta) and Rab7ΔC22•GDP (cyan) in complex with REP-1 (dark blue).

3.4.5 Cyclization as an aid for crystallization

Cyclized Rab7• GDP

Rab7•GDP has been extensively structurally characterized. Both monoprenylated Rab7•GDP and Rab7ΔC22•GDP each in complex with REP-1, as well as Rab7•GDP and Rab7•GppNHp alone have been crystallized and their structures have been determined by X-ray crystallography (Rak *et al.*, 2004). Switch I and II were found to be largely disordered in the Rab7•GDP structure, in keeping with the inherent flexibility of these regions in the GDP form of Rab GTPases in general (Stroupe and Brunger, 2000; Eathiraj *et al.*, 2005). Structures of Rab7ΔC22•GDP and monoprenylated Rab7•GDP in complex with REP-1 allowed for the visualization of Switch II, which makes key interactions with the REP-1 molecule. In contrast, Switch I was disordered in each structure, arising from the minimal contact of this region with REP-1, which predominantly interacts with Switch II. With this motivation, Rab7 was cyclized to determine if this could stabilize the Switch I region enough to obtain structural information on this area. Indeed, cyclized Rab7•GDP crystallized readily, and diffracted to very high resolution (1.16 Å), resulting in a complete picture that includes Switch I (Dr. Olena Pylypenko, *unpublished results*).

The overall structures of Rab7•GDP and cyclized Rab7•GDP do not differ significantly from each other, with a rmsd of C_α atoms of 0.83 Å. The main difference lies in the ordering of Switch I and II in the cyclized version (Figure 60A). These regions are stabilized by several crystal contacts. Rab7•GDP and cyclized Rab7•GDP crystallized in different space groups, and therefore possess different crystal packing. The observed conformation of Switch I in cyclized Rab7•GDP is affected by hydrophobic contacts with the linker region of a symmetry related molecule. The side chain of Ile 4 in the linker packs against a hydrophobic environment created by the methylene groups of Gln 36 and Lys 38, as well as the aromatic ring of Tyr 37 in Switch I. A salt bridge between Arg 69 in Switch II and Glu 158 of a second symmetry related molecule allows for a second hydrophobic environment, with Ile 127 and Ile 160 of the same symmetry molecule packing against Tyr 37 on the other side of its aromatic ring (Figure 60C). This stabilized conformation of Switch I allows Ala 39 to form key backbone hydrogen bonds to both the α-phosphate and an axial water which coordinates the Mg^{2+} ion (Figure 60D), thus stabilizing GDP binding. Cyclized Rab7 was found to require a more stringent nucleotide exchange protocol to fully exchange the endogenously bound GDP compared to wild type Rab7 (see next section), which suggests that these interactions between Ala 39 and GDP may also be present in solution. Knowledge of the conformation of Switch I in the apo-form of Rab7•GDP allows for comparative analysis with structures of Rab7 bound to effectors like REP-1 to understand the molecular details of Rab7 conformational changes upon binding (see Effector binding section).

Switch II is also stabilized by interactions of neighboring symmetry related molecules as well as intramolecular interactions. The salt bridge between Arg 69 and Glu 158 of a symmetry related molecule provides one anchor point, which is enhanced with hydrophobic interactions between Phe 70 and the methylene groups of Glu 130 of the same symmetry related molecule. A second area, the extended loop region of Switch II, is ordered through a hydrogen bond between the side chain of Ser 72 and Gln 109, which further hydrogen bonds to the side chain of Glu 105. Additional hydrophobic interactions occur between the side chains of Leu 73 and Phe 77 (Figure 60B).

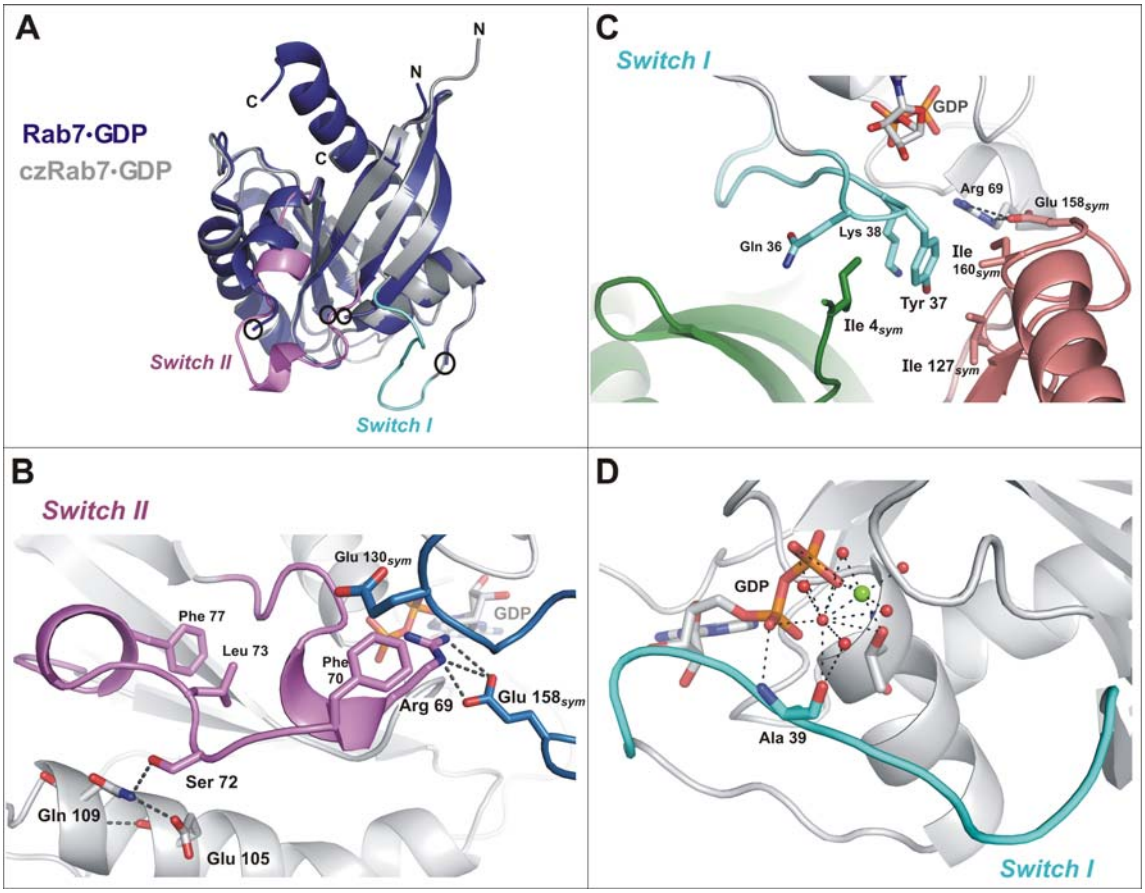

Figure 60. Stabilization of Switch I and II in cyclized Rab7•GDP. *A*, Superposition of ribbon representations of Rab7•GDP (navy) and cyclized Rab7•GDP (white). Black circles indicate the extent of the switch regions visible in Rab7•GDP, with Switch I and Switch II in cyclized Rab7•GDP highlighted in cyan and lilac. *B*, Stabilization of Switch II in cyclized Rab7•GDP through favorable interactions (dashes) between Arg 69 and Glu 158 of a symmetry related molecule (blue) on one end, and Ser 72 with Gln 109 on the other. Additional hydrophobic interactions occur between Leu 73 and Phe 77, as well as between Phe 70 and the methylene groups of Glu 130 of the same symmetry related molecule. *C*, Stabilization of Switch I in cyclized Rab7•GDP via interactions with symmetry related molecules. Glu 36, Lys 38, and Tyr 37 in Switch I surround Ile 4 of the linker region from one symmetry related molecule (green). A salt bridge between Arg 69 in Switch II and Glu 158 of a second symmetry related molecule (dark peach) allows Ile 127 and Ile 160 of the same symmetry molecule to pack against Tyr 37 on the other side of its aromatic ring. *D*, Ribbon representation of the nucleotide binding region of cyclized Rab7•GDP. Switch I is shown in cyan, with interactions made by Ala 39, Mg^{2+} (green sphere) and active site waters (red spheres) shown with dashes.

Cyclized Rab7• GppNHp

Additional structural studies were carried out to determine whether cyclization permitted crystallization of the GTP-state of Rab7 as well. Crystallization studies on cyclized Rab7•GDP highlighted two base conditions that promoted protein crystal growth: 1) 25% PEG 3350, 100 mM Tris-HCl, pH 8.5, and 2) 1.6 M ammonium sulfate, 100 mM HEPES, pH 7.4 with microseeding, each with a protein concentration of 7 mg/ml (Nathalie

Bleimling, unpublished results). These conditions were probed first as an initial screen for cyclized Rab7 in complex with GppNHp (a nonhydrolyzable GTP analogue) at a concentration of 5 mg/ml, and both produced crystals. Crystals appeared 3 days after setup without microseeding in the ammonium sulfate conditions, and these were probed further by varying the pH and concentration of precipitant to encourage single crystal growth suitable for X-ray diffraction studies. A pH value other than 7.4 only delayed the onset of crystallization, and did not improve crystal form. Different seeding techniques such as microseeding and streak seeding were employed, as well as varying the time the seeds were introduced to the crystallization drops. Though the crystal forms improved to rods, they remained striated and flawed even at the stage of initial crystal growth. These observations led to suspicions that there was an inherent problem with the protein samples used for crystallization.

Though requiring a significantly longer time (months), crystals were also eventually observed in the PEG conditions. When these crystals were subsequently used to seed fresh drops, crystals appeared overnight, with successive "generations" of seeding producing crystals with greatly improved quality and form. The resulting crystals strikingly resembled the form obtained for cyclized Rab7•GDP, and these results strengthened the growing suspicions that these crystals and those obtained from ammonium sulfate contained GDP or GDP-like nucleotides.

Crystallization proved to be somewhat sensitive to different batches of purified protein, and surprisingly insensitive to the nucleotide state of the protein. HPLC analysis on crystals obtained in 21-22% w/v PEG 3350 with 100 mM Tris-HCl, pH 8.5 showed occupancy for three different nucleotides: 59.6% GDP, 8.8% of a contaminant found in GppNHp used for nucleotide exchange (possibly $GppNH_2$), and 31.6% GppNHp. Analysis of crystals obtained from ammonium sulfate also contained a significant amount of this GDP-like contaminant, with a putative $GppNH_2$ content 8-fold higher than GppNHp (Table 3). These results demanded a more stringent nucleotide exchange protocol than the one typically used for wild type Rab7 to produce exclusively GppNHp-bound protein for the present crystallization studies. Inclusion of alkaline phosphatase (Simon *et al.*, 1996) to ensure complete removal of GDP successfully produced 97.8% cyclized Rab7•GppNHp. It is interesting to note that with this procedure, the amount of bound $GppNH_2$ was significantly reduced to 2.2%.

Table 3. Nucleotide identification and quantification using HPLC analysis of crystals of cyclized Rab7. Standards containing 10 µM GDP and 10 µM GppNHp were analyzed alongside samples under isocratic conditions using 50 mM potassium phosphate, pH 6.6, 10 mM TBAB and 8% Acetonitrile. Crystals from PEG 3350 conditions, AP treated cyclized Rab7, and their respective standards were analyzed using a buffer containing slightly less than 8% Acetonitrile. Retention times for the respective standards are shown in parentheses.

Sample	Retention Time (min)	% nucleotide
Crystals from PEG 3350 conditions:		
$GppNH_2$	5.89 (5.92)	8.79
GDP	10.10 (10.03)	59.60
GppNHp	14.32 (14.26)	31.61
Crystals from $AmSO_4$ conditions:		
$GppNH_2$	5.26 (5.27)	89.02
GppNHp	11.61 (11.65)	10.98
AP treated cyclized Rab7:		
$GppNH_2$	5.94 (5.93)	2.22
GppNHp	14.32 (14.31)	97.78

This alkaline phosphatase prepared cyclized Rab7•GppNHp (10 mg/ml) produced initial crystals 2 days after set up in 1.6M ammonium sulfate and 100 mM HEPES, pH 7.4 without seeding. Several factors were optimized to produce crystals large enough for diffraction studies. These include streak seeding drops at the time of setup, decreasing the concentration of precipitant to 1.3M or 1.4M, and increasing the drop volume from 0.6 µl to 1.4 µl. These measures resulted in a flat crystal approximately 60 x 100 microns large (Figure 61A). Unfortunately, it was discovered that this crystal consisted of a collection of tiny rods, which splintered during separation attempts from the rest of the crystal bundle.

As mentioned earlier, PEG 3350 provided an alternative crystallization condition and parameters were also probed in parallel using the alkaline phosphatase generated cyclized Rab7•GppNHp. Two concentrations of protein (5.15 mg/ml and 10.3 mg/ml), several pH values (4.5 to 10.6), and varying PEG concentrations were scanned and tested with cross-seeding from GDP-containing cyclized Rab7 crystals that were originally seen in PEG 3350. Crystals were more reluctant to form in PEG conditions than was observed with the ammonium sulfate conditions (Figure 61B and C). Crystals were rather sensitive to pH, and found only to form with 100 mM Tris-HCl, pH 8.5. In general, 5-7 days were required before crystals were observed, and although most had thin-plate morphology, there was considerable striation observed along the surfaces (Figure 61, E and F). Unfortunately, crystals grown from PEG 3350 proved to be less robust than their ammonium sulfate counterparts. Heat from a standard light microscope was enough to create a temperature gradient within the vapor diffusion wells, which effectively melted the crisp edged plates. In

addition, initial tests for diffraction showed weak reflections to 12 Å. To see whether other compounds could improve the form and quality, a commercially available PEG Suite Nextal screen composed of 96 conditions with different molecular weight PEGs, pHs and salts, was made. Long thin needles were found 5 days later in 20% PEG 3350 with 200 mM magnesium sulfate. When reproduced on a larger scale, 23% PEG 3350 with 100 mM Tris-HCl, pH 8.5 and 200 mM magnesium sulfate produced very large clusters of striated plates 5 days after setup without seeding (Figure 61D). When tested for diffraction, the crystals diffracted to 3Å, but the reflections were diffuse, and subsequent screening for diffraction did not identify any crystal that would be suitable for structure determination.

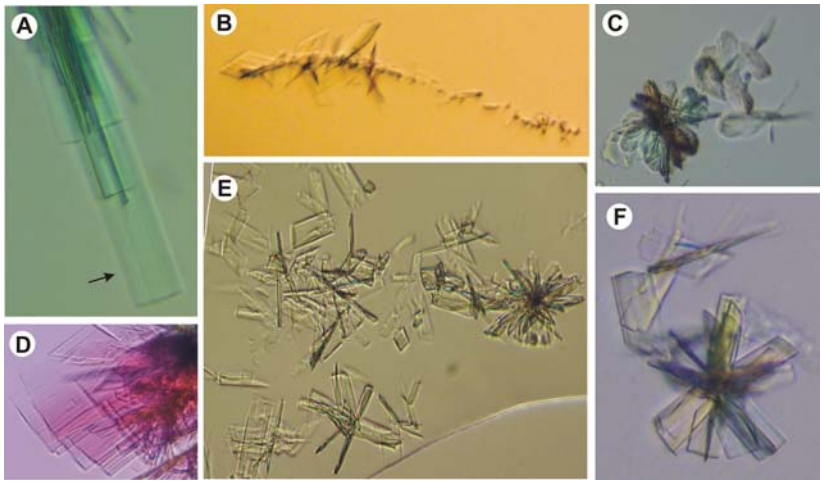

Figure 61. Crystals grown from alkaline phosphatase-prepared cyclized Rab7•GppNHp. *A*, Crystals obtained from optimized conditions containing 1.4 M Ammonium sulfate, 100 mM HEPES, pH 7.4 with seeding at a protein concentration of 10.3 mg/ml. A volume of 0.7 µl protein to 0.7 µl reservoir solution was used over a final reservoir solution of 500 µl. Arrow indicates the crystal described in the text. *B and C*, Initial crystals of cyclized Rab7•GppNHp obtained in 23% and 25% PEG 3350, 100 mM Tris-HCl, pH 8.5. *D*, Striated plates obtained from 23% PEG 3350 with 100 mM Tris-HCl, pH 8.5 and 200 mM $MgSO_4$. *E and F*, Improved crystals obtained after streak seeding with crystals from B and C.

In an effort to determine if other factors might improve the ammonium sulfate crystal form or provide new crystal forms, an additive screen (Hampton Research) of 96 different small molecules was made using 1.6M ammonium sulfate and 100 mM HEPES, pH 7.4 as a base solution. In this commercially available screen, 96 reagents ranging from various salts, small organic molecules to detergents, are diluted 10-fold with the base solution. Crystals were found in a few conditions containing monovalent salts one week after setup. One condition containing 200 mM NaCl produced a cluster of crystals, some of which were thin

plates (Figure 62A), which was subsequently used as a seed stock to reproduce the conditions on a larger scale. Streak seeded drops produced showers of small, sometimes flat, rods overnight (as opposed to the originally observed thin plates) and crystal formation was surprisingly insensitive to varying concentrations of NaCl (50-400 mM). The number of crystals formed was proportional to the concentration of ammonium sulfate used, with 1.3 and 1.4 M ammonium sulfate providing slower equilibration to improve crystal growth. Sequential seeding, where nice looking crystals of a flat rod form were crushed and used as seeds in fresh drops, aided in producing "generations" of more desirable looking crystals. Drop sizes were also varied to additionally increase equilibration time and allow for more controlled crystal formation. Reproducibility was a continual problem, but conditions were optimized to a range of 1.3-1.44 M ammonium sulfate, 100 mM HEPES, pH 7.4 and 200-300 mM NaCl, with 0.6 µl or 1µl total drop volume. Unfortunately these crystals either did not diffract or produced smeary reflections in the diffraction pattern when tested on a home X-ray generator source.

Another condition containing 100 mM KCl was found to produce a cluster of predominantly thin plates 19 days after the original additive screen setup (Figure 62B). Two thin plates were isolated from this original drop and cryocooled in 70% saturated ammonium sulfate, 100 mM HEPES, pH 7.4, and 10% glycerol. One of the crystals diffracted to 3.5 Å in house, the best diffraction from any ammonium sulfate grown crystal obtained thus far. Reflections were diffuse, but this result encouraged further optimization to improve diffraction quality. Crystals could be reproduced with seeding from this original crystal cluster, and similar optimization strategies employed for the NaCl conditions were made with the KCl conditions. These produced more consistently (though not exclusively) thin plates, albeit often with striated surfaces. One protein batch set up in the sitting drop format at 13 mg/ml with 1.3 M ammonium sulfate, 100 mM HEPES, pH 7.4, and 500 mM KCl, with an altered protein to reservoir ratio of 0.5 µl to 1 µl or 0.5 µl to 1.5 µl and microseeding, gave three clean, glass-like thin plates measuring 200 µm in the longest dimension (Figure 62C to E). This success, however, was limited by the fact that the plates were indeed very thin and manipulation with cryoloops to cryocool for diffraction testing was quite demanding. Many factors contributed to the difficulty of this task. The sitting drop pedestals that were used are

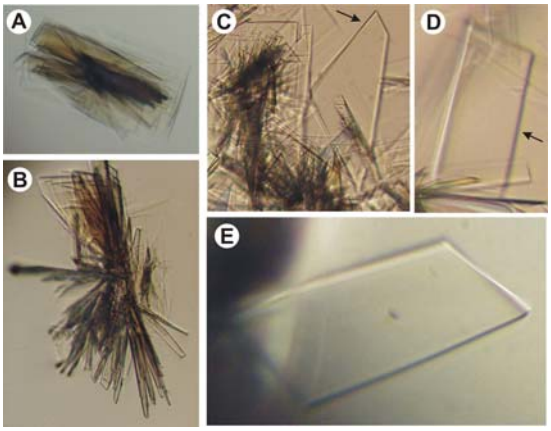

Figure 62. Flat plate crystals of alkaline phosphatase-prepared cyclized Rab7•GppNHp obtained in ammonium sulfate with NaCl and KCl. *A*, Crystal cluster found in the original additive screen with 200 mM NaCl. *B*, Initial crystal cluster found in the original additive screen with 100 mM KCl. *C*, *D*, and *E*, Improved crystals of cyclized Rab7•GppNHp, in ammonium sulfate, 500 mM KCl, and 100 mM HEPES, pH 7.4.

quite deep, and the need to add cryoprotectant solution at approximately 3 times the volume of the original drop results in a very narrow plane of focus for viewing through the light microscope. In addition, the few thin plates were often surrounded by a large network of rods, which made the technical aspect of crystal handling extremely problematic to coordinate this in a short period of time before ammonium sulfate salt crystals invaded the drop due to high vapor pressure. The nature of the thin plate morphology also makes uniform cryocooling of the crystals without bending at the edges quite tricky, especially if the plates are large. Thus many crystals were screened for diffraction to find any which would be suitable for structure determination. The most common problems encountered were clean diffraction in one direction, and streaky, diffuse diffraction at phi= 90°.

Data collection and structure solution

One such crystal was found, which surpassed all previously tested crystals, diffracting to the edge of the home source detector at 2.2 Å in one direction. Diffraction data were collected at the Swiss Light Source (SLS) synchrotron to 1.8 Å. Diffraction data were processed with *XDS* (Kabsch, 1993), which indicated that the highest possible symmetry of the diffraction pattern corresponded to an orthorhombic space group. The structure was solved with molecular replacement using *MOLREP* (Collaborative Computational Project Number 4, 1994) with Rab7•GDP (PDB code 1VG1) as a search model, indicating a space group of $P22_12_1$ with two molecules of cyclized Rab7•GppNHp in the asymmetric unit. This model was refined using *REFMAC5* (Murshudov *et al.*, 1997), but the *R* factors failed to converge to acceptable values. The data were re-examined, and it was discovered that the crystal was

actually twinned, with a true space group of $P2_1$ and four molecules in the asymmetric unit (Table 4).

Table 4. Data collection and refinement statistics of cyclized Rab7•GppNHp. Data processed in the correct space group, $P2_1$, are compared to values from original processing in $P22_12_1$. Values in parentheses are for the highest resolution shell, 1.85-1.80Å.

Data collection		
X-ray source	SLS beamline, Paul Scherrer Institute	
Wavelength (Å)	0.9796	
	Processing in $P2_1$ (correct space group)	Processing in $P22_12_1$ (incorrect space group)
Unit cell parameters (Å, °)	a = 40.62, b = 47.15, c = 189.94 α = 90.000, β = 89.991, γ = 90.000	a = 47.07, b = 190.04, c = 40.55 α = 90.000, β = 90.000, γ = 90.000
Resolution range	20-1.8 Å	20-1.8 Å
No. of observations	156841	153872
No. of unique reflections	62728	33970
R_{merge} (%)	12.2 (50.6)	9.1 (36.0)
Completeness (%)	93.3 (83.3)	97.6 (92.2)
Redundancy	2.5 (2.3)	4.5 (4.0)
$<(I/\sigma(I)>$	11.1 (2.7)	12.9 (3.2)

Refinement	
R factor (%)	18.4
R_{free} (%)	26.6
Included residues	
molecule 1	5-179
molecule 2	6-71, 74-175
molecule 3	6-178
molecule 4	5-71, 74-179
No. protein atoms	5464
No. ligand atoms	132
No. solvent atoms	345
Twinning operator	$-h,-k,l$
refined twinning fraction	0.49
R.m.s.d. bond lengths (Å)	0.014
R.m.s.d. angles (°)	2.1
Average B values (Å^2)	
Overall	22.3
Main chain	21.6
Side chain	23.0
Mg-GppNHp	17.2
Solvent	28.0
Ramachandran plot , % residing in	
Core regions	87.2
Additional allowed regions	11.8
Generously allowed regions	1.0
Disallowed regions	0

$R_{merge} = \Sigma \mid A_{I_{h,P}} - A_{I_{h,Q}} \mid / (0.5 * \Sigma A_{I_{h,P}} + A_{I_{h,Q}})$, a quality indicator of the final merged structure factor amplitudes.
Multiple observations of reflection h are assigned to two disjoint sets, where $I_{h,P}$ and $I_{h,Q}$ are the partially averaged estimates of the intensity. A_I are pseudoamplitudes, which take the contribution of negative reflections into account.
$R = \Sigma \mid |Fo| - |Fc| \mid / \Sigma |Fo|$, where Fo and Fc are the structure factor amplitudes of the data and the model, respectively.
R_{free} is R using a 5.6% test set of randomly chosen reflections with twinning taken into account.

The complications of twinning in crystallography

When molecules crystallize out of solution, they search for the lowest free energy state, which is most easily accomplished by packing in a regular fashion. A perfect crystal is a three-dimensional ordered array of molecules possessing identical conformations.

Molecules within the crystal are related to each other by symmetry relationships such as rotation about an axis, which if performed on one of the molecules will produce another molecule in the lattice. Thus, molecules which are related by crystallographic symmetry have identical crystallographic environments (Drenth, 1999). A phenomenon in crystallography that macromolecular crystallographers are becoming increasingly aware of is that of twinning. Twinning is a special type of crystal growth defect where molecules may pack together in a way that is more favorable, but which violates the crystal symmetry (Yeates and Fam, 1999). This creates two or more regions termed "domains" that relate to each other by a specific symmetry operation known as the twin law.

The presence of these specially related domains gives rise to certain properties of the resulting diffraction patterns depending on the number of dimensions in which their respective lattices coincide (Yeates, 1997; Yeates and Fam, 1999). If the domains share a common interface, where only two of the three dimensions coincide, the resulting diffraction pattern will be a composite of the two lattices. Such twinning is referred to as epitaxial, or non-merohedral twinning, and usually does not present large obstacles for structure determination, since the two diffraction patterns can be identified at the data collection stage. If one lattice can be indexed, the reflections from the second can then be ignored as long as they do not lie close to reflections from the first lattice (Yeates, 1997). A more problematic form of twinning (for the crystallographer) is when all three dimensions of each domain coincide perfectly, termed merohedral twinning. In this case, the diffraction patterns from each domain superimpose and resemble that of a single crystal because the respective real space lattices superimpose exactly. They are, however, oriented differently toward one another inside the crystal. This means that although the reflections of each domain superimpose in reciprocal space, their intensities are actually made up of contributions from the respective intensities of each twin reflection. Every reflection $I_{obs}(\mathbf{h}_1)$ will have a twin related reflection $I_{obs}(\mathbf{h}_2)$ related by the twin law, and the resulting measured intensities will be a linear combination of the intensity of each twin reflection weighted by the relative volume of each domain present in the crystal (Rees, 1980; Larsen *et al.*, 2002):

$$I_{obs}(\mathbf{h}_1) = (1 - \alpha)\, I(\mathbf{h}_1) + \alpha\, I(\mathbf{h}_2)$$

$$I_{obs}(\mathbf{h}_2) = \alpha\, I(\mathbf{h}_1) + (1 - \alpha)\, I(\mathbf{h}_2)$$

where α is called the twinning fraction. The complement (1 - α) and α describe the relative volumes of each domain to each other (Yeates and Fam, 1999). If α is 0.5, the twinning is termed perfect and if α is less than 0.5 it is termed partial twinning.

Perfect merohedral twinning is particularly difficult to detect because it provides additional symmetry to the crystal lattice that is not found in the actual Laue space group of the crystal. Hence the space group is often misidentified as a higher symmetry group of the same Laue system. This is possible in tetragonal, trigonal, hexagonal, and cubic crystal systems (Yeates, 1997). It has also been found in highly twinned monoclinic crystals, which appear to have orthorhombic symmetry. Such twinning of monoclinic crystals requires certain unit cell parameters that happen to mimic those of an orthorhombic cell. This has been found to occur if the β angle approaches 90° (Larsen *et al.*, 2002), or if unit cell lengths *a* and *c* approximate each other (Ito *et al.*, 1995; Declercq and Evrard, 2001). If the twinned lattices overlap approximately in three dimensions, this is termed pseudomerohedral twinning, and the resulting diffraction pattern will show split reflections at high resolution. In the present work, β refined to 89.991°, with $a \neq b \neq c$, and $\alpha=\gamma=90°$, emulating a primitive orthorhombic unit cell. Close inspection of the cyclized Rab7•GppNHp diffraction pattern revealed split spots, indicating pseudomerohedral twinning (Figure 63).

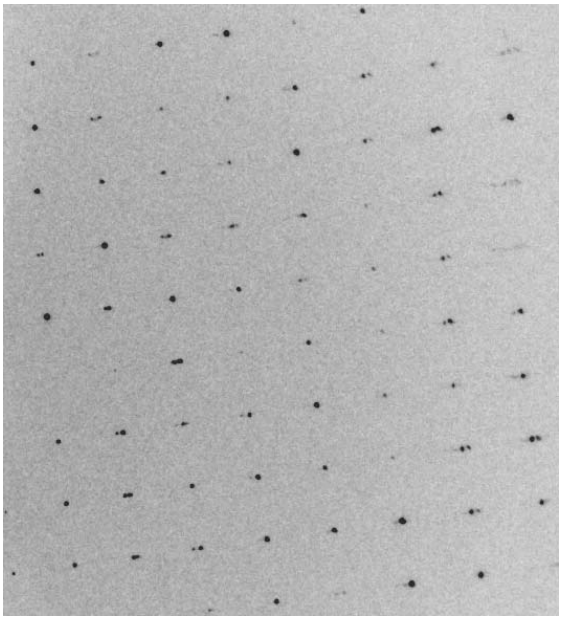

Figure 63. Excerpt of cyclized Rab7•GppNHp diffraction pattern showing split spots indicative of pseudomerohedral twinning.

Confirmation of twinning and estimation of twinning fraction

To confirm that twinning was present in the crystal, the program *TRUNCATE* (Collaborative Computational Project Number 4, 1994) was utilized to perform statistical analysis on the measured intensities, which can be a simple test of twinning without knowledge of the twinning law (Rees, 1980). Single crystals follow Wilson's statistics (Wilson, 1942), which predicts a broad distribution of intensities. Twinned crystals, as mentioned above, have measured intensities which are made up of contributions from twin-related reflections, and this results in an averaging effect on the intensities (Barends *et al.*, 2005). A plot of the cumulative intensity distribution of the measured intensities for cyclized Rab7•GppNHp showed clear sigmoidal behavior for the acentric case, indicative of this averaging effect.

Other common indications of twinning include specific statistical trends based on the normalized intensities (*E)* of twinned data versus that obtained for single crystals. One such indication is if $|E^2-1|<<0.736$. Since intensities of the twin domains overlap, they tend to have less extreme (very sharp or very weak) types of intensities (http://xrayweb.chem.ou.edu/notes/twin.html#indicators). The mean $|E^2-1|$ value calculated using *ECALC* (Collaborative Computational Project Number 4, 1994) was significantly lower than the value of 0.736 expected for acentric zones of an untwinned crystal (Table 5). Similarly the fourth moment of *E*, $<E^4>$, was also found to be lower than what is expected for single crystals, again, demonstrating that the measured data do not have a broad distribution of intensities, which is typical of twinned crystals.

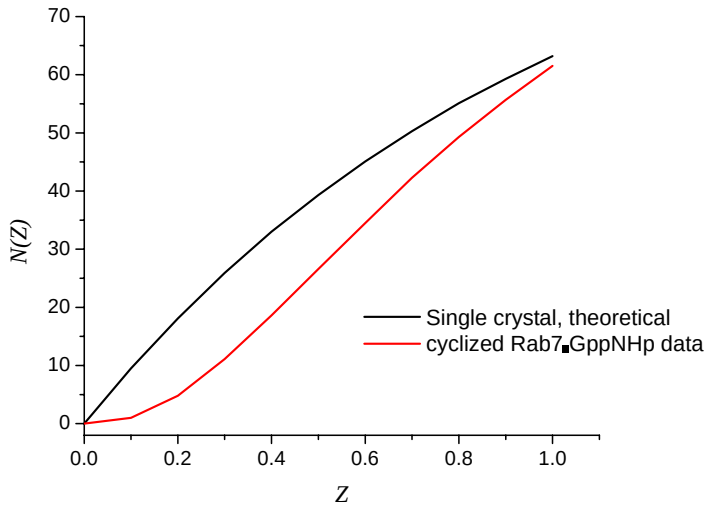

Figure 64. Cumulative Intensity distribution for cyclized Rab7•GppNHp data compared to the theoretical distribution for a single crystal. *N(Z)* represents the cumulative distribution function, i.e. the cumulative frequency of reflections that have an intensity of *Z*, with *Z* as the intensity relative to the mean intensity.

Table 5. Statistical values for experimentally measured intensities compared with those expected for a single and twinned crystal, respectively.

Statistical quantity (for acentric data)	cyclized Rab7•GppNHp data	Theoretical single crystal	Theoretical perfect hemihedral twin
Mean first moment of E, $\langle E \rangle$	0.93	0.89	0.94
Mean third moment of E, $\langle E^3 \rangle$	1.21	1.33	1.175
Mean fourth moment of E, $\langle E^4 \rangle$	1.741	2.00	1.5
$\lvert E^2-1 \rvert$	0.590	0.736	0.541

Structures from pseudomerohedrally twinned crystals can be refined using the program *SHELXL* (Sheldrick, 2008) with the addition of just two parameters that describe the twinning: an estimate of the twinning fraction and the twinning law. These two parameters can be obtained from *SFCHECK* (Collaborative Computational Project Number 4, 1994) and were found to be 0.441, with a twinning law of –h, -k, l. Refining with *SHELXL* has the advantage that refinement can be made against all of the data, and *SHELXL* will refine the twinning fraction as well. Taking this into account, molecular replacement was repeated using the refined model before twinning was diagnosed as the search model, and the true space group was found to be monoclinic $P2_1$ with 4 molecules in the asymmetric unit.

Definition of a new test set and removing model bias

Since the previously *REFMAC5* refined model was refined using a test set that did not take into account twin-related reflections, two procedures were implemented first before proceeding with further refinement of the twinned data (Larsen et al., 2002; Barends and Dijkstra, 2003). First, a test set that considers the twinning was generated using the script make_cv_twin in *CNS* (Brunger *et al.*, 1998). This ensures that twin-related reflections do not lie both in the working set (reflections that contribute to R) and the test set (reflections that contribute to R_{free}), which would eliminate the purpose for having the test set as cross-validation. Second, simulated annealing was performed on the model to erase any bias from refinement against a test set that did not take twinning into account. In this procedure, the molecule is heated up to high temperatures to randomize the positions of the atoms in the model (effectively erasing its memory) and then allowed to cool slowly.

Refinement against twinned data

The resulting model was then further refined using *SHELXL* (Sheldrick, 2008) which allows refinement against the twinned data if the twinning fraction and twinning law are known. Using the twinning fraction of 0.441 obtained from *SFCHECK* and a twinning law of -h, -k, l, (corresponding to a twin axis parallel to c), 20 cycles of conjugated least squares refinement were performed on all of the data. Surprisingly, R and R_{free} again failed to converge, and although R was reduced by ~2.5%, R_{free} did not reduce significantly from values obtained from *REFMAC5* where no twinning was accounted for (Table 6).

Table 6. Comparison of different refinement strategies for the cyclized Rab7•GppNHp model.

Refinement strategy	R	R_{free}
REFMAC5, $P22_12_1$, 2 molecules in a.u., no twinning	21.5	27.3
SHELXL, $P2_1$, 4 molecules in a.u., no twinning	25.3	32.4
SHELXL, $P2_1$, 4 molecules in a.u., *Twinning: -h,- k, l BASF=0.441*	19.1	28.2
Iterative cycles of model building, *SHELXL*, $P2_1$, 4 molecules in a.u., *Twinning: -h,- k, l BASF=0.49*	18.4	26.6

Refinement with *SHELXL* proved to be less straightforward than other typical examples of high resolution data that refined to respectable R factors without much effort. Of concern was the observation that in many of the molecules, the axial waters coordinating the Mg^{2+} ions were either slightly off-linear or had no electron density. To address this, both the nucleotide and magnesium ion for each of the four molecules in the asymmetric unit were removed from the model. The model was then fit to the resulting electron density maps, which returned positive density at 2.55σ (3σ is the standard for significant) for each nucleotide and magnesium ion. Indeed, the occupancy of the axial magnesium waters was highly variable among the four molecules, and this slightly distorted octahedral geometry was most prevalent in the difference density of the fourth molecule in the asymmetric unit. The lack of full occupancy for the axial waters of the Mg^{2+} ions often led to distortion by *SHELXL* of the octahedral geometry, and was found to be corrected when the Mg^{2+} and GppNHp were allowed to refine together as a rigid body. This was made using the command "AFIX 6" before the Mg^{2+} coordinates and "AFIX 0" after the GppNHp coordinates of each nucleotide in the refinement input file. The axial waters in the Mg^{2+} coordination sphere of the first molecule required inclusion within these rigid body

restraints, to prevent the generation of a distorted 1.48 Å bond to Mg^{2+} after refinement in *SHELXL*.

In spite of refining the entire data set using the twin law and the twinning fraction, R_{free} remained relatively high (28%). As recommended by the *SHELXL* manual, the global standard deviations (the DEFS command) for different aspects of geometry were systematically varied to see if they might lower R_{free}. In general, all changes to the DEFS values indicated that the default settings were the most beneficial. It was noted in the resulting PDB files after *SHELXL* refinement that the temperature factors (B-factors) for each amino acid varied significantly, even for atoms belonging to the same residue. To remedy this, the current model at the time was refined with a single 20-cycle *REFMAC5* run, which, although it does not take twinning into account, was sufficient to average the B-factors. All subsequent changes to the model (see below) were then made with this *REFMAC5*-refined model to produce an optimized "final" model, that was then refined in one 10-cycle *SHELXL* run with tighter SIMU restraints set to a value of 0.02. The most significant improvements (albeit gradual) to the R_{free} resulted from many iterative cycles of omitting regions from the model and observing what positive density (if any) actually returned. In this way, it was soon discovered that each molecule varied in what was actually described by the data with regards to each termini, Switch I, Switch II, Loop 3 (residues 52-55), and Loop 7 (residues 111-118). Through this procedure, it was observed that *SHELXL* has a tendency for model bias, often returning good electron density whatever the model may be. Such properties have been observed by others with lower resolution (2.2 Å) merohedrally twinned data sets that used *SHELX* for refinement (Esser, 2007), and may represent a limitation of using this program. With respect to refining twinned data sets, *SHELX* is at present one of the few programs that can refine against the entire twinned data set, but future users are highly advised to make extensive use of Fo-Fc maps to guide their model building to avoid the stall in refinement progress that was experienced with cyclized Rab7•GppNHp. The difficulties experienced in the refinement of cyclized Rab7• GppNHp may also be due to the extremely high twinning fraction present in the crystal, with a final refined twinning fraction of 0.49.

As mentioned earlier, twinning in the crystal was noticed only after refinement, when the *R* factors failed to converge. The near perfect twinning present in the crystal, which reduces the number of measured intensities by half of what would be expected at each resolution,

results in an observable-to-parameter ratio of 2.3. This is extremely low and examples like this ultimately lead to an effective lower resolution of the maps as compared to what would have been expected had twinning not been present (Rudolph *et al.*, 2004). In the case of Rudolph *et al*, they report near perfect (α ~0.46) pseudomerohedral twinning with a data set collected to 2.5 Å, but with an information content equivalent to an untwinned data set collected to 3.1 Å. Their low observable-to-parameter ratio led to unstable refinement and suboptimal geometry of their resulting model, with 71.2% of all residues in the most favored regions of the Ramachandran plot. Other examples in the PDB include the structures of rat apo-Heme Oxygenase-1 (PDB code 1IRM) and human topoisomerase I covalently bound to double stranded DNA (PDB code 1K4S), both of which have lower percentages of residues in the most favored regions (Table 7) (Sugishima *et al.*, 2002; Staker *et al.*, 2002). When compared with these values, the final refined model of cyclized Rab7•GppNHp shows reasonable geometry with 87.2% of residues in the most favored region, close to the normally acceptable value of over 90%.

Table 7. Comparison of the overall geometry of cyclized Rab7•GppNHp with that of other twinned structures.

Protein/PDB Code	α	Resolution	*R*	R_{free}	% most favored	Reference
1R3H	0.46	2.5 Å	23.1%	27.2%	71.2	Rudolph *et al*, 2004
1IRM	0.45	2.55 Å	20.4%	30.7%	69.9	Sugishima *et al*, 2002
1K4S	NR*	3.2	21.7%	22.2%	78.1	Staker *et al*, 2002
1NJ9	0.43	2.35	18%	27%	81.2%	Larsen *et al*, 2002
cyclized Rab7•GppNHp	0.49	1.8	18.4%	26.6%	87.2	present work

*NR, not reported

Structure of cyclized Rab7•GppNHp and comparison with wild type Rab7•GppNHp

The overall structure of cyclized Rab7•GppNHp is quite similar to that of wild type Rab7•GppNHp, with an overall rmsd of C_α atoms of 0.52 Å. All four molecules in the asymmetric unit possess a similar overall fold, with differences in the extent of what is visible for each terminus, Switch II, Loop 3 and Loop 7. The first and fourth molecules contain the longest visible regions (residues 5-179), followed by the third molecule with residues 6-178 visible, while the second has the most disordered C-terminus (residues 6-175 visible). This may result from the close proximity of this region to the side chains of Arg 69 and Gln 71 in Switch II of a symmetry related molecule, which themselves have sparse

electron density as well as high Bfactors, an indication of mobility. This may affect the packing of the C-terminus and contribute to the poor electron density describing this area.

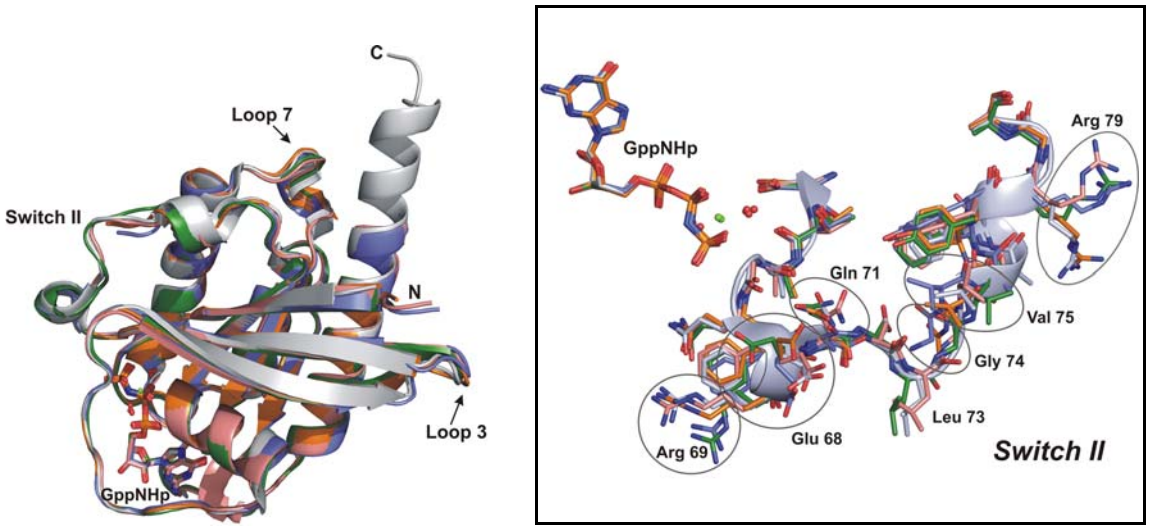

Figure 65. Comparison of the overall structure of cyclized and linear Rab7•GppNHp (white). Each molecule of cyclized Rab7•GppNHp is colored (1, salmon; 2, orange; 3, green; 4, dull blue). The flexibility of Switch II is shown in the boxed inset, with residues displaying varied conformations circled for clarity and shown in stick representation against the white ribbon representation of linear Rab7•GppNHp. Ser 72 and Leu 73 are not clearly defined in molecules 2 and 4, and were therefore omitted from the final model. Stick representation of the overlay of GppNHp from each molecule is shown for comparison.

Superposition of all four molecules of the asymmetric unit revealed the regions of flexibility for cyclized Rab7•GppNHp, which occur primarily at the surface in solvent exposed loops and the termini (Figure 65). Whereas the cyclized version of Rab7•GDP was found to stabilize the Switch I region such that it could actually be modeled, cyclized Rab7•GppNHp shows a high degree of flexibility in Switch II, as evidenced by the sparse electron density that returned as positive density when residues 72-76 were omitted from each of the four molecules in the asymmetric unit, as well as the conformational variability observed among the four molecules (Figure 65). In the second and fourth molecule, residues 72-73 were omitted from the final model because they could not be modeled with confidence. The residues in Switch II are also characterized by high B-factors, indicating conformational mobility. It is worthy to note that these regions are visible in the wild type uncyclized Rab7•GppNHp crystal structure (PDB code 1VG8) (Rak *et al.*, 2004), with much more of the C-terminus visible (residues 7-190) compared to the cyclized Rab7•GppNHp structure.

Small shifts in Loop3 (Val 52-Arg 55) and Loop 7 (Ser 111-Asp 114) are also seen in the cyclized Rab7•GppNHp structure when compared to Rab7•GppNHp. The lack of electron density in regions otherwise visible in linear Rab7 suggest that cyclization of Rab7 may allow for increased mobility of certain regions in the GTP state. Superposition of several active Rab7 structures reveals that the choice of the site of truncation and length of the linker may add strain to the molecule, forcing it to adopt a conformation that is not identical to wild type Rab7•GppNHp. The number of residues for the linker of cyclized Rab7 is the same as the number of residues at the N- and C-termini observed in the structures, which point away from each other (Figure 66A). The linker, therefore, may not be long enough to really allow the protein to adopt the GTP conformation that uncyclized Rab7 can reach. This additional strain may slightly destabilize cyclized Rab7•GppNHp, which may allow for flexibility in Switch II because the protein cannot adopt the conformation it normally would in a "relaxed" state.

Although the two termini point in opposite directions in the Rab7•GppNHp structure, they do lie close to each other in the Rab7•GTP:RILP complex structure (Wu *et al.*, 2005). Rab7 in this case was mutated to the constitutively active Q67L mutant (which impairs its intrinsic GTP hydrolysis). The Rab7 binding domain of RILP was found to form a coiled-coil homodimer of four helices that binds two identical Rab7 molecules on either side. The Rab7 binding domain of RILP contacts Rab7 at two interfaces: one involving the switch and interswitch regions which is typically observed in other complexes between Ras-like GTPases and their effectors, and another involving the RabSF1 and RabSF4 regions which correspond to the N- and C-terminal regions. Rab7 undergoes significant conformational changes in its C-terminus upon RILP binding. The C-terminal helix (residues 175-185) was found to unfold halfway to a short β-strand, which forms an antiparallel β-sheet with strand β1, and makes important contacts with RILP. Mutation or deletion of Leu 8, Lys 10 or Val 180 significantly reduced or abolished Rab7 binding to RILP, confirming their role in complex formation. Although the N- and C-termini are not structurally defined in the model of cyclized Rab7, the construct contains the residues necessary for RILP binding. It would be interesting to know whether covalent linkage of the termini still permits such a conformational change in the C-terminus upon RILP binding. Unfortunately for the present work, a well-behaved purified RILP sample could not be obtained, and these functional measurements could not be performed.

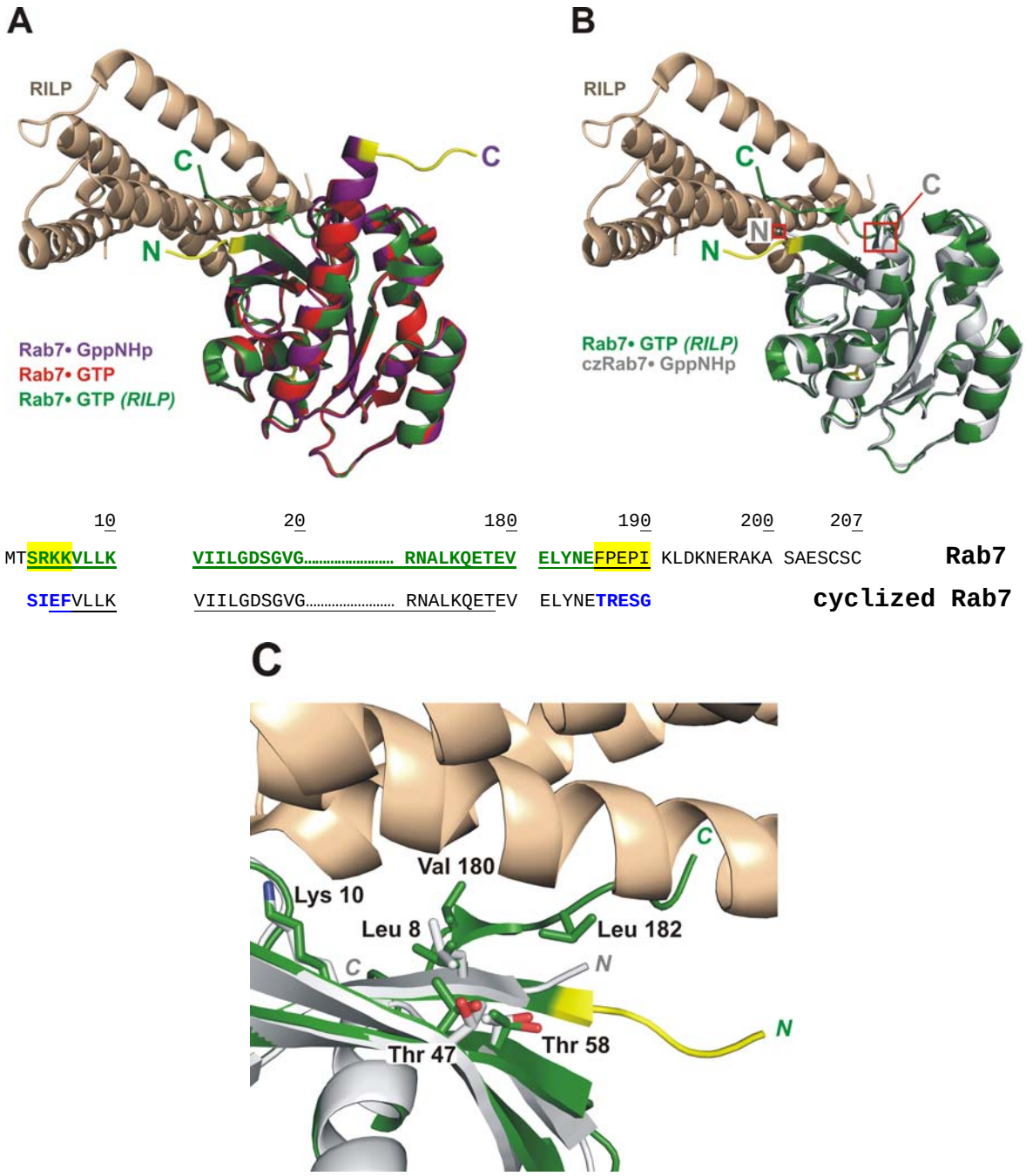

Figure 66. *A*, Rab 7•GTP (1T91, red), and Rab 7•GppNHp (1VG8, purple) superimposed on Rab7•GTP (green) in complex with the Rab7 binding domain of RILP (1YHN, peach). For the purpose of the overlay, only one molecule of Rab7•GTP is shown from the Rab7•GTP:RILP heterodimer. The structure of the Rab7 C-terminus changes significantly upon RILP binding. *B*, Cyclized Rab7•GppNHp (white) superimposed on Rab7•GTP in complex with RILP (1YHN, green). *Below*, protein sequence alignment of the N- and C-termini of wild type Rab7 and cyclized Rab7. Residues visible from the ribbon representations are underlined, with the linker used in cyclized Rab7 colored in blue. N- and C-terminal residues observed in the Rab7•GTP:RILP complex and Rab7•GppNHp structures are highlighted in yellow (as in the ribbon representation). Residues visible in the Rab7•GTP:RILP complex structure are colored green. *C*, Zoom of *B* showing residues of Rab7 in the N- and C-termini that contact RILP. Cyclized Rab7•GppNHp maintains most of the binding site, and the flexible termini (unobserved in the structure) may allow for complete RILP binding.

3.5 SUMMARY AND PERSPECTIVES

A cyclized version of Rab7 was produced via intein-mediated expressed protein ligation, and characterized to determine the effect of cyclization on protein stability, biological function, crystallization, and structure. Cyclization imparted a modest increase in the thermal stability of Rab7, with a 3.7°C increase in the melting temperature. Although cyclized Rab7 is not capable of C-terminal prenylation and membrane targeting, it does mimic a C-terminally truncated Rab7, displaying similar rates of GTP hydrolysis, effector binding and dissociation kinetics. Residues in the linker of cyclized Rab7 provided favorable crystal contacts that significantly stabilized the notoriously flexible Switch I loop in the GDP bound form. This stabilization allows interactions between the backbone of Ala 39 and both the α-phosphate of GDP and an axial water, which coordinates the active site Mg^{2+} ion. Cyclization also permitted crystallization of the GppNHp bound form. Crystals in this form were found to be pseudomerohedrally twinned with a near perfect twinning fraction of 0.49. In contrast to the stabilization seen in cyclized Rab7•GDP, cyclized Rab 7 • GppNHp showed several regions of flexibility, most notably in Switch II. Structures of active Rab7 reveal that the N- and C-termini lie in opposite directions in the GTP form, in contrast to Rab7•GDP. The choice of linker length and site of truncation may strain the protein by forcing the two ends of the molecule together, allowing for more flexibility in Switch II.

In general, cyclization is a useful method for increasing the stability of proteins of interest. It can also be a useful tool to aid in the crystallization of proteins, by reducing the inherent flexibility of loops that may have important roles in biological function. An important prerequisite is the close proximity of the termini to each other in the target protein, in all forms in which it will be studied, as well as the lack of interference of cyclization with its biological function.

Chapter 4.

Materials and Methods

4. MATERIALS AND METHODS

4.1 MATERIALS

4.1.1 Chemicals and enzymes

acetonitrile	Sigma-Aldrich, Munich
alkaline phosphatase (calf intestinal)	Roche Diagnostics, Mannheim
ammonium sulfate	Applichem, Darmstadt
ampicillin	Gerbu Biotechnik, Gaiberg
anti-His antibody	Roche Diagnostics, Mannheim; Santa Cruz Biotechnology, Santa Cruz, CA, USA
anti-mouse IgG conjugated with AP	Pierce, Rockford, IL, USA
anti-rabbit IgG conjugated with AP	Pierce, Rockford, IL, USA
$CaCl_2$	Merck Biosciences, Darmstadt
chloramphenicol	Genaxxon Biosciences, Biberach/Riß
Complete EDTA-free protease inhibitor cocktail	Roche Diagnostics, Mannheim
DNase, bovine pancreas, grade II	Roche Diagnostics, Mannheim
DTE	Gerbu Biotechnik, Gaiberg
DTT	Gerbu Biotechnik, Gaiberg
EDTA	Gerbu Biotechnik, Gaiberg
FAD	Sigma-Aldrich, Munich
Fos-choline-12	Anatrace, Maumee, OH, USA
GDP	Pharma Waldhof, Düsseldorf
gel filtration standards	Bio-Rad, Munich
Genapol X-80	Merck Biosciences, Darmstadt
glutathione, reduced	Sigma-Aldrich, Munich
glycerol	Gerbu Biotechnik, Gaiberg
GMP	Pharma Waldhof, Düsseldorf
GppNHp	Sigma-Aldrich, Munich
GTP	Pharma Waldhof, Düsseldorf
guanidinium hydrochloride	Gerbu Biotechnik, Gaiberg Sigma-Aldrich, Munich
HEPES	Sigma-Aldrich, Munich; Gerbu Biotechnik, Gaiberg
Imidazole	Fluka, Deisenhofen; Merck Biosciences, Darmstadt
IPTG	Gerbu Biotechnik, Gaiberg
kanamycin	Gerbu Biotechnik, Gaiberg
low molecular weight marker	Amersham Biosciences/GE Healthcare, Freiburg
mantGDP	Invitrogen, Carlsbad, CA, USA
mantGppNHp	Jena Biosciences, Jena; Invitrogen, Carlsbad, CA, USA
$MgCl_2$	Merck Biosciences, Darmstadt; JT Baker, Deventer, Holland

NADPH	Sigma-Aldrich, Munich; Serva Electrophoresis, Heidelberg
NBT	Sigma-Aldrich, Munich
NBT/BCIP staining solution	Pierce, Rockford, IL, USA
phosphodiesterase	Sigma-Aldrich, Munich
popular detergent kit	Anatrace, Maumee, OH, USA
potassium chloride	Merck Biosciences, Darmstadt
potassium phosphate, dibasic	Merck Biosciences, Darmstadt
potassium phosphate, monobasic	Merck Biosciences, Darmstadt
Pre-stained molecular weight marker	Fermentas, St. Leon-Rot
restriction enzymes	New England Biolabs, Frankfurt/Main
sodium chloride	Merck Biosciences, Darmstadt; Fluka, Deisenhofen
sodium phosphate, monobasic	Merck Biosciences, Darmstadt
sucrose	Serva Electrophoresis, Heidelberg
T4-DNA ligase	Roche Diagnostics, Mannheim
Tetra-n-butyl ammonium bromide	Sigma-Aldrich, Munich
thrombin	Sigma-Aldrich, Munich
Triton X-100	Merck Biosciences, Darmstadt
Trizma Base	Sigma-Aldrich, Munich; Roth, Karlsruhe
tween	Serva Electrophoresis, Heidelberg
urea	Gerbu Biotechnik, Gaiberg
δ-aminolevulinic acid	Sigma-Aldrich, Munich

All chemicals used for crystallization were from Fluka, Deisenhofen.

4.1.2 Bacterial strains and media

XL1Blue (Stratagene, Heidelberg):

recA1 endA1 gyrA96 thi-1 hsdR17 supE44 relA1 lac [F'*proAB lacI*^{q}*ZΔM15 Tn10* (Tet^{r})]

XL10 Gold (Stratagene, Heidelberg):

Tet^{r} Δ(mcrA)183 Δ(mcrCB-hsdSMR-mrr)173 endA1 supE44 thi-1 recA1 gyrA96 relA1 lac Hte [F' proAB lacI^{q}ZΔM15 Tn10 (Tet^{r}) Amy Cam^{r}]

BL21(DE3) (Merck Biosciences, Darmstadt):

F^{-} *ompT hsdS*$_{B}$ ($r_B^- m_B^-$) *gal dcm* (DE3)

BL21(DE3) Codon Plus RIL (Merck Biosciences, Darmstadt):

E. coli B F^{-} *ompT hsdS* ($r_B^- m_B^-$) *dcm*$^{+}$ Tet^{r} *gal* λ(DE3) *endA* Hte [*argU ileY leuW* Cam^{r}]

C41(DE3) (Prof. Dr. Axel Scheidig, ZBM, Christian-Albrechts-Universität Kiel):

[*E. coli* F^{-} *ompT hsdS*$_{B}$ ($r_B^- m_B^-$) *gal dcm* (DE3)]

Media

LB, TB, ST1, and 2YT media and LB agar plates with the appropriate antibiotics were made by the media kitchens at the MPI of Molecular Physiology (Dortmund) and the MPI for Medical Research (Heidelberg).

4.1.3 Vectors and primers

Vectors

pET 32a	Novagen/Merck Biosciences, Darmstadt
pET 19b	Novagen/Merck Biosciences, Darmstadt
pET 30a	Novagen/Merck Biosciences, Darmstadt
pET 41a	Novagen/Merck Biosciences, Darmstadt
pGEX 2T	Amersham Biosciences/GE Healthcare, Freiburg

Sequencing primers:

All non-commercially available primers were synthesized by MWG Biotech (Ebersberg) as HPSF (Highly purified salt free) grade.

Primer	Sequence (5' to 3')
T7 promoter	CGA AAT TAA TAC GAC TCA CTA TAG GG
T7 terminator[1]	GCT AGT TAT TGC TCA GCG G
S•Tag™ Primer[1]	CGA ACG CCA GCA CAT GGA CA
hNox1SM1 Primer	GGG GGT TCT TGG CTA AAT CCC
hNox1SM2 Primer	GGC TTC AGC ATG GAA GTG GGG
rEK-TEVseqF	C CAT CAT CAT CAT CAT TCT TCT GG
pGEX 3' [2]	CCG GGA GCT GCA TGT GTC AGA GG
pGEX 5' [2]	GGG CTG GCA AGC CAC GTT TGG TG

[1]Novagen/ Merck Biosciences, Darmstadt
[2]Amersham Biosciences/GE Healthcare, Freiburg

4.1.4 Chromatographic matrices

2'5'ADP Sepharose 4B	Amersham Biosciences/GE Healthcare, Freiburg
DEAE-Sepharose FF	Amersham Biosciences/GE Healthcare, Freiburg
Glutathione Sepharose 4B	Amersham Biosciences/GE Healthcare, Freiburg
HiTrap Benzamidine FF (high sub)	Amersham Biosciences/GE Healthcare, Freiburg
HiTrap Desalting columns	Amersham Biosciences/GE Healthcare, Freiburg
HiTrap Ni-Chelating Sepharose	Amersham Biosciences/GE Healthcare, Freiburg

HiTrap Ni-Sepharose High Performance	Amersham Biosciences/GE Healthcare, Freiburg
NAP-5 column	Amersham Biosciences/GE Healthcare, Freiburg
Ni-NTA resin	Qiagen, Hilden
ODS Prontosil Hypersorb, reversed phase C18	Bischoff Chromatography, Leonberg
Resource Q	Amersham Biosciences/GE Healthcare, Freiburg
Superdex 200	Amersham Biosciences/GE Healthcare, Freiburg
Superdex 75	Amersham Biosciences/GE Healthcare, Freiburg
POROS® HQ resin	Applied Biosystems, Foster City, CA, USA

4.1.5 Miscellaneous materials

Amicon Ultra centrifugal concentrator	Millipore, Schwalbach
Greiner low profile 96-well microplate	Greiner Bio-One GmbH, Frickenhausen
Nunc nuclon 96-well microtiter plate	Nunc, Wiesbaden
Qiagen Gel Extraction Kit	Qiagen, Hilden
Qiagen Miniprep Kit	Qiagen, Hilden
Vivapore static concentrator	Sartorius, Göttingen
Wizard plus SV Miniprep-Kit	Promega, Mannheim

4.1.6 Equipment

ÄKTA Prime	Amersham Biosciences/GE Healthcare, Freiburg
Beckman Avanti^{TM} J-20 XP Centrifuge	Beckman Coulter, Krefeld
Beckman DU®640 spectrophotometer	Beckman Instruments, Munich
Beckman L8-70M Ultracentrifuge	Beckman Coulter, Krefeld
Beckman Optima L-70K Ultracentrifuge	Beckman Coulter, Krefeld
Criterion Blotter	Bio-Rad, Munich
Finnigan LCQ Advantage Max	Thermo Electron Corp, Langenselbold
Fluoromax-3	Horiba Jobin Yvon, Munich
GeneQuant /pro/ spectrophotometer	Amersham Biosciences/GE Healthcare, Freiburg
INFORS Multitron Shakers	INFORS HT, Bottmingen, Switzerland
Labsystem iEMS Reader MF	Thermo Electron, Langenselbold
Latek HPLC	Latek, Eppelheim
Microfluidizer	Microfluidics, Lampertheim
MJ Research PTC-200 thermocycler	Biozym Diagnostik, Hess. Oldendorf
Mosquito Crystallization Robot	TTP Labtech, Royston, UK
SX20 Stopped Flow apparatus	Applied Photophysics, Leatherhead, UK
Waters HPLC	Waters, Eschborn

4.2 HUMAN NOX1 METHODS

4.2.1 Coexpression of full-length human Nox1 and subunit b of E. coli F_1F_o ATP synthase

Chemically competent C41(DE3) cells were transformed via heat shock with 2 µl of either 1) full-length human Nox1 cloned into pET41a via *Nco*I and *Xho*I (Prof. Dr. H.H.W. Schmidt, Monash University, Melbourne, Australia), 2) a plasmid containing subunit b (Prof. John E. Walker, MRC Cambridge), or 3) both plasmids, and plated on LB agar plates containing the appropriate antibiotic (subunit b: 100 µg/ml ampicillin; full-length human Nox1: 50 µg/ml kanamycin; both plasmids: 100 µg/ml ampicillin and 50 µg/ml kanamycin). Seven colonies were obtained from cells transformed with both plasmids, and each was used to inoculate seven individual flasks containing 100 ml of 2YT media supplemented with 100 µg/ml ampicillin and 50 µg/ml kanamycin. A control for each individual plasmid was made likewise, inoculating 100 ml of 2YT containing the appropriate antibiotic with a single colony. All cultures were grown at 37°C until the cell density reached specific values: 0.6 for subunit b alone, human Nox1 alone and two cultures containing both plasmids; 0.4-0.5 for two cultures containing both plasmids; and 0.3 for three cultures containing both plasmids. Protein expression was induced with the addition of IPTG at a final concentration of 0.7 mM. The control with subunit b only and three cultures of cells transformed with both plasmids at cell densities of 0.3, 0.4 and 0.6 were incubated at 37°C for 3 hours, and the control with human Nox1 only and four cultures of cells transformed with both plasmids at cell densities of 0.3, 0.3, 0.4 and 0.6 were incubated at 25°C for 18 hours. Non-induced samples were included for each temperature set. 50 µl of each culture was centrifuged for analysis on 15% SDS-PAGE.

The above protocol was repeated with some adjustments to determine the effect of the heme precursor, δ-aminolevulinic acid, on expression of human Nox1. Due to the unusually slow growth observed previously with cultures containing kanamycin, this antibiotic was used in a reduced final concentration of 35 µg/ml. Starter cultures of 4 ml 2YT and the appropriate antibiotic were inoculated with a single colony containing subunit b alone, human Nox1 alone, or both plasmids together. These cultures were first grown at 37°C for 9 hours, then supplemented with fresh antibiotic and allowed to continue growth at 25°C overnight. The overnight cultures were used to inoculate 100 ml of 2YT with the appropriate antibiotic and

grown at 25°C until a cell density at 600 nm of about 1. δ-aminolevulinic acid was added to each culture at a final concentration of 25 μg/ml. Each culture was divided in half to generate 50 ml of a non-induced sample and 50 ml of an induced sample. IPTG was added to each induced sample to a final concentration of 0.7 mM and all cultures were incubated at 20°C for 2 days.

4.2.2 Cloning of H_6-Nox1$_{cyt}$ and Trx$_T$-Nox1$_{cyt}$

H_6-Nox1$_{cyt}$

Residues 290-564 of human Nox1 were amplified by PCR from the Trx$_E$-Nox1$_{cyt}$ plasmid (Prof. Dr. H.H.W. Schmidt, Monash University, Melbourne, Australia) using Hot Star Taq polymerase (Qiagen) and the following primers, which simultaneously exchanged the *Nco*I restriction site for *Nde*I (bold and underlined). The *Xho*I restriction site is bold and italic.

ΔhNox1NdeF *5'* GCA GTG TAC **CAT ATG** CGC TCC CAG CAG AAG G *3'*

hNox1XhoR *5'* CCA G***CT CGA G*** TC AAA AAT TTT CTT TGT TGA AG *3'*

This PCR reaction utilized the following program:

Temperature	Time	No. of Cycles
95°C	15 min	---
94°C 52°C 72°C	1 min 1 min 1 min 45 sec	10
94°C 62°C 72°C	1 min 1 min 1 min 45 sec	20

The vector, coding for an N-terminal His-tag followed by a TEV protease site (Dr. Kirill Alexandrov, MPI of Molecular Physiology, Dortmund), was sequentially digested with *Nde*I followed by *Xho*I, each for 4 hours at 37°C. The digested vector was treated with calf intestinal alkaline phosphatase (to remove the 5' phosphate and prevent vector re-ligation), and purified by gel extraction (Qiagen). The PCR-amplified human Nox1$_{cyt}$ insert was purified by gel extraction (Qiagen) and digested with *Nde*I and *Xho*I for 4 hours at 37°C. 20 ng of digested vector was ligated with the human Nox1$_{cyt}$ insert at a vector:insert ratio of

1:5 using T4 DNA Ligase and overnight incubation at 16°C. Ligated plasmids containing the human $Nox1_{cyt}$ insert were transformed into XL1-Blue competent cells and plasmids were isolated (Miniprep Kit, Qiagen) from 4 ml cultures. Plasmids containing the desired human $Nox1_{cyt}$ insert were identified by restriction enzyme digest with *Nde*I and *Xho*I, as well as analytical PCR using the above primers. Sequences were verified with DNA sequencing.

Trx_T-$Nox1_{cyt}$

The Trx_T-$Nox1_{cyt}$ construct was made with two sequential mutagenesis reactions utilizing the QuikChange® Site-Directed Mutagenesis Kit (Stratagene) and the plasmid for Trx_E-$Nox1_{cyt}$ as a template. The enterokinase protease site was removed with the following primers:

-rEKforward *5'* CCA GAT CTG GGT ACC GCC ATG GGT CGC TCC *3'*

-rEKreverse *5'* GGA GCG ACC CAT GGC GGT ACC CAG ATC TGG *3'*

DNA sequencing identified plasmids with the desired deletion, which became the template for the second mutagenesis reaction, using the following primers to insert the TEV protease site:

TEVforward *5'* CCA GAT CTG GGT ACC GAG AAT CTT TAT TTT CAG GGC GCC ATG GGT CGC TC *3'*

TEVreverse *5'* GA GCG ACC CAT GGC GCC CTG AAA ATA AAG ATT CTC GGT ACC CAG ATC TGG *3'*

Plasmids containing the desired TEV protease site were verified with DNA sequencing.

4.2.3 Expression of recombinant human Nox1 constructs

Chemically competent C41(DE3) cells were transformed via heat shock with 2 µl of either Trx_E-$Nox1_{cyt}$, H_6-$Nox1_{cyt}$, or Trx_T-$Nox1_{cyt}$ miniprepped plasmid, and plated onto LB agar plates containing a final concentration of 100 µg/ml of ampicillin. Starter cultures of 50-100 ml of LB supplemented with ampicillin at a final concentration of 100 µg/ml (used at this

concentration in all subsequent cultures) were inoculated with a single colony and grown at 37°C overnight. Typically 5-10L of TB or ST1 media were used for large-scale protein expression and inoculated with the starter culture using a volume 1:200 of the final volume per flask. Cultures were grown at 37°C until the cell density at 600 nm reached 0.3-0.5, and then chilled on ice at 4°C prior to induction. Protein expression was induced at 20°C overnight with the addition of IPTG to a final concentration of 0.1 mM. Subsequent expressions indicated that 0.05 mM final IPTG was also sufficient for protein expression. Cells were harvested at 4°C by centrifugation for 15 minutes at 3500 rpm, flash frozen in liquid nitrogen and stored at -80°C. In some cases the cells were resuspended in the respective Buffer Ni-A with 1 Complete EDTA-free protease inhibitor cocktail tablet (Roche)/50 ml buffer at a volume 2x the mass of the cells, and flash frozen as a suspension in liquid nitrogen for storage at –80°C.

Small scale expression of H_6-$Nox1_{220-564}$ was made from a single colony of BL21(DE3) cells containing the H_6-$Nox1_{220-564}$ plasmid (prepared by Monika Berthel). 1L of TB supplemented with kanamycin at a final concentration of 50 µg/ml was inoculated with 50 ml of an overnight culture and grown at 37°C until the cell density at 600 nm reached approximately 1. Protein expression was induced at 37°C for 4 hours with the addition of IPTG to a final concentration 1 mM. Cells were harvested at 4°C by centrifugation for 15 minutes at 5000 rpm, flash frozen in liquid nitrogen and stored at -80°C.

4.2.4 Purification of recombinant human Nox1 constructs

Due to the temperature instability of the Nox1 proteins, all chromatographic steps were carried out at 4°C. All stated pH values represent the pH of the respective buffer at 4°C, unless otherwise noted. All buffers were sterile filtered and degassed prior to use.

Trx_E-$Nox1_{cyt}$

Frozen cell pellets were thawed at room temperature and resuspended in ice-cold Buffer Ni-A containing 1 Complete EDTA-free protease inhibitor cocktail tablet (Roche)/50 ml buffer at a volume 2x the mass of the cells. Resuspended cells were lysed 2-3 times with a microfluidizer (Microfluidics). Genomic DNA was digested with DNase (35µg/ml lysate) in

the presence of 10 mM $MgCl_2$ with stirring for 10 minutes at 4°C. The lysate was then clarified via ultracentrifugation at 40,000 rpm for 1 hr at 4°C.

Ni-NTA Chromatography

Early purifications of Trx_E-$Nox1_{cyt}$ were made using two 5 ml HiTrap Ni-Chelating Sepharose columns (Amersham Biosciences/GE Healthcare) connected in series for the initial capture. Separation was found to improve with the addition of a third 5 ml HiTrap Ni-Sepharose column (Amersham Biosciences/GE Healthcare). Lysate containing Trx_E-$Nox1_{cyt}$ was loaded onto these three columns connected in series at 1 ml/min with a peristaltic pump (Amersham Biosciences/GE Healthcare). The columns were washed with Buffer Ni-A until the absorbance reading at 280 nm returned to baseline and remained constant, and were then connected to an ÄKTA Prime (Amersham Biosciences/GE Healthcare). Initial separation was achieved with a linear gradient of 0-80% Buffer Ni-B in 150 ml at 2 ml/min, with 3 ml fractions. Fractions containing Trx_E-$Nox1_{cyt}$ were identified with 15% SDS-PAGE.

Buffer Ni-A: 20 mM Tris-HCl, pH 8, 300 mM NaCl, 5 mM Imidazole, 10% glycerol, 2 mM β-mercaptoethanol

Buffer Ni-B: 20 mM Tris-HCl, pH 8, 300 mM NaCl, 1 M Imidazole, 10% glycerol, 2 mM β-mercaptoethanol

Desalting Chromatography

Fractions containing Trx_E-$Nox1_{cyt}$ were desalted over 5 x 5 ml HiTrap Desalting columns (Amersham Biosciences/GE Healthcare) pre-equilibrated with Buffer Res Q-A. 6 ml of sample was loaded with a syringe, attached to an ÄKTA Prime, and desalted at 2 ml/min, with 1.5 ml fractions.

Resource Q Anion Exchange Chromatography

Desalted fractions containing Trx_E-$Nox1_{cyt}$ were loaded with a syringe onto a 6 ml Resource Q anion exchange column (Amersham Biosciences/GE Healthcare) pre-equilibrated with Buffer Res Q-A. The column was then attached to an ÄKTA Prime, and washed with 3 column volumes of Buffer Res Q-A, at a flow rate of 8 ml/min, collecting 3 ml fractions. Protein was eluted with a linear gradient of 0-100% Buffer Res Q-B over 300 ml. At 17% Buffer Res Q-B, the gradient was manually held until the absorbance reading at 280 nm

returned to baseline and remained constant. The linear gradient was then allowed to continue to completion. Fractions containing Trx_E-$Nox1_{cyt}$ were identified with 15% SDS-PAGE.

Buffer Res Q-A: 20 mM Tris-HCl, pH 8, 25 mM NaCl, 10% glycerol, 2 mM β-mercaptoethanol

Buffer Res Q-B: 20 mM Tris-HCl, pH 8, 1M NaCl, 10 % glycerol, and 2 mM β-mercaptoethanol

2'5' ADP Sepharose Chromatography

Fractions from Resource Q chromatography containing Trx_E-$Nox1_{cyt}$ were loaded directly onto 4 ml of 2'5' ADP Sepharose resin pre-equilibrated with Buffer ADP-A. The column was washed by gravity with two column volumes of Buffer ADP-A, and a series of step elutions were made with 4 ml of Buffer ADP-A containing 200 mM, 300 mM, 400 mM, 500 mM, 700 mM and 1M NaCl, respectively. Competitive elution was made with 4 ml of 8 mM $NADP^+$. Fractions were analyzed on 15% SDS-PAGE.

Buffer ADP-A: 10 mM NaH_2PO_4, pH 7.3, 150 mM NaCl, 10 % glycerol, and 2 mM DTT

Optimized Purification

Due to the effectiveness achieved with 2'5' ADP Sepharose chromatography, the above protocol was streamlined to two chromatographic steps: initial capture with Ni-NTA chromatography, followed by purification with 2'5' ADP Sepharose chromatography. For this reason, the linear gradient used in Ni-NTA chromatography was changed to 0-80% Buffer Ni-B in 70 ml, with 5 ml fractions to concentrate the protein in a minimal volume. Desalting chromatography was replaced with a simple 6-fold dilution of the pooled fractions containing Trx_E-$Nox1_{cyt}$ with a pre-ADP Dilution Buffer containing no salt.

pre-ADP Dilution Buffer: 10 mM NaH_2PO_4, pH 7.3, 10 % glycerol, and 2 mM DTT

This diluted sample was loaded via an ÄKTA Prime onto a 10 ml 2'5' ADP Sepharose column, and washed with 50 ml of Buffer ADP-A, or until the absorbance reading at 280 nm returned to baseline and remained constant. Step elution of Trx_E-$Nox1_{cyt}$ was made with 70 ml of 100% Buffer ADP-B.

Buffer ADP-A: 10 mM NaH_2PO_4, pH 7.3, 150 mM NaCl, 10 % glycerol, and 2 mM DTT

Buffer ADP-B: 10 mM NaH_2PO_4, pH 7.3, 1M NaCl, 10 % glycerol, and 2 mM DTT

Fractions containing Trx_E-$Nox1_{cyt}$ were pooled, diluted with a post-ADP Dilution Buffer to a final concentration of 500 mM NaCl, and concentrated in 30 kDa MWCO (molecular weight cut-off) centrifugal concentrators (Millipore) at 4°C with 10 minute spins. The protein was buffer-exchanged into a Final Storage Buffer via concentration. Protein concentration was determined by Bradford assay (Bradford, 1976) using BSA as a standard, aliquoted, flash frozen in liquid nitrogen, and stored at –80°C.

post-ADP Dilution Buffer: 10 mM NaH_2PO_4, pH 8, 10 % glycerol, and 2 mM DTT

Final Storage Buffer: 10 mM NaH_2PO_4, pH 8, 500 mM NaCl, 10 % glycerol, and 2 mM DTT

Purification under denaturing conditions

The insoluble fraction of ~1L of lysed cells expressing Trx_E-$Nox1_{cyt}$ was homogenized in Denaturing Buffer to a final volume of 30 ml and allowed to incubate with mild agitation for 20-30 min at room temperature. Buffers containing guanidinium hydrochloride were at room temperature when pHed. The solubilized fraction was clarified with ultracentrifugation at 40,000 *xg*, 4°C for 1 hour. Chromatography was carried out at 4°C. The supernatant was loaded via a peristaltic pump onto 10 ml of Ni-NTA resin (Qiagen) and washed with 100 ml of Wash Buffer. Refolding buffer was introduced with a manual gradient maker at 1.75 ml/min over 100 ml. Renatured protein was step eluted with Elution Buffer, and fractions were concentrated in a 30 kDa MWCO centrifugal concentrator.

Denaturing buffer: 50 mM HEPES, pH 7.4, 150 mM NaCl, 20 mM Imidazole, 6 M guanidinium hydrochloride

Wash Buffer: 50 mM HEPES, pH 7.4, 150 mM NaCl, 40 mM Imidazole, 6 M guanidinium hydrochloride

Refolding buffer: 50 mM NaH_2PO_4, pH 7.4, 150 mM NaCl, 30 μM FAD, 0.3% Triton X-100

Elution Buffer: 50 mM NaH_2PO_4, pH 7.5, 150 mM NaCl, 250 mM Imidazole, 30 µM FAD, 0.3% Triton X-100

H_6-Nox1$_{220-564}$

Frozen cells from 1L of culture expressing H_6-Nox1$_{220-564}$ were thawed at room temperature and resuspended in ice-cold Lysis Buffer containing 1 Complete EDTA-free protease inhibitor cocktail tablet/50 ml buffer at a volume 2x the mass of the cells. Resuspended cells were lysed in re-circulation mode for 20-30 pulses with a microfluidizer. Genomic DNA was digested with DNase (35µg/ml lysate) in the presence of 10 mM $MgCl_2$ with stirring for 10 minutes at 4°C. The lysate was then clarified via ultracentrifugation at 12,100 rpm for 40 min at 4°C.

Ni-NTA Chromatography

200 µl of a slurry of Ni-NTA resin pre-equilibrated with Lysis buffer was added to the clarified lysate and collected in a gravity column. The resin was washed with 1 ml of Lysis Buffer followed by 1ml of a series of step washes with Lysis Buffer containing 20, 40 and 60 mM Imidazole, respectively, with a reduced detergent concentration of 0.3% Triton X-100. H_6-Nox1$_{220-564}$ was eluted in 1.5 ml of Elution Buffer and collected in 300 µl fractions.

Lysis Buffer: 20 mM NaH_2PO_4, pH 7.3, 5 mM Imidazole, 300 mM NaCl, 10% glycerol, 2% Triton X-100

Elution Buffer: 20 mM NaH_2PO_4, pH 7.3, 250 mM Imidazole, 300 mM NaCl, 10% glycerol, 0.3% Triton X-100

H_6-Nox1$_{cyt}$

Frozen cell pellets were thawed at room temperature and resuspended in ice-cold Buffer Ni-A containing one Complete EDTA-free protease inhibitor cocktail tablet/50 ml buffer at a volume 2x the mass of the cells. Resuspended cells were lysed 2-3 times with a microfluidizer. Genomic DNA was digested with DNase (35µg/ml lysate) in the presence of 10 mM $MgCl_2$ with stirring for 10 minutes at 4°C. The lysate was then clarified via ultracentrifugation at 40,000 rpm for 1 hr at 4°C.

Ni-NTA Chromatography

Lysate containing H_6-Nox1$_{cyt}$ was loaded at 1 ml/min with a peristaltic pump onto a 5 ml HiTrap Ni-Sepharose column connected to two 5 ml HiTrap Ni-Chelating Sepharose columns in series. The columns were washed with Buffer Ni-A until the absorbance reading at 280 nm returned to a stable baseline and were then connected to an ÄKTA Prime. Purification was achieved with a linear gradient of 0-80% Buffer Ni-B in 250 ml at 2 ml/min, with 5 ml fractions. Fractions containing H_6-Nox1$_{cyt}$ were identified with 15% SDS-PAGE, diluted with Dilution Buffer to ~300 mM Imidazole and concentrated in Vivapore solvent absorption concentrators (Sartorius, Göttingen).

Buffer Ni-A: 20 mM NaH_2PO_4, pH 7.3, 300 mM NaCl, 5 mM Imidazole, 10% glycerol

Buffer Ni-B: 20 mM NaH_2PO_4, pH 7.3, 300 mM NaCl, 1M Imidazole, 10% glycerol

Dilution Buffer: 20 mM NaH_2PO_4, pH 7.4, 500 mM NaCl, 10% glycerol

Protein Concentration Determination

Protein concentration was determined by SDS-PAGE analysis of various amounts of H_6-Nox1$_{cyt}$ run alongside known amounts (1, 2, 4, 5, and 7 µg) of a low molecular weight marker (Amersham Biosciences/GE Healthcare). The absorbance at 280 nm of the concentrated H_6-Nox1$_{cyt}$ sample was measured and amounts corresponding to 1, 2, and 5 µg were calculated using the approximation of 1 OD = 1 mg/ml. The actual amounts of H_6-Nox1$_{cyt}$ loaded were then determined from direct comparison with the known quantities of the chymotrypsin marker at 30 kDa.

2'5' ADP Sepharose Chromatography

Fractions containing H_6-Nox1$_{cyt}$ previously purified with Ni-NTA and size exclusion chromatography (Superdex 75, Amersham Biosciences/GE Healthcare) were dialyzed in 10 mM NaH_2PO_4, pH 7.3, 150 mM NaCl, 10 % glycerol, and 2 mM DTE. This sample was then loaded via an ÄKTA Prime onto a 10 ml 2'5' ADP Sepharose column pre-equilibrated with Buffer ADP-A, and washed with 50 ml of Buffer ADP-A. Step elution of H_6-Nox1$_{cyt}$ was made with 70 ml of 100% Buffer ADP-B, and fractions were analyzed on 15% SDS-PAGE.

Buffer ADP-A: 10 mM NaH_2PO_4, pH 7.3, 150 mM NaCl, 10 % glycerol, and 2 mM DTT

Buffer ADP-B: 10 mM NaH_2PO_4, pH 7.3, 1M NaCl, 10 % glycerol, and 2 mM DTT

Trx_T-$Nox1_{cyt}$

Cells expressing Trx_T-$Nox1_{cyt}$ were flash frozen in liquid nitrogen as a resuspension in ice-cold Buffer Ni-A containing 1 Complete EDTA-free protease inhibitor cocktail tablet/50 ml buffer at a volume 2x the mass of the cells. This resuspension was thawed and lysed by 4 passes through a microfluidizer. The soluble fraction was separated via ultracentrifugation at 30,000 rpm for 30 minutes at 4°C. The clarified lysate was loaded onto 12 ml Ni-NTA resin (Qiagen) by gravity and washed with 350 ml of Buffer Ni-A. Step elutions were made with approximately 30 ml of Buffer Ni-A containing 50 mM, 100 mM and 250 mM Imidazole, respectively. Fractions (~10 ml) were manually collected and analyzed on 15% SDS-PAGE. Fractions containing Trx_T-$Nox1_{cyt}$ were concentrated in a centrifugal concentrator (30 kDa MWCO) at 4000 rpm, 4°C, and loaded at 2 ml/min via a Waters HPLC onto a Superdex 75 column (Amersham Biosciences/GE Healthcare) pre-equilibrated with Buffer S75. Fractions were analyzed on 15% SDS-PAGE.

Buffer Ni-A: 50 mM Tris-HCl, pH 7.5, 300 mM NaCl, 20 mM Imidazole, 10% glycerol

Buffer S75: 20 mM HEPES, pH 7, 300 mM NaCl, 10% glycerol

4.2.5 Isoelectric Focusing

The pI of refolded Trx_E-$Nox1_{cyt}$ was experimentally determined with isoelectric focusing. A sample was made consisting of 4 µl of 9.4 mg/ml refolded Trx_E-$Nox1_{cyt}$ mixed with 4 µl 100% glycerol and run alongside standards on a Ready Gel IEF gel (Bio-Rad) using a cathode buffer of 20 mM arginine and 20 mM lysine, and an anode buffer of 7 mM phosphoric acid. The following run conditions were used on a PowerPac 3000 power supply (Bio-Rad) at 4°C:

Voltage	Current	Time
100 V (constant)	limit 25 mA max	1 hour
205 V (constant)	limit 25 mA max	1 hour
500 V (constant)	limit 25 mA max	30 min

The gel was stained for 45 min in IEF staining solution (Bio-Rad), and destained with 10% acetic acid and 40% methanol overnight.

4.2.6 Western Blot

Proteins were electrophoresed on SDS-PAGE, and the gel was rinsed three times with doubly distilled water to remove all traces of running buffer. The gel was then soaked in transfer buffer (10 mM CAPS, pH 11) for 15-20 minutes. Proteins were transferred to PVDF membrane (pre-wet with methanol) using tank transfer in a Criterion Blotter (Bio-Rad) with 100 volts for 40 minutes at 4°C. After transfer, the PVDF membrane was blocked with shaking for 1 hour at room temperature in 10% milk in TBST, and then washed 4 times with 30 ml TBST (20 mM Tris-HCl, pH 7.5, 150 mM NaCl, 0.1% Tween) for 10 min, with shaking. To detect His-tagged proteins, the membrane was incubated with either mouse monoclonal Anti-His antibody (Roche) at a concentration of 1:333 or rabbit polyclonal Anti-His antibody (Santa Cruz Biotechnology) at a concentration of 1:1000 in 3% milk in TBST for 1 hour at room temperature. To identify Nox1 proteins, the membrane was incubated with rabbit polyclonal Anti-Nox1 antibody (Prof. Dr. H.H.W. Schmidt, Monash University, Melbourne, Australia) at a concentration of 1:6700 in 3% milk in TBST for 1 hour at room temperature. The membrane was again washed 4 times with 30 ml TBST for 10 min, with shaking. The membrane was then incubated with anti-mouse IgG or anti-rabbit IgG secondary antibodies conjugated with alkaline phosphatase (Pierce) at a concentration of 1:30,000 in 3% milk in TBST for 1 hour at room temperature. The membrane was again washed 4 times with 30 ml TBST for 10 min, with shaking. Bands were visualized with NBT/BCIP one-step stain (Pierce). For Trx_T-$Nox1_{cyt}$, the blot was visualized with a chemiluminescence kit (Roche).

4.2.7 MALDI-TOF

MALDI-TOF analysis (Dr. Robert Shoeman) was performed using sinapinic acid (3,5-dimethoxy-4-hydroxy cinnamic acid) as the matrix. Samples were made via a "matrix sandwich": a layer of sinapinic acid was first added to the plate and allowed to dry, followed by the protein sample, and then another layer of sinapinic acid, allowing each layer to dry before application of the next layer. Due to the high salt and complex buffer composition present in the protein samples, the samples were washed twice with 1-2 µl of 0.1% TFA. Calibration was made with lysozyme and BSA standards.

4.2.8 Screen for detergent stability

This protocol is based on one used in a course on membrane proteins (NCCR course, 2004). Detergents at ~10x the CMC are incubated with an equal volume of target protein for one week at 4°C. Stability is determined by SDS-PAGE analysis of the soluble fraction. Detergent solutions were made with the following concentrations in 10 mM Tris-HCl, pH 7.5 and 100 mM NaCl: 0.2% n-Dodecyl-β-D-maltopyranoside (DDM), 2% n-Decyl-β-D-maltopyranoside (DM), 5% CHAPS, 1.2% CYMAL-5, 0.5% Fos-Choline-12, 0.15% Triton X-100, and 0.083% Genapol X-80. Due to solubility issues, n-Octyl-β-D-glucopyranoside (OG) was used as a 10% aqueous solution without buffer or NaCl. Trx_{E}-$Nox1_{cyt}$ and H_6-$Nox1_{cyt}$ were each subjected to this screen. For Trx_{E}-$Nox1_{cyt}$, 7.2 µg in 5 µl was incubated individually with 5 µl of each respective detergent solution. An equivalent amount of Trx_{E}-$Nox1_{cyt}$ was incubated with 5 µl of the storage buffer for the protein, which does not contain detergent (10 mM NaH_2PO_4, 500 mM NaCl, 10% glycerol, 2 mM DTE, pH 8.0). To control the total protein amount for each sample, a gel sample of an equivalent amount was made from a freshly thawed sample of Trx_{E}-$Nox1_{cyt}$ prior to running the SDS-PAGE. H_6-$Nox1_{cyt}$ (7 µg) was processed in a similar way with the exception that the buffer used for the detergent solutions (10 mM Tris-HCl, pH 7.5 and 100 mM NaCl) was used for the no-detergent control. Gel samples of the supernatant were made after centrifugation of each sample at 14,000 rpm for 30 min at 4°C. All gel samples (excluding markers) were made without boiling at 100°C.

4.2.9 NADPH-dependent diaphorase activity

Spectrophotometric format

H_6-Nox1$_{cyt}$ was assayed for NADPH-dependent diaphorase activity at 37°C after an established procedure (Nisimoto *et al.*, 2004). Intrinsic activity and activity in the presence of p67N-Rac(Q61L)•GTP or p67N-Rac•GppNHp was assayed in a final volume of 1 ml. For measurement of intrinsic activity, 100 µl of protein pre-incubation buffer containing 4.5 µM H_6-Nox1$_{cyt}$ was allowed to incubate for 15 minutes on ice. For the measurement of activity in the presence of p67N-Rac(Q61L)•GTP or p67N-Rac•GppNHp, 100 µl of protein pre-incubation buffer containing 4.5 µM H_6-Nox1$_{cyt}$ and either 14.8 µM p67N-Rac(Q61L)•GTP or 12.3 µM pre-loaded p67N-Rac•GppNHp was pre-incubated for 15 minutes on ice. 100 µl of each sample was added to assay buffer and pre-incubated in a 39-40°C water bath for 5 minutes. NADPH was added to a final concentration of 200 µM and the samples were assayed at 595 nm in a Beckman DU®640 spectrophotometer for 20-60 minutes at 37°C. The spectrophotometer was blanked at 595 nm with 100 µl of protein pre-incubation buffer in assay buffer after NADPH had been added to a final concentration of 200 µM. Storage buffers for the respective proteins were assayed using volumes identical to the volumes of protein used in protein-containing assay samples. The change in absorbance at 595 nm over time produced by each storage buffer were subtracted from that of the respective protein-containing samples to buffer correct the measured values. For p67N-Rac, this particular protein sample did not contain DTT in the buffer. In the future, the assay buffer should contain 4 mM $MgCl_2$, to ensure optimal nucleotide binding to Rac. To prevent light catalyzed reduction of NBT, all sample preparation was made in low light conditions.

Assay Buffer: 50 mM NaH_2PO_4, pH 7.3, 50 mM NaCl, 20 µM FAD, 0.1 mM NBT final concentrations in 1ml

Protein Pre-incubation Buffer: 25 mM NaH_2PO_4, pH 7.3, 20 µM FAD, and either 10 µM GTP (for p67N-RacQ61L) or 10 µM GppNHp (for p67N-Rac)

Microtiter format

The NADPH-dependent diaphorase activity assay was modified for microtiter format with a few changes. Since H_6-Nox1$_{cyt}$ is not active at 20°C, the assay samples were made at 20°C,

and were likewise prepared under low light conditions. Assay buffer was made as a 2-fold concentrated stock and 50 µl was added to wells in a Nunc Nunclon microtiter plate. H_6-$Nox1_{cyt}$, detergent, p67N-Rac(Q61L)•GTP, and buffer controls were added as detailed below, and each sample was made to a final volume of 98 µl with water. Three concentrations of H_6-$Nox1_{cyt}$ (0.46 µM, 2.3 µM, and 4.6 µM final concentration in 100 µl) were assayed and a concentration of 2.3 µM was used in all subsequent assays. Fos-choline-12 was assayed with and without H_6-$Nox1_{cyt}$, at the following concentrations: 0.5x CMC (0.75 mM), 1x CMC (1.5 mM), 2x CMC (3 mM), 5x CMC (7.5 mM), and 10x CMC (15 mM) from a freshly prepared 10% aqueous stock solution. H_6-$Nox1_{cyt}$ was assayed with and without p67N-Rac(Q61L)•GTP, in the absence and presence of 2x CMC of Fos-choline-12. 11 µM H_6-$Nox1_{cyt}$ and 39 µM p67N-Rac(Q61L)•GTP were pre-incubated in pre-incubation buffer in a final volume of 21 µl for 15 minutes on ice prior to the assay. Buffer controls were made in exactly the same way as protein-containing samples, except the proteins were substituted by the respective protein storage buffer. For example, the buffer control for a sample containing 10 µl of H_6-$Nox1_{cyt}$ in assay buffer with a final volume of 100 µl, consisted of 10 µl of the storage buffer for H_6-$Nox1_{cyt}$ in assay buffer with a final volume of 100 µl. For a sample containing 10 µl of H_6-$Nox1_{cyt}$ and 0.5 µl of p67N-Rac(Q61L)•GTP pre-incubated with 10.5 µl of 2x protein pre-incubation buffer, all in assay buffer at a final volume of 100µl, the buffer control contained 10 µl of the storage buffer for H_6-$Nox1_{cyt}$, 0.5 µl of the storage buffer for p67N-Rac(Q61L)•GTP, and 10.5 µl of 2x protein pre-incubation buffer, all in assay buffer at a final volume of 100µl. A 20 mM solution of NADPH in 10 mM HEPES, pH 7.5 was made and the concentration checked spectrophotometrically using an extinction coefficient of 6.22 $mM^{-1}cm^{-1}$. 2µl of this NADPH solution was added to each sample. The plate was then sealed with Crystal Clear Tape and inserted into a Labsystem iEMS Reader MF (Thermo Electron, Langenselbold) preheated at 37°C. The plate was shaken for 10 seconds and read at 595 nm and 340 nm for 1 hour, with samples reaching 37°C in the first 5 minutes.

2x Assay Buffer: 100 mM NaH_2PO_4, pH 7.3, 100 mM NaCl, 8 mM $MgCl_2$,0.2 mM NBT, 40 µM FAD

2x Protein Pre-incubation Buffer: 50 mM NaH_2PO_4, pH 7.3, 40 µM FAD, 20 µM GTP, 8 mM $MgCl_2$

Calculation of activity and turnover number

Activity (mol of reduced NBT/min/mol of Nox1) can be calculated from the measured change in absorbance at 595 nm over time using the Beer-Lambert law:

$$\Delta c = \frac{\Delta A_{595}}{\varepsilon_{595} \cdot b \cdot \Delta t} \qquad \text{Eq. 1}$$

where ε_{595} is the molar extinction coefficient of NBT at 595 nm (12.6 $mM^{-1}cm^{-1}$), and b is the pathlength, which is 1 cm in the spectrophotometric assay. Data were buffer corrected by subtracting the data of the corresponding buffer control, and the linear portion fit with linear regression in Origin version 6.0 (Microcal Software, Northampton, MA). The slopes obtained were used in Equation 1 to calculate the change in concentration of reduced NBT per minute. Moles of reduced NBT were calculated by multiplying Equation 1 with the volume of the assay sample and activity was calculated by dividing this value with the moles of Nox1 used in the assay. Rates of electron flow were calculated in electrons/min/molecule of protein assuming NBT is a 4 electron acceptor and using:

$$N_e/\text{min/molecule protein} = \frac{N_A \cdot n_{redNBT} \cdot (4mol_e / mol_{redNBT})}{N_A \cdot n_{Nox1}} \qquad \text{Eq. 2}$$

where N_e is the number of electrons, N_A is Avogadro's number of 6.022 x 10^{23} molecules/mole, n_{redNBT} is the number of moles of reduced NBT, mol_e is mole of electrons, mol_{redNBT} is mole of reduced NBT and n_{Nox1} is the number of moles of Nox1.

4.2.10 Analytical size exclusion chromatography

Two batches of H_6-$Nox1_{cyt}$ were analyzed with analytical size exclusion chromatography. 100 µg of H_6-$Nox1_{cyt}$ was incubated with a 50-fold molar excess of FAD at 4°C for at least 1 hour. 125 µl of this solution was injected with an autosampler using a Waters HPLC at 0.5 ml/min onto an analytical Superdex 75 column pre-equilibrated with 20 mM NaH_2PO_4, pH 7.3, 300 mM NaCl, 250 mM Imidazole, and 10% glycerol. For the second batch of H_6-$Nox1_{cyt}$, 280 µg was incubated with a 25-fold molar excess of FAD for 2.5 hours at 4°C. 190 µl of this solution was loaded at 0.5 ml/min onto an analytical Superdex 75 column pre-equilibrated with 50 mM NaH_2PO_4, pH 7.3, 300 mM NaCl, 250 mM Imidazole, and 10% glycerol. For each H_6-$Nox1_{cyt}$ chromatographic run, Bio-Rad gel filtration standards were

run using identical volumes as the loaded protein samples with identical buffers and flow rates.

4.2.11 Expression, purification, and characterization of p67N-Rac and p67N-Rac(Q61L)

Expression

Chemically competent BL21(DE3) cells (Dr. Konstanze von König), were transformed via heat shock with the plasmid pGEX-2T containing either p67N-Rac or p67N-Rac(Q61L) (Dr. Minoru Tamura, Ehime University, Japan), and plated on LB agar plates containing a final concentration of 100 μg/ml of ampicillin (used at this concentration in all subsequent cultures). Typically, 3-4L of LB/ampicillin were inoculated with an overnight culture using a volume 1:500 of the final volume, and grown at 37°C until a cell density at 600 nm of 0.7-0.8. Cultures were chilled at 4°C for 30-60 min, and protein expression was induced with IPTG at a final concentration of 0.05 mM, with overnight incubation at 20°C. Cells were harvested at 4000 rpm for 20 min at 4°C, flash frozen in liquid nitrogen and stored at –80°C.

Glutathione Sepharose Chromatography

In contrast to the Nox1 constructs, both Rac fusion proteins overexpress well, and cells from 0.5 or 1L will provide more than enough protein in the end. Purification was performed at 4°C and pH values of all buffers represent values at 4°C. Generally, cells from 1L of culture were thawed at room temperature and resuspended in Lysis Buffer with one Complete EDTA-free protease inhibitor cocktail tablet/50 ml buffer at a volume 2x the mass of the cells. Cells were lysed with 2 passes through a microfluidizer and genomic DNA was digested with DNase I (35μg/ml lysate) in the presence of 10 mM $MgCl_2$ with stirring for 10 minutes at 4°C. The lysate was then clarified via ultracentrifugation at 40,000 rpm for 1 hr at 4°C. The supernatant was incubated with ~7ml of Glutathione Sepharose 4B resin at 4°C for 1.5-2 hours with gentle shaking. This was then transferred to a gravity column and the resin was washed with 70 ml of Lysis Buffer, followed by 30 ml of Wash 1 Buffer and 30 ml of Wash 2 buffer. Bound proteins were batch eluted with 20 ml of Elution Buffer and allowed to incubate at 4°C for 1.5 hours on a wheel. Eluted fusion proteins were dialyzed into Thrombin Digest buffer and digested with thrombin (2U/mg protein), with complete digestion requiring about one week at 4°C. To remove thrombin, NaCl was added to the

digest to a final concentration of 0.5 M and the sample was loaded on a HiTrap Benzamidine FF (high sub) column pre-equilibrated with Benzamidine Binding Buffer. The flow through was collected and concentrated in centrifugal concentrators (30 MWCO) to 3 ml, then diluted 10-fold with Dilution Buffer. The GST tag and any uncut GST-fusion protein were removed with a second application over Glutathione Sepharose 4B resin. The desired fusion proteins were collected in the flow through fractions and concentrated in centrifugal concentrators (30 MWCO) to 1.5 ml.

Lysis buffer: 50 mM Tris-HCl, pH 7.5, 300 mM NaCl, 4 mM DTT, 2 mM EDTA, 5 mM $MgCl_2$

Wash 1 buffer: 50 mM Tris-HCl, pH 7.5, 1M NaCl, 4 mM DTT, 2 mM EDTA, 5 mM $MgCl_2$

Wash 2 buffer: 50 mM Tris-HCl, pH 7.5, 50 mM NaCl, 2 mM DTT, 1 mM EDTA, 5 mM $MgCl_2$

Elution Buffer: 100 mM Tris-HCl, pH 7.5, 50 mM reduced glutathione

Thrombin Digest Buffer: 50 mM Tris-HCl, pH 7.5, 150 mM NaCl, 2 mM DTT, 5 mM $MgCl_2$, 2.5 mM $CaCl_2$

Benzamidine Binding Buffer: 50 mM Tris-HCl, pH 7.4, 0.5 M NaCl

Dilution Buffer: 50 mM Tris-HCl, pH 7.5, 2 mM DTT, 1 mM EDTA, 5 mM $MgCl_2$

Size Exclusion Chromatography

The concentrated elution from the second Glutathione Sepharose 4B column was loaded with an ÄKTA Prime onto a Superdex 200 gel filtration column at 1 ml/min, and 3 ml fractions were collected. Fractions containing the Rac fusion proteins were identified by SDS-PAGE and concentrated in centrifugal concentrators (30 MWCO).

Superdex 200 Buffer: 50 mM Tris-HCl, pH 7.5, 50 mM NaCl, 2 mM DTT, 5 mM $MgCl_2$

Nucleotide Identification and Quantification

Bound nucleotide for each Rac fusion protein was identified and quantified with HPLC. 100 µl of 10 µM Rac fusion protein in water was heated for 3 min at 95°C, then centrifuged for 20 min at 14,000 rpm, 4°C. 20 µl of the supernatant was analyzed on a Latek HPLC

(Latek, Eppelheim) over a ODS Prontosil Hypersorb, reversed phase C18 column (Bischoff Chromatography, Leonberg) using isocratic elution with 0.1M potassium phosphate, pH 6.8, 10 mM Tetra-n-butyl ammonium bromide, and 7.5% Acetonitrile. The amount of bound nucleotide was calculated from the average of three trials using the areas obtained from 20 µl of a 30.8 µM GXP standard containing 10.27µM of GMP, GDP and GTP, respectively. This value was compared with the protein concentration as determined by the Ehresmann method (Ehresmann *et al.*, 1973) to give the percent nucleotide bound, and the adjusted concentration of active protein.

Intrinsic GTPase Activity of p67N-Rac(Q61L)

720 µg of p67N-Rac(Q61L) was loaded with a 5-fold molar excess of GTP in 20 mM Tris-HCl, pH 7.45, 3 mM NaCl, and 50 mM KCl at 20°C for 15 minutes. Excess nucleotide was removed with NAP 5 chromatography and simultaneously buffer exchanged into 50 mM Tris-HCl, pH 7.45, 50 mM NaCl, 2 mM DTT, and 5 $MgCl_2$. A 200 µl solution of p67N-Rac(Q61L) at a concentration of 54.5 µM was incubated at 37°C and aliquots were removed to make 100µl of a 10µM protein sample for each time point, which were then flash frozen in liquid nitrogen. Samples for each time point were analyzed in triplicate with HPLC and the amount of GTP bound was calculated from a GXP standard of known concentration in the same manner described for nucleotide identification and quantification.

4.2.12 Fluorescence measurements

Fluorescence measurements were made with a FluoroMax-3 at 20°C, after Nisimoto *et al*, 1997. A 800 µl solution of mantGppNHp at a final concentration of 0.12 µM in 20 mM Tris-HCl, pH 7.45, 3 mM NaCl, 50 mM KCl, and 0.1 µM $MgCl_2$, was excited with a wavelength of 355 nm and the emission at 445 nm was monitored over 5 minutes. p67N-Rac•GDP (in 50 mM Tris-HCl, pH 7.5, 50 mM NaCl, 2 mM DTT, 5 mM $MgCl_2$) was added to this solution at a final concentration of 0.25 µM and the emission was monitored further over 30 minutes. Trx_E-$Nox1_{cyt}$ (in 10 mM NaH_2PO_4, pH 7.3, 500 mM NaCl, 10 % glycerol, and 2 mM DTT) was then added at a final concentration of 0.35 µM and the emission monitored further over 20 minutes. Data were corrected for volume changes, which did not exceed 1%.

4.3 CYCLIZED RAB7 METHODS

4.3.1 Protein expression

Cells transformed with a plasmid containing the intein and Rab7, residues 7-185 (a kind gift from Prof. Nick Dixon, University of Wollongong, New South Wales, Australia) were grown in LB at 30°C until an OD_{600} of 0.6-0.7 was reached. Protein expression was thermally induced by initially exposing the cultures to 45°C for 30 minutes, followed by 2.5-3.5 hours at 42°C. Cyclization was promoted by cooling the flasks at 4°C for 2 hours. Cells were harvested via centrifugation and flash frozen at -80°C.

4.3.2 Purification

Cells expressing cyclized Rab7 were thawed and homogenized in lysis buffer and lysed in a microfluidizer. The lysate was clarified via ultracentrifugation and subjected to ammonium sulfate precipitation (40g/100 ml of lysate). The suspension was clarified via ultracentrifugation and the pellet was resuspended in Buffer DEAE-A, and subsequently dialyzed against the same buffer to remove the ammonium sulfate prior to application on a DEAE Sepharose Fast Flow column (Amersham Biosciences/GE Healthcare). After washing the column with Buffer DEAE-A until the absorbance reached baseline and remained stable, cyclized Rab7 was eluted with a linear gradient of 0-250mM NaCl in Buffer DEAE-A over 5 column volumes, and fractions were analyzed with SDS-PAGE. Cyclized Rab7 typically eluted at 100 mM NaCl, and fractions were pooled and concentrated with ammonium sulfate precipitation (0.5 g/ml). Higher molecular weight contaminants were removed with gel filtration chromatography on a Superdex 75 column (Amersham Biosciences/GE Healthcare) in Superdex 75 Buffer. Fractions were analyzed with SDS-PAGE, and fractions containing cyclized Rab7 were pooled, diluted 10 times with Buffer HQ-A, and applied to a POROS® HQ anion exchange column (Applied Biosystems). Cyclized Rab7 was eluted with a step gradient of 80 mM NaCl, and purity was checked with SDS-PAGE. The final protein preparation was buffer exchanged into Final Buffer via centrifugal concentration (10 MWCO, Millipore). Cyclization of Rab7 was confirmed with ESI-MS, showing a mass of 21,353 Da (21,355 expected), which indicates the loss of a molecule of water upon cyclization (cf. linear mass 21,373 Da).

Lysis Buffer: 50 mM Tris-HCl, pH 7.6, 100 mM NaCl, 10%w/v sucrose, 1 mM EDTA, 2 mM DTT

Buffer DEAE-A: 50 mM Tris-HCl, pH 7.6, 15% glycerol, 1 mM EDTA, 2 mM DTT

Buffer DEAE-B: 50 mM Tris-HCl, pH 7.6, 500 mM NaCl, 15% glycerol, 1 mM EDTA, 2 mM DTT

Superdex 75 Buffer: 50 mM Tris-HCl, pH 7.6, 100 mM NaCl, 15% glycerol, 1 mM EDTA, 2 mM DTT.

Buffer HQ-A: 50 mM Tris-HCl, pH 8.5, 1 mM EDTA, 1 mM DTT

Buffer HQ-B: 50 mM Tris-HCl, pH 8.5, 1M NaCl, 1 mM EDTA, 1 mM DTT

Final Buffer: 20 mM Tris-HCl, pH 7.6, 80 mM NaCl, 2 mM DTT

4.3.3 ESI-MS

Electrospray ionization mass spectrometry (ESI-MS) measurements were made with a LCQ Advantage Max mass spectrometer (Finnigan, San Jose, CA, USA). 2 µl of each protein sample were diluted with 28 µl of water to reduce the concentration of salt and buffer, and 25 µl of this solution was analyzed. Deconvolution was made using Xcalibur software.

4.3.4 Fluorescence measurements

Fluorescence measurements were made on a Fluoromax-3 monitoring the intrinsic tryptophan fluorescence at an excitation wavelength of 290 nm. Protein samples were made at a concentration of 5 µM in 40 mM HEPES, pH 7.5, 1 mM $MgCl_2$, 2 mM DTT. Spectra were recorded from 20°C to 85°C, with 10 minute equilibration at each temperature. Thermal recovery of the respective proteins was checked after the last temperature by cooling the sample to 20°C and re-measuring its fluorescence emission.

4.3.5 Circular Dichroism (CD) spectroscopy

Protein secondary structure was determined by CD measurements using a Jasco J-720 spectropolarimeter. CD spectra were collected over the wavelength range from 190 to

260 nm at 0.2 nm intervals with a spectral bandwidth of 0.8 nm, 1 s integration time and a scanning speed of 200 nm/min, using a 0.1 cm quartz cuvette. Protein samples were prepared in a buffer consisting of 25 mM sodium phosphate, pH 7.5, 1 mM $MgCl_2$, and 1 mM DTT at a final concentration of 0.5 mg/ml (0.05 %w/v) and spectra were taken immediately after preparation. Thermal denaturation was monitored from 25°C to 85°C, with 10 minute equilibration at each respective temperature. Thermal recovery was checked after the last temperature by cooling the sample to 20°C and re-measuring its circular dichroism.

All CD spectra are shown after buffer subtraction and smoothing with Origin 7 (Dr. Dahabada Lopes). The data are expressed as molar ellipticity [θ] in units of deg cm^2 $dmol^{-1}$, according to (Myers *et al.*, 1997):

$$[\theta] = \frac{100(signal)}{Cnl} \qquad \text{Eq. 3}$$

where *C* is the protein concentration in mM, *n* is the number of residues and *l* is the pathlength in cm. The percentage of secondary structural elements was determined using the CONTIN program (Provencher, 1982) (Dr. Dahabada Lopes).

4.3.6 Nucleotide exchange

Endogenously bound GDP was exchanged for mantGDP or GTP by removing excess Mg^{2+} with incubation in 5 mM EDTA and a 20-fold molar excess of the desired nucleotide at 25°C for 2 hours. The exchange was stopped with the addition of 10 mM $MgCl_2$, and excess nucleotide was removed with Nap-5 columns. The incubation time was doubled to 4 hours for cyclized Rab7. GppNHp bound cyclized Rab7 used for crystallization was prepared by incubation with 10 mM EDTA for one hour at 4°C, followed by removal of excess EDTA with a Nap-5 column. A 10-fold molar excess of GppNHp was added, and residually bound GDP was hydrolyzed by incubation for 3-4 hours at 25°C with alkaline phosphatase (5U/mg protein) in the presence of 200 mM ammonium sulfate and 500 µM $ZnCl_2$. The extent of nucleotide exchange/GDP hydrolysis was monitored by HPLC and was stopped after completion by the addition of 10 mM $MgCl_2$. Excess nucleotides were removed with a Nap-5 column and the protein was concentrated in centrifugal ultrafiltration concentrators (10 MWCO).

4.3.7 GTPase activity

GTPase activity was measured by incubating 150 µM of either Rab7 ΔC22•GTP or cyclized Rab7•GTP in 40 mM HEPES, pH 7.5 at 37°C in the presence of 10 mM $MgCl_2$. Aliquots were removed at given time points, flash frozen in liquid nitrogen and analyzed on HPLC to quantify the amounts of GTP and GDP. The amount of GTP for each time point was normalized with the initial amount of GTP. Data were plotted with Origin version 6.0 (Microcal Software, Northampton, MA, U.S.A.) and fit with the following single exponential equation:

$$y = y_o + A_1 e^{\left(\frac{-x}{t_1}\right)} \qquad \text{Eq. 4}$$

Rates were calculated from t_1^{-1}.

4.3.8 Effector binding and dissociation

Cyclized Rab7•mantGDP or Rab7ΔC22•mantGDP at a final concentration of 0.5 µM in 50 mM HEPES, pH 7.5, 50 mM NaCl, 2 mM $MgCl_2$, 2 mM DTT, was mixed with various excess concentrations of Mrs6 in a SX 18MV-R stopped flow apparatus (Applied Photophysics, Surrey, UK) using a sample volume of 100 µl, at 20°C. FRET from tryptophan to the mant moiety was measured using an excitation wavelength of 295 nm and a 400 nm cutoff filter, with slit width of 1 mm. Association curves were fit using the corresponding manufacturer's program to the following double exponential equation:

$$y = A_1 e^{(rate1 \cdot x)} + A_2 e^{(rate2 \cdot x)} + endpt \qquad \text{Eq. 5}$$

K_D was determined independently using amplitude analysis, by calculating signal change as a percentage of the total signal and plotting this against Mrs6 concentration. The data were then fit to the following equation to obtain K_D:

$$\Delta A = \frac{\Delta A_o}{1 + \frac{K_d}{[Mrs6]}} \qquad \text{Eq. 6}$$

where ΔA is the signal change observed for a given Mrs6 concentration and ΔA_o is the maximal change (i.e. that at infinite [Mrs6]). Displacement kinetics were measured by incubating a final concentration of 0.5 μM cyclized Rab7•mantGDP or Rab7ΔC22•mantGDP with Mrs6 in a 1:1 molar ratio for 5 minutes at 20°C. Bound Rab7 was displaced by the addition of a 10-fold molar excess of full-length Rab7SSSS, containing mutations in the two C-terminal cysteines for solubility. FRET was monitored using an excitation wavelength of 290 nm and a 400 nm cutoff filter. Displacement curves were fit to the following double exponential equation:

$$y = A_1 e^{(-k_1 \cdot t)} + A_2 e^{(-k_2 \cdot t)} + endpt \qquad \text{Eq. 7}$$

4.3.9 Crystallization

Cyclized Rab7 bound with GppNHp was crystallized using hanging drop vapor diffusion. 1 μl of reservoir solution consisting of 1.3 M ammonium sulfate, 100 mM HEPES, pH 7.4, and 500 mM KCl was added to 0.5 μl of a 13 mg/ml protein solution, and suspended over 500 ml of reservoir solution. Microseeding was employed to improve crystal quality. Briefly, larger bundles of crystals not suitable for x-ray diffraction studies were gathered in a stabilizing solution of 70% saturated ammonium sulfate and 100 mM HEPES, pH 7.4, and crushed with a needle. The stock microseed solution was serially diluted and scanned by adding 0.2 μl of each seed solution to crystallization drops to find the concentration of seed that would give 1-5 crystals per drop.

4.3.10 X-ray data collection and processing

Cyclized Rab7•GppNHp crystals were placed briefly in a cryoprotectant containing 70% saturated ammonium sulfate, 100 mM HEPES, pH 7.4, and 10% glycerol and cryocooled in liquid nitrogen. X-ray diffraction data (120° with an oscillation of 0.25°) were collected at the Swiss Light Source (SLS) synchrotron (Villingen, Switzerland) (Dr. Thomas Barends, Dr. Anton Meinhart), at 100K, with a detector distance of 180 mm. Data were processed with *XDS*, and the structure was solved with molecular replacement (CCP4) using Rab7•GDP (PDB code 1VG1) as a search model. The structure was initially refined with

REFMAC5 (CCP4) until twinning was discovered and confirmed with *TRUNCATE* (CCP4). A new reflection test set was generated to exclude twin-related reflections from belonging to both working and test sets with *CNS*, and the previous model bias was erased with simulated annealing (*CNS*). The resulting model was then refined against the twinned data set in *SHELXL* using the twin law -h, -k, l and an initial twinning fraction of 0.441. All structure figures were made using PyMOL (DeLano Scientific LLC, Palo Alto, U.S.A.)

REFERENCES

3rd NCCR Practical Course: Membrane protein expression, purification, 2-D crystallization and imaging. (October 4-8, 2004) Biozentrum, University of Basel, Basel, Switzerland.

Abo, A., Pick, E., Hall, A., Totty, N., Teahan, C.G. and Segal, A.W. (1991) Activation of the NADPH oxidase involves the small GTP-binding protein p21rac1. *Nature* **353**, 668-670.

Abo, A., Webb, M.R., Grogan, A. and Segal, A.W. (1994) Activation of NADPH oxidase involves the dissociation of p21rac from its inhibitory GDP/GTP exchange protein (rhoGDI) followed by its translocation to the plasma membrane. *Biochem. J.* **298 Pt 3**, 585-591.

Abramson, J. and Wright, J.M. (2007) Are lipid-lowering guidelines evidence-based? *Lancet* **369**, 168-169.

Ago, T., Kitazono, T., Ooboshi, H., Iyama, T., Han, Y.H., Takada, J., Wakisaka, M., Ibayashi, S., Utsumi, H. and Iida, M. (2004) Nox4 as the major catalytic component of an endothelial NAD(P)H oxidase. *Circulation* **109**, 227-233.

Ago, T., Kuribayashi, F., Hiroaki, H., Takeya, R., Ito, T., Kohda, D. and Sumimoto, H. (2003) Phosphorylation of p47phox directs phox homology domain from SH3 domain toward phosphoinositides, leading to phagocyte NADPH oxidase activation. *Proc. Natl. Acad. Sci. U. S. A* **100**, 4474-4479.

Ago, T., Nunoi, H., Ito, T. and Sumimoto, H. (1999) Mechanism for phosphorylation-induced activation of the phagocyte NADPH oxidase protein p47(phox). Triple replacement of serines 303, 304, and 328 with aspartates disrupts the SH3 domain-mediated intramolecular interaction in p47(phox), thereby activating the oxidase. *J. Biol. Chem.* **274**, 33644-33653.

Ago, T., Takeya, R., Hiroaki, H., Kuribayashi, F., Ito, T., Kohda, D. and Sumimoto, H. (2001) The PX domain as a novel phosphoinositide- binding module. *Biochem. Biophys. Res. Commun.* **287**, 733-738.

Ahmed, S., Prigmore, E., Govind, S., Veryard, C., Kozma, R., Wientjes, F.B., Segal, A.W. and Lim, L. (1998) Cryptic Rac-binding and p21(Cdc42Hs/Rac)-activated kinase phosphorylation sites of NADPH oxidase component p67(phox). *J. Biol. Chem.* **273**, 15693-15701.

Alderton, W.K., Cooper, C.E. and Knowles, R.G. (2001) Nitric oxide synthases: structure, function and inhibition. *Biochem. J.* **357**, 593-615.

Alexandrov, K., Simon, I., Iakovenko, A., Holz, B., Goody, R.S. and Scheidig, A.J. (1998) Moderate discrimination of REP-1 between Rab7 x GDP and Rab7 x GTP arises from a difference of an order of magnitude in dissociation rates. *FEBS Lett.* **425**, 460-464.

Alloul, N., Gorzalczany, Y., Itan, M., Sigal, N. and Pick, E. (2001) Activation of the superoxide-generating NADPH oxidase by chimeric proteins consisting of segments of the cytosolic component p67(phox) and the small GTPase Rac1. *Biochemistry* **40**, 14557-14566.

Alory, C. and Balch, W.E. (2001) Organization of the Rab-GDI/CHM superfamily: the functional basis for choroideremia disease. *Traffic.* **2**, 532-543.

Altman, F.P. (1974) Studies on the reduction of tetrazolium salts. 3. The products of chemical and enzymic reduction. *Histochemistry* **38**, 155-171.

Ambasta, R.K., Kumar, P., Griendling, K.K., Schmidt, H.H., Busse, R. and Brandes, R.P. (2004) Direct interaction of the novel Nox proteins with p22phox is required for the formation of a functionally active NADPH oxidase. *J. Biol. Chem.* **279**, 45935-45941.

Ambasta, R.K., Schreiber, J.G., Janiszewski, M., Busse, R. and Brandes, R.P. (2006) Noxa1 is a central component of the smooth muscle NADPH oxidase in mice. *Free Radic. Biol. Med.* **41**, 193-201.

Arechaga, I., Miroux, B., Karrasch, S., Huijbregts, R., de, K.B., Runswick, M.J. and Walker, J.E. (2000) Characterisation of new intracellular membranes in Escherichia coli accompanying large scale over-production of the b subunit of F(1)F(o) ATP synthase. *FEBS Lett.* **482**, 215-219.

Azumi, H., Inoue, N., Ohashi, Y., Terashima, M., Mori, T., Fujita, H., Awano, K., Kobayashi, K., Maeda, K., Hata, K., Shinke, T., Kobayashi, S., Hirata, K., Kawashima, S., Itabe, H., Hayashi, Y., Imajoh-Ohmi, S., Itoh, H. and Yokoyama, M. (2002) Superoxide generation in directional coronary atherectomy specimens of patients with angina pectoris: important role of NAD(P)H oxidase. *Arterioscler. Thromb. Vasc. Biol.* **22**, 1838-1844.

Azumi, H., Inoue, N., Takeshita, S., Rikitake, Y., Kawashima, S., Hayashi, Y., Itoh, H. and Yokoyama, M. (1999) Expression of NADH/NADPH oxidase p22phox in human coronary arteries. *Circulation* **100**, 1494-1498.

Babior, B.M. and Kipnes, R.S. (1977) Superoxide-forming enzyme from human neutrophils: evidence for a flavin requirement. *Blood* **50**, 517-524.

Babior, B.M., Lambeth, J.D. and Nauseef, W. (2002) The neutrophil NADPH oxidase. *Arch. Biochem. Biophys.* **397**, 342-344.

Bae, Y.S., Sung, J.Y., Kim, O.S., Kim, Y.J., Hur, K.C., Kazlauskas, A. and Rhee, S.G. (2000) Platelet-derived growth factor-induced H(2)O(2) production requires the activation of phosphatidylinositol 3-kinase. *J. Biol. Chem.* **275**, 10527-10531.

Baeuerle, P.A. and Baltimore, D. (1996) NF-kappa B: ten years after. *Cell* **87**, 13-20.

Baldwin, A.S., Jr. (2001) Series introduction: the transcription factor NF-kappaB and human disease. *J. Clin. Invest* **107**, 3-6.

Banfi, B., Clark, R.A., Steger, K. and Krause, K.H. (2003) Two novel proteins activate superoxide generation by the NADPH oxidase NOX1. *J. Biol. Chem.* **278**, 3510-3513.

Banfi, B., Malgrange, B., Knisz, J., Steger, K., Dubois-Dauphin, M. and Krause, K.H. (2004) NOX3, a superoxide-generating NADPH oxidase of the inner ear. *J. Biol. Chem.* **279**, 46065-46072.

Banfi, B., Molnar, G., Maturana, A., Steger, K., Hegedus, B., Demaurex, N. and Krause, K.H. (2001) A Ca(2+)-activated NADPH oxidase in testis, spleen, and lymph nodes. *J. Biol. Chem.* **276**, 37594-37601.

Barbacanne, M.A., Souchard, J.P., Darblade, B., Iliou, J.P., Nepveu, F., Pipy, B., Bayard, F. and Arnal, J.F. (2000) Detection of superoxide anion released extracellularly by endothelial cells using cytochrome c reduction, ESR, fluorescence and lucigenin-enhanced chemiluminescence techniques. *Free Radic. Biol. Med.* **29**, 388-396.

Barends, T.R., de Jong, R.M., van Straaten, K.E., Thunnissen, A.M. and Dijkstra, B.W. (2005) Escherichia coli MltA: MAD phasing and refinement of a tetartohedrally twinned protein crystal structure. *Acta Crystallogr. D Biol. Crystallogr.* **61**, 613-621.

Barends, T.R. and Dijkstra, B.W. (2003) Acetobacter turbidans alpha-amino acid ester hydrolase: merohedral twinning in P21 obscured by pseudo-translational NCS. *Acta Crystallogr. D Biol. Crystallogr.* **59**, 2237-2241.

Barry-Lane, P.A., Patterson, C., van der, M.M., Hu, Z., Holland, S.M., Yeh, E.T. and Runge, M.S. (2001) p47phox is required for atherosclerotic lesion progression in ApoE(-/-) mice. *J. Clin. Invest* **108**, 1513-1522.

Bauersachs, J., Bouloumie, A., Fraccarollo, D., Hu, K., Busse, R. and Ertl, G. (1999) Endothelial dysfunction in chronic myocardial infarction despite increased vascular endothelial nitric oxide synthase and soluble guanylate cyclase expression: role of enhanced vascular superoxide production. *Circulation* **100**, 292-298.

Bauersachs, J., Bouloumie, A., Mulsch, A., Wiemer, G., Fleming, I. and Busse, R. (1998) Vasodilator dysfunction in aged spontaneously hypertensive rats: changes in NO synthase III and soluble guanylyl cyclase expression, and in superoxide anion production. *Cardiovasc. Res.* **37**, 772-779.

Bayraktutan, U., Blayney, L. and Shah, A.M. (2000) Molecular characterization and localization of the NAD(P)H oxidase components gp91-phox and p22-phox in endothelial cells. *Arterioscler. Thromb. Vasc. Biol.* **20**, 1903-1911.

Bayraktutan, U., Draper, N., Lang, D. and Shah, A.M. (1998) Expression of functional neutrophil-type NADPH oxidase in cultured rat coronary microvascular endothelial cells. *Cardiovasc. Res.* **38**, 256-262.

Beckman, J.S., Beckman, T.W., Chen, J., Marshall, P.A. and Freeman, B.A. (1990) Apparent hydroxyl radical production by peroxynitrite: implications for endothelial injury from nitric oxide and superoxide. *Proc. Natl. Acad. Sci. U. S. A* **87**, 1620-1624.

Beckman, J.S. and Koppenol, W.H. (1996) Nitric oxide, superoxide, and peroxynitrite: the good, the bad, and ugly. *Am. J. Physiol* **271**, C1424-C1437.

Beckman, K.B. and Ames, B.N. (1998) The free radical theory of aging matures. *Physiol Rev.* **78**, 547-581.

Bedard, K. and Krause, K.H. (2007) The NOX family of ROS-generating NADPH oxidases: physiology and pathophysiology. *Physiol Rev.* **87**, 245-313.

Behrendt, D. and Ganz, P. (2002) Endothelial function. From vascular biology to clinical applications. *Am. J. Cardiol.* **90**, 40L-48L.

Berry, C., Hamilton, C.A., Brosnan, M.J., Magill, F.G., Berg, G.A., McMurray, J.J. and Dominiczak, A.F. (2000) Investigation into the sources of superoxide in human blood vessels: angiotensin II increases superoxide production in human internal mammary arteries. *Circulation* **101**, 2206-2212.

Bianca, V.D., Dusi, S., Bianchini, E., Dal, P., I and Rossi, F. (1999) beta-amyloid activates the O-2 forming NADPH oxidase in microglia, monocytes, and neutrophils. A possible inflammatory mechanism of neuronal damage in Alzheimer's disease. *J. Biol. Chem.* **274**, 15493-15499.

Biberstine-Kinkade, K.J., DeLeo, F.R., Epstein, R.I., LeRoy, B.A., Nauseef, W.M. and Dinauer, M.C. (2001) Heme-ligating histidines in flavocytochrome b(558): identification of specific histidines in gp91(phox). *J. Biol. Chem.* **276**, 31105-31112.

Bisby, R.H. and Parker, A.W. (1991) Reactions of the alpha-tocopheroxyl radical in micellar solutions studied by nanosecond laser flash photolysis. *FEBS Lett.* **290**, 205-208.

Bokoch, G.M. and Zhao, T. (2006) Regulation of the phagocyte NADPH oxidase by Rac GTPase. *Antioxid. Redox. Signal.* **8**, 1533-1548.

Bowry, V.W. and Stocker, R. (1993) Tocopherol-mediated peroxidation. The prooxidant effect of vitamin E on the radical-initiated oxidation of human low-density lipoprotein. *J. Am. Chem. Soc.* **115**, 6029-6044.

Bradford, M.M. (1976) A rapid and sensitive method for the quantitation of microgram quantities of protein utilizing the principle of protein-dye binding. *Anal. Biochem.* **72**, 248-254.

Bravo, J., Karathanassis, D., Pacold, C.M., Pacold, M.E., Ellson, C.D., Anderson, K.E., Butler, P.J., Lavenir, I., Perisic, O., Hawkins, P.T., Stephens, L. and Williams, R.L. (2001) The crystal structure of the PX domain from p40(phox) bound to phosphatidylinositol 3-phosphate. *Mol. Cell* **8**, 829-839.

Bredt, D.S. and Snyder, S.H. (1990) Isolation of nitric oxide synthetase, a calmodulin-requiring enzyme. *Proc. Natl. Acad. Sci. U. S. A* **87**, 682-685.

Brown, M.S. and Goldstein, J.L. (1986) A receptor-mediated pathway for cholesterol homeostasis. *Science* **232**, 34-47.

Brunger, A.T., Adams, P.D., Clore, G.M., DeLano, W.L., Gros, P., Grosse-Kunstleve, R.W., Jiang, J.S., Kuszewski, J., Nilges, M., Pannu, N.S., Read, R.J., Rice, L.M., Simonson, T. and Warren, G.L. (1998) Crystallography & NMR system: A new software suite for macromolecular structure determination. *Acta Crystallogr. D Biol. Crystallogr.* **54**, 905-921.

Bucci, C., Thomsen, P., Nicoziani, P., McCarthy, J. and van, D.B. (2000) Rab7: a key to lysosome biogenesis. *Mol. Biol. Cell* **11**, 467-480.

Burton, G.W. and Ingold, K.U. (1986) Vitamin E: application of the principles of physical organic chemistry to the exploration of its structure and function. *Acc. Chem. Res.* **19**, 194-201.

Cai, H. (2005) NAD(P)H oxidase-dependent self-propagation of hydrogen peroxide and vascular disease. *Circ. Res.* **96**, 818-822.

Cantalupo, G., Alifano, P., Roberti, V., Bruni, C.B. and Bucci, C. (2001) Rab-interacting lysosomal protein (RILP): the Rab7 effector required for transport to lysosomes. *EMBO J.* **20**, 683-693.

Castier, Y., Brandes, R.P., Leseche, G., Tedgui, A. and Lehoux, S. (2005) p47phox-dependent NADPH oxidase regulates flow-induced vascular remodeling. *Circ. Res.* **97**, 533-540.

Cave, A.C., Brewer, A.C., Narayanapanicker, A., Ray, R., Grieve, D.J., Walker, S. and Shah, A.M. (2006) NADPH oxidases in cardiovascular health and disease. *Antioxid. Redox. Signal.* **8**, 691-728.

Chance, B., Sies, H. and Boveris, A. (1979) Hydroperoxide metabolism in mammalian organs. *Physiol Rev.* **59**, 527-605.

Chen, X. and Medford, R. (1999) Oxidation-reduction sensitive regulation of inflammatorygene expression in vasculature. In *Vascular Adhesion Molecules and Inflammation* (ed. Pearson JD) Birkhauser Press, Basel, 161-178.

Cheng, G., Cao, Z., Xu, X., van Meir, E.G. and Lambeth, J.D. (2001) Homologs of gp91phox: cloning and tissue expression of Nox3, Nox4, and Nox5. *Gene* **269**, 131-140.

Cheng, G. and Lambeth, J.D. (2004) NOXO1, regulation of lipid binding, localization, and activation of Nox1 by the Phox homology (PX) domain. *J. Biol. Chem.* **279**, 4737-4742.

Cheng, G. and Lambeth, J.D. (2005) Alternative mRNA splice forms of NOXO1: differential tissue expression and regulation of Nox1 and Nox3. *Gene* **356**, 118-126.

Cheung, M.C., Zhao, X.Q., Chait, A., Albers, J.J. and Brown, B.G. (2001) Antioxidant supplements block the response of HDL to simvastatin-niacin therapy in patients with coronary artery disease and low HDL. *Arterioscler. Thromb. Vasc. Biol.* **21**, 1320-1326.

Chiu, J.J., Wung, B.S., Shyy, J.Y., Hsieh, H.J. and Wang, D.L. (1997) Reactive oxygen species are involved in shear stress-induced intercellular adhesion molecule-1 expression in endothelial cells. *Arterioscler. Thromb. Vasc. Biol.* **17**, 3570-3577.

Chuang, T.H., Bohl, B.P. and Bokoch, G.M. (1993) Biologically active lipids are regulators of Rac.GDI complexation. *J. Biol. Chem.* **268**, 26206-26211.

Collaborative Computational Project Number 4 (1994) The CCP4 Suite: Programs for Protein Crystallography. *Acta Cryst.* **D50**, 760-763.

Collins, T. (1993) Endothelial nuclear factor-kappa B and the initiation of the atherosclerotic lesion. *Lab Invest* **68**, 499-508.

Collins, T. and Cybulsky, M.I. (2001) NF-kappaB: pivotal mediator or innocent bystander in atherogenesis? *J. Clin. Invest* **107**, 255-264.

Constantinescu, A. T. (2001) Structural and functional studies on the small GTPase Ypt7p and its interacting partners. p. 98. Bucharest, Romania, Romanian Academy Institute of Biochemistry.

Cornwell, T.L., Arnold, E., Boerth, N.J. and Lincoln, T.M. (1994) Inhibition of smooth muscle cell growth by nitric oxide and activation of cAMP-dependent protein kinase by cGMP. *Am. J. Physiol* **267**, C1405-C1413.

Cross, A.R. and Curnutte, J.T. (1995) The cytosolic activating factors p47phox and p67phox have distinct roles in the regulation of electron flow in NADPH oxidase. *J. Biol. Chem.* **270**, 6543-6548.

Cross, A.R., Parkinson, J.F. and Jones, O.T. (1985) Mechanism of the superoxide-producing oxidase of neutrophils. O2 is necessary for the fast reduction of cytochrome b-245 by NADPH. *Biochem. J.* **226**, 881-884.

Cross, A.R., Rae, J. and Curnutte, J.T. (1995) Cytochrome b-245 of the neutrophil superoxide-generating system contains two nonidentical hemes. Potentiometric studies of a mutant form of gp91phox. *J. Biol. Chem.* **270**, 17075-17077.

Cross, A.R. and Segal, A.W. (2004) The NADPH oxidase of professional phagocytes--prototype of the NOX electron transport chain systems. *Biochim. Biophys. Acta* **1657**, 1-22.

Cross, A.R., Yarchover, J.L. and Curnutte, J.T. (1994) The superoxide-generating system of human neutrophils possesses a novel diaphorase activity. Evidence for distinct regulation of electron flow within NADPH oxidase by p67-phox and p47-phox. *J. Biol. Chem.* **269**, 21448-21454.

Cucoranu, I., Clempus, R., Dikalova, A., Phelan, P.J., Ariyan, S., Dikalov, S. and Sorescu, D. (2005) NAD(P)H oxidase 4 mediates transforming growth factor-beta1-induced differentiation of cardiac fibroblasts into myofibroblasts. *Circ. Res.* **97**, 900-907.

Cushing, S.D., Berliner, J.A., Valente, A.J., Territo, M.C., Navab, M., Parhami, F., Gerrity, R., Schwartz, C.J. and Fogelman, A.M. (1990) Minimally modified low density lipoprotein induces monocyte chemotactic protein 1 in human endothelial cells and smooth muscle cells. *Proc. Natl. Acad. Sci. U. S. A* **87**, 5134-5138.

Dana, R., Leto, T.L., Malech, H.L. and Levy, R. (1998) Essential requirement of cytosolic phospholipase A2 for activation of the phagocyte NADPH oxidase. *J. Biol. Chem.* **273**, 441-445.

Dana, R., Malech, H.L. and Levy, R. (1994) The requirement for phospholipase A2 for activation of the assembled NADPH oxidase in human neutrophils. *Biochem. J.* **297 (Pt 1)**, 217-223.

Darley-Usmar, V., Wiseman, H. and Halliwell, B. (1995) Nitric oxide and oxygen radicals: a question of balance. *FEBS Lett.* **369**, 131-135.

Davies, K.J. (1995) Oxidative stress: the paradox of aerobic life. *Biochem. Soc. Symp.* **61**, 1-31.

De Deken, X., Wang, D., Dumont, J.E. and Miot, F. (2002) Characterization of ThOX proteins as components of the thyroid H(2)O(2)-generating system. *Exp. Cell Res.* **273**, 187-196.

De Deken, X., Wang, D., Many, M.C., Costagliola, S., Libert, F., Vassart, G., Dumont, J.E. and Miot, F. (2000) Cloning of two human thyroid cDNAs encoding new members of the NADPH oxidase family. *J. Biol. Chem.* **275**, 23227-23233.

de Graaf, J.C., Banga, J.D., Moncada, S., Palmer, R.M., de Groot, P.G. and Sixma, J.J. (1992) Nitric oxide functions as an inhibitor of platelet adhesion under flow conditions. *Circulation* **85**, 2284-2290.

Declercq, J.P. and Evrard, C. (2001) A twinned monoclinic crystal form of human peroxiredoxin 5 with eight molecules in the asymmetric unit. *Acta Crystallogr. D Biol. Crystallogr.* **57**, 1829-1835.

DeLeo, F.R., Burritt, J.B., Yu, L., Jesaitis, A.J., Dinauer, M.C. and Nauseef, W.M. (2000) Processing and maturation of flavocytochrome b558 include incorporation of heme as a prerequisite for heterodimer assembly. *J. Biol. Chem.* **275**, 13986-13993.

DeLeo, F.R. and Quinn, M.T. (1996) Assembly of the phagocyte NADPH oxidase: molecular interaction of oxidase proteins. *J. Leukoc. Biol.* **60**, 677-691.

Dendorfer, A., Wolfrum, S., Wagemann, M., Qadri, F. and Dominiak, P. (2001) Pathways of bradykinin degradation in blood and plasma of normotensive and hypertensive rats. *Am. J. Physiol Heart Circ. Physiol* **280**, H2182-H2188.

Diatchuk, V., Lotan, O., Koshkin, V., Wikstroem, P. and Pick, E. (1997) Inhibition of NADPH oxidase activation by 4-(2-aminoethyl)-benzenesulfonyl fluoride and related compounds. *J. Biol. Chem.* **272**, 13292-13301.

Diebold, B.A. and Bokoch, G.M. (2001) Molecular basis for Rac2 regulation of phagocyte NADPH oxidase. *Nat. Immunol.* **2**, 211-215.

Diekmann, D., Abo, A., Johnston, C., Segal, A.W. and Hall, A. (1994) Interaction of Rac with p67phox and regulation of phagocytic NADPH oxidase activity. *Science* **265**, 531-533.

Doussiere, J. and Vignais, P.V. (1992) Diphenylene iodonium as an inhibitor of the NADPH oxidase complex of bovine neutrophils. Factors controlling the inhibitory potency of diphenylene iodonium in a cell-free system of oxidase activation. *Eur. J. Biochem.* **208**, 61-71.

Drenth, J. (1999) Principles of protein X-ray crystallography. Springer-Verlag, Heidelberg.

Droge, W. (2002) Free radicals in the physiological control of cell function. *Physiol Rev.* **82**, 47-95.

Dupuy, C., Ohayon, R., Valent, A., Noel-Hudson, M.S., Deme, D. and Virion, A. (1999) Purification of a novel flavoprotein involved in the thyroid NADPH oxidase. Cloning of the porcine and human cdnas. *J. Biol. Chem.* **274**, 37265-37269.

Dusi, S., Donini, M. and Rossi, F. (1996) Mechanisms of NADPH oxidase activation: translocation of p40phox, Rac1 and Rac2 from the cytosol to the membranes in human neutrophils lacking p47phox or p67phox. *Biochem. J.* **314 (Pt 2)**, 409-412.

Dyer, G. and Fifer, M. (2003) Heart Failure. In *Pathophysiology of Heart Disease: a collaborative project of medical students and faculty* (ed. Lilly, L.) Lippincott Williams & Wilkins, Philadelphia, 211-236.

Eathiraj, S., Pan, X., Ritacco, C. and Lambright, D.G. (2005) Structural basis of family-wide Rab GTPase recognition by rabenosyn-5. *Nature* **436**, 415-419.

Edinger, A.L., Cinalli, R.M. and Thompson, C.B. (2003) Rab7 prevents growth factor-independent survival by inhibiting cell-autonomous nutrient transporter expression. *Dev. Cell* **5**, 571-582.

Ehresmann, B., Imbault, P. and Weil, J.H. (1973) Spectrophotometric determination of protein concentration in cell extracts containing tRNA's and rRNA's. *Anal. Biochem.* **54**, 454-463.

Eisenbrandt, R., Kalkum, M., Lai, E.M., Lurz, R., Kado, C.I. and Lanka, E. (1999) Conjugative pili of IncP plasmids, and the Ti plasmid T pilus are composed of cyclic subunits. *J. Biol. Chem.* **274**, 22548-22555.

El Benna, J., Faust, L.P. and Babior, B.M. (1994) The phosphorylation of the respiratory burst oxidase component p47phox during neutrophil activation. Phosphorylation of sites recognized by protein kinase C and by proline-directed kinases. *J. Biol. Chem.* **269**, 23431-23436.

Ellson, C.D., Anderson, K.E., Morgan, G., Chilvers, E.R., Lipp, P., Stephens, L.R. and Hawkins, P.T. (2001a) Phosphatidylinositol 3-phosphate is generated in phagosomal membranes. *Curr. Biol.* **11**, 1631-1635.

Ellson, C.D., Gobert-Gosse, S., Anderson, K.E., Davidson, K., Erdjument-Bromage, H., Tempst, P., Thuring, J.W., Cooper, M.A., Lim, Z.Y., Holmes, A.B., Gaffney, P.R., Coadwell, J., Chilvers, E.R., Hawkins, P.T. and Stephens, L.R. (2001b) PtdIns(3)P regulates the neutrophil oxidase complex by binding to the PX domain of p40(phox). *Nat. Cell Biol.* **3**, 679-682.

Ermolova, N.V., Ann, C.M., Taybi, T., Condon, S.A., Cushman, J.C. and Chollet, R. (2003) Expression, purification, and initial characterization of a recombinant form of plant PEP-carboxylase kinase from CAM-induced Mesembryanthemum crystallinum with enhanced solubility in Escherichia coli. *Protein Expr. Purif.* **29**, 123-131.

Esser, L. (2007) Refinement in cases of twinning. *NIH X-ray Diffraction Interest Group Newsletter* **158**.

Esterbauer, H., Striegl, G., Puhl, H. and Rotheneder, M. (1989) Continuous monitoring of in vitro oxidation of human low density lipoprotein. *Free Radic. Res. Commun.* **6**, 67-75.

Evans, T.C., Jr., Martin, D., Kolly, R., Panne, D., Sun, L., Ghosh, I., Chen, L., Benner, J., Liu, X.Q. and Xu, M.Q. (2000) Protein trans-splicing and cyclization by a naturally split intein from the dnaE gene of Synechocystis species PCC6803. *J. Biol. Chem.* **275**, 9091-9094.

Faraci, F.M. and Didion, S.P. (2004) Vascular protection: superoxide dismutase isoforms in the vessel wall. *Arterioscler. Thromb. Vasc. Biol.* **24**, 1367-1373.

Felizmenio-Quimio, M.E., Daly, N.L. and Craik, D.J. (2001) Circular proteins in plants: solution structure of a novel macrocyclic trypsin inhibitor from Momordica cochinchinensis. *J. Biol. Chem.* **276**, 22875-22882.

Feng, Y., Press, B. and Wandinger-Ness, A. (1995) Rab 7: an important regulator of late endocytic membrane traffic. *J. Cell Biol.* **131**, 1435-1452.

Fichtlscherer, S., Breuer, S. and Zeiher, A.M. (2004) Prognostic value of systemic endothelial dysfunction in patients with acute coronary syndromes: further evidence for the existence of the "vulnerable" patient. *Circulation* **110**, 1926-1932.

Finan, P., Shimizu, Y., Gout, I., Hsuan, J., Truong, O., Butcher, C., Bennett, P., Waterfield, M.D. and Kellie, S. (1994) An SH3 domain and proline-rich sequence mediate an interaction between two components of the phagocyte NADPH oxidase complex. *J. Biol. Chem.* **269**, 13752-13755.

Freeman, J.L., Abo, A. and Lambeth, J.D. (1996) Rac "insert region" is a novel effector region that is implicated in the activation of NADPH oxidase, but not PAK65. *J. Biol. Chem.* **271**, 19794-19801.

Freeman, J.L., Kreck, M.L., Uhlinger, D.J. and Lambeth, J.D. (1994) Ras effector-homologue region on Rac regulates protein associations in the neutrophil respiratory burst oxidase complex. *Biochemistry* **33**, 13431-13435.

Fridovich, I. (1995) Superoxide radical and superoxide dismutases. *Annu. Rev. Biochem.* **64**, 97-112.

Fukui, T., Ishizaka, N., Rajagopalan, S., Laursen, J.B., Capers, Q., Taylor, W.R., Harrison, D.G., de, L.H., Wilcox, J.N. and Griendling, K.K. (1997) p22phox mRNA expression and NADPH oxidase activity are increased in aortas from hypertensive rats. *Circ. Res.* **80**, 45-51.

Fung, Y.C. and Liu, S.Q. (1993) Elementary mechanics of the endothelium of blood vessels. *J. Biomech. Eng* **115**, 1-12.

Gabig, T.G. (1983) The NADPH-dependent O-.2-generating oxidase from human neutrophils. *J. Biol. Chem.* **258**, 6352-6356.

Galis, Z.S., Asanuma, K., Godin, D. and Meng, X. (1998) N-acetyl-cysteine decreases the matrix-degrading capacity of macrophage-derived foam cells: new target for antioxidant therapy? *Circulation* **97**, 2445-2453.

Galis, Z.S., Sukhova, G.K., Lark, M.W. and Libby, P. (1994) Increased expression of matrix metalloproteinases and matrix degrading activity in vulnerable regions of human atherosclerotic plaques. *J. Clin. Invest* **94**, 2493-2503.

Gardner, P.R. and Fridovich, I. (1992) Inactivation-reactivation of aconitase in Escherichia coli. A sensitive measure of superoxide radical. *J. Biol. Chem.* **267**, 8757-8763.

Gardner, P.R. and Fridovich, I. (1991) Superoxide sensitivity of the Escherichia coli aconitase. *J. Biol. Chem.* **266**, 19328-19333.

Gardner, P.R., Nguyen, D.D. and White, C.W. (1994) Aconitase is a sensitive and critical target of oxygen poisoning in cultured mammalian cells and in rat lungs. *Proc. Natl. Acad. Sci. U. S. A* **91**, 12248-12252.

Gardner, P.R., Raineri, I., Epstein, L.B. and White, C.W. (1995) Superoxide radical and iron modulate aconitase activity in mammalian cells. *J. Biol. Chem.* **270**, 13399-13405.

Gasteiger, E., Gattiker, A., Hoogland, C., Ivanyi, I., Appel, R.D. and Bairoch, A. (2003) ExPASy: The proteomics server for in-depth protein knowledge and analysis. *Nucleic Acids Res.* **31**, 3784-3788.

Gauthier, T.W., Scalia, R., Murohara, T., Guo, J.P. and Lefer, A.M. (1995) Nitric oxide protects against leukocyte-endothelium interactions in the early stages of hypercholesterolemia. *Arterioscler. Thromb. Vasc. Biol.* **15**, 1652-1659.

Geiszt, M., Kopp, J.B., Varnai, P. and Leto, T.L. (2000) Identification of renox, an NAD(P)H oxidase in kidney. *Proc. Natl. Acad. Sci. U. S. A* **97**, 8010-8014.

Geiszt, M., Lekstrom, K., Brenner, S., Hewitt, S.M., Dana, R., Malech, H.L. and Leto, T.L. (2003a) NAD(P)H oxidase 1, a product of differentiated colon epithelial cells, can partially replace glycoprotein 91phox in the regulated production of superoxide by phagocytes. *J. Immunol.* **171**, 299-306.

Geiszt, M., Lekstrom, K., Witta, J. and Leto, T.L. (2003b) Proteins homologous to p47phox and p67phox support superoxide production by NAD(P)H oxidase 1 in colon epithelial cells. *J. Biol. Chem.* **278**, 20006-20012.

Giasson, B.I., Ischiropoulos, H., Lee, V.M. and Trojanowski, J.Q. (2002) The relationship between oxidative/nitrative stress and pathological inclusions in Alzheimer's and Parkinson's diseases. *Free Radic. Biol. Med.* **32**, 1264-1275.

Gimbrone, M.A., Jr., Cybulsky, M.I., Kume, N., Collins, T. and Resnick, N. (1995) Vascular endothelium. An integrator of pathophysiological stimuli in atherogenesis. *Ann. N. Y. Acad. Sci.* **748**, 122-131.

Godin, C., Caprani, A., Dufaux, J. and Flaud, P. (1993) Interactions between neutrophils and endothelial cells. *J. Cell Sci.* **106 (Pt 2)**, 441-451.

Goody, R.S., Rak, A. and Alexandrov, K. (2005) The structural and mechanistic basis for recycling of Rab proteins between membrane compartments. *Cell Mol. Life Sci.* **62**, 1657-1670.

Gorlach, A., Brandes, R.P., Nguyen, K., Amidi, M., Dehghani, F. and Busse, R. (2000) A gp91phox containing NADPH oxidase selectively expressed in endothelial cells is a major source of oxygen radical generation in the arterial wall. *Circ. Res.* **87**, 26-32.

Gotoh, N. and Niki, E. (1992) Rates of interactions of superoxide with vitamin E, vitamin C and related compounds as measured by chemiluminescence. *Biochim. Biophys. Acta* **1115**, 201-207.

Graham, A., Hogg, N., Kalyanaraman, B., O'Leary, V., Darley-Usmar, V. and Moncada, S. (1993) Peroxynitrite modification of low-density lipoprotein leads to recognition by the macrophage scavenger receptor. *FEBS Lett.* **330**, 181-185.

Graham, D.J., Staffa, J.A., Shatin, D., Andrade, S.E., Schech, S.D., La, G.L., Gurwitz, J.H., Chan, K.A., Goodman, M.J. and Platt, R. (2004) Incidence of hospitalized rhabdomyolysis in patients treated with lipid-lowering drugs. *JAMA* **292**, 2585-2590.

Gray, H. (1918) Anatomy of the Human Body. Lea & Febiger, Cambridge, Massachusetts.

Greenwood, J., Steinman, L. and Zamvil, S.S. (2006) Statin therapy and autoimmune disease: from protein prenylation to immunomodulation. *Nat. Rev. Immunol.* **6**, 358-370.

Gregg, D., Rauscher, F.M. and Goldschmidt-Clermont, P.J. (2003) Rac regulates cardiovascular superoxide through diverse molecular interactions: more than a binary GTP switch. *Am. J. Physiol Cell Physiol* **285**, C723-C734.

Griendling, K.K., Minieri, C.A., Ollerenshaw, J.D. and Alexander, R.W. (1994) Angiotensin II stimulates NADH and NADPH oxidase activity in cultured vascular smooth muscle cells. *Circ. Res.* **74**, 1141-1148.

Griendling, K.K., Sorescu, D., Lassegue, B. and Ushio-Fukai, M. (2000) Modulation of protein kinase activity and gene expression by reactive oxygen species and their role in vascular physiology and pathophysiology. *Arterioscler. Thromb. Vasc. Biol.* **20**, 2175-2183.

Grizot, S., Fieschi, F., Dagher, M.C. and Pebay-Peyroula, E. (2001) The active N-terminal region of p67phox. Structure at 1.8 A resolution and biochemical characterizations of the A128V mutant implicated in chronic granulomatous disease. *J. Biol. Chem.* **276**, 21627-21631.

Groemping, Y., Lapouge, K., Smerdon, S.J. and Rittinger, K. (2003) Molecular basis of phosphorylation-induced activation of the NADPH oxidase. *Cell* **113**, 343-355.

Groemping, Y. and Rittinger, K. (2005) Activation and assembly of the NADPH oxidase: a structural perspective. *Biochem. J.* **386**, 401-416.

Grosshans, B.L., Ortiz, D. and Novick, P. (2006) Rabs and their effectors: achieving specificity in membrane traffic. *Proc. Natl. Acad. Sci. U. S. A* **103**, 11821-11827.

Grote, K., Flach, I., Luchtefeld, M., Akin, E., Holland, S.M., Drexler, H. and Schieffer, B. (2003) Mechanical stretch enhances mRNA expression and proenzyme release of matrix metalloproteinase-2 (MMP-2) via NAD(P)H oxidase-derived reactive oxygen species. *Circ. Res.* **92**, e80-e86.

Guzik, T.J. and Harrison, D.G. (2006) Vascular NADPH oxidases as drug targets for novel antioxidant strategies. *Drug Discov. Today* **11**, 524-533.

Guzik, T.J., West, N.E., Black, E., McDonald, D., Ratnatunga, C., Pillai, R. and Channon, K.M. (2000) Vascular superoxide production by NAD(P)H oxidase: association with endothelial dysfunction and clinical risk factors. *Circ. Res.* **86**, E85-E90.

Halcox, J.P., Schenke, W.H., Zalos, G., Mincemoyer, R., Prasad, A., Waclawiw, M.A., Nour, K.R. and Quyyumi, A.A. (2002) Prognostic value of coronary vascular endothelial dysfunction. *Circulation* **106**, 653-658.

Hall, A. (1994) Small GTP-binding proteins and the regulation of the actin cytoskeleton. *Annu. Rev. Cell Biol.* **10**, 31-54.

Halliwell, B. and Gutteridge, J.M. (1986) Oxygen free radicals and iron in relation to biology and medicine: some problems and concepts. *Arch. Biochem. Biophys.* **246**, 501-514.

Halliwell, B. and Gutteridge, J.M. (1989) Free Radicals in Biology and Medicine. Oxford Univ. Press, Oxford, UK.

Hampton, M.B., Kettle, A.J. and Winterbourn, C.C. (1998) Inside the neutrophil phagosome: oxidants, myeloperoxidase, and bacterial killing. *Blood* **92**, 3007-3017.

Han, C.H., Freeman, J.L., Lee, T., Motalebi, S.A. and Lambeth, J.D. (1998) Regulation of the neutrophil respiratory burst oxidase. Identification of an activation domain in p67(phox). *J. Biol. Chem.* **273**, 16663-16668.

Han, C.H., Nisimoto, Y., Lee, S.H., Kim, E.T. and Lambeth, J.D. (2001) Characterization of the flavoprotein domain of gp91phox which has NADPH diaphorase activity. *J. Biochem. (Tokyo)* **129**, 513-520.

Hanna, I.R., Hilenski, L.L., Dikalova, A., Taniyama, Y., Dikalov, S., Lyle, A., Quinn, M.T., Lassegue, B. and Griendling, K.K. (2004) Functional association of nox1 with p22phox in vascular smooth muscle cells. *Free Radic. Biol. Med.* **37**, 1542-1549.

Harman, D. (1981) The aging process. *Proc. Natl. Acad. Sci. U. S. A* **78**, 7124-7128.

Harper, A.M., Chaplin, M.F. and Segal, A.W. (1985) Cytochrome b-245 from human neutrophils is a glycoprotein. *Biochem. J.* **227**, 783-788.

Harrison, D., Griendling, K.K., Landmesser, U., Hornig, B. and Drexler, H. (2003) Role of oxidative stress in atherosclerosis. *Am. J. Cardiol.* **91**, 7A-11A.

Hathaway, C.A., Heistad, D.D., Piegors, D.J. and Miller, F.J., Jr. (2002) Regression of atherosclerosis in monkeys reduces vascular superoxide levels. *Circ. Res.* **90**, 277-283.

Hattori, H. (1961) Studies on the labile, stable Nadi oxidase and peroxidase staining reactions in the isolated particles of horse granulocyte. *Nagoya J. Med. Sci.* **23**, 362-378.

Hazell, L.J., Davies, M.J. and Stocker, R. (1999) Secondary radicals derived from chloramines of apolipoprotein B-100 contribute to HOCl-induced lipid peroxidation of low-density lipoproteins. *Biochem. J.* **339 (Pt 3)**, 489-495.

Hazell, L.J. and Stocker, R. (1993) Oxidation of low-density lipoprotein with hypochlorite causes transformation of the lipoprotein into a high-uptake form for macrophages. *Biochem. J.* **290 (Pt 1)**, 165-172.

Hazell, L.J. and Stocker, R. (1997) Alpha-tocopherol does not inhibit hypochlorite-induced oxidation of apolipoprotein B-100 of low-density lipoprotein. *FEBS Lett.* **414**, 541-544.

Heinecke, J.W. (1999) Mass spectrometric quantification of amino acid oxidation products in proteins: insights into pathways that promote LDL oxidation in the human artery wall. *FASEB J.* **13**, 1113-1120.

Hessler, J.R., Morel, D.W., Lewis, L.J. and Chisolm, G.M. (1983) Lipoprotein oxidation and lipoprotein-induced cytotoxicity. *Arteriosclerosis* **3**, 215-222.

Heymes, C., Bendall, J.K., Ratajczak, P., Cave, A.C., Samuel, J.L., Hasenfuss, G. and Shah, A.M. (2003) Increased myocardial NADPH oxidase activity in human heart failure. *J. Am. Coll. Cardiol.* **41**, 2164-2171.

Heyworth, P.G., Bohl, B.P., Bokoch, G.M. and Curnutte, J.T. (1994) Rac translocates independently of the neutrophil NADPH oxidase components p47phox and p67phox. Evidence for its interaction with flavocytochrome b558. *J. Biol. Chem.* **269**, 30749-30752.

Heyworth, P.G., Curnutte, J.T., Nauseef, W.M., Volpp, B.D., Pearson, D.W., Rosen, H. and Clark, R.A. (1991) Neutrophil nicotinamide adenine dinucleotide phosphate oxidase assembly. Translocation of p47-phox and p67-phox requires interaction between p47-phox and cytochrome b558. *J. Clin. Invest* **87**, 352-356.

Hilenski, L.L., Clempus, R.E., Quinn, M.T., Lambeth, J.D. and Griendling, K.K. (2004) Distinct subcellular localizations of Nox1 and Nox4 in vascular smooth muscle cells. *Arterioscler. Thromb. Vasc. Biol.* **24**, 677-683.

Hiroaki, H., Ago, T., Ito, T., Sumimoto, H. and Kohda, D. (2001) Solution structure of the PX domain, a target of the SH3 domain. *Nat. Struct. Biol.* **8**, 526-530.

Holland, J.A., Meyer, J.W., Schmitt, M.E., Sauro, M.D., Johnson, D.K., bdul-Karim, R.W., Patel, V., Ziegler, L.M., Schillinger, K.J., Small, R.F. and Lemanski, L.F. (1997) Low-density lipoprotein stimulated peroxide production and endocytosis in cultured human endothelial cells: mechanisms of action. *Endothelium* **5**, 191-207.

Holland, J.A., Ziegler, L.M. and Meyer, J.W. (1996) Atherogenic levels of low-density lipoprotein increase hydrogen peroxide generation in cultured human endothelial cells: possible mechanism of heightened endocytosis. *J. Cell Physiol* **166**, 144-151.

Honbou, K., Minakami, R., Yuzawa, S., Takeya, R., Suzuki, N.N., Kamakura, S., Sumimoto, H. and Inagaki, F. (2007) Full-length p40phox structure suggests a basis for regulation mechanism of its membrane binding. *EMBO J.* **26**, 1176-1186.

Hong, Y.H., Peng, H.B., La, F., V and Liao, J.K. (1997) Hydrogen peroxide-mediated transcriptional induction of macrophage colony-stimulating factor by TGF-beta1. *J. Immunol.* **159**, 2418-2423.

Huang, J. and Kleinberg, M.E. (1999) Activation of the phagocyte NADPH oxidase protein p47(phox). Phosphorylation controls SH3 domain-dependent binding to p22(phox). *J. Biol. Chem.* **274**, 19731-19737.

Huie, R.E. and Padmaja, S. (1993) The reaction of NO with superoxide. *Free Radic. Res. Commun.* **18**, 195-199.

Hwang, J., Saha, A., Boo, Y.C., Sorescu, G.P., McNally, J.S., Holland, S.M., Dikalov, S., Giddens, D.P., Griendling, K.K., Harrison, D.G. and Jo, H. (2003) Oscillatory shear stress stimulates endothelial production of O2- from p47phox-dependent NAD(P)H oxidases, leading to monocyte adhesion. *J. Biol. Chem.* **278**, 47291-47298.

Infanger, D.W., Sharma, R.V. and Davisson, R.L. (2006) NADPH oxidases of the brain: distribution, regulation, and function. *Antioxid. Redox. Signal.* **8**, 1583-1596.

Ito, N., Komiyama, N.H. and Fermi, G. (1995) Structure of deoxyhaemoglobin of the antarctic fish Pagothenia bernacchii with an analysis of the structural basis of the root effect by comparison of the liganded and unliganded haemoglobin structures. *J. Mol. Biol.* **250**, 648-658.

Ito, T., Matsui, Y., Ago, T., Ota, K. and Sumimoto, H. (2001) Novel modular domain PB1 recognizes PC motif to mediate functional protein-protein interactions. *EMBO J.* **20**, 3938-3946.

Iwai, H., Lingel, A. and Pluckthun, A. (2001) Cyclic green fluorescent protein produced in vivo using an artificially split PI-PfuI intein from Pyrococcus furiosus. *J. Biol. Chem.* **276**, 16548-16554.

Iwai, H. and Pluckthun, A. (1999) Circular beta-lactamase: stability enhancement by cyclizing the backbone. *FEBS Lett.* **459**, 166-172.

Jaeger, J., Sorensen, K. and Wolff, S.P. (1994) Peroxide accumulation in detergents. *J. Biochem. Biophys. Methods* **29**, 77-81.

Jennings, C., West, J., Waine, C., Craik, D. and Anderson, M. (2001) Biosynthesis and insecticidal properties of plant cyclotides: the cyclic knotted proteins from Oldenlandia affinis. *Proc. Natl. Acad. Sci. U. S. A* **98**, 10614-10619.

Jo, H., Song, H. and Mowbray, A. (2006) Role of NADPH oxidases in disturbed flow- and BMP4-induced inflammation and atherosclerosis. *Antioxid. Redox. Signal.* **8**, 1609-1619.

Jones, S.A., O'Donnell, V.B., Wood, J.D., Broughton, J.P., Hughes, E.J. and Jones, O.T. (1996) Expression of phagocyte NADPH oxidase components in human endothelial cells. *Am. J. Physiol* **271**, H1626-H1634.

Joneson, T. and Bar-Sagi, D. (1998) A Rac1 effector site controlling mitogenesis through superoxide production. *J. Biol. Chem.* **273**, 17991-17994.

Kabsch, W. (1993) Automatic Processing of Rotation Diffraction Data from Crystals of Internally Unknown Symmetry and Cell Constants. *J. Appl. Cryst.* **26**, 795-800.

Kaiser, L. and Sparks, H.V., Jr. (1987) Endothelial cells. Not just a cellophane wrapper. *Arch. Intern. Med.* **147**, 569-573.

Kami, K., Takeya, R., Sumimoto, H. and Kohda, D. (2002) Diverse recognition of non-PxxP peptide ligands by the SH3 domains from p67(phox), Grb2 and Pex13p. *EMBO J.* **21**, 4268-4276.

Kanai, F., Liu, H., Field, S.J., Akbary, H., Matsuo, T., Brown, G.E., Cantley, L.C. and Yaffe, M.B. (2001) The PX domains of p47phox and p40phox bind to lipid products of PI(3)K. *Nat. Cell Biol.* **3**, 675-678.

Karathanassis, D., Stahelin, R.V., Bravo, J., Perisic, O., Pacold, C.M., Cho, W. and Williams, R.L. (2002) Binding of the PX domain of p47(phox) to phosphatidylinositol 3,4-bisphosphate and phosphatidic acid is masked by an intramolecular interaction. *EMBO J.* **21**, 5057-5068.

Katsuyama, M., Fan, C. and Yabe-Nishimura, C. (2002) NADPH oxidase is involved in prostaglandin F2alpha-induced hypertrophy of vascular smooth muscle cells: induction of NOX1 by PGF2alpha. *J. Biol. Chem.* **277**, 13438-13442.

Kawahara, B.T., Quinn, M.T. and Lambeth, J.D. (2007) Molecular evolution of the reactive oxygen-generating NADPH oxidase (Nox/Duox) family of enzymes. *BMC. Evol. Biol.* **7**, 109.

Kawahara, T., Kohjima, M., Kuwano, Y., Mino, H., Teshima-Kondo, S., Takeya, R., Tsunawaki, S., Wada, A., Sumimoto, H. and Rokutan, K. (2005) Helicobacter pylori lipopolysaccharide activates Rac1 and transcription of NADPH oxidase Nox1 and its organizer NOXO1 in guinea pig gastric mucosal cells. *Am. J. Physiol Cell Physiol* **288**, C450-C457.

Kawahara, T., Kuwano, Y., Teshima-Kondo, S., Takeya, R., Sumimoto, H., Kishi, K., Tsunawaki, S., Hirayama, T. and Rokutan, K. (2004) Role of nicotinamide adenine dinucleotide phosphate oxidase 1 in oxidative burst response to Toll-like receptor 5 signaling in large intestinal epithelial cells. *J. Immunol.* **172**, 3051-3058.

Kawahara, T. and Lambeth, J.D. (2007) Molecular evolution of Phox-related regulatory subunits for NADPH oxidase enzymes. *BMC. Evol. Biol.* **7**, 178.

Kawahara, T., Teshima, S., Oka, A., Sugiyama, T., Kishi, K. and Rokutan, K. (2001) Type I Helicobacter pylori lipopolysaccharide stimulates toll-like receptor 4 and activates mitogen oxidase 1 in gastric pit cells. *Infect. Immun.* **69**, 4382-4389.

Kikuchi, H., Hikage, M., Miyashita, H. and Fukumoto, M. (2000) NADPH oxidase subunit, gp91(phox) homologue, preferentially expressed in human colon epithelial cells. *Gene* **254**, 237-243.

Klein, J.A. and Ackerman, S.L. (2003) Oxidative stress, cell cycle, and neurodegeneration. *J. Clin. Invest* **111**, 785-793.

Kleinberg, M.E., Rotrosen, D. and Malech, H.L. (1989) Asparagine-linked glycosylation of cytochrome b558 large subunit varies in different human phagocytic cells. *J. Immunol.* **143**, 4152-4157.

Klug, D., Rabani, J. and Fridovich, I. (1972) A direct demonstration of the catalytic action of superoxide dismutase through the use of pulse radiolysis. *J. Biol. Chem.* **247**, 4839-4842.

Knaus, U.G., Heyworth, P.G., Evans, T., Curnutte, J.T. and Bokoch, G.M. (1991) Regulation of phagocyte oxygen radical production by the GTP-binding protein Rac 2. *Science* **254**, 1512-1515.

Knoller, S., Shpungin, S. and Pick, E. (1991) The membrane-associated component of the amphiphile-activated, cytosol-dependent superoxide-forming NADPH oxidase of macrophages is identical to cytochrome b559. *J. Biol. Chem.* **266**, 2795-2804.

Koga, H., Terasawa, H., Nunoi, H., Takeshige, K., Inagaki, F. and Sumimoto, H. (1999) Tetratricopeptide repeat (TPR) motifs of p67(phox) participate in interaction with the small GTPase Rac and activation of the phagocyte NADPH oxidase. *J. Biol. Chem.* **274**, 25051-25060.

Kojda, G. and Harrison, D. (1999) Interactions between NO and reactive oxygen species: pathophysiological importance in atherosclerosis, hypertension, diabetes and heart failure. *Cardiovasc. Res.* **43**, 562-571.

Koshkin, V., Lotan, O. and Pick, E. (1996) The cytosolic component p47(phox) is not a sine qua non participant in the activation of NADPH oxidase but is required for optimal superoxide production. *J. Biol. Chem.* **271**, 30326-30329.

Koshkin, V. and Pick, E. (1993) Generation of superoxide by purified and relipidated cytochrome b559 in the absence of cytosolic activators. *FEBS Lett.* **327**, 57-62.

Koshkin, V. and Pick, E. (1994) Superoxide production by cytochrome b559. Mechanism of cytosol-independent activation. *FEBS Lett.* **338**, 285-289.

Kreck, M.L., Uhlinger, D.J., Tyagi, S.R., Inge, K.L. and Lambeth, J.D. (1994) Participation of the small molecular weight GTP-binding protein Rac1 in cell-free activation and assembly of the respiratory burst oxidase. Inhibition by a carboxyl-terminal Rac peptide. *J. Biol. Chem.* **269**, 4161-4168.

Ku, D.N., Giddens, D.P., Zarins, C.K. and Glagov, S. (1985) Pulsatile flow and atherosclerosis in the human carotid bifurcation. Positive correlation between plaque location and low oscillating shear stress. *Arteriosclerosis* **5**, 293-302.

Kubes, P., Suzuki, M. and Granger, D.N. (1991) Nitric oxide: an endogenous modulator of leukocyte adhesion. *Proc. Natl. Acad. Sci. U. S. A* **88**, 4651-4655.

Kuo, C.F., Mashino, T. and Fridovich, I. (1987) alpha, beta-Dihydroxyisovalerate dehydratase. A superoxide-sensitive enzyme. *J. Biol. Chem.* **262**, 4724-4727.

Kuribayashi, F., Nunoi, H., Wakamatsu, K., Tsunawaki, S., Sato, K., Ito, T. and Sumimoto, H. (2002) The adaptor protein p40(phox) as a positive regulator of the superoxide-producing phagocyte oxidase. *EMBO J.* **21**, 6312-6320.

Kuroda, J., Nakagawa, K., Yamasaki, T., Nakamura, K., Takeya, R., Kuribayashi, F., Imajoh-Ohmi, S., Igarashi, K., Shibata, Y., Sueishi, K. and Sumimoto, H. (2005) The superoxide-producing NAD(P)H oxidase Nox4 in the nucleus of human vascular endothelial cells. *Genes Cells* **10**, 1139-1151.

Kwon, J., Lee, S.R., Yang, K.S., Ahn, Y., Kim, Y.J., Stadtman, E.R. and Rhee, S.G. (2004) Reversible oxidation and inactivation of the tumor suppressor PTEN in cells stimulated with peptide growth factors. *Proc. Natl. Acad. Sci. U. S. A* **101**, 16419-16424.

Lambeth, J.D. (2004) NOX enzymes and the biology of reactive oxygen. *Nat. Rev. Immunol.* **4**, 181-189.

Landmesser, U. and Harrison, D.G. (2001) Oxidant stress as a marker for cardiovascular events: Ox marks the spot. *Circulation* **104**, 2638-2640.

Lapouge, K., Smith, S.J., Groemping, Y. and Rittinger, K. (2002) Architecture of the p40-p47-p67phox complex in the resting state of the NADPH oxidase. A central role for p67phox. *J. Biol. Chem.* **277**, 10121-10128.

Lapouge, K., Smith, S.J., Walker, P.A., Gamblin, S.J., Smerdon, S.J. and Rittinger, K. (2000) Structure of the TPR domain of p67phox in complex with Rac.GTP. *Mol. Cell* **6**, 899-907.

Larsen, N.A., Heine, A., de, P.P., Redwan, e., Yeates, T.O., Landry, D.W. and Wilson, I.A. (2002) Structure determination of a cocaine hydrolytic antibody from a pseudomerohedrally twinned crystal. *Acta Crystallogr. D Biol. Crystallogr.* **58**, 2055-2059.

Lassegue, B. and Clempus, R.E. (2003) Vascular NAD(P)H oxidases: specific features, expression, and regulation. *Am. J. Physiol Regul. Integr. Comp Physiol* **285**, R277-R297.

Lassegue, B., Sorescu, D., Szocs, K., Yin, Q., Akers, M., Zhang, Y., Grant, S.L., Lambeth, J.D. and Griendling, K.K. (2001) Novel gp91(phox) homologues in vascular smooth muscle cells : nox1 mediates angiotensin II-induced superoxide formation and redox-sensitive signaling pathways. *Circ. Res.* **88**, 888-894.

Laursen, J.B., Somers, M., Kurz, S., McCann, L., Warnholtz, A., Freeman, B.A., Tarpey, M., Fukai, T. and Harrison, D.G. (2001) Endothelial regulation of vasomotion in apoE-deficient mice: implications for interactions between peroxynitrite and tetrahydrobiopterin. *Circulation* **103**, 1282-1288.

Lee, I.M., Cook, N.R., Manson, J.E., Buring, J.E. and Hennekens, C.H. (1999) Beta-carotene supplementation and incidence of cancer and cardiovascular disease: the Women's Health Study. *J. Natl. Cancer Inst.* **91**, 2102-2106.

Lee, S.R., Kwon, K.S., Kim, S.R. and Rhee, S.G. (1998) Reversible inactivation of protein-tyrosine phosphatase 1B in A431 cells stimulated with epidermal growth factor. *J. Biol. Chem.* **273**, 15366-15372.

Leto, T.L., Adams, A.G. and de, M., I (1994) Assembly of the phagocyte NADPH oxidase: binding of Src homology 3 domains to proline-rich targets. *Proc. Natl. Acad. Sci. U. S. A* **91**, 10650-10654.

Leung, K.F., Baron, R. and Seabra, M.C. (2006) Thematic review series: lipid posttranslational modifications. geranylgeranylation of Rab GTPases. *J. Lipid Res.* **47**, 467-475.

Leusen, J.H., Fluiter, K., Hilarius, P.M., Roos, D., Verhoeven, A.J. and Bolscher, B.G. (1995) Interactions between the cytosolic components p47phox and p67phox of the human neutrophil NADPH oxidase that are not required for activation in the cell-free system. *J. Biol. Chem.* **270**, 11216-11221.

Lever, M. (1977) Peroxides in detergents as interfering factors in biochemical analysis. *Anal. Biochem.* **83**, 274-284.

Li, J.M. and Shah, A.M. (2002) Intracellular localization and preassembly of the NADPH oxidase complex in cultured endothelial cells. *J. Biol. Chem.* **277**, 19952-19960.

Li, N. and Karin, M. (1999) Is NF-kappaB the sensor of oxidative stress? *FASEB J.* **13**, 1137-1143.

Libby, P., Ridker, P.M. and Maseri, A. (2002) Inflammation and atherosclerosis. *Circulation* **105**, 1135-1143.

Linnemann, T., Geyer, M., Jaitner, B.K., Block, C., Kalbitzer, H.R., Wittinghofer, A. and Herrmann, C. (1999) Thermodynamic and kinetic characterization of the interaction between the Ras binding domain of AF6 and members of the Ras subfamily. *J. Biol. Chem.* **274**, 13556-13562.

Liochev, S.I. and Fridovich, I. (1994) The role of O2.- in the production of HO.: in vitro and in vivo. *Free Radic. Biol. Med.* **16**, 29-33.

Liu, J., Ormsby, A., Oja-Tebbe, N. and Pagano, P.J. (2004) Gene transfer of NAD(P)H oxidase inhibitor to the vascular adventitia attenuates medial smooth muscle hypertrophy. *Circ. Res.* **95**, 587-594.

Lonn, E., Bosch, J., Yusuf, S., Sheridan, P., Pogue, J., Arnold, J.M., Ross, C., Arnold, A., Sleight, P., Probstfield, J. and Dagenais, G.R. (2005) Effects of long-term vitamin E supplementation on cardiovascular events and cancer: a randomized controlled trial. *JAMA* **293**, 1338-1347.

Lusis, A.J. (2000) Atherosclerosis. *Nature* **407**, 233-241.

Madamanchi, N.R., Vendrov, A. and Runge, M.S. (2005) Oxidative stress and vascular disease. *Arterioscler. Thromb. Vasc. Biol.* **25**, 29-38.

Maehama, T., Taylor, G.S. and Dixon, J.E. (2001) PTEN and myotubularin: novel phosphoinositide phosphatases. *Annu. Rev. Biochem.* **70**, 247-279.

Mahmoudi, M., Curzen, N. and Gallagher, P.J. (2007) Atherogenesis: the role of inflammation and infection. *Histopathology* **50**, 535-546.

Maly, F.E., Schuerer-Maly, C.C., Quilliam, L., Cochrane, C.G., Newburger, P.E., Curnutte, J.T., Gifford, M. and Dinauer, M.C. (1993) Restitution of superoxide generation in autosomal cytochrome-negative chronic granulomatous disease (A22(0) CGD)-derived B lymphocyte cell lines by transfection with p22phax cDNA. *J. Exp. Med.* **178**, 2047-2053.

Martyn, K.D., Frederick, L.M., von, L.K., Dinauer, M.C. and Knaus, U.G. (2006) Functional analysis of Nox4 reveals unique characteristics compared to other NADPH oxidases. *Cell Signal.* **18**, 69-82.

Marui, N., Offermann, M.K., Swerlick, R., Kunsch, C., Rosen, C.A., Ahmad, M., Alexander, R.W. and Medford, R.M. (1993) Vascular cell adhesion molecule-1 (VCAM-1) gene transcription and expression are regulated through an antioxidant-sensitive mechanism in human vascular endothelial cells. *J. Clin. Invest* **92**, 1866-1874.

Mashima, R., Witting, P.K. and Stocker, R. (2001) Oxidants and antioxidants in atherosclerosis. *Curr. Opin. Lipidol.* **12**, 411-418.

Matsuno, K., Yamada, H., Iwata, K., Jin, D., Katsuyama, M., Matsuki, M., Takai, S., Yamanishi, K., Miyazaki, M., Matsubara, H. and Yabe-Nishimura, C. (2005) Nox1 is involved in angiotensin II-mediated hypertension: a study in Nox1-deficient mice. *Circulation* **112**, 2677-2685.

McCord, J.M. and Day, E.D., Jr. (1978) Superoxide-dependent production of hydroxyl radical catalyzed by iron-EDTA complex. *FEBS Lett.* **86**, 139-142.

McGuire, J.J., Anderson, D.J., McDonald, B.J., Narayanasami, R. and Bennett, B.M. (1998) Inhibition of NADPH-cytochrome P450 reductase and glyceryl trinitrate biotransformation by diphenyleneiodonium sulfate. *Biochem. Pharmacol.* **56**, 881-893.

McMurray, H.F., Parthasarathy, S. and Steinberg, D. (1993) Oxidatively modified low density lipoprotein is a chemoattractant for human T lymphocytes. *J. Clin. Invest* **92**, 1004-1008.

Meier, B., Jesaitis, A.J., Emmendorffer, A., Roesler, J. and Quinn, M.T. (1993) The cytochrome b-558 molecules involved in the fibroblast and polymorphonuclear leucocyte superoxide-generating NADPH oxidase systems are structurally and genetically distinct. *Biochem. J.* **289 (Pt 2)**, 481-486.

Mello Filho, A.C., Hoffmann, M.E. and Meneghini, R. (1984) Cell killing and DNA damage by hydrogen peroxide are mediated by intracellular iron. *Biochem. J.* **218**, 273-275.

Mello Filho, A.C. and Meneghini, R. (1984) In vivo formation of single-strand breaks in DNA by hydrogen peroxide is mediated by the Haber-Weiss reaction. *Biochim. Biophys. Acta* **781**, 56-63.

Melville, M.W., Katze, M.G. and Tan, S.L. (2000) P58IPK, a novel cochaperone containing tetratricopeptide repeats and a J-domain with oncogenic potential. *Cell Mol. Life Sci.* **57**, 311-322.

Menshikov, M., Plekhanova, O., Cai, H., Chalupsky, K., Parfyonova, Y., Bashtrikov, P., Tkachuk, V. and Berk, B.C. (2006) Urokinase plasminogen activator stimulates vascular smooth muscle cell proliferation via redox-dependent pathways. *Arterioscler. Thromb. Vasc. Biol.* **26**, 801-807.

Meresse, S., Gorvel, J.P. and Chavrier, P. (1995) The rab7 GTPase resides on a vesicular compartment connected to lysosomes. *J. Cell Sci.* **108 (Pt 11)**, 3349-3358.

Meyer, J.W., Holland, J.A., Ziegler, L.M., Chang, M.M., Beebe, G. and Schmitt, M.E. (1999) Identification of a functional leukocyte-type NADPH oxidase in human endothelial cells :a potential atherogenic source of reactive oxygen species. *Endothelium* **7**, 11-22.

Miki, T. and Orii, Y. (1985) The reaction of horseradish peroxidase with hydroperoxides derived from Triton X-100. *Anal. Biochem.* **146**, 28-34.

Miller, E.R., III, Pastor-Barriuso, R., Dalal, D., Riemersma, R.A., Appel, L.J. and Guallar, E. (2005) Meta-analysis: high-dosage vitamin E supplementation may increase all-cause mortality. *Ann. Intern. Med.* **142**, 37-46.

Miroux, B. and Walker, J.E. (1996) Over-production of proteins in Escherichia coli: mutant hosts that allow synthesis of some membrane proteins and globular proteins at high levels. *J. Mol. Biol.* **260**, 289-298.

Mitsushita, J., Lambeth, J.D. and Kamata, T. (2004) The superoxide-generating oxidase Nox1 is functionally required for Ras oncogene transformation. *Cancer Res.* **64**, 3580-3585.

Miyano, K., Fukuda, H., Ebisu, K. and Tamura, M. (2003) Remarkable stabilization of neutrophil NADPH oxidase using RacQ61L and a p67phox-p47phox fusion protein. *Biochemistry* **42**, 184-190.

Miyano, K., Ogasawara, S., Han, C.H., Fukuda, H. and Tamura, M. (2001) A fusion protein between rac and p67phox (1-210) reconstitutes NADPH oxidase with higher activity and stability than the individual components. *Biochemistry* **40**, 14089-14097.

Mizuno, K., Kitamura, A. and Sasaki, T. (2003) Rabring7, a novel Rab7 target protein with a RING finger motif. *Mol. Biol. Cell* **14**, 3741-3752.

Mochizuki, T., Furuta, S., Mitsushita, J., Shang, W.H., Ito, M., Yokoo, Y., Yamaura, M., Ishizone, S., Nakayama, J., Konagai, A., Hirose, K., Kiyosawa, K. and Kamata, T. (2006) Inhibition of NADPH oxidase 4 activates apoptosis via the AKT/apoptosis signal-regulating kinase 1 pathway in pancreatic cancer PANC-1 cells. *Oncogene* **25**, 3699-3707.

Moncada, S., Palmer, R.M. and Higgs, E.A. (1991) Nitric oxide: physiology, pathophysiology, and pharmacology. *Pharmacol. Rev.* **43**, 109-142.

Moon, S.Y. and Zheng, Y. (2003) Rho GTPase-activating proteins in cell regulation. *Trends Cell Biol.* **13**, 13-22.

Mugge, A., Elwell, J.H., Peterson, T.E. and Harrison, D.G. (1991) Release of intact endothelium-derived relaxing factor depends on endothelial superoxide dismutase activity. *Am. J. Physiol* **260**, C219-C225.

Mulrooney, S.B. and Waskell, L. (2000) High-level expression in Escherichia coli and purification of the membrane-bound form of cytochrome b(5). *Protein Expr. Purif.* **19**, 173-178.

Murphy, G., Willenbrock, F., Crabbe, T., O'Shea, M., Ward, R., Atkinson, S., O'Connell, J. and Docherty, A. (1994) Regulation of matrix metalloproteinase activity. *Ann. N. Y. Acad. Sci.* **732**, 31-41.

Murshudov, G.N., Vagin, A.A. and Dodson, E.J. (1997) Refinement of macromolecular structures by the maximum-likelihood method. *Acta Crystallogr. D Biol. Crystallogr.* **53**, 240-255.

Myers, J.K., Pace, C.N. and Scholtz, J.M. (1997) Helix propensities are identical in proteins and peptides. *Biochemistry* **36**, 10923-10929.

Nauseef, W.M. (2004) Assembly of the phagocyte NADPH oxidase. *Histochem. Cell Biol.* **122**, 277-291.

Nerem, R.M., Harrison, D.G., Taylor, W.R. and Alexander, R.W. (1993) Hemodynamics and vascular endothelial biology. *J. Cardiovasc. Pharmacol.* **21 Suppl 1**, S6-10.

Neuzil, J., Thomas, S.R. and Stocker, R. (1997) Requirement for, promotion, or inhibition by alpha-tocopherol of radical-induced initiation of plasma lipoprotein lipid peroxidation. *Free Radic. Biol. Med.* **22**, 57-71.

Nisimoto, Y., Freeman, J.L., Motalebi, S.A., Hirshberg, M. and Lambeth, J.D. (1997) Rac binding to p67(phox). Structural basis for interactions of the Rac1 effector region and insert region with components of the respiratory burst oxidase. *J. Biol. Chem.* **272**, 18834-18841.

Nisimoto, Y., Ogawa, H., Miyano, K. and Tamura, M. (2004) Activation of the flavoprotein domain of gp91phox upon interaction with N-terminal p67phox (1-210) and the Rac complex. *Biochemistry* **43**, 9567-9575.

Nisimoto, Y., Otsuka-Murakami, H. and Lambeth, D.J. (1995) Reconstitution of flavin-depleted neutrophil flavocytochrome b558 with 8-mercapto-FAD and characterization of the flavin-reconstituted enzyme. *J. Biol. Chem.* **270**, 16428-16434.

Nobuhisa, I., Takeya, R., Ogura, K., Ueno, N., Kohda, D., Inagaki, F. and Sumimoto, H. (2006) Activation of the superoxide-producing phagocyte NADPH oxidase requires co-operation between the tandem SH3 domains of p47phox in recognition of a polyproline type II helix and an adjacent alpha-helix of p22phox. *Biochem. J.* **396**, 183-192.

Norris, E.H. and Giasson, B.I. (2005) Role of oxidative damage in protein aggregation associated with Parkinson's disease and related disorders. *Antioxid. Redox. Signal.* **7**, 672-684.

O'Donnell, V.B., Tew, D.G., Jones, O.T. and England, P.J. (1993) Studies on the inhibitory mechanism of iodonium compounds with special reference to neutrophil NADPH oxidase. *Biochem. J.* **290 (Pt 1)**, 41-49.

Ohara, Y., Peterson, T.E. and Harrison, D.G. (1993) Hypercholesterolemia increases endothelial superoxide anion production. *J. Clin. Invest* **91**, 2546-2551.

Ohgushi, M., Kugiyama, K., Fukunaga, K., Murohara, T., Sugiyama, S., Miyamoto, E. and Yasue, H. (1993) Protein kinase C inhibitors prevent impairment of endothelium-dependent relaxation by oxidatively modified LDL. *Arterioscler. Thromb.* **13**, 1525-1532.

Omar, M.A. and Wilson, J.P. (2002) FDA adverse event reports on statin-associated rhabdomyolysis. *Ann. Pharmacother.* **36**, 288-295.

Ostermeier, C. and Brunger, A.T. (1999) Structural basis of Rab effector specificity: crystal structure of the small G protein Rab3A complexed with the effector domain of rabphilin-3A. *Cell* **96**, 363-374.

Paclet, M.H., Coleman, A.W., Vergnaud, S. and Morel, F. (2000) P67-phox-mediated NADPH oxidase assembly: imaging of cytochrome b558 liposomes by atomic force microscopy. *Biochemistry* **39**, 9302-9310.

Paffenholz, R., Bergstrom, R.A., Pasutto, F., Wabnitz, P., Munroe, R.J., Jagla, W., Heinzmann, U., Marquardt, A., Bareiss, A., Laufs, J., Russ, A., Stumm, G., Schimenti, J.C. and Bergstrom, D.E. (2004) Vestibular defects in head-tilt mice result from mutations in Nox3, encoding an NADPH oxidase. *Genes Dev.* **18**, 486-491.

Pagano, P.J., Clark, J.K., Cifuentes-Pagano, M.E., Clark, S.M., Callis, G.M. and Quinn, M.T. (1997) Localization of a constitutively active, phagocyte-like NADPH oxidase in rabbit aortic adventitia: enhancement by angiotensin II. *Proc. Natl. Acad. Sci. U. S. A* **94**, 14483-14488.

Palinski, W. (2001) New evidence for beneficial effects of statins unrelated to lipid lowering. *Arterioscler. Thromb. Vasc. Biol.* **21**, 3-5.

Paravicini, T.M., Gulluyan, L.M., Dusting, G.J. and Drummond, G.R. (2002) Increased NADPH oxidase activity, gp91phox expression, and endothelium-dependent vasorelaxation during neointima formation in rabbits. *Circ. Res.* **91**, 54-61.

Park, H.S., Lee, S.H., Park, D., Lee, J.S., Ryu, S.H., Lee, W.J., Rhee, S.G. and Bae, Y.S. (2004) Sequential activation of phosphatidylinositol 3-kinase, beta Pix, Rac1, and Nox1 in growth factor-induced production of H2O2. *Mol. Cell Biol.* **24**, 4384-4394.

Park, H.S., Park, D. and Bae, Y.S. (2006) Molecular interaction of NADPH oxidase 1 with betaPix and Nox Organizer 1. *Biochem. Biophys. Res. Commun.* **339**, 985-990.

Parkos, C.A., Dinauer, M.C., Jesaitis, A.J., Orkin, S.H. and Curnutte, J.T. (1989) Absence of both the 91kD and 22kD subunits of human neutrophil cytochrome b in two genetic forms of chronic granulomatous disease. *Blood* **73**, 1416-1420.

Parkos, C.A., Dinauer, M.C., Walker, L.E., Allen, R.A., Jesaitis, A.J. and Orkin, S.H. (1988) Primary structure and unique expression of the 22-kilodalton light chain of human neutrophil cytochrome b. *Proc. Natl. Acad. Sci. U. S. A* **85**, 3319-3323.

Patel, K.D., Zimmerman, G.A., Prescott, S.M., McEver, R.P. and McIntyre, T.M. (1991) Oxygen radicals induce human endothelial cells to express GMP-140 and bind neutrophils. *J. Cell Biol.* **112**, 749-759.

Paulus, H. (2000) Protein splicing and related forms of protein autoprocessing. *Annu. Rev. Biochem.* **69**, 447-496.

Pereira-Leal, J.B. and Seabra, M.C. (2000) The mammalian Rab family of small GTPases: definition of family and subfamily sequence motifs suggests a mechanism for functional specificity in the Ras superfamily. *J. Mol. Biol.* **301**, 1077-1087.

Perler, F.B. and Adam, E. (2000) Protein splicing and its applications. *Curr. Opin. Biotechnol.* **11**, 377-383.

Petry, A., Djordjevic, T., Weitnauer, M., Kietzmann, T., Hess, J. and Gorlach, A. (2006) NOX2 and NOX4 mediate proliferative response in endothelial cells. *Antioxid. Redox. Signal.* **8**, 1473-1484.

Pfeffer, S.R. (2001) Rab GTPases: specifying and deciphering organelle identity and function. *Trends Cell Biol.* **11**, 487-491.

Ponting, C.P. (1996) Novel domains in NADPH oxidase subunits, sorting nexins, and PtdIns 3-kinases: binding partners of SH3 domains? *Protein Sci.* **5**, 2353-2357.

Porter, C.D., Parkar, M.H., Verhoeven, A.J., Levinsky, R.J., Collins, M.K. and Kinnon, C. (1994) p22-phox-deficient chronic granulomatous disease: reconstitution by retrovirus-mediated expression and identification of a biosynthetic intermediate of gp91-phox. *Blood* **84**, 2767-2775.

Provencher, S.W. (1982) A general purpose constrained regularization program for inverting noisy linear algebraic and integral equations. *Comput. Phys. Commun.* **27**, 229.

Quinn, M.T. and Gauss, K.A. (2004) Structure and regulation of the neutrophil respiratory burst oxidase: comparison with nonphagocyte oxidases. *J. Leukoc. Biol.* **76**, 760-781.

Rajagopalan, S. and Harrison, D.G. (1996) Reversing endothelial dysfunction with ACE inhibitors. A new trend. *Circulation* **94**, 240-243.

Rajagopalan, S., Kurz, S., Munzel, T., Tarpey, M., Freeman, B.A., Griendling, K.K. and Harrison, D.G. (1996a) Angiotensin II-mediated hypertension in the rat increases vascular superoxide production via membrane NADH/NADPH oxidase activation. Contribution to alterations of vasomotor tone. *J. Clin. Invest* **97**, 1916-1923.

Rajagopalan, S., Meng, X.P., Ramasamy, S., Harrison, D.G. and Galis, Z.S. (1996b) Reactive oxygen species produced by macrophage-derived foam cells regulate the activity of vascular matrix metalloproteinases in vitro. Implications for atherosclerotic plaque stability. *J. Clin. Invest* **98**, 2572-2579.

Rajavashisth, T.B., Andalibi, A., Territo, M.C., Berliner, J.A., Navab, M., Fogelman, A.M. and Lusis, A.J. (1990) Induction of endothelial cell expression of granulocyte and macrophage colony-stimulating factors by modified low-density lipoproteins. *Nature* **344**, 254-257.

Rak, A., Pylypenko, O., Niculae, A., Pyatkov, K., Goody, R.S. and Alexandrov, K. (2004) Structure of the Rab7:REP-1 complex: insights into the mechanism of Rab prenylation and choroideremia disease. *Cell* **117**, 749-760.

Rapoport, R.M., Draznin, M.B. and Murad, F. (1983) Endothelium-dependent relaxation in rat aorta may be mediated through cyclic GMP-dependent protein phosphorylation. *Nature* **306**, 174-176.

Ray, R. and Shah, A.M. (2005) NADPH oxidase and endothelial cell function. *Clin. Sci. (Lond)* **109**, 217-226.

Rees, D.C. (1980) The influence of twinning by merohedry on intensity statistics. *Acta Cryst.* **A36**, 578-581.

Reid, I.A. (1998) The Renin-Angiotensin system: Physiology, pathophysiology, and pharmacology. *Advances in Physiology Education* **275**, 236-245.

Ren, R., Mayer, B.J., Cicchetti, P. and Baltimore, D. (1993) Identification of a ten-amino acid proline-rich SH3 binding site. *Science* **259**, 1157-1161.

Reth, M. (2002) Hydrogen peroxide as second messenger in lymphocyte activation. *Nat. Immunol.* **3**, 1129-1134.

Ridley, A.J. (1996) Rho: theme and variations. *Curr. Biol.* **6**, 1256-1264.

Ross, R. (1993) The pathogenesis of atherosclerosis: a perspective for the 1990s. *Nature* **362**, 801-809.

Ross, R. (1999) Atherosclerosis--an inflammatory disease. *N. Engl. J. Med.* **340**, 115-126.

Rotilio, G., Bray, R.C. and Fielden, E.M. (1972) A pulse radiolysis study of superoxide dismutase. *Biochim. Biophys. Acta* **268**, 605-609.

Rotrosen, D., Yeung, C.L., Leto, T.L., Malech, H.L. and Kwong, C.H. (1992) Cytochrome b558: the flavin-binding component of the phagocyte NADPH oxidase. *Science* **256**, 1459-1462.

Rudolph, M.G., Wingren, C., Crowley, M.P., Chien, Y.H. and Wilson, I.A. (2004) Combined pseudo-merohedral twinning, non-crystallographic symmetry and pseudo-translation in a monoclinic crystal form of the gammadelta T-cell ligand T10. *Acta Crystallogr. D Biol. Crystallogr.* **60**, 656-664.

Salonen, J.T., Nyyssonen, K., Salonen, R., Lakka, H.M., Kaikkonen, J., Porkkala-Sarataho, E., Voutilainen, S., Lakka, T.A., Rissanen, T., Leskinen, L., Tuomainen, T.P., Valkonen, V.P., Ristonmaa, U. and Poulsen, H.E. (2000) Antioxidant Supplementation in Atherosclerosis Prevention (ASAP) study: a randomized trial of the effect of vitamins E and C on 3-year progression of carotid atherosclerosis. *J. Intern. Med.* **248**, 377-386.

Scott, C.P., bel-Santos, E., Wall, M., Wahnon, D.C. and Benkovic, S.J. (1999) Production of cyclic peptides and proteins in vivo. *Proc. Natl. Acad. Sci. U. S. A* **96**, 13638-13643.

Segal, A.W. (2005) How neutrophils kill microbes. *Annu. Rev. Immunol.* **23**, 197-223.

Segal, A.W. and Jones, O.T. (1978) Novel cytochrome b system in phagocytic vacuoles of human granulocytes. *Nature* **276**, 515-517.

Segal, A.W., Jones, O.T., Webster, D. and Allison, A.C. (1978) Absence of a newly described cytochrome b from neutrophils of patients with chronic granulomatous disease. *Lancet* **2**, 446-449.

Segal, A.W., West, I., Wientjes, F., Nugent, J.H., Chavan, A.J., Haley, B., Garcia, R.C., Rosen, H. and Scrace, G. (1992) Cytochrome b-245 is a flavocytochrome containing FAD and the NADPH-binding site of the microbicidal oxidase of phagocytes. *Biochem. J.* **284 (Pt 3)**, 781-788.

Sheldrick, G.M. (2008) A short history of SHELX. *Acta Crystallogr. A* **64**, 112-122.

Shi, Y., Niculescu, R., Wang, D., Patel, S., Davenpeck, K.L. and Zalewski, A. (2001) Increased NAD(P)H oxidase and reactive oxygen species in coronary arteries after balloon injury. *Arterioscler. Thromb. Vasc. Biol.* **21**, 739-745.

Shihabi, A., Li, W.G., Miller, F.J., Jr. and Weintraub, N.L. (2002) Antioxidant therapy for atherosclerotic vascular disease: the promise and the pitfalls. *Am. J. Physiol Heart Circ. Physiol* **282**, H797-H802.

Shimohama, S., Tanino, H., Kawakami, N., Okamura, N., Kodama, H., Yamaguchi, T., Hayakawa, T., Nunomura, A., Chiba, S., Perry, G., Smith, M.A. and Fujimoto, S. (2000) Activation of NADPH oxidase in Alzheimer's disease brains. *Biochem. Biophys. Res. Commun.* **273**, 5-9.

Shiose, A., Kuroda, J., Tsuruya, K., Hirai, M., Hirakata, H., Naito, S., Hattori, M., Sakaki, Y. and Sumimoto, H. (2001) A novel superoxide-producing NAD(P)H oxidase in kidney. *J. Biol. Chem.* **276**, 1417-1423.

Shiose, A. and Sumimoto, H. (2000) Arachidonic acid and phosphorylation synergistically induce a conformational change of p47phox to activate the phagocyte NADPH oxidase. *J. Biol. Chem.* **275**, 13793-13801.

Siebold, C. and Erni, B. (2002) Intein-mediated cyclization of a soluble and a membrane protein in vivo: function and stability. *Biophys. Chem.* **96**, 163-171.

Sikorski, R.S., Boguski, M.S., Goebl, M. and Hieter, P. (1990) A repeating amino acid motif in CDC23 defines a family of proteins and a new relationship among genes required for mitosis and RNA synthesis. *Cell* **60**, 307-317.

Simon, I., Zerial, M. and Goody, R.S. (1996) Kinetics of interaction of Rab5 and Rab7 with nucleotides and magnesium ions. *J. Biol. Chem.* **271**, 20470-20478.

Sleight, P. (2002) The renin-angiotensin system: a review of trials with angiotensin-converting enzyme inhibitors and angiotensin receptor blocking agents. *European Heart Journal Supplements* **4 (Supplement A)**, A53-A57.

SoRelle, R. (2001) Baycol withdrawn from market. *Circulation* **104**, E9015-E9016.

Sorescu, D., Weiss, D., Lassegue, B., Clempus, R.E., Szocs, K., Sorescu, G.P., Valppu, L., Quinn, M.T., Lambeth, J.D., Vega, J.D., Taylor, W.R. and Griendling, K.K. (2002) Superoxide production and expression of nox family proteins in human atherosclerosis. *Circulation* **105**, 1429-1435.

Sorescu, G.P., Song, H., Tressel, S.L., Hwang, J., Dikalov, S., Smith, D.A., Boyd, N.L., Platt, M.O., Lassegue, B., Griendling, K.K. and Jo, H. (2004) Bone morphogenic protein 4 produced in endothelial cells by oscillatory shear stress induces monocyte adhesion by stimulating reactive oxygen species production from a nox1-based NADPH oxidase. *Circ. Res.* **95**, 773-779.

Southworth, M.W., Adam, E., Panne, D., Byer, R., Kautz, R. and Perler, F.B. (1998) Control of protein splicing by intein fragment reassembly. *EMBO J.* **17**, 918-926.

Sparrow, C.P., Burton, C.A., Hernandez, M., Mundt, S., Hassing, H., Patel, S., Rosa, R., Hermanowski-Vosatka, A., Wang, P.R., Zhang, D., Peterson, L., Detmers, P.A., Chao, Y.S. and Wright, S.D. (2001) Simvastatin has anti-inflammatory and antiatherosclerotic activities independent of plasma cholesterol lowering. *Arterioscler. Thromb. Vasc. Biol.* **21**, 115-121.

Spiecker, M., Darius, H., Kaboth, K., Hubner, F. and Liao, J.K. (1998) Differential regulation of endothelial cell adhesion molecule expression by nitric oxide donors and antioxidants. *J. Leukoc. Biol.* **63**, 732-739.

Spiecker, M., Peng, H.B. and Liao, J.K. (1997) Inhibition of endothelial vascular cell adhesion molecule-1 expression by nitric oxide involves the induction and nuclear translocation of IkappaBalpha. *J. Biol. Chem.* **272**, 30969-30974.

Staffa, J.A., Chang, J. and Green, L. (2002) Cerivastatin and reports of fatal rhabdomyolysis. *N. Engl. J. Med.* **346**, 539-540.

Staker, B.L., Hjerrild, K., Feese, M.D., Behnke, C.A., Burgin, A.B., Jr. and Stewart, L. (2002) The mechanism of topoisomerase I poisoning by a camptothecin analog. *Proc. Natl. Acad. Sci. U. S. A* **99**, 15387-15392.

Stroupe, C. and Brunger, A.T. (2000) Crystal structures of a Rab protein in its inactive and active conformations. *J. Mol. Biol.* **304**, 585-598.

Stuehr, D.J., Fasehun, O.A., Kwon, N.S., Gross, S.S., Gonzalez, J.A., Levi, R. and Nathan, C.F. (1991) Inhibition of macrophage and endothelial cell nitric oxide synthase by diphenyleneiodonium and its analogs. *FASEB J.* **5**, 98-103.

Sturrock, A., Cahill, B., Norman, K., Huecksteadt, T.P., Hill, K., Sanders, K., Karwande, S.V., Stringham, J.C., Bull, D.A., Gleich, M., Kennedy, T.P. and Hoidal, J.R. (2006) Transforming growth factor-beta1 induces Nox4 NAD(P)H oxidase and reactive oxygen species-dependent proliferation in human pulmonary artery smooth muscle cells. *Am. J. Physiol Lung Cell Mol. Physiol* **290**, L661-L673.

Sugishima, M., Sakamoto, H., Kakuta, Y., Omata, Y., Hayashi, S., Noguchi, M. and Fukuyama, K. (2002) Crystal structure of rat apo-heme oxygenase-1 (HO-1): mechanism of heme binding in HO-1 inferred from structural comparison of the apo and heme complex forms. *Biochemistry* **41**, 7293-7300.

Suh, Y.A., Arnold, R.S., Lassegue, B., Shi, J., Xu, X., Sorescu, D., Chung, A.B., Griendling, K.K. and Lambeth, J.D. (1999) Cell transformation by the superoxide-generating oxidase Mox1. *Nature* **401**, 79-82.

Sumimoto, H., Kage, Y., Nunoi, H., Sasaki, H., Nose, T., Fukumaki, Y., Ohno, M., Minakami, S. and Takeshige, K. (1994) Role of Src homology 3 domains in assembly and activation of the phagocyte NADPH oxidase. *Proc. Natl. Acad. Sci. U. S. A* **91**, 5345-5349.

Sumimoto, H., Sakamoto, N., Nozaki, M., Sakaki, Y., Takeshige, K. and Minakami, S. (1992) Cytochrome b558, a component of the phagocyte NADPH oxidase, is a flavoprotein. *Biochem. Biophys. Res. Commun.* **186**, 1368-1375.

Suzuki, K., Enghild, J.J., Morodomi, T., Salvesen, G. and Nagase, H. (1990) Mechanisms of activation of tissue procollagenase by matrix metalloproteinase 3 (stromelysin). *Biochemistry* **29**, 10261-10270.

Sydor, J.R., Engelhard, M., Wittinghofer, A., Goody, R.S. and Herrmann, C. (1998) Transient kinetic studies on the interaction of Ras and the Ras-binding domain of c-Raf-1 reveal rapid equilibration of the complex. *Biochemistry* **37**, 14292-14299.

Szatrowski, T.P. and Nathan, C.F. (1991) Production of large amounts of hydrogen peroxide by human tumor cells. *Cancer Res.* **51**, 794-798.

Takemoto, M. and Liao, J.K. (2001) Pleiotropic effects of 3-hydroxy-3-methylglutaryl coenzyme a reductase inhibitors. *Arterioscler. Thromb. Vasc. Biol.* **21**, 1712-1719.

Takemoto, M., Node, K., Nakagami, H., Liao, Y., Grimm, M., Takemoto, Y., Kitakaze, M. and Liao, J.K. (2001) Statins as antioxidant therapy for preventing cardiac myocyte hypertrophy. *J. Clin. Invest* **108**, 1429-1437.

Takeya, R. and Sumimoto, H. (2006) Regulation of novel superoxide-producing NAD(P)H oxidases. *Antioxid. Redox. Signal.* **8**, 1523-1532.

Takeya, R., Taura, M., Yamasaki, T., Naito, S. and Sumimoto, H. (2006) Expression and function of Noxo1gamma, an alternative splicing form of the NADPH oxidase organizer 1. *FEBS J.* **273**, 3663-3677.

Takeya, R., Ueno, N., Kami, K., Taura, M., Kohjima, M., Izaki, T., Nunoi, H. and Sumimoto, H. (2003) Novel human homologues of p47phox and p67phox participate in activation of superoxide-producing NADPH oxidases. *J. Biol. Chem.* **278**, 25234-25246.

Taylor, W.R., Jones, D.T. and Segal, A.W. (1993) A structural model for the nucleotide binding domains of the flavocytochrome b-245 beta-chain. *Protein Sci.* **2**, 1675-1685.

Tegtmeier, F., Walter, U., Schinzel, R., Wingler, K., Scheurer, P. and Schmidt, H.H. (2005) Compounds containing a N-heteroaryl moiety linked to fused ring moieties for the inhibition of NAD(P)H oxidases and platelet activation. *EP 1 598 354 A1*.

ten Freyhaus H., Huntgeburth, M., Wingler, K., Schnitker, J., Baumer, A.T., Vantler, M., Bekhite, M.M., Wartenberg, M., Sauer, H. and Rosenkranz, S. (2006) Novel Nox inhibitor VAS2870 attenuates PDGF-dependent smooth muscle cell chemotaxis, but not proliferation. *Cardiovasc. Res.* **71**, 331-341.

Thomas, S.R., Neuzil, J. and Stocker, R. (1996) Cosupplementation with coenzyme Q prevents the prooxidant effect of alpha-tocopherol and increases the resistance of LDL to transition metal-dependent oxidation initiation. *Arterioscler. Thromb. Vasc. Biol.* **16**, 687-696.

Thomas, S.R. and Stocker, R. (2000) Molecular action of vitamin E in lipoprotein oxidation: implications for atherosclerosis. *Free Radic. Biol. Med.* **28**, 1795-1805.

Toporik, A., Gorzalczany, Y., Hirshberg, M., Pick, E. and Lotan, O. (1998) Mutational analysis of novel effector domains in Rac1 involved in the activation of nicotinamide adenine dinucleotide phosphate (reduced) oxidase. *Biochemistry* **37**, 7147-7156.

Traenckner, E.B., Wilk, S. and Baeuerle, P.A. (1994) A proteasome inhibitor prevents activation of NF-kappa B and stabilizes a newly phosphorylated form of I kappa B-alpha that is still bound to NF-kappa B. *EMBO J.* **13**, 5433-5441.

Ucar, M., Mjorndal, T. and Dahlqvist, R. (2000) HMG-CoA reductase inhibitors and myotoxicity. *Drug Saf* **22**, 441-457.

Ueyama, T., Geiszt, M. and Leto, T.L. (2006) Involvement of Rac1 in activation of multicomponent Nox1- and Nox3-based NADPH oxidases. *Mol. Cell Biol.* **26**, 2160-2174.

Ungvari, Z., Csiszar, A., Kaminski, P.M., Wolin, M.S. and Koller, A. (2004) Chronic high pressure-induced arterial oxidative stress: involvement of protein kinase C-dependent NAD(P)H oxidase and local renin-angiotensin system. *Am. J. Pathol.* **165**, 219-226.

Ungvari, Z. and Koller, A. (2000) Endothelin and prostaglandin H(2)/thromboxane A(2) enhance myogenic constriction in hypertension by increasing Ca(2+) sensitivity of arteriolar smooth muscle. *Hypertension* **36**, 856-861.

Ungvari, Z. and Koller, A. (2001) Selected contribution: NO released to flow reduces myogenic tone of skeletal muscle arterioles by decreasing smooth muscle Ca(2+) sensitivity. *J. Appl. Physiol* **91**, 522-527.

Ungvari, Z., Wolin, M.S. and Csiszar, A. (2006) Mechanosensitive production of reactive oxygen species in endothelial and smooth muscle cells: role in microvascular remodeling? *Antioxid. Redox. Signal.* **8**, 1121-1129.

Vasquez-Vivar, J., Kalyanaraman, B., Martasek, P., Hogg, N., Masters, B.S., Karoui, H., Tordo, P. and Pritchard, K.A., Jr. (1998) Superoxide generation by endothelial nitric oxide synthase: the influence of cofactors. *Proc. Natl. Acad. Sci. U. S. A* **95**, 9220-9225.

Verhoeven, A.J., Bolscher, B.G., Meerhof, L.J., van, Z.R., Keijer, J., Weening, R.S. and Roos, D. (1989) Characterization of two monoclonal antibodies against cytochrome b558 of human neutrophils. *Blood* **73**, 1686-1694.

Vetter, I.R. and Wittinghofer, A. (2001) The guanine nucleotide-binding switch in three dimensions. *Science* **294**, 1299-1304.

Visse, R. and Nagase, H. (2003) Matrix metalloproteinases and tissue inhibitors of metalloproteinases: structure, function, and biochemistry. *Circ. Res.* **92**, 827-839.

von Sonntag, C. (1987) New aspects in the free-radical chemistry of pyrimidine nucleobases. *Free Radic. Res. Commun.* **2**, 217-224.

Vora, D.K., Fang, Z.T., Liva, S.M., Tyner, T.R., Parhami, F., Watson, A.D., Drake, T.A., Territo, M.C. and Berliner, J.A. (1997) Induction of P-selectin by oxidized lipoproteins. Separate effects on synthesis and surface expression. *Circ. Res.* **80**, 810-818.

Wallach, T.M. and Segal, A.W. (1997) Analysis of glycosylation sites on gp91phox, the flavocytochrome of the NADPH oxidase, by site-directed mutagenesis and translation in vitro. *Biochem. J.* **321 (Pt 3)**, 583-585.

Wang H.D., Hope, S., Du, Y., Quinn, M.T., Cayatte, A., Pagano, P.J. and Cohen, R.A. (1999) Paracrine role of adventitial superoxide anion in mediating spontaneous tone of the isolated rat aorta in angiotensin II-induced hypertension. *Hypertension* **33**, 1225-1232.

Wang, H.D., Xu, S., Johns, D.G., Du, Y., Quinn, M.T., Cayatte, A.J. and Cohen, R.A. (2001) Role of NADPH oxidase in the vascular hypertrophic and oxidative stress response to angiotensin II in mice. *Circ. Res.* **88**, 947-953.

Warnholtz, A., Nickenig, G., Schulz, E., Macharzina, R., Brasen, J.H., Skatchkov, M., Heitzer, T., Stasch, J.P., Griendling, K.K., Harrison, D.G., Bohm, M., Meinertz, T. and Munzel, T. (1999) Increased NADH-oxidase-mediated superoxide production in the early stages of atherosclerosis: evidence for involvement of the renin-angiotensin system. *Circulation* **99**, 2027-2033.

Wassmann, S., Laufs, U., Muller, K., Konkol, C., Ahlbory, K., Baumer, A.T., Linz, W., Bohm, M. and Nickenig, G. (2002) Cellular antioxidant effects of atorvastatin in vitro and in vivo. *Arterioscler. Thromb. Vasc. Biol.* **22**, 300-305.

West, N., Guzik, T., Black, E. and Channon, K. (2001) Enhanced superoxide production in experimental venous bypass graft intimal hyperplasia: role of NAD(P)H oxidase. *Arterioscler. Thromb. Vasc. Biol.* **21**, 189-194.

Wientjes, F.B., Hsuan, J.J., Totty, N.F. and Segal, A.W. (1993) p40phox, a third cytosolic component of the activation complex of the NADPH oxidase to contain src homology 3 domains. *Biochem. J.* **296 (Pt 3)**, 557-561.

Wientjes, F.B., Panayotou, G., Reeves, E. and Segal, A.W. (1996) Interactions between cytosolic components of the NADPH oxidase: p40phox interacts with both p67phox and p47phox. *Biochem. J.* **317 (Pt 3)**, 919-924.

Williams, N.K., Prosselkov, P., Liepinsh, E., Line, I., Sharipo, A., Littler, D.R., Curmi, P.M., Otting, G. and Dixon, N.E. (2002) In vivo protein cyclization promoted by a circularly permuted Synechocystis sp. PCC6803 DnaB mini-intein. *J. Biol. Chem.* **277**, 7790-7798.

Wilson, A.J.C. (1942) *Nature* **150**, 152.

Wilson, M.I., Gill, D.J., Perisic, O., Quinn, M.T. and Williams, R.L. (2003) PB1 domain-mediated heterodimerization in NADPH oxidase and signaling complexes of atypical protein kinase C with Par6 and p62. *Mol. Cell* **12**, 39-50.

Wingler, K., Wunsch, S., Kreutz, R., Rothermund, L., Paul, M. and Schmidt, H.H. (2001) Upregulation of the vascular NAD(P)H-oxidase isoforms Nox1 and Nox4 by the renin-angiotensin system in vitro and in vivo. *Free Radic. Biol. Med.* **31**, 1456-1464.

Woo, T. T. (2003) Expression and purification studies on human Nox1. Final Report for entrance into Ph.D. studies at the University of Dortmund, MPI for Molecular Physiology, Dortmund.

Wu, H., Hu, Z. and Liu, X.Q. (1998a) Protein trans-splicing by a split intein encoded in a split DnaE gene of Synechocystis sp. PCC6803. *Proc. Natl. Acad. Sci. U. S. A* **95**, 9226-9231.

Wu, H., Xu, M.Q. and Liu, X.Q. (1998b) Protein trans-splicing and functional mini-inteins of a cyanobacterial dnaB intein. *Biochim. Biophys. Acta* **1387**, 422-432.

Wu, M., Wang, T., Loh, E., Hong, W. and Song, H. (2005) Structural basis for recruitment of RILP by small GTPase Rab7. *EMBO J.* **24**, 1491-1501.

Xia, Y., Tsai, A.L., Berka, V. and Zweier, J.L. (1998) Superoxide generation from endothelial nitric-oxide synthase. A Ca2+/calmodulin-dependent and tetrahydrobiopterin regulatory process. *J. Biol. Chem.* **273**, 25804-25808.

Xiao, H.D., Fuchs, S., Cole, J.M., Disher, K.M., Sutliff, R.L. and Bernstein, K.E. (2003) Role of bradykinin in angiotensin-converting enzyme knockout mice. *Am. J. Physiol Heart Circ. Physiol* **284**, H1969-H1977.

Xiao, L., Pimentel, D.R., Wang, J., Singh, K., Colucci, W.S. and Sawyer, D.B. (2002) Role of reactive oxygen species and NAD(P)H oxidase in alpha(1)-adrenoceptor signaling in adult rat cardiac myocytes. *Am. J. Physiol Cell Physiol* **282**, C926-C934.

Xu, X., Barry, D.C., Settleman, J., Schwartz, M.A. and Bokoch, G.M. (1994) Differing structural requirements for GTPase-activating protein responsiveness and NADPH oxidase activation by Rac. *J. Biol. Chem.* **269**, 23569-23574.

Yang, H.Y., Erdos, E.G. and Levin, Y. (1970) A dipeptidyl carboxypeptidase that converts angiotensin I and inactivates bradykinin. *Biochim. Biophys. Acta* **214**, 374-376.

Yang, S., Madyastha, P., Bingel, S., Ries, W. and Key, L. (2001) A new superoxide-generating oxidase in murine osteoclasts. *J. Biol. Chem.* **276**, 5452-5458.

Yeates, T.O. (1997) Detecting and overcoming crystal twinning. *Methods Enzymol.* **276**, 344-358.

Yeates, T.O. and Fam, B.C. (1999) Protein crystals and their evil twins. *Structure.* **7**, R25-R29.

Yu, B.P. (1994) Cellular defenses against damage from reactive oxygen species. *Physiol Rev.* **74**, 139-162.

Yu, L., Zhen, L. and Dinauer, M.C. (1997) Biosynthesis of the phagocyte NADPH oxidase cytochrome b558. Role of heme incorporation and heterodimer formation in maturation and stability of gp91phox and p22phox subunits. *J. Biol. Chem.* **272**, 27288-27294.

Zabel, U. and Baeuerle, P.A. (1990) Purified human I kappa B can rapidly dissociate the complex of the NF-kappa B transcription factor with its cognate DNA. *Cell* **61**, 255-265.

Zarins, C.K., Giddens, D.P., Bharadvaj, B.K., Sottiurai, V.S., Mabon, R.F. and Glagov, S. (1983) Carotid bifurcation atherosclerosis. Quantitative correlation of plaque localization with flow velocity profiles and wall shear stress. *Circ. Res.* **53**, 502-514.

Zerial, M. and McBride, H. (2001) Rab proteins as membrane organizers. *Nat. Rev. Mol. Cell Biol.* **2**, 107-117.

Zhang, F.L. and Casey, P.J. (1996) Protein prenylation: molecular mechanisms and functional consequences. *Annu. Rev. Biochem.* **65**, 241-269.

Zou, M.H., Shi, C. and Cohen, R.A. (2002) Oxidation of the zinc-thiolate complex and uncoupling of endothelial nitric oxide synthase by peroxynitrite. *J. Clin. Invest* **109**, 817-826.

ACKNOWLEDGEMENTS

I would like to thank the following people for their contributions to this work:

My supervisors, Prof. Dr. Roger Goody, Dr. Alexey Rak, and Prof. Dr. Ilme Schlichting for the opportunity to participate in the cyclized Rab7 and human Nox1 projects, for their time, support, constructive discussions and helpful comments on the respective thesis chapters. Additional thanks to Prof. Dr. Roger Goody for taking time to make stopped flow measurements on human Nox1. I thank Dr. Alexey Rak for purifying the Mrs6 protein used in this work.

Prof. Dr. Roland Winter, for being the second referee of this work and for the collaborative work on the characterization of cyclized Rab7 by circular dichroism. I would also like to thank Dr. Stefan Grudzielanek and Dr. Dahabada Lopes for assisting me with the measurements and data analysis.

I would like to thank the Max-Planck-Gesellschaft and the IMPRS for financial support.

At the MPI for Medical Research in Heidelberg, I would like to thank Dr. Robert Shoeman for MALDI measurements and analysis, as well as many helpful discussions. I thank Monika Berthel for her work on H_6-Nox1$_{220-564}$. I thank PD Dr. Jochen Reinstein for discussions about mant-GppNHp and fluorescence. I thank Dr. Yvonne Groemping for helpful discussions on the phagocytic oxidase system. Many thanks to Thorsten Lorenz for his patient advice on the human Nox1 fluorescence measurements. I thank Dr. Lars Blumenstein for many discussions on human Nox1 as well as Carsten Kintscher for his help with fluorescence and HPLC. I would like to thank members of the Schlichting, Reinstein, Groemping, Shoeman and Meinhart groups for the nice working environment.

At the MPI of Molecular Physiology in Dortmund I would like to thank Dr. Olena Pylypenko for her assistance with the crystallography, her diagnosis of twinning in the cyclized Rab7•GppNHp data set, her critical reading of the cyclized Rab7 chapter and helpful suggestions. I would like to thank Dr. Kirill Alexandrov and members of his group for allowing me to work in their lab. Many thanks to Dr. Yaowen Wu, Dr. Tim Bergbrede and Dr. Aymelt Itzen for helping to orient me in the lab and their helpful discussions on kinetics and fluorescence. Many thanks to Nathalie Bleimling for her patient help in several aspects of the cyclized Rab7 project. I thank Dr. Sergei Mureev for his help with the

microplate reader and Dr. Christian Becker for discussions on ESI-MS. I thank members of AG Rak, AG Alexandrov, and AG Blankenfeldt for the pleasant working environment.

I wish to thank the X-ray group in Dortmund, particularly Dr. Ingrid Vetter and Dr. Michael Weyand for their help with the computational aspects of crystallographic analysis and initial advice with regards to twinning.

Special thanks to Dr. Thomas Barends (MPImF) for his clear and patient explanations about twinning and crystallography, as well as critically reading the cyclized Rab7 chapter.

Many heartfelt thanks to my fellow Woinemers: Raphael Aponte, Dr. Thomas Barends, Vinod Veetil, Dr. Konstanze von König, Dr. Gina Dumitru, Dr. Tatiana Domratcheva, and Dr. Julia Rumpf, as well as Dr. Anna Dondzillo, Anna Scherer and Dr. Susanne Eschenburg for the many laughs, continual support and good memories that I will cherish. Special thanks to Dr. Konstanze von König, for her warm friendship, help in many ways, continual encouragement, and belief in me.

Special thanks to Prof. Dr. Elizabeth Getzoff for being a wonderful source of support and encouragement at a critical time. We need more mentors like you!

Thanks also to Morgan O'Hayre for her helpful comments on this manuscript.

To Dr. Björn Klink, Dr. Niki Ahuja, and Dr. Ljiljana Fruk- my home away from home…you have been the crutches I have leaned on through these hard years. Thank you for your support and belief in me, and for all of the wonderful ways you have brought the sunshine into my life.

My deepest thanks to my family for bearing with the many years of separation with their constant love and support. Special, deep thanks to my twin sister Linda and Björn for their continual encouragement, for critically reading this dissertation, and for their helpful suggestions. Special, deep thanks to Björn for many stimulating discussions, help in many ways, patient understanding, and support, especially during the time of this writing.

To the Greatest Teacher I know, thank You that Your strength is made perfect in weakness. The way was very different, more than I ever imagined. Thank You for never letting go of me even though You had all reason to. *Ps. 40* *PTL CLJC*

Epilogue

Here the heart may give an useful lesson to the head,
And learning wiser grow without his books.
Knowledge and wisdom, far from being one,
Have ofttimes no connection.
Knowledge dwells in heads replete with thoughts of other men;
Wisdom in minds attentive to their own.
Knowledge, a rude unprofitable mass,
The mere materials with which wisdom builds,
Till smoothed and squared and fitted to its place,
Does but encumber whom it seems to enrich.
Knowledge is proud that he has learned so much,
Wisdom is humble that he knows no more.

William Cowper, *The Task*, Book 6, 1785